Development, characterization and evaluation of advanced therapies for the treatment of cardiac pathologies

by

Lidia Gómez Cid

A dissertation submitted by in partial fulfillment of the requirements for the degree of Doctor of Philosophy in

Biomedical Science and Technology

Universidad Carlos III de Madrid

Advisors:

Francisco Fernández-Avilés Díaz
Lilian Grigorian Shamagian

Tutor:

Juan José Vaquero López

March 2022

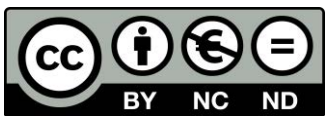

Para Carlos, por tu apoyo incondicional e infinito

"Do, or do not. There is no try"

Master Yoda

"Hazlo o no lo hagas, pero no lo intentes"

Maestro Yoda

AGRADECIMIENTOS

En primer lugar, quiero dar las gracias al Dr. Francisco Fernández-Avilés y a la Dra. Lilian Grigorian por confiar en mí para dirigirme esta tesis y permitirme hacer este bonito trabajo. Gracias Lilian por todo lo que me has enseñado, por tu gran apoyo y tu admirable motivación. Gracias también por haberme sabido llevar durante todo este tiempo y sacar lo mejor de mí.

También quiero agradecer al resto de personas del Servicio de Cardiología del Hospital Gregorio Marañón, del edificio experimental, del Laboratorio de Imagen, del Laboratorio de Genética Hematológica, de la Universidad Carlos III y del CSIC, y en particular a todos los co-autores de los trabajos, su contribución para sacar adelante los diferentes estudios.

A mis compañeros del día a día en el Laboratorio, Ana, Ana I., Gonzalo e Ismael, quiero agradeceros vuestra compañía, vuestros ánimos, vuestro apoyo, y todos los momentos agradables que hemos pasado juntos y que sin duda han hecho este periodo mucho más llevadero y divertido. Gracias también a los amigos que habéis cumplido este papel fuera del entorno laboral.

A los que me habéis apoyado y acompañado desde la universidad, en particular a David, Rigo, Juanjo, Arrate, Javier, Diego y Marisa. Gracias Juanjo por ser el tutor de esta tesis, por confiar en mí, y por estar ahí siempre que lo he necesitado. Gracias a Diego y a Marisa por el tiempo y la ayuda que me habéis dedicado de forma totalmente desinteresada.

Gracias a los estudiantes de TFG que también habéis formado parte de estos estudios y que siempre lo habéis hecho con una sonrisa: Víctor, Alexia, Mar y Marina.

Por último, quiero dar las gracias a mi familia. Gracias por ser mi gran apoyo en lo personal y en lo profesional, y por estar siempre dispuestos a ayudarme con todo lo que estuviera en vuestra mano. Gracias a mi madre por mantenerme alimentada con comida sana durante todos estos años. Soy consciente de todo el trabajo y tiempo que me has regalado. Gracias a mi padre por hacerme piezas a medida de todos los tamaños y materiales posibles para que mis experimentos y mis hidrogeles siempre salieran perfectos. Gracias a mi hermana por su actitud risueña, siempre quitándole hierro a los problemas y recordándome que también tengo que dedicarle tiempo a disfrutar. Gracias a Carlos por ser un perfecto compañero de vida. Aunque todas las palabras de esta tesis se quedan cortas al lado de todo lo que tengo que agradecerte, gracias por estar ahí siempre, por echarme una mano con todo lo que puedes y por aguantarme en mis malos momentos. Gracias sobre todo por entender siempre lo importante que han sido y son mi profesión y esta tesis para mí, a pesar de que eso te haya supuesto renunciar a ciertas cosas. Sin duda no podría haber hecho esta tesis sin ti. No podría cerrar estos agradecimientos sin mencionar a mis abuelas/os y a mi segunda madre, Mari. Gracias por todo vuestro cariño. Sé que cada uno desde donde estáis hoy, estáis contentos y orgullosos de que me convierta en Doctora.

PUBLISHED AND SUBMITTED CONTENT

Journal Articles

1. **Gómez-Cid L**, Grigorian-Shamagian L, Sanz-Ruiz R, de la Nava AS, Fernández AI, Fernández-Santos ME, Fernández-Avilés F. The essential need for a validated potency assay for cell-based therapies in cardiac regenerative and reparative medicine. A practical approach to test development. *Stem Cell Rev Rep* 2021; 17: 2235–2244. https://doi.org/10.1007/s12015-021-10244-5.

   L. Gómez-Cid and L. Grigorian-Shamagian performed the literature search and drafted the manuscript. F. Fernández-Avilés and L. Grigorian-Shamagian had the idea for the article. R. Sanz-Ruiz, AS. de la Nava, AI. Fernández, ME Fernández-Santos and F Fernández-Avilés critically revised the work. All authors read and approved the final manuscript.

   Contribution completely included in Chapter 3.

2. **Gómez-Cid L**, López-Donaire ML, Velasco D, Marín V, González MI, Salinas B, Cussó L, García Á, Bravo SB, Fernández-Santos ME, Elvira C, Sierra J, Arroba E, Bañares R, Grigorian-Shamagian L, Fernández-Avilés F. Cardiac extracellular matrix hydrogel enriched with polyethylene glycol presents improved gelation time and increased on-target site retention of extracellular vesicles. *Int J Mol Sci.* 2021; 22(17):9226. https://doi.org/10.3390/ijms22179226.

   L. Gómez-Cid performed most of the experiments, analyzed and interpreted the data, prepared the figures and drafted the manuscript. M. López-Donaire and D. Velasco helped performing some of the experiments and conceptualizing the work. V. Marín, MI. González, SB. Bravo, C. Elvira, J. Sierra and E. Arroba provided technical assistance. M. López-Donaire, D. Velasco, B. Salinas, L. Cussó, A. García, ME. Fernández Santos, C. Elvira and R. Bañares provided resources and critically revised the work. Lilian Grigorian-Shamagian supervised and validated the work and the manuscript. Francisco-Fernández Avilés acquired the funding, supervised the project and critically revised the work. All authors read and approved the final manuscript.

   Contribution completely included in Chapter 6.

3. **Gómez-Cid L**, Moro-López M, de la Nava AS, Hernández-Romero I, Fernández AI, Suárez-Sancho S, Atienza F, Grigorian-Shamagian L, Fernández-Avilés F. Electrophysiological effects of extracellular vesicles secreted by cardiosphere-derived cells: unraveling the antiarrhythmic properties of cell therapies. *Processes* 2020; 8: 924. https://doi.org/10.3390/pr8080924.

   L. Gómez-Cid performed the experiments, analyzed the data and prepared the figures with M. Moro-López. Lidia interpreted the results and drafted the manuscript. I. Hernández Romero helped conceptualizing the work. AS de la Nava, I. Hernández-Romero, AI. Fernández and S. Suárez-Sancho provided technical assistance. F. Atienza critically revised the work. L. Grigorian-Shamagian supervised and validated the work and the manuscript. F. Fernández-Avilés acquired the funding, supervised the project and critically revised the work. All authors read and approved the final manuscript.

   Contribution completely included in Chapter 7.

4. **Gómez-Cid L**, Cervera-Negueruela M, Campo-Fonseca A, Pinto A, Gil-Jaurena JM, Suárez-Sancho S, Fernández-Santos ME, Fernández-Avilés F, Grigorian-Shamagian L. Anti-senescence in vitro potency of extracellular vesicles secreted by cardiosphere-derived cells predicts their rejuvenating effects in an ageing rodent model (submitted).

   L. Gómez-Cid performed most of the experiments, analyzed and interpreted the data, prepared the figures and drafted the manuscript. M Cervera-Negueruela and A. Campo-Fonseca helped performing some of the experiments. A. Pinto and JM. Gil-Jaurena contributed to sample collection. S. Suárez-Sancho provided technical assistance. Francisco-Fernández Avilés acquired the funding, supervised the project and critically revised the work. Lilian Grigorian-Shamagian designed, supervised and validated the work and the manuscript. All authors read and approved the final manuscript.

   Contribution completely included in Chapters 4 and 5.

Conference Abstracts

1. **Gómez-Cid L**, Campo-Fonseca A, Suárez-Sancho S, Chicano M, Pinto A, Gil-Jaurena JM, Climent AM, Fernández-Santos ME, Fernández-Avilés F, Grigorian L. Digging into the rejuvenating properties of cardiosphere-derived cell therapy. *In: Frontiers in Cardiovascular Biomedicine – April 23-26, 2020.*

L. Gómez-Cid performed most of the experiments, analyzed and interpreted the data, prepared the figures and drafted the abstract.

Contribution completely included in Chapter 4.

2. **Gómez-Cid L**, Cervera-Negueruela M, Campo-Fonseca A, Suárez-Sancho S, Pinto A, Gil-Jaurena JM, Fernández-Santos ME, Fernández-Avilés F, Grigorian L. Senescence-based predicted potency of extracellular vesicles determines their rejuvenating cardiac effects in an ageing rodent model. *In: Frontiers in Cardiovascular Biomedicine – April 29-May 01, 2022* (accepted).

   L. Gómez-Cid performed most of the experiments, analyzed and interpreted the data, prepared the figures and drafted the abstract.

   Contribution completely included in Chapter 5.

3. **Gómez-Cid L**, López-Donaire ML, Velasco D, Fernández-Santos ME, Grigorian-Shamagian L, Fernández-Avilés F. The combination of extracellular vesicles in a cardiac extracellular matrix hydrogel with polyethylene glycol presents promising physico-chemical properties and bioactivity for cardiac applications. *In: Frontiers in Cardiovascular Biomedicine – April 29-May 01, 2022* (accepted).

   L. Gómez-Cid performed the experiments, analyzed and interpreted the data, prepared the figures and drafted the abstract.

   Contribution completely included in Chapter 6.

4. **Gómez-Cid L**, Cervera-Negueruela M, Campo-Fonseca A, Suárez-Sancho S, Pinto A, Gil-Jaurena JM, Fernández-Santos ME, Fernández-Avilés F, Grigorian-Shamagian L. Anti-senescence in vitro potency of extracellular vesicles secreted by cardiosphere-derived cells predicts the antihypertrophic effect in a rat model of cardiac ageing. *In: ESC Congress 2021 – The Digital Experience, August 27-30, 2021. European Heart Journal.* October 2021;42 (Supplement_1):ehab724.3270. https://doi.org/10.1093/eurheartj/ehab724.3270.

   L. Gómez-Cid performed most of the experiments, analyzed and interpreted the data, prepared the figures and drafted the abstract.

Contribution completely included in Chapter 5.

5. **Gómez-Cid L**, Moro-López M, de la Nava AS, Fernández AI, Fernández-Santos ME, Atienza F, Grigorian-Shamagian L, Fernández-Avilés F. Extracellular vesicles secreted by human cardiosphere-derived cells attenuate electrophysiological remodelling in an in vitro model of atrial fibrillation. *In: ESC Congress 2021 – The Digital Experience, August 27-30, 2021. European Heart Journal.* October 2021;42 (Supplement_1):ehab724.3317. https://doi.org/10.1093/eurheartj/ehab724.3317

   L. Gómez-Cid performed the experiments, analyzed the data and prepared the figures with Marina Moro-López. L. Gómez-Cid interpreted the results and drafted the abstract.

   Contribution completely included in Chapter 7.

The material from these sources included in this thesis are not singled out with typographic means and references.

OTHER RESEARCH MERITS

Journal Articles

1. Del-Canto I, **Gómez-Cid L**, Hernández Romero I, Guillem MS, Fernández-Santos ME, Atienza F, Such L, Fernández-Avilés F, Chorro FJ, Climent AM. Ranolazine-mediated Attenuation of Mechanoelectric Feedback in Atrial Myocyte Monolayers**.** *Frontiers in Physiology* 2020; 11: 922. https://doi.org/10.3389/fphys.2020.00922

   L. Gómez-Cid helped in performing the experiments and analyzing the data.

Conference Abstracts

1. Del-Canto I, **Gómez-Cid L,** de la Nava AS, Guillem MS, Fernández-Santos ME, Climent AM, Atienza F, Such L, Fernández-Avilés F, Chorro FJ. The selective late sodium current inhibitor eleclazine reduces atrial fibrillation dominant frequency and facilitates the suppression of arrhythmia in HL-1 cells. *In: ESC Congress 2020 – The Digital Experience, August 29-September 1, 2020. European Heart Journal.* November 2020;41 (Supplement_2):ehaa946.3704 https://doi.org/10.1093/ehjci/ehaa946.3704

   L. Gómez-Cid helped in performing the experiments.

2. Sánchez de la Nava AM, Ríos-Muñoz GR, **Gómez-Cid L**, Grigorian-Shamagian L, Fernández-Santos ME, Arenal A, Atienza F, Fernández-Avilés F. Influence of highest dominant frequency area on fibrillation dynamics and frequency spectrum on electrograms. *In: ESC Congress 2021 – The Digital Experience, August 27-30, 2021. European Heart Journal.* October 2021;42 (Supplement_1):ehab724.3318. https://doi.org/10.1093/eurheartj/ehab724.3318

   L. Gómez-Cid helped in performing the experiments.

3. Ríos-Muñoz GR, Sánchez de la Nava AM, **Gómez-Cid L,** Grigorian-Shamagian L, Fernández-Santos ME, Atienza F, Arenal A, Fernández-Avilés F. Unveiling the impact of fibrosis presence in fibrillatory electrograms. *In: ESC Congress 2021 – The Digital Experience, August 27-30, 2021. European Heart Journal.* October 2021;42 (Supplement_1):ehab724.0417. https://doi.org/10.1093/eurheartj/ehab724.0417

   L. Gómez-Cid helped in performing the experiments.

4. Sánchez de la Nava AM, Ríos-Muñoz GR, **Gómez-Cid L**, Grigorian-Shamagian L, Fernández-Santos ME, Arenal A, Atienza F, Fernández-Avilés F. Influencia del área de la frecuencia dominante en las dinámicas de fibrilación y el espectro de frecuencia en los

electrogramas. *En: SEC 2021 – El Congreso de la Salud Cardiovascular, Zaragoza, Octubre 28-30, 2021. Revista Española de Cardiología*. 2021;74 (Supl 1):1046. https://www.revespcardiol.org/en-congresos-sec-2021-el-congreso-138-sesion-fibrilacion-auricular-ii-6575-influencia-del-area-de-la-79063-pdf

L. Gómez-Cid helped in performing the experiments.

5. Ríos-Muñoz GR, Sanchez de la Nava AM, **Gómez-Cid L,** Grigorian-Shamagian L, Fernández-Santos ME, Arenal A, Atienza F, Fernández-Avilés F. Desvelando el impacto de la fibrosis en electrogramas de fibrilación auricular. *En: SEC 2021 – El Congreso de la Salud Cardiovascular, Zaragoza, Octubre 28-30, 2021. Revista Española de Cardiología*. 2021;74 (Supl 1):5001. https://www.congresosec.org/2021/sec/public/sessions/abstracts/8590.pdf

L. Gómez-Cid helped in performing the experiments.

Table of Contents

Abstract ..... **xiii**
List of Figures ..... **xv**
List of Tables ..... **xix**
List of Abbreviations and Acronyms ..... **xxi**
1. Introduction **1**
1.1 The heart 1
1.1.1 Heart anatomy 1
1.1.2 Blood circulation 3
1.1.3 Cardiac tissue 4
1.1.4 Conduction system 5
1.1.5 The cardiac cycle and cardiac output 5
1.2 Cardiac aging and heart disease 8
1.2.1 Functional changes 8
1.2.2 Structural and cellular changes 9
1.2.3 Molecular mechanisms 9
1.2.4 Treatment, challenges, and new directions 13
1.3 Advanced reparative and regenerative therapies in the cardiovascular field 17
1.3.1 Stem cells 17
1.3.2 Stem cell-derived products: extracellular vesicles (EVs) 20
1.3.3 Hydrogels 22
1.3.4 Limitations and challenges for translation of cardiac regenerative and reparative products 25
2. Motivation, objectives and thesis outline **31**
2.1 Motivation 31
2.2 Objectives 32
2.3 Thesis outline 32
3. The essential need for a validated potency assay for cell-based therapies in cardiac regenerative and reparative medicine. A practical approach to test development **35**
3.1 Abstract 35
3.2 Introduction 35
3.3 Potency assay as regulatory recommendation to optimize research results 36
3.4 Requirements of an "ideal" potency assay 38
3.5 Challenges in the development of potency assays for cell-based therapies 38

3.6 Disease-targeted and mechanism of action-guided potency tests in cardiovascular regenerative medicine 40
3.7 Possible ways of measuring potency according to the expected mechanism of action 42
3.7.1 Cardiomyogenesis 42
3.7.2 Electromechanical maturation and coupling 43
3.7.3 Immunomodulation 44
3.7.4 Cardioprotection 44
3.7.5 Angiogenesis 45
3.7.6 Anti-fibrotic mechanism 45
3.8 Examples of potency assays for cell-based therapy products in the cardiovascular field 46
3.9 Conclusions 46
4. Exploring the determinants of rejuvenating potency of cardiosphere-derived cells: chronological vs. biological age 49
4.1 Abstract 49
4.2 Introduction 50
4.3 Materials and Methods 52
4.3.1 CDCs and derived extracellular vesicle isolation 52
4.3.2 Experimental protocol 53
4.3.3 Cell culture 59
4.3.4 Gene expression analysis 60
4.3.5 Histochemistry 62
4.3.6 Cardiosphere diameter 63
4.3.7 Flow cytometry 64
4.3.8 Telomere length 65
4.3.9 Proliferation 66
4.3.10 Migration 66
4.3.11 Factor secretion - ELISA 66
4.3.12 Tube formation 67
4.3.13 Statistical analysis 67
4.4 Results 68
4.4.1 CDC's bioactivity is correlated to the cellular senescence status but not to the donor's chronological age 68
4.4.2 Cardiosphere size and CDC surface markers relate to VEGF secretion, but not to other CDC properties 70
4.4.3 CDC-EVs have an anti-senescent effect on different cell types in the heart 71
4.4.4 CDC-EVs have other "pro-rejuvenating" and pro-angiogenic effects on different cell types in the heart 71
4.4.5 The extent of the CDC-EVs efficacy cannot be predicted by the cellular senescence status as surrogate marker 72
4.5 Discussion 74

4.6 Conclusions 79
5. Anti-senescence *in vitro* potency of extracellular vesicles secreted by cardiosphere-derived cells predicts their rejuvenating effects in an aging rodent model 81
5.1 Abstract 81
5.2 Introduction 82
5.3 Materials and methods 83
5.3.1 Experimental protocol 83
5.3.2 *In vitro* characterization and classification 87
5.3.3 *In vivo* evaluation 88
5.3.4 Statistical analysis 92
5.4 Results 92
5.4.1 CDC-EVs present variable anti-senescent and pro-angiogenic potency *in vitro*, which allows their classification as potent (P-EVs) and non-potent (NP-EVs) 92
5.4.2 P-EVs have more rejuvenating cardiac effect *in vivo* than NP-EVs 93
5.4.3 P-EVs have more beneficial systemic effects *in vivo* than NP-EVs 96
5.5 Discussion 100
5.6 Conclusions 102
6. Cardiac extracellular matrix hydrogel enriched with polyethylene glycol presents improved gelation time and increased on-target site retention of extracellular vesicles 103
6.1 Abstract 103
6.2 Introduction 103
6.3 Materials and methods 105
6.3.1 EDCs, CDCs, and derived extracellular vesicle isolation 105
6.3.2 Porcine myocardial matrix decellularization, lyophilization, and characterization 105
6.3.3 Cardiac extracellular matrix hydrogel (cECMH) synthesis 107
6.3.4 Gelation kinetics 108
6.3.5 Scanning electron microscopy 108
6.3.6 Rheometry and injectability 108
6.3.7 Enzymatic degradation assay 110
6.3.8 EV bioactivity — anti-senescent effect 110
6.3.9 EV release from cECMH 110
6.3.10 EV *in vivo* retention 111
6.3.11 Statistical analysis 112
6.4 Results 112
6.4.1 Lyophylized cECM retained native ECM proteins and sGAGs. 112
6.4.2 cECM hydrogels incorporating EVs and PEG have shorter gelation times, larger fiber diameter, and improved mechanical properties while remaining injectable and biodegradable 112

6.4.3 The combined product of EVs–PEG–cECMH maintains the bioactivity of the individual components ... 116
6.4.4 The combined product of EVs–PEG–cECMH shows a higher local EV retention *in vivo* ... 119
6.5 Discussion ... 119
6.6 Conclusions ... 123
7. Electrophysiological effects of extracellular vesicles secreted by cardiosphere-derived cells: unraveling the antiarrhythmic properties of cell therapies ... 125
7.1 Abstract ... 125
7.2 Introduction ... 125
7.3 Materials and methods ... 127
7.3.1 CDCs and derived extracellular vesicle isolation ... 127
7.3.2 Experimental protocol ... 127
7.3.3 Optical mapping recordings ... 128
7.3.4 Calcium image processing ... 128
7.3.5 Gene expression analysis ... 130
7.3.6 Statistical analysis ... 131
7.4 Results ... 131
7.4.1 Effects of extracellular vesicles derived from CDCs on activation dominant frequency, complexity and rotor dynamics ... 132
7.4.2 Extracellular vesicles derived from CDCs increase conduction velocity in arrhythmogenic substrate and increase ion channel expression ... 134
7.4.3 Activation complexity electrophysiological mechanisms ... 135
7.5 Discussion ... 135
7.6 Conclusions ... 137
8. Discussion and conclusions ... 139
8.1 Main findings ... 139
8.2 Comparison with previous studies ... 141
8.3 Limitations ... 143
8.4 Future work ... 144
8.5 Conclusions ... 145
References ... 149
Declarations ... 183
Funding ... 183
Institutional review board statement and informed consent ... 183

Abstract

Cardiovascular diseases (CVDs) are the leading cause of disease burden and mortality in the world, as well as a major cause of disability and health care costs. With the average lifespan of the human population continuously increasing, it is expected that the problem of CVDs will only continue to grow in the following years. Current pharmacological treatments for age-associated cardiac pathologies such as heart failure and atrial fibrillation present severe clinical efficacy and safety problems and are not regarded as definitive cures. This makes it necessary to develop new treatment strategies that target the involved molecular pathways and trigger endogenous reparative responses.

Contrary to current molecular treatments, advanced therapy medicinal products (ATMPs) such as stem cells, extracellular vesicles (EVs) and biomaterials such as hydrogels could have the potential to treat cardiac aging-associated pathologies from a more fundamental level. However, many problems and unknowns still need to be solved before they can reach the clinical scenario. Some of the most highlighted limitations we focus on in this work are: (i) the lack of deep understanding of their mechanism of action (MoA), (ii) their large variability and lack of standardization (including inadequate potency tests) and (iii) low *in vivo* retention at the site of interest. Therefore, the main objective of this thesis is to develop, characterize and evaluate advanced therapies for the treatment of cardiac pathologies solving some of their current limitations to enhance their therapeutic potential.

To achieve this aim, we first focus on improving standardization and development of potency assays. We describe the main characteristics and challenges for a cell therapy based potency test in the cardiovascular field and we review and propose different types of assays that could be taken into consideration based on the product's expected MoA and the target cardiovascular disease**.** Secondly, as cardiosphere-derived cells (CDCs) and their secreted EVs (CDC-EVs) have previously reported to have anti-senescent effects and this is considered important in aging-related cardiac diseases, we explore potential predictors of rejuvenating potency with a special focus on the chronological age of the CDC-donors and CDC-senescence, among others. Multiple *in vitro* tests allow us to conclude that more than cell particular biological markers or characteristics, the cell bioactivity relative to the expected MoA should be a better predictor for the ATMP potency. Thus, we evaluate if the *in vitro* anti-senescent and pro-angiogenic effect of the CDC-EVs, scored with a matrix assay, can be used to predict the *in vivo* potency of the CDC-EVs in an animal model of cardiac aging. Our results show that EVs classified *in vitro* as potent with the matrix assay have more cardiac reparative potential *in vivo* than

EVs classified as non-potent. After further validation, the matrix assay proposed here could be a suitable *in vitro* potency test for discerning suitable allogenic biological products in the cardiac aging clinical scenario.

Next, with the purpose of improving EV retention at the site of interest, we develop an optimized product combining hydrogels from cardiac extracellular matrix (cECM), polyethylene glycol and EVs to overcome some of their individual limitations: long gelation time of the cECM and poor retention of the EVs. We conclude that the combined product rapidly gels at physiological temperature and presents improved mechanical properties while maintaining the injectability, the biodegradability, and the bioactivity of its individual components. In addition, it serves to better retain the EVs on-site *in vivo*.

Finally, we explore the electrophysiological modifications induced by CDC-EVs on arrhythmogenic tissue to better understand the mechanisms behind their antiarrhythmic effect. We found that CDC-EVs reduce spontaneous activation complexity and increase conduction velocity of cardiomyocytes leading to a less arrhythmogenic profile. If validated in other cellular models, CDC-EVs may be used specifically as antiarrhythmic agents in a wide range of cardiac pathologies.

Although future work should aim to further validate these results both at preclinical and clinical level, these findings together partially overcome some of the main challenges for the therapeutic use of cellular therapies and open a new horizon for the treatment of cardiac-aging related pathologies, some still considered as unmet medical needs.

List of Figures

Figure 1.1. Heart anatomy. 2

Figure 1.2. Blood circulation. 3

Figure 1.3. Ventricular action potential and conduction system of the heart. 5

Figure 1.4. Cardiac cycle. 7

Figure 1.5. Markers of senescent cells. Indirect markers characterizing cellular senescence are as follows, and these vary among tissues and cells. 10

Figure 1.6. Key mechanisms of cardiac aging. Abnormal expression of ncRNAs can cause dysregulation of their downstream target genes, which cause telomere damage and cardiac aging. 12

Figure 1.7. The concept of cardiac aging and its biological mechanism. 13

Figure 1.8. A schematic summary of the molecular mechanisms of cardiac aging and potential cardiac aging interventions. 16

Figure 1.9. Advantages and disadvantages in cellular and acellular therapy [194]. 22

Figure 1.10. Regenerative therapies. Classification of the different type of therapies in cell-based, cell-free or tissue engineering is done mostly from an academic perspective. In reality many of them converge and the combined use of different strategies may lead to better results. 25

Figure 1.11. Priority concepts in cardiac regenerative and reparative medicine according to the field of research. 29

Figure 3.1. Development and challenges in potency assay development in the cardiovascular field. 37

Figure 3.2. Steps in the development of a potency assay. 39

Figure 3.3. Potency tests based on the expected mechanism of action (MoA) for different cardiac diseases. 42

Figure 4.1. Methodology employed for cardiosphere-derived cell extracellular vesicle (CDC-EV) isolation. 53

Figure 4.2. Cardiac biopsies donor distribution by age. 54

Figure 4.3. Procedure followed for explant-derived cells (EDCs), cardiosphere and cardiosphere-derived cells (CDCs) characterization. 56

Figure 4.4. Procedure followed for evaluating the CDC-EV bioactivity in different cell types present in the heart 58

Figure 4.5. Percentage of CDCs expressing CD105, CD117, CD90, CD31 and CD45 by flow cytometry (n = 18 donors). 64

Figure 4.6. CDC nuclei from two different donors after merged DAPI and Telomere PNA FISH Kit/Cy3 staining. First image shows nuclei with shorter telomere length with respect to the second image, as length of the telomeres is directly correlated to the fluorescence intensity of the red spots. Scale bar corresponds to 25 μm. 65

Figure 4.7. Donor chronological age vs. CDC biological age effect on different CDC properties. 69

Figure 4.8. Cardiosphere size and surface markers relationship to VEGFA expression and secretion. * $p < 0.05$, ** $p < 0.01$. 70

Figure 4.9. Anti-senescent effect of CDC-EVs from a low senescent CDC donor and from a highly senescent CDC donor on different cell types in the heart. Senescent cells in blue. 72

Figure 4.10. Other rejuvenating and pro-angiogenic effects of CDC-EVs from a low senescent CDC donor and from a highly senescent CDC donor on different cell types in the heart.. 73

Figure 4.11. Correlation between the characteristics at different stages of product development and final CDC-EVs anti-senescent and pro-angiogenic potency *in vitro*. 75

Figure 5.1. Experimental protocol. 86

Figure 5.2. Glucose level changes in time and the corresponding parameters measured. 91

Figure 5.3. Performance of CDC-EVs from the different donors in the different tests in the potency matrix-assay. 94

Figure 5.4. Cardiac effects of D-gal and P- and NP-EV administration. 97

Figure 5.5. Systemic effects induced by D-gal and by P- and NP-EVs in the rodent model.....99

Figure 6.1. Procedure followed for the preparation of the cardiac extracellular matrix hydrogel (cECMH). 107

Figure 6.2. Set up for the rheometry and injectability tests. 109

Figure 6.3. Proteins identified by liquid chromatography–tandem mass spectrometry (LC–MS/MS) in the lyophilized cardiac extracellular matrix (cECM) (n = 3). 113

Figure 6.4. Gelation kinetics and fiber diameter. 115

Figure 6.5. Mechanical properties and degradation of the cECMH alone, with PEG, and with PEG-isolated EVs. 117

Figure 6.6. Bioactivity of EVs alone, cECMH, and EVs–PEG–cECMH, measured as anti-senescent effect. 118

Figure 6.7. EV release from the EVs–PEG–cECMH and EV *in vivo* retention. 120

Figure 7.1. Experimental protocol and methodology employed for calcium transient (CaT) recording analysis. 129

Figure 7.2. Representative images of the HL-1 culture at 100% confluency on day 4 of the experiment in control and CDC-EVs group. 132

Figure 7.3. Electrophysiological characteristics comparison (n = 12 in each group) and representative examples of control (CNT) and CDC-EV treated cultures. Examples of complexity, dominant frequency, rotor dynamics and conduction velocity are illustrated for both groups. 133

Figure 7.4. Relative gene expression results (n = 9 in each group) normalized to *ACTB* and *36B4* housekeeping genes. Relative gene expression of *SCN5A* (** $p < 0.01$), *CACNA1C* (** $p < 0.01$) and *GJA1* (* $p < 0.05$) was significantly higher in the CDC-EV treated group. 134

Figure 7.5. Relative gene expression relationship with CV and complexity, and relationship of the different electrophysiological parameters with activation complexity. 136

List of Tables

Table 1.1. Clinical trials using CDCs. 19

Table 4.1. Cardiac biopsies donor distribution by age group and sex. 54

Table 4.2. Primers used for RT-PCR in EDC characterization 60

Table 4.3. Surface markers characteristic of each subpopulation of cells inside the CDC mixture. 64

Table 5.1. CDC-EV score assigned according to the extent of the beneficial effect in each of the different tests in the matrix-assay.....85

Table 5.2. Primers used for RT-PCR in heart samples from rat experiments. 89

Table 7.1. Primers used for RT-PCR in HL-1 cells 131

List of Abbreviations and Acronyms

2D	Two-dimensional
3D	Three-dimensional
AF	Atrial fibrillation
ATMPs	Advanced therapy medicinal products
AUC	Area under the curve
AV	Atrioventricular
BM	Bone marrow
BM-MNCs	Bone marrow mononuclear cells
BM-MSCs	Bone marrow mesenchymal stem cells
CaT	Calcium transients
CDC-EVs	Extracellular vesicles secreted by cardiosphere-derived cells
CDCs	Cardiosphere-derived cells
cECM	Cardiac extracellular matrix
cECMH	Cardiac extracellular matrix hydrogel
CMs	Cardiomyocytes
CNT	Control
CO	Cardiac output
CPCs	Cardiac progenitor cells
CSCs	Cardiac stromal cells
CT	Computer Tomography
Cx43	Connexin 43
D-gal	D-galactose
dECM	Decellularized extracellular matrix
DF	Dominant frequency
ECG	Electrocardiogram
ECM	Extracellular matrix
ECs	Endothelial cells
EDCs	Cardiac explant-derived cells
EDP	End-diastolic pressure
EDV	End-diastolic volume

EF	Ejection fraction
ELISA	Enzyme-linked immunosorbent assay
EMA	European Medicines Agency
ESCs	Embryonic stem cells
ESP	End-systolic pressure
ESV	End-systolic volume
EVs	Extracellular vesicles
FBS	Fetal Bovine Serum
FDA	Food and Drug Administration
HF	Heart failure
HFpEF	Heart failure with preserved ejection fraction
HFrEF	Heart failure with reduced ejection fraction
HGF	Hepatic growth factor
HR	Heart rate
HS-CDC-EVs	Extracellular vesicles secreted by highly senescent cardiosphere-derived cells
HUVEC	Human Umbilical Vein Endothelial Cells
I_{CaL}	Low L-type calcium current
IGF-1	Insulin growth factor 1
IL	Interleukin
IMDM	Iscove's Modified Dulbecco's Medium
I_{Na}	Late sodium current
IP	Intraperitoneal
iPSCs	Induced by reprogramming pluripotent stem cells
LC–MS/MS	Liquid chromatography–tandem mass spectrometry
LS-CDC-EVs	Extracellular vesicles secreted by low senescent cardiosphere-derived cells
LV	Left ventricle
LVEDV	Left ventricular end-diastolic volume
LVEF	Left ventricular ejection fraction
LVESV	Left ventricular end-systolic volume
NP-EVs	Non-potent extracellular vesicles
NTA	Nanoparticle tracking analysis
MMP	Matrix metalloproteinase
MoA	Mechanism of action
MPI	Myocardial performance index
MSCs	Mesenchymal stem cells

OD	Optical density
P#	Passage number # (e.g. P1, passage 1)
P-EVs	Potent extracellular vesicles
PDT	Population doubling time
PEG	Polyethylene glycol
PSs	Point singularities
RAAS	Renin angiotensin aldosterone system
ROS	Reactive oxygen species
RT	Room temperature
RT-PCR	Real-Time Polymerase Chain Reaction
RV	Right ventricle
SA	Sinoatrial
SA-β-gal	Senescence-associated with β-galactosidase
SASP	Senescence-associated secretory phenotype
SDF-1	Stromal cell-derived factor 1
SEM	Scanning Electron Microscopy
SFM	Serum free medium
sGAG	Sulfated glycosaminoglycans
SPECT	Single Photon Emission Computer Tomography
$t_{1/2}$	Half gelation time
TGF-β	Transforming growth factor-β
TIMP	Tissue inhibitor of metalloproteinases
t_{lag}	Lag time
TNF-α	Tumor necrosis factor-α
VEGF	Vascular endothelial growth factor

Chapter 1

Introduction

Cardiovascular diseases (CVDs), particularly associated to increasing age, are the leading cause of disease burden and mortality in the world, as well as a major cause of disability and health care costs [1]. However, current treatments present severe clinical efficacy and safety problems [2, 3] and are not regarded as definitive cures [4]. The use of advanced therapies, including stem cell therapy, extracellular vesicles (EVs) and biomaterials such as hydrogels has emerged as a potential breakthrough [5]. Nevertheless, many problems and unknowns still remain that need to be solved before they can reach the clinical scenario. In this section, we revise heart anatomy and physiology, the pathophysiological changes associated with cardiac aging and heart disease at functional, structural, cellular and molecular level, and the limitations of current available treatments. Then, we introduce the state of the art of advanced reparative and regenerative therapies in the cardiovascular field, including stem cells, stem cell-derived EVs and hydrogels and the main limitations they face towards successful translation into the clinical scenario.

1.1 The heart

The heart is the natural pump of the body in charge of maintaining blood circulation. Blood flow ensures a constant oxygen and nutrient supply to all the cells in our body, as well as a removal of waste from the cellular processes. To perform this task efficiently, the heart presents unique molecular, cellular, and structural characteristics that translate into a coordinated electrical and mechanical activity. In this section, we are going to review the heart anatomy and its role in maintaining blood circulation, the main cell types involved and their characteristics, and how these, together with the conduction system, cooperate to lead to effective pumping.

1.1.1 Heart anatomy

The heart is an organ forming part of the cardiovascular system and located near the midline of the thoracic cavity, in the mediastinum (Figure 1.1a). Inside the mediastinum, the heart is protected by the pericardium and the pericardial fluid, that confine the heart to its position but

allow the vigorous movement required for contraction. The heart wall is composed of three layers: the epicardium (the more external layer), the myocardium (the middle layer) and the endocardium (the inner layer) (Figure 1.1b). The epicardium and the endocardium are of connective tissue (mesothelium and endothelium respectively) to provide smooth surfaces that diminish friction of the heart with the pericardial fluid in the exterior and with blood in the interior. The myocardium, composed of cardiac muscle, is responsible for the relaxation-contraction that leads to the pumping. The human heart walls arrange to form four chambers: two superior atria and two inferior ventricles (Figure 1.1c). The right and left atria are separated by the interatrial septum and the right and left ventricles (RV and LV) are separated by the interventricular septum. The thickness of the myocardium is not constant and depends on each chamber's function. On one hand, atria pump blood under lower pressure and smaller distances, having thinner walls. On the other hand, ventricles, specially the left one, pump over higher distances and have higher workload, requiring thicker walls (Figure 1.1d).

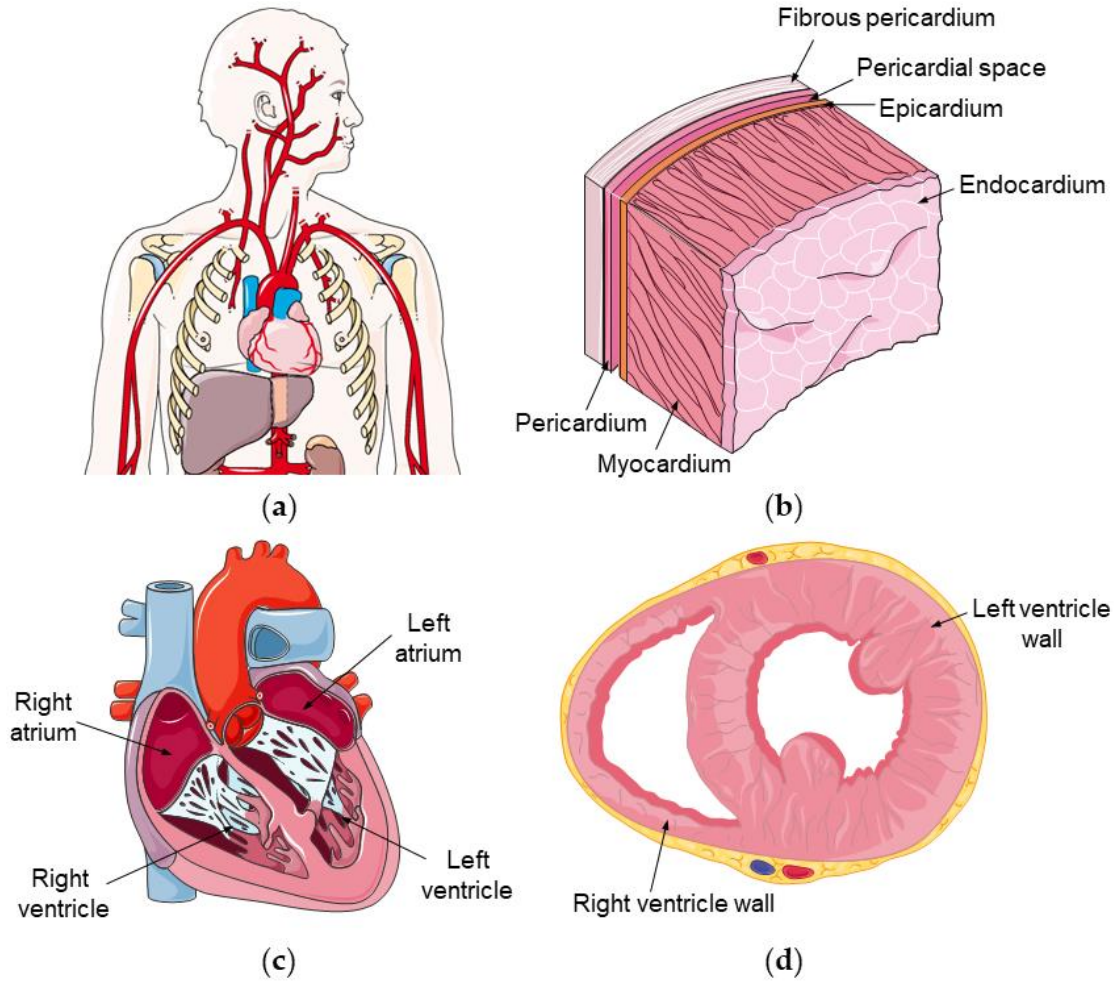

Figure 1.1. Heart anatomy. (**a**) Heart location inside the thoracic cavity, in the mediastinum. (**b**) Different layers composing the heart wall. (**c**) Heart chambers. (**d**) Inferior transversal view of the left and right ventricles [6].

1.1.2 Blood circulation

As atria and ventricles contract, they push blood from one chamber to the other and along the circulatory system to enable blood flow. The circulatory system can be divided into two main circulatory pathways: the pulmonary (Figure 1.2a) and the systemic circulation (Figure 1.2b). The right atrium receives deoxygenated blood from the superior and the inferior vena cava and the coronary sinus. Once it contracts, it pushes blood through the tricuspid valve into the right ventricle. Blood passes from the RV through the pulmonary valve into the pulmonary arteries, that carry blood to the lungs. In the lungs, gas exchange (carbon dioxide by oxygen) takes place in the alveoli and deoxygenated blood becomes oxygenated. Oxygenated blood returns to the heart (left atrium) via the pulmonary veins, closing the pulmonary circulation. In the left atrium, blood is passed into the LV through the bicuspid valve. From the LV, blood is pushed through the aortic valve into the aorta, initiating the systemic circulation. From the aorta, smaller arteries and arterioles will branch to finally reach all the organs, tissues, and cells in the body via the capillaries. Gas (oxygen by carbon dioxide), nutrients and waste are exchanged between the blood and the cells in the organism and systemic deoxygenated blood returns to the heart via the capillaries, the venules, the veins, and the inferior and superior vena cava into the right atrium, closing the systemic circulation and the circulatory system loop. Cells in the heart itself have its own network of blood vessels to receive oxygen and nutrients, called the coronary circulation (Figure 1.2c). The coronary arteries branch from the aorta and then divide into capillaries to feed the myocardium. After gas and nutrients exchange, deoxygenated blood returns to the right atrium through the coronary sinus.

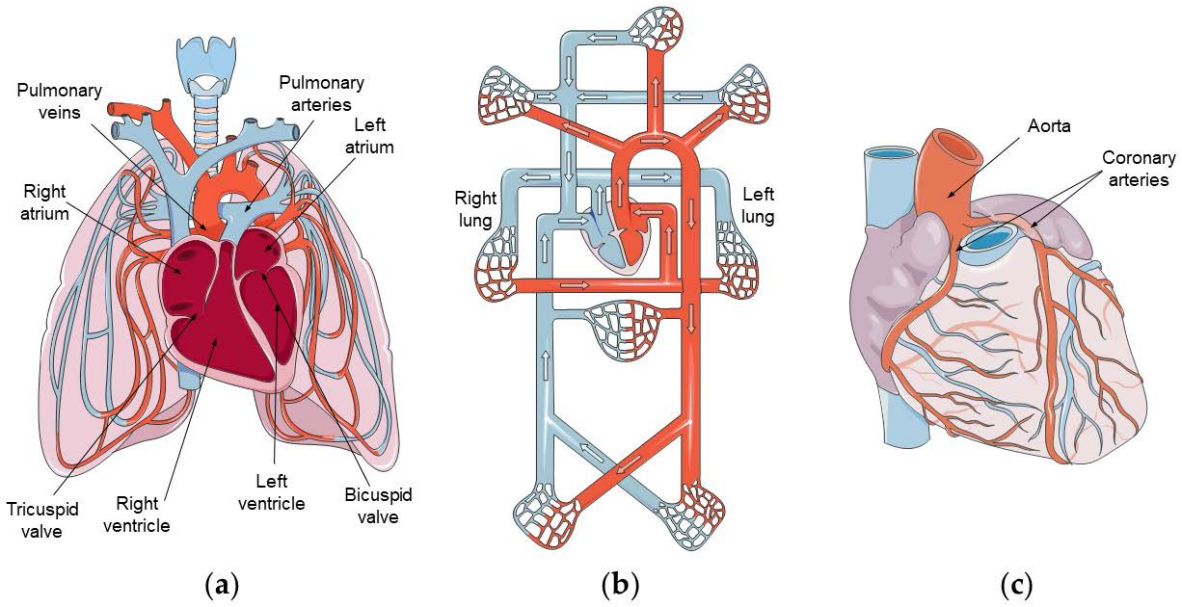

Figure 1.2. Blood circulation. (**a**) Pulmonary circulation (**b**) Systemic circulation (**c**) Coronary circulation [6].

1.1.3 Cardiac tissue

Cardiac tissue contraction is possible because it is mainly composed of cardiomyocytes (CMs, cardiac muscle cells). As muscle cells, CMs are electrically excitable (they can initiate action potentials) and the electrical activity leads to the mechanical response (contraction). CMs connect to each other electrically through proteins formed by connexins and called gap junctions. Gap junctions allow the flow of ions for action potentials to propagate from one CM to its neighbors to lead to coordinated contraction. CMs have a stable resting potential. Action potentials in neighboring cells bring the transmembrane potential of a CM to its threshold potential and voltage-gated fast Na^+ channels open, Na^+ enters the cell, and the depolarization phase initiates. Following the depolarization phase, there is a plateau phase. During this plateau phase, voltage-gated slow Ca^{2+} channels in the cell membrane open and Ca^{2+} enters the cell to maintain depolarization. This Ca^{2+} inflow causes more Ca^{2+} to leave the sarcoplasmic reticulum and to trigger contraction. Some voltage-gated K^+ channels are also open during the plateau phase, allowing K^+ to leave the cell and balance Ca^{2+} inflow to sustain depolarization. After the plateau phase, the repolarization phase restores the membrane potential with additional voltage-gated K^+ channels opening (more K^+ outflow) and Ca^{2+} channels closing. As intracellular Ca^{2+} concentration increases during the plateau phase, it triggers contraction by binding to troponin, which allows the actin and myosin filaments in the cardiac fiber to slide and to generate the required tension for contraction. The refractory period (time at which a second action potential cannot be triggered) of cardiac fibers is considerably longer than the contraction itself. This ensures a contraction is not initiated before full relaxation to ensure efficient pumping. The action potential of a ventricular CM and the different phases are illustrated in Figure 1.3a [7].

Although CMs constitute most of the cardiac mass (~70% in volume) and are responsible for heart contraction, they are only around 30% of the total cell number in the heart [8]. The proportion of other cell types in the heart still remains controversial, but the approximate remaining 70% of the cells are smaller-volume cells such as cardiac fibroblasts, smooth muscle cells, endothelial cells, pericytes, adipocytes, mesothelial cells, immune cells (myeloid and lymphoid) and neural [9]. All these cell types also play important roles in cardiac functioning, pathology, and repair. Cardiac fibroblasts produce and organize the extracellular matrix (ECM) supporting CMs with biophysical stimuli [9] and constitute around half of the heart cells [10]. Smooth muscle cells support the vascular system, endothelial cells form the endocardium, the blood vessels and the cardiac valves [8], and pericytes are the mural cells of the microcirculation [11]. Adipocytes surround the heart and the great vessels and should be less than 1% of the myocardial mass in healthy individuals [12]. Mesothelial cells mainly form the epicardium [13]. Immune cells interact with fibroblast and CMs to maintain cardiac homeostasis and normal organ function [14].

1.1.4 Conduction system

One of the main highlights of the heart is its inherent electrical activity resulting from a network of specialized cells. Whether these specialized autorhythmic cells are closer to CMs or neurons still remains under debate [15]. Regardless of their identity, these cells are able to spontaneously generate action potentials without the need of the nervous system. Therefore, they act as a pacemaker and ensure a coordinated and effective heart contraction. Heart activation starts periodically in the sinoatrial node (SA), located in the right atrial wall. SA node cells do not have a stable resting potential, so they depolarize to threshold and initiate action potentials spontaneously. From the SA node, the action potential propagates to CMs in the atrium through gap junctions. Then the impulse reaches the atrioventricular (AV) node, where the conduction velocity (CV) is considerably lower to allow for the atria to contract and fill in the ventricles before the impulse reaches the ventricles. The atria are electrically isolated from the ventricles except at the AV node. From the AV node, the impulse travels to the bundle of His, the right and left bundle branches and finally to the Purkinje fibers where the action potentials propagate to the rest of the ventricular myocardium and cause ventricular contraction. Action potential propagation through the conduction system and the myocardial tissue leads to electrical currents that can be recorded from the surface as an electrocardiogram (ECG). The conduction system of the heart is illustrated in Figure 1.3b

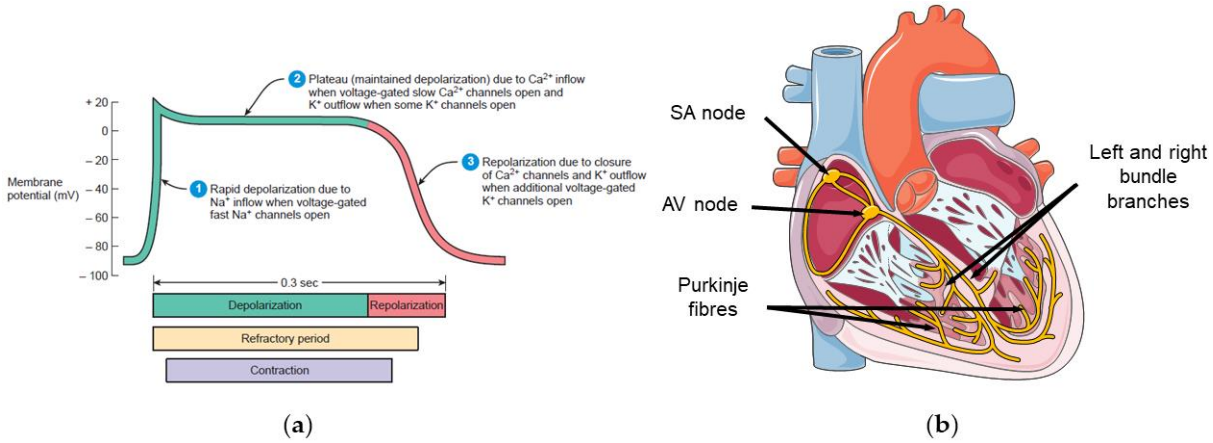

Figure 1.3. Ventricular action potential and conduction system of the heart. (**a**) Action potential in a ventricular contractile fiber and the different phases. Reproduced with permission [7]. Copyright © 2009, John Wiley & Sons, Inc. (**b**) Conduction system of the heart [6]. SA: sinoatrial. AV: atrioventricular.

1.1.5 The cardiac cycle and cardiac output

During the cardiac cycle, the atria and the ventricles contract and relax sequentially to force blood from places of higher pressure to areas of lower pressure. First, atrial depolarization

causes atrial systole: the atria contract and their pressure increases while the ventricles are relaxed. This process pushes blood through the tricuspid and bicuspid valves into the ventricles. As the atria empty, their pressure drops, and they start relaxing (atrial diastole). The end of the atrial systole coincides with the end of the ventricular diastole as ventricular depolarization triggers the initiation of ventricular systole. The ventricles contract and their pressure rise (isovolumetric contraction) until the aortic and pulmonary valves open and allow blood to be ejected from the ventricles. During ventricular repolarization, ventricles relax and enter diastole. The ventricular pressure drops and the pulmonary and aortic valves close, initiating the isovolumetric relaxation phase. Ventricular pressure drops until it is below atrial pressure and the cycle initiates again. The cardiac cycle, and the correspondence between the ECG signal, the pressure, the volumes and the phases of the cardiac cycle are shown in Figure 1.4 [7].

Important parameters regarding the cardiac cycle and assessing ventricular performance are:

- Heart rate (HR): Number of cardiac cycles (beats) in one minute.
- End-diastolic volume and pressure (EDV, EDP). Blood volume/pressure of a ventricle at the end of the relaxation period.
- End-systolic volume and pressure (ESV, ESP). Blood volume remaining/pressure at the end of ventricular systole.
- Stroke volume (SV): Blood volume ejected by a ventricle in each cardiac cycle. It is equal to the EDV minus the ESV.
- Cardiac output (CO): Blood volume ejected by a ventricle in each minute. It is the SV multiplied by the HR.
- Ejection fraction (EF): Percentage of blood leaving the ventricles in the cardiac cycle. It is the SV divided by the EDV and multiplied by 100.
- Cardiac reserve: Increase in CO related to an increase in the HR or the SV.
- Myocardial performance index (MPI): Assesses global cardiac dysfunction. It is the sum of the isovolumetric contraction time and the isovolumetric relaxation time divided by the ejection time.

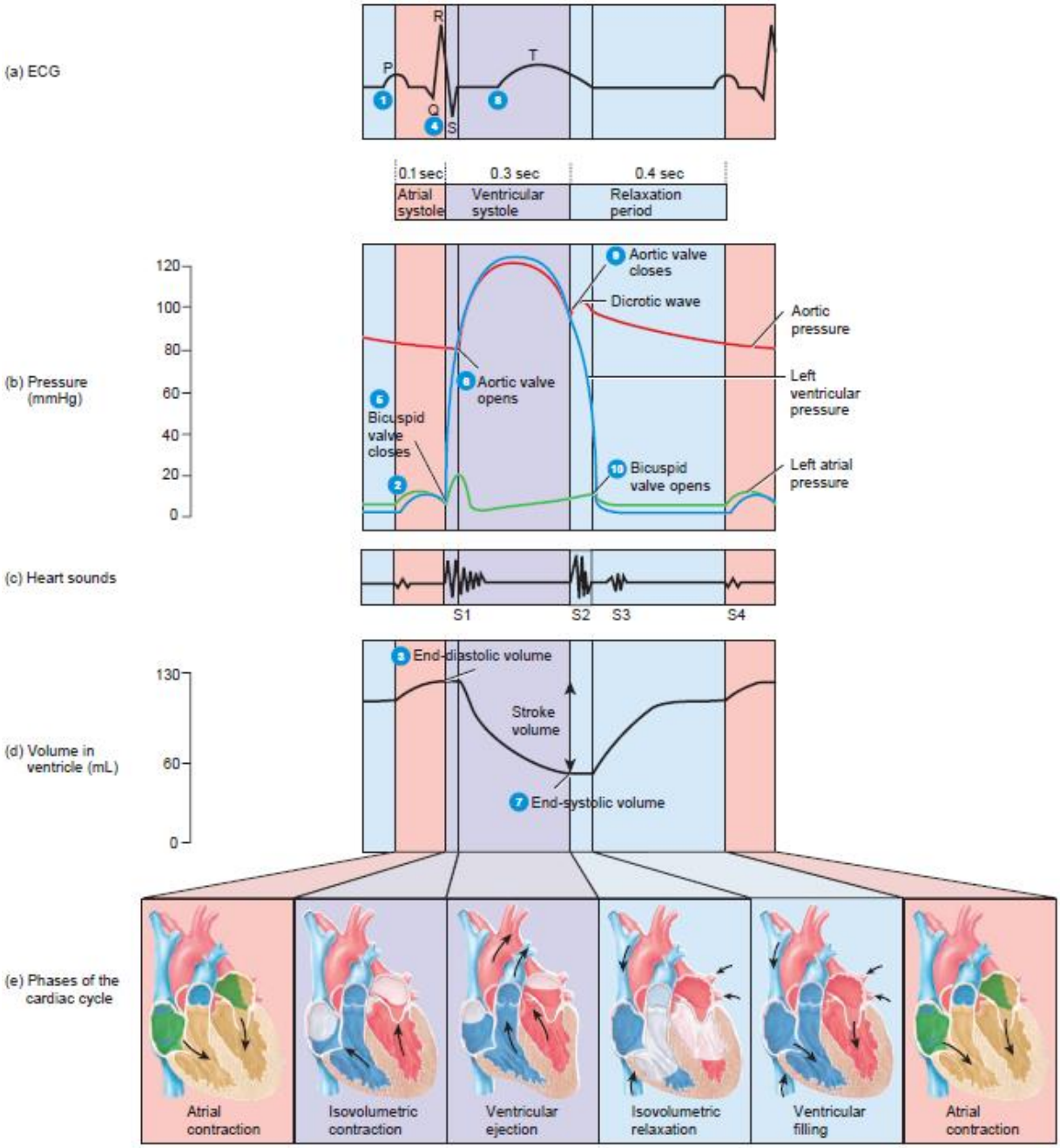

Figure 1.4. Cardiac cycle. (**a**) Electrocardiogram (ECG) (**b**) Changes in left atrial pressure (green line), left ventricular pressure (blue line) and aortic pressure (red line) as they relate to the opening and closing of heart valves. (**c**) Heart sounds (**d**) Changes in left ventricular volume. (**e**) Phases of the cardiac cycle. Reproduced with permission [7]. Copyright © 2009, John Wiley & Sons, Inc.

1.2 Cardiac aging and heart disease

Pathological alterations in cardiac tissue and functioning lead to CVDs, which are the leading cause of disease burden and mortality in the world. They are also a major cause of disability and health care costs [1]. The main risk factor for the development of cardiovascular diseases is increasing age [16]. Aging is a natural biological process in which the body's homeostatic adaptive response is progressively altered, increasing the susceptibility to environmental stress and disease. With the average lifespan of the human population continuously increasing, it is expected that the problem of cardiovascular diseases will only continue to grow in the following years [1]. In this section, we revise the pathophysiological functional, structural, cellular and molecular changes behind cardiac aging and age-associated heart diseases, available treatments, current needs, and new research directions.

1.2.1 Functional changes

The prevalence of heart-related pathologies, such as heart failure (HF), arrhythmia, microcirculatory dysfunction, valvular disease and inflammation increase considerably with age [16, 17]. At functional level, cardiac aging is mostly characterized by a decline in diastolic function. However, systolic function at rest (measured by the EF) is relatively preserved [16]. This has led to a designation of two types of HF, each representing around half of the patients [18]: with preserved EF (HFpEF), especially prevalent in aged women [19] and responsible of a high number of hospital admissions [20], and with reduced EF (HFrEF). Therefore, HFpEF characterizes by delayed relaxation, increased myocardial stiffness and decreased filling rate [21]. As ventricular filling shifts to later in diastole, atria commonly enlarge to compensate it and preserve the EF. Nevertheless, patients with atrial arrhythmias (such as atrial fibrillation, AF) have reduced atrial contraction and cannot compensate the diastolic dysfunction by increasing the late LV filling [22]. Despite EF at rest being generally preserved during aging, other indicators of cardiac function and indirect systolic performance are affected. For example, during exercise, maximum HR, cardiac reserve and EF do decrease [23]. With age, there is also a decrease of myocardial contractility and MPI increase, implying that a greater fraction of systole is devoted to overcoming the pressure changes during the isovolumetric phases. At electrical level, age relates to increased incidence of SA node, AV node, bundle of His and bundle branches dysfunction (which may manifests as palpitations, dizziness, syncope and confusion) [24], increasing the predisposition to arrhythmias, and in particular, AF.

1.2.2 Structural and cellular changes

Main structural changes responsible for altered functionality in aged hearts are increased hypertrophy and cardiac fibrosis. Despite some cellular types having the ability to divide and regenerate damage tissue (e.g. fibroblasts and endothelial cells), others, such as adult CMs, present limited dividing and regeneration capacity. In humans, CMs exhibit cell cycle arrest shortly after birth, and although they may retain their proliferative capacity, CM turnover is rare in the human heart (less than 1% of CMs per year [25]) and it even further decreases with age [10]. Decreases in proliferative capacity and in numbers of CMs and other cell types present in the heart mainly occur when they become senescent or apoptotic. Age- and pathology-induced alterations in homeostasis can lead to increased numbers of senescent and apoptotic cells, so to compensate for CM loss and maintain contractility and CO, remaining CMs increase in size becoming hypertrophic [26]. If CM size increases in length, the LV is able to accept more venous return, but the energy cost of ejection is higher, promoting more dilation in a vicious cycle and leading to HFrEF (systolic failure). Nevertheless, if CM size increases in thickness, LV wall becomes thicker and the size of the LV cavity decreases (and so the LVEDV), affecting LV diastolic function [27] (HFpEF). As already mentioned above, to compensate for this, atrial cavities tend to dilate. However, this makes them more susceptible to arrhythmias.

The ECM is a complex protein network providing structural and mechanical support and aligning the heart cells. The ECM composition includes several types of collagens (type I, II, III, IV, V and VI) as well as elastin, fibronectin, laminin and fibrinogen [28]. The proportion and amount of the different proteins in the ECM varies with age [29], and in excess deposition, it can increase myocardial stiffness and affect diastolic function [30]. Cardiac aging is associated with deregulation of ECM synthesis and degradation, and therefore, with increased collagen deposition and increased number of fibroblasts (primary sources of ECM proteins) [17]. Cardiac fibroblasts, opposite to CMs, lack electrical excitability and mechanical contractility but have considerable proliferative capability [31]. As a result, excess numbers of fibroblasts reduce the CV in the cardiac tissue and make it more susceptible to developing arrhythmias [31]. In response to CM injury, such as that derived after an ischemic episode of myocardial infarction (MI), large numbers of dead CMs are not replaced by newly formed CMs (which lack regenerative potential), but by fibrotic tissue [32]. Apart from the electrophysiological implications, large areas of fibrotic tissue lack contractility, considerably affecting the heart pumping efficiency.

1.2.3 Molecular mechanisms

Several factors and mechanisms can bring cardiac cells into the pathological phenotypes that lead to the structural and functional deficiencies. Lack of oxygen and nutrients supply, lack

of adequate waste removal, inflammation, and alterations in homeostasis can drive cells to senescence and apoptosis, to dysfunction, and ultimately, to death.

In senescence, cells are metabolically active but arrested in the cell cycle [33]. It is a natural cellular response that limits proliferation of aged or damaged cells to allow for normal development and maintaining of tissue homeostasis [34]. However, senescent cells accumulate with chronological aging and under some pathological situations. Senescence is associated to morphological changes, such as increased volume and flattening, to a loss of regenerative function, and to secretion of pro-inflammatory cytokines, interleukins, and growth factors (secretory phenotype associated with senescence, SASP). The main molecular pathways controlling the senescence state are p53/p21 and p16/pRB [35], and although there are other known regulators, those are not totally clarified in the cardiovascular system [36]. Senescence-associated with β-galactosidase (SA-β-gal) indicates lysosomal activity and is considered the gold standard for senescent cells. Still, markers of cell cycle arrest (p16, p21, p53), absence of proliferation markers (e.g. Ki-67), secretion of pro-inflammatory factors, and DNA damage response markers (e.g. γ-H2AX) are commonly used in combination to SA-β-gal to confirm senescence [37] (Figure 1.5). Some factors that lead to senescence are oxidative stress and inflammation, which provoke DNA damage, mitochondrial dysfunction, activation of oncogenes, telomere shortening and deficiencies in autophagy.

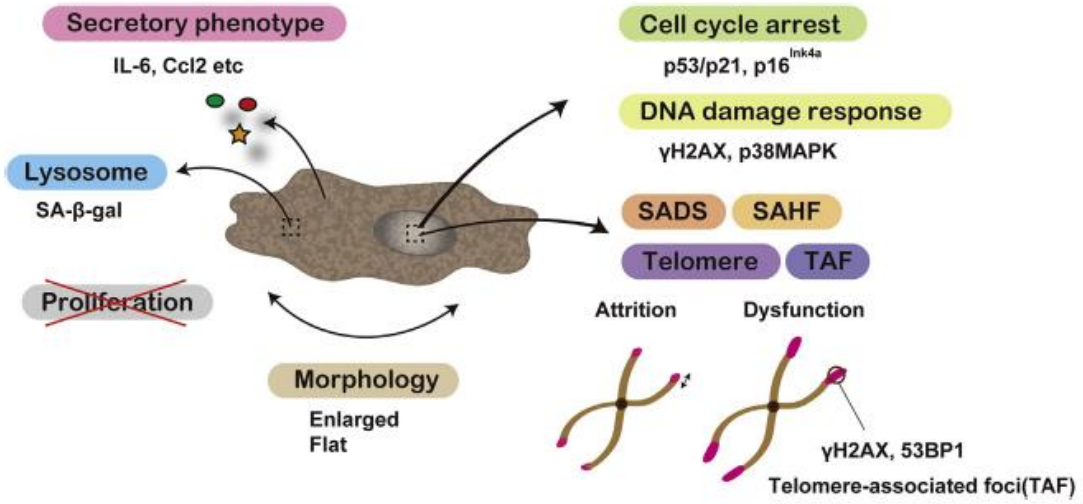

Figure 1.5. Markers of senescent cells. Indirect markers characterizing cellular senescence are as follows, and these vary among tissues and cells. (1) Enlarged and flat morphology, (2) cell cycle arrest (p53/p21, p16Ink4a signals become high), (3) DNA damage response (γ-H2AX, p38 MAPK signals become high), (4) irreversible termination of proliferation, (5) high senescence-associated beta-galactosidase (SA-β-gal) activity, (6) telomere attrition, (7) telomere dysfunction, (8) senescence-associated distention of satellites (SADs), and (9) senescence-associated heterochromatin foci (SAHF) [38].

The heart presents higher basal oxygen consumption than other organs and produces more reactive oxygen species (ROS) [39]. Disturbances in ROS are associated to increased cell apoptosis and inflammation [40] and to multiple cardiovascular diseases such as HF, hypertension, atherosclerosis, cardiac fibrosis and hypertrophy [41, 42]. Increased ROS stimulate the production of transforming growth factor-β (TGF-β) in fibroblasts [41]. TGF-β is a pro-fibrotic factor that increases the expression of ECM proteins and inhibits matrix degradation [43]. Elevation of TGF-β also promotes senescence and induces cardiac aging [44].

As CMs have little ability to proliferate during human lifetime, telomere shortening caused by the number of cell divisions does not seem the main mechanism by which CMs enter senescence in aged hearts (despite length-independent telomere injury can also activate senescence and lead to cardiac fibrosis and hypertrophy) [45]. CM senescence is mainly associated with dysfunctional organelles, misfolded proteins and cell death [46]. In particular, excessive mitochondrial ROS provoke damage in mitochondrial DNA and redox-sensitive mitochondrial proteins [47]. This causes mitochondrial dysfunction and more ROS are produced, leading to a "vicious cycle" that leads to necrosis, apoptosis, inflammation [48] and finally ends with cellular and organ dysfunction (such as HF [49] and AF [50]). Increasing evidence in animals also points towards specific miRNAs as regulators of aging and cardiovascular diseases [51]: miR-18a, miR19a and miR-19b (decreased in HF and ECM remodeling mediators [52]), miR-22 (regulator of cardiac fibroblast senescence [53]), miR-29 (related to cellular senescence and cardiac aging [44]), miR-34a (regulator of cardiac aging and function [54]), miR-125b (antifibrotic [55]), miR-133a (inhibitor of angiogenesis, inflammation, apoptosis and fibrosis [56]) and miR-378 (antifibrotic [57]).

Autophagy plays an important role in cellular homeostasis and serves to protect cells against stress by eliminating misfolded proteins and damaged organelles, including the mitochondria [58]. It also provides nutrients and energy through the degradation of the autophagic cargo [59]. Therefore, impaired autophagy associated with age can lead to accumulation of misfolded proteins and mitochondrial dysfunction that provoke cardiac hypertrophy, fibrosis, and dysfunction [45]. It is also a cell death mechanism, so in excess, it can also be pathological [59]. One of the pathways regulating autophagy and nutrient and growth signaling is the mammalian target of rapamycin (mTOR) [58]. Reduced mTOR signaling is associated to improved resistance against cardiac aging [45]. These main mechanisms and pathways behind cardiac aging are shown in Figure 1.6.

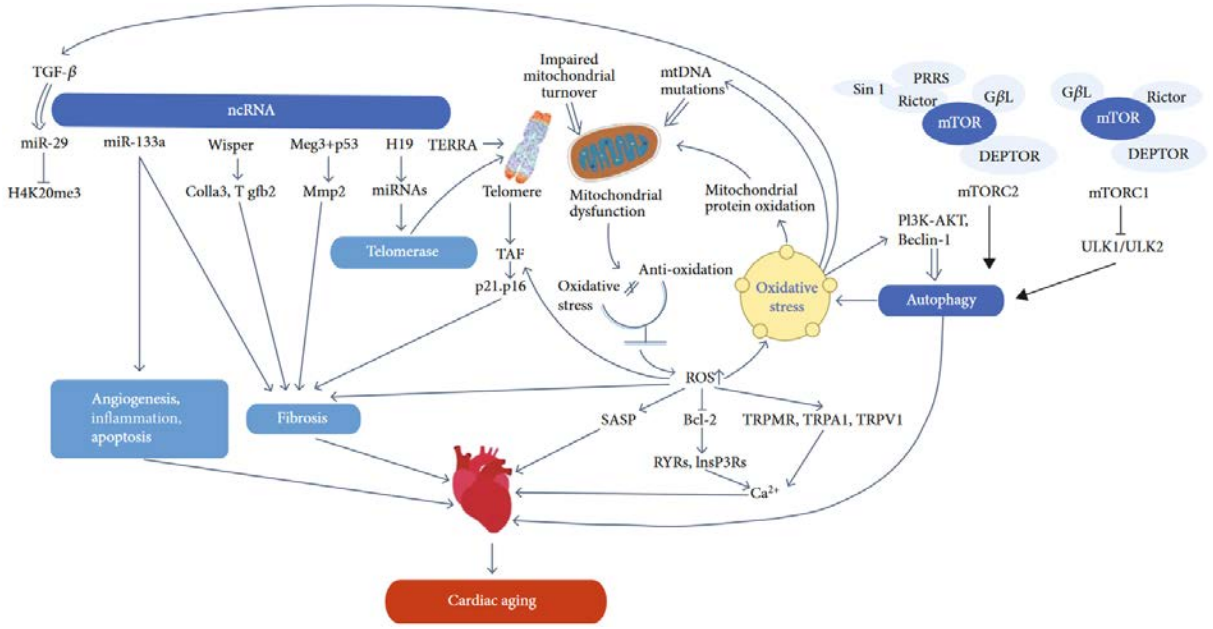

Figure 1.6. Key mechanisms of cardiac aging. Abnormal expression of ncRNAs can cause dysregulation of their downstream target genes, which cause telomere damage and cardiac aging. MtDNA mutations, mitochondrial protein oxidation, and impaired mitochondrial turnover can cause the loss of mitochondrial function and lead to inadequate ATP synthesis and increased ROS production. Increased ROS can lead to further mitochondrial dysfunction, forming a vicious cycle. Elevated ROS also lead to telomere dysfunction, DNA damage, and autophagy. Wisper indicates Wisp2 super-enhancer–associated RNA; Meg3: maternally expressed gene 3; TERRA: telomeric repeat-containing RNA; TAF: telomere-associated DNA damage foci; mtDNA: mitochondrial DNA; ROS: reactive oxygen species; and SASP: senescence-associated secretory phenotype [45].

Age-mitochondria dysfunction and increased ROS have other consequences in other organelles such as in the sarcoplasmic reticulum. Impaired sarcoplasmic reticulum activity can lead to prolonged relaxation of CMs, which has also been identified as one of the reasons behind diastolic dysfunction associated to aging [60, 61]. Alterations in CM relaxation can be caused by impaired Ca^{2+} cycling, by increased myofilaments stiffness, by reduced Ca^{2+} sensitivity or by alterations in actin or myosin [17, 60–62]. To compensate these effects, in aged hearts there may be an increase in the L-type Ca^{2+} current [63] and prolongation of the action potential duration to maintain Ca^{2+} transients and contraction [64]. Although the density of L-type Ca^{2+} channels does not seem to be affected by age [65], the density of L-type Ca^{2+} channels is reduced in atrial myocytes from patients with chronic AF [66].

Other related pathways in cardiac aging and pathology are growth and neurohormonal signaling. Insulin growth factor 1 (IGF-1) is a characterized pathway related to lifespan regulation, and is associated to mitochondrial and cardiovascular protection [67–69] and to

reduced cardiac fibrosis [70]. In humans, age-related low serum IGF-1 levels [71] correlate to an increased risk of HF [72]. IGF-1 interacts with the renin angiotensin aldosterone system (RAAS) to inhibit or activate inflammation and oxidative stress, nevertheless, this mechanism is impaired with aging [73]. RAAS is the part of the endocrine system controlling hypertension and stress-induced cardiac hypertrophy [45]. Upregulation of the RAAS is related to increased cardiac hypertrophy, fibrosis, impaired CM relaxation [74], increased ROS [75] and increased arrhythmogenicity [76]. β-adrenergic receptors are also part of neurohormonal signaling in heart function. They regulate HR, myocardial contractility, blood pressure, wall stress and metabolic demand [17, 22], however, their excessive stimulation to maintain CO at early stages of cardiac disease is related to increased ROS and heart damage [75]. This leads to a reduction of β-adrenergic receptor density observed with age (desensitization), which gives rise to further pathological changes and remodeling [77], such as hypertrophy, systolic dysfunction, apoptosis and fibrosis [78].

The relationship between the molecular changes described, the cellular phenotypic changes, the structural alterations, the functional consequences and the impact on the patients suffering from cardiac aging-derived heart disease are summarized in Figure 1.7.

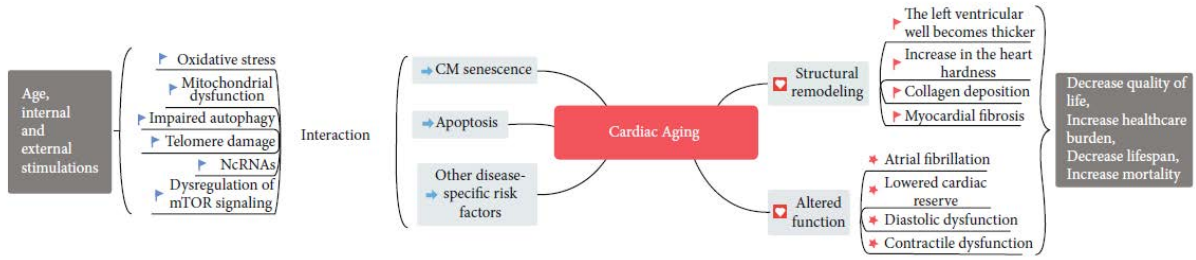

Figure 1.7. The concept of cardiac aging and its biological mechanism. Cardiac aging is a pathophysiological process affected by many factors triggered under various intrinsic and external stimuli with age. Many factors can affect key cellular processes and pathways during cardiac aging, such as oxidative stress, mitochondrial dysfunction, impaired autophagy, telomere damage, ncRNAs, and dysregulation of mTOR signaling. These factors can also influence each other and lead to cardiomyocyte senescence, apoptosis, and other cell damages. Cardiac aging causes changes in heart structure and function, such as progressive myocardial remodeling, decreases in systolic and diastolic function. CM indicates cardiomyocytes [45].

1.2.4 Treatment, challenges, and new directions

Although large progresses have been made in the last years in elucidating molecular mechanisms behind cardiac aging and cardiac pathology, many unknowns and obstacles still

remain [79]. In this section, we review the potential and the limitations of possible treatment strategies targeting the known mechanisms behind cardiac aging.

In the current clinical scenario, cardiac aging itself is not treated until there are symptoms or altered cardiac function. As earlier discussed, these are commonly manifested in the form of HF and AF. HFpEF treatment, despite its high prevalence and known impact in the quality of life and patient prognosis, remains largely as an unsolved clinical need. In these patients, the European Society (ESC) clinical guidelines from 2021 only advise the screening and treatment of other cardiovascular and non-cardiovascular comorbidities (hypertension, diabetes, cholesterol levels…) and the use of diuretics to alleviate the symptoms [80]. In patients with HFrEF, pharmacological treatments are advised before considering device therapy to try to reduce mortality, prevent recurrent hospitalizations and improve clinical status, functional capacity and quality of life [80]. Most of these drugs act by targeting neurohormonal signaling at different levels (RAAS and β-adrenergic receptors). These drugs include angiotensin-converting enzyme inhibitors (ACE-I), angiotensin receptor-neprilysin inhibitor (ARNI), angiotensin-receptor blockers (ARB), mineralocorticoid receptor antagonists (MRA, that bind to aldosterone and other steroid hormones) and β-blockers (β-adrenergic receptors blockers), either used alone or in combination. Novel therapies being introduced in the clinical guidelines include sodium-glucose cotransporter-2-inhibitors (SGLT2i), that inhibit glucose reabsorption at the kidneys to reduce blood glucose levels [81], soluble guanylate cyclase stimulators [82] and cardiac myosin activators [83]. For the treatment of AF, β-blockers and specific ion channels/pump blockers are used with the purpose of controlling the rate and lengthening the action potential [84]. However, current pharmacological treatments for HF and AF present severe clinical efficacy and safety problems [2, 3] and are not regarded as definitive cures [4]. This makes it necessary to develop new treatment strategies that target other involved molecular pathways and that aim to promote cardiac cell survival and protection, cardiomyogenesis, cell to cell communication, angiogenesis, and vascularization, and to reduce inflammation.

For the development of more successful treatments, CM survival and protection are critical to preserve electrical and contractile ability of the cardiac tissue, especially because of CM low proliferative capacity after injury. Mechanisms to promote cardiac cell survival include reducing senescence and apoptosis, preventing mitochondrial dysfunction and maintaining autophagy. Senolytics are genetic or pharmacological compounds that target the elimination of senescent cells by inducing them to apoptosis. They have shown potential to reverse cardiac age-related dysfunction and could become a new generation therapy for cardiac disorders [85–90]. Nevertheless, the use of senolytics leads to depletion in the number of CMs, and whether this allows to preserve myocardial function in the long term still remains unknown. While excess senescence is pathological, senescence also plays a role in coordinating inflammation, fibrosis and

remodeling. Therefore, other pitfalls of using senolytics include enhanced fibrosis, difficult translation of the preclinical studies into the clinical scenario, and potential adverse effects [91].

Interventions targeting mitochondrial dysfunction are also gaining interest and could have large potential. For example, Szeto-Schiller (SS) compounds can reduce mitochondrial ROS in CMs and improve diastolic function in aged mice [17, 92, 93]. Mitochondria-targeting therapies are still in its infancy and require many more preliminary studies before moving to clinical testing [94]. Caloric restriction (CR), which refers to reducing caloric intake but without malnutrition, has also shown multiple benefits related to cardiac aging [95], such as attenuation of cardiac hypertrophy and fibrosis [96]. Its main mechanisms of action (MoA) are reduction of mitochondrial ROS production [97, 98] and reduction in autophagy by the inhibition of the mTOR signaling [45, 99]. However, its use in humans would be challenging and developing CR mimetics that target similar cellular and metabolic responses is of great interest [17]. In this line, rapamycin is a well-established inhibitor of the mTOR signaling pathway, enhancing autophagy, regulating oxidative stress, inflammation and organelle function and promoting CM survival [45]. Rapamycin treatment can inhibit senescence, reverse age-related diastolic dysfunction [100–102] and cardiac hypertrophy [103]. Despite rapamycin being a drug approved by the United States Food and Drug Administration (FDA) and the European Medicines Agency (EMA) due to its immunosuppressive effects for some non-cardiac pathologies, its use for the treatment of heart diseases presents important limitations, such as a high frequency of administration and side effects, including anemia and nephrotoxicity [104]. In addition, whether it has the potential to treat cardiac pathology in humans still needs to be determined [45, 105].

The use of growth factors and miRNAs has also been explored to prevent cardiac damage associated to age. Growth hormone therapy increases IGF-1 signaling and may have benefits for the treatment of HF [67, 68] and cardiac aging [69] by protecting mitochondria from ROS [106]. Growth differentiation factor 11 (GDF11), a member of the TGF-β superfamily has been attributed rejuvenating potential and has reported beneficial effects for controlling age-related hypertrophy in animals [107], but in excess concentration, it can have deleterious effects at cardiac and systemic levels [108, 109]. Therefore, despite promising, more knowledge needs to be gained before moving this potential therapy into the clinical scenario [107]. As recent studies are also highlighting the role of miRNAs in regulating cardiac aging, gene therapy is being explored as a potential treatment [54]. However, miRNAs are likely to have multiple targets, resulting in a high risk of undesirable effects that need to be adequately studied [17].

The above-mentioned treatments, although they show potential for the treatment of cardiac aging related pathologies, are still under investigation, not used in the clinical scenario, and in principle do not cover all the molecular mechanisms associated with cardiac aging, such as adverse extracellular matrix remodeling and impaired calcium homeostasis (Figure 1.8). Thus,

future work is required to better understand the mechanisms, their effects on animals of both genders, and their therapeutic potential in humans. For the treatment of cardiac aging, it is important to bear in mind that short-term treatments applied later in life when the symptoms are initiated will be more translational than long-term or life-long treatments. This becomes particularly important if they are delivered systemically, to minimize irreversible side effects [17].

In this context of limited therapeutic efficacy and a high clinical need, the use of advanced therapies, including stem cell therapy, has emerged as a potential breakthrough [5]. Contrary to current available treatments, biological products could have the potential to treat cardiac aging-associated pathologies from a more fundamental level [110], as they are able to interact beneficially with some of the pathophysiological pathways involved and to induce changes at molecular, cellular and structural level that can translate into enhanced functionality. For example, they can improve cell survival and protection, cell-cell communication, angiogenesis, cardiomyogenesis, reduce inflammation and molecularly regulate proliferation and cell cycle [79]. However, despite the promising potential of biological therapies, many problems and unknowns remain that need to be solved before they can reach the clinical scenario.

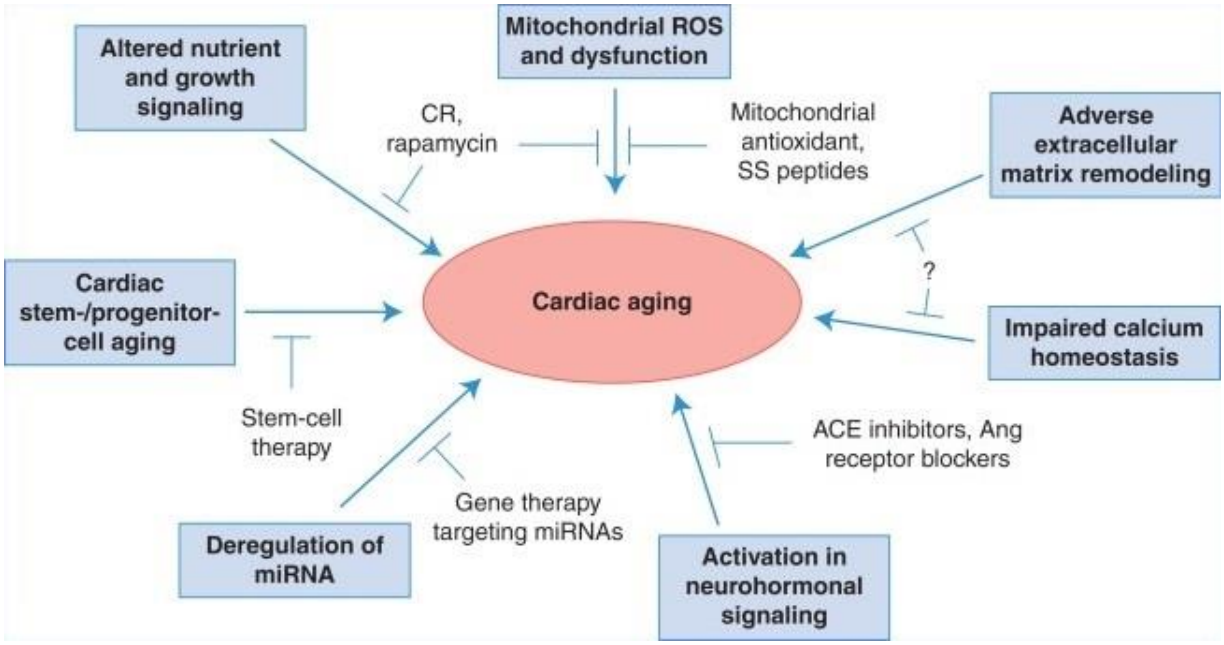

Figure 1.8. A schematic summary of the molecular mechanisms of cardiac aging and potential cardiac aging interventions. ROS, Reactive oxygen species; CR, caloric restriction; SS, Szeto–Schiller; miRNA, microRNA; ACE, angiotensin-converting enzyme; Ang, angiotensin. Reproduced with permission [17]**.** Copyright © 2015, Cold Spring Harbor Laboratory Press.

1.3 Advanced reparative and regenerative therapies in the cardiovascular field

Advanced therapy medicinal products (ATMPs), according to the EMA, are medicines for human use based on genes, tissues or cells [111]. In general, they are considered innovative therapies that target diseases with high unmet clinical needs [112]. Since the first ATMPs were authorized in 2009 by the EMA and in 2010 by the US FDA [113], many products have followed. In the cardiovascular field, the discovery of stem cell niches in the heart drove significant attention towards ATMPs due to the limited regenerative capacity of the human heart and the large clinical need [114]. Despite the results of the preclinical studies using cell therapy for cardiac repair and regeneration seemed very promising, rapid implementation into clinical trials led only to modest outcomes [79]. This made the scientific community to re-think and re-define the field of cell therapy in cardiac applications, stablishing which were the main limitations and the priorities that needed to be solved before further moving them into the cardiac clinical scenario [115]. In this section, we revise stem cells and their use for the treatment in cardiac pathologies both at preclinical and clinical level, with a focus on cardiosphere-derived cells (CDCs). Then, we review knowledge about their MoA and how using cell-derived products, and in particular extracellular vesicles (EVs), may overcome some of the stem cell limitations. We also discuss the use of biomaterials, focusing on hydrogels, as ATMPs used alone or in combination with stem cells or their derived products. Finally, we highlight current limitations and possible solutions for enhancing translation of cardiac regenerative and reparative ATMPs into the clinical scenario.

1.3.1 Stem cells

Stem cells are defined as immature and unspecialized cells capable of differentiating into different and multiple types of specialized cells [116]. From the human heart, cells with different molecular and functional properties have been isolated, some called stem or progenitor cells (CPCs) as they have the ability to self-renew in culture and differentiate into different lineages [115, 117]. *In vivo*, these cells are involved in maintaining homeostasis and heart repair [118]. Despite these cells being capable of differentiating mostly into endothelial and mesenchymal cells (MSCs), they present limited ability to differentiate into functional and mature CMs, and if so, only under exceptional circumstances [119]. Apart from that, the only stem cells capable of generating CMs under the culture of specific factors are pluripotent stem cells (PSCs), that can be of embryonic origin (ESCs) or induced by reprogramming differentiated adult cells (iPSCs) [115]. Other cell types explored in preclinical and clinical trials in the cardiovascular field include stem cells of non-cardiac origin, such as bone marrow (BM) mononuclear cells (BM-MNCs), bone

marrow MSCs (isolated from BM-MNCs and denoted BM-MSCs) or MSCs cultured from a variety of tissue sources (such as adipogenic tissue, AT-MSCs) [120, 121].

First approaches used stem cells of non-cardiac origin, such as BM-MNCs and MSCs. BM-MNCs are a heterogeneous population of myeloid and lymphoid cells, endothelial progenitors, hematopoietic stem cells and small fractions of MSCs [122]. These are easy to obtain (from BM aspirates) and do not require culture or expansion [123]. However, in clinical trials, they only showed limited regenerative potential and minimal improved cardiac function [115], if any [122]. MSCs are defined as plastic-adherent cells in serum-containing medium expressing the following surface markers: CD105, CD73 and CD90 and able to differentiate into chondrocytes, osteoblasts, adipocytes and fibroblasts [124]. MSC differentiation into other cell types, such as CMs has been described but remains controversial [122], as well as whether if MSCs are formed by heterogeneous cell populations [115]. They should also lack the expression of hematopoietic markers (CD45, CD34, CD14/CD11b, CD79α and HLA-DR) and can be isolated from different tissues [124]. Their main advantages are easy isolation and expansion together with numerous bioactive properties [122], but therapeutically they present limited regenerative potential and minimal improved cardiac function [115].

The use of ESC or iPSCs seemed promising because of their ability to differentiate into CMs under specific stimulus. Nevertheless, their use includes several problems such as genomic instability, potential risk of teratomas [125] and potential graft rejection requiring immunosuppression in the case of ESCs [126, 127]. In addition, ESC and iPSCs derived CMs (ESC-CM and iPSC-CMs) are largely immature in terms of structure and function, differing considerably from adult CMs [128] what can trigger life-threatening arrhythmias *in vivo* [125, 126, 129, 130]. Moreover, to serve these purpose of heart re-muscularization, ESC and iPSCs need high engraftment rates after transplantation, but evidence shows that they disappear rapidly after transplantation in the heart [131].

CPCs are purified cell populations of cardiac origin with greater potential for cardiac repair after being selected and/or modified *in vitro* to enhance their reparative properties (e.g. engraftment, survival, plasticity and paracrine activity) [115]. Although their isolation from cardiac biopsies is more invasive, they can be cultured *in vitro* to yield adequate numbers for transplantation [120]. Among CPCs, different subpopulations have been isolated and explored in both preclinical and clinical trials: CDCs, c-kit+ (or CD117+) cells, and Sca-1+ cells. These cells, and in particular CDCs, have shown superior regenerative potential and improved cardiac function vs. BM-MNCs and MSCs *in vivo* [132]. However, comparison between MSCs and CPCs, and between the different types of CPCs has not been done in clinical studies [115].

Cardiospheres are self-organized three-dimensional (3D) structures obtained after established 3D culturing system from cardiac explant-derived cells (EDCs) [133]. Cardiospheres are a complex, niche-like environment that favors proliferation and stemness of CPCs. CDCs, obtained after further culture of cardiospheres, are multipotent and clonogenic [134]. They express CD105 and are negative for the expression of hematopoietic markers (CD45) [133]. Inside the CDC population, there are a variable proportion of cells expressing other surface markers: CD117 (c-kit), CD90 (Thy-1) and CD31 [133]. Therefore, they include different subpopulations such as c-kit+ cells, endothelial cells, and MSCs. *In vivo*, CDCs stimulate angiogenesis and left ventricular functional improvement [132, 135] by increasing microvessel formation, by activating endogenous cardiomyogenesis [136], by attenuating CM apoptosis and hypertrophy and by reducing collagen deposition and enhancing collagen degradation [137, 138]. They also present immunomodulatory effects [137, 139], ability to elongate telomere length and to reduce cell senescence [140]. *In vitro* and *in vivo*, the use of CDCs has shown superior efficacy compared to c-kit+ and CD90+ populations alone [132, 138]. In clinical trials, the use of CDCs has been proven to be safe and to have some beneficial effects. However, improvements in cardiac function and scar size reduction have been moderate and variable, with some clinical trials failing to meet their primary endpoint. Main clinical trials using CDCs for the treatment of cardiac and non-cardiac pathologies are summarized in Table 1.1.

Clinical Trial	Treated pathology	Administration Route	CDCs origin	Patients included	Benefits	No observed changes
CADUCEUS *Phase I* *2014* [141, 142]	MI	Intracoronary	Autologous	31	↓ Scar size ↑ Viable myocardium ↑ Segmental myocardial function	↔ LVEF ↔ LVEDV ↔ LVESV ↔ NYHA class ↔ Functional capacity ↔ QoL
ALLSTAR *Phase I/II* *2021* [143–145]	MI	Intracoronary	Allogenic	142	↓ LVEDV ↓ LVESV ↓ NT-proBNP ↑ Segmental myocardial function	↔ LVEF ↔ Scar size
HOPE *Phase I/II* *2019* [146]	DMD	Intracoronary	Allogenic	25	↓ Scar size ↑ Inferior wall systolic thickening ↑ Upper limb performance	↔ LVEF ↔ LVEDV ↔ LVESV
HOPE-2 *Phase II* *2020* [147, 148]	DMD	Multi-doses, Intravenous	Allogenic	20, planned 80 *	↑ LVEF ↓ LVEDV ↓ LVESV ↓ CK-MB isozyme ↑ Upper limb performance	
DYNAMIC *Phase I* *2020* [149]	HFrEF / Dilated cardiomyopathy	Intracoronary	Allogenic	14	↑ LVEF ↓ LVESV ↑ NYHA class ↑ QoL	

TICAP Phase I 2015 [150, 151]	HLHS	Intracoronary	Autologous	18	↑ RVEF ↓ RVESVI ↑ Weight-for-age z score ↓ NYUPHFI ↓ Incidence of coil occlusion for collaterals ↓ BNP ↓ Unplanned catheter interventions	↔ RVESVI
PERSEUS Phase II 2017 [152]	Single ventricle physiology	Intracoronary	Autologous	41	↑ VEF ↓ VESV ↓ VEDV ↑ Weight-for-age z score ↓ NYUPHFI ↑ IGF-1 ↑ HGF ↑ QoL ↓ Cardiac fibrosis ↓ BNP	
Regress-HFpEF Phase I [153]	HFpEF	Intracoronary	Allogenic	Planned 40 #		
ALPHA Phase I 2018 [154, 155]	Pulmonary hypertension	Infusion in RV outflow tract	Allogenic	6 Planned 26 #		
CAP-1002 in Severe COVID-19 Disease 2020 Compassionate-use [156, 157]	COVID-19	Intravenous	Allogenic	6	Safety only	

Table 1.1. Clinical trials using CDCs. MI: Myocardial infarction. BNP: Brain natriuretic peptide. DMD: Duchenne muscular dystrophy. HFrEF: Heart failure with reduced ejection fraction. HLHS: Hypoplastic left heart syndrome. HFpEF: Heart failure with preserved ejection fraction. NYHA: New York Heart Association Classification for heart failure. QoL: Quality of life. NYUPHFI: New York University Pediatric Heart Failure Index. * Preliminary results only. # Still recruiting.

1.3.2 Stem cell-derived products: extracellular vesicles (EVs)

In the early stages of cell-therapy development for cardiac applications, the hypothesis was that stem cells exerted their beneficial effects by engrafting into the cardiac tissue, differentiating into CM, and therefore regenerating/remuscularizing heart muscle. However, later evidence showed that this could not be the main mechanism: (i) transplanted cells engrafted poorly after administration and practically disappeared after a certain amount of time, but the effects persisted [138, 158–162], and (ii) implanted cells, regardless of the type, very barely

differentiate into CMs *in vivo* [122, 163–165]. This shifted the paradigm to exploring whether if transplanted cells exerted their MoA though paracrine secretion that activated endogenous cardiac repair [120]. It is now well accepted that stem cells secrete signaling molecules (cytokines, growth factors, vesicles, exosomes…) that are capable of recruiting and activating endogenous CPCs, inducing vessel formation, reducing fibrosis, modulating inflammation, inhibiting apoptosis and promoting CM proliferation [166–168].

Most of the paracrine action of stem cells is exerted by biomolecules enclosed in EVs [169]. Several studies have shown that EVs secreted by different types of stem cells are able to recapitulate the beneficial effects of their parenteral cells in cardiac applications [138, 170–175]. EVs from BM-MSCs, ESCs, CPCs and CDCs have shown efficacy after intramyocardial injection in MI models [172, 176–181] and after intravenous administration in myocardial ischemia, dilated cardiomyopathy and muscular dystrophy [182–189]. EVs are nanosized particles secreted by cells (not necessarily stem cells) and formed by a lipid bilayer transporting inside proteins, noncoding nucleic acids (including miRNAs), and lipids rafts intended to be delivered to other cells as a mechanism of cell to cell communication [190]. The term EVs includes two main subcategories of particle classification: exosomes and microvesicles [191]. EVs regulate diverse functions such as maintaining cardiovascular homeostasis, structure, and function, and may have neutral, beneficial or deleterious effects in target cells. However, under pathological situations, their content and number can vary. Thus, they hold prevention, diagnostic and therapeutic potential to treat cardiovascular diseases [190].

CDC-derived EVs (CDC-EVs) present many cardiac beneficial effects for their potential use as treatments and have shown superior efficacy for cardiac applications compared to EVs from other non-cardiac cells [192–194]. *In vitro*, CDC-EVs inhibit apoptosis, promote proliferation of CMs and enhance angiogenesis [180, 195, 196]. These results have translated into animal models, where CDC-EVs attenuated scar size, necrotic myocardium and adverse remodeling while improving cardiac function and inducing neovascularization [176, 180, 181]. However, despite knowledge about their MoA being continuously increasing, there is still no clear understanding of the mechanisms and signaling pathways by which stem cell EVs exert their promotion of cell survival and proliferation, angiogenesis, differentiation of endogenous stem cells, extracellular matrix homeostasis and by which they reduce inflammation and fibrosis [197]. Pinpointing specific components inside the EVs that recapitulate all their beneficial effect is highly desirable in terms of treatment simplification, standardization, and optimization. Nevertheless, it may be a hard task because it is likely that several bioactive molecules inside the EVs target multiple signaling pathways synergistically [198]. When looking at specific CDC-EV cargo, several proteins, miRNAs and RNA fragments have been identified as particularly abundant and relevant (although not exclusive) for exerting efficacy [180, 192, 198, 199].

The use of EVs versus their parenteral cells offers many advantages. In the first place, they are more stable [200] (even after repeated freeze-thaw cycles [201]) and are immune tolerant [181]. In the second place, contrary to cells, high doses of EVs do not face the problem of microvascular plugging and partial loss of the injected dose due to reduced transplanted viability [110]. From the regulatory point of view, EVs may be regulated as biological medications rather than ATMPs, as the manufacturing process is more similar to a drug than to cells and they are easier to standardize [202]. Still, clinical use of EVs and their commercial development is in early stages [110]. In 2021 there were only 22 clinical trials testing the beneficial effects of EVs, and none were in the cardiac field [202]. There is now one planned clinical trial with EVs from iPSC-derived CPCs [203]. Main advantages of cellular and acellular products (which include EVs) are summarized in Figure 1.9.

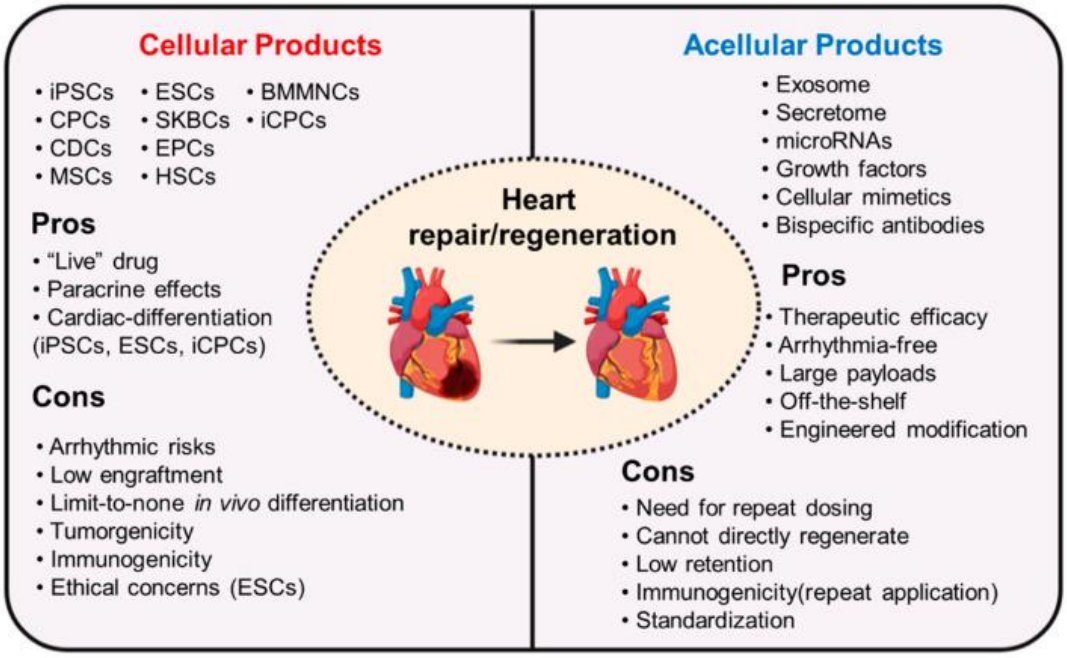

Figure 1.9. Advantages and disadvantages in cellular and acellular therapy [197]. iPSCs: induced Pluripotent Stem Cells. CPCs: cardiac progenitor cells. CDCs: cardiosphere-derived cells. MSCs: mesenchymal stem cells. ESCs: embryonic stem cells. SKBCs: skeletal blast cells. EPCs: endothelial progenitor cells. HSCs: hematopoietic stem cells. BMMNCs: bone marrow-derived mononuclear cells. iCPCs: induced cardiac progenitor cells.

1.3.3 Hydrogels

Hydrogels are a form of biomaterials consisting in cross-linked polymeric networks with high water content that form soft, 3D structures that mimic the structure of natural tissues [204]. When used alone, they have the potential to improve function of the damaged myocardium by providing structural and chemical support and inducing endogenous repair [205]. Hydrogels are

mainly classified in two types: natural and synthetic hydrogels. Natural hydrogels explored with cardiac applications include collagen [206], decellularized ECM (dECM) [205], silk fibroin [207, 208], chitosan [209, 210], cellulose [211], alginate [212, 213], gelatin [214] and hyaluronic acid hydrogels [215]. Their main advantages are that they are highly biocompatible [216] and are *in vivo* degraded by cellular enzymes (or ion exchange in the case of alginate). This makes them very safe, but their degradation is hard to control and they offer batch-to-batch variations. In addition, their mechanical and electrical properties are different from that of the myocardial tissue [204] and they present long gelation times [217]. In contrast, synthetic hydrogels such as polyvinyl alcohol (PVA) [218], polyacrylamide, poly(N-isopropylacrylamide) (PNIPAm) [219], polyethylene glycol (PEG) [220] and poly(3,4-ethylenedioxythiophen) polysterene sulfonate (PEDOT:PSS) [221] are highly controllable and customizable, but are less biocompatible and not degraded *in vivo* unless modified. The field is moving towards developing combined hydrogels that include natural and synthetic materials to obtain desirable mechanical and biochemical properties while maintaining biocompatibility and biodegradability [217].

Hydrogels can be used as a standalone therapy to provide mechanical and chemical support, as drug-delivery vehicles, and to construct artificial tissue in the form of patches. While the use of patches requires surgery for implementation in cardiac applications, the use of injectable hydrogels offers the possibility of minimally invasive delivery through a catheter [222]. In this case, a partially cross-linked hydrogel is injected and when reaching the cardiac tissue it self-assembles in-situ performing the solution to gel transition to retain this structure [204]. Ideal injectable hydrogels exhibit shear thinning behavior, gel fast after injection and once gelled have physicochemical properties similar to that of cardiac tissue while being biodegradable [217, 223]. These are essential properties to properly integrate with the host tissue, offer mechanical support, decrease wall stress and inhibit pathological remodeling [224]. Three different hydrogels have been tested in clinical trials with cardiac applications: fibrin [225], alginate [226] and dECM hydrogels [227] for the treatment of MI, being the last two injectable. Despite alginate showing improved benefits, in some studies fatalities occurred in the hydrogel injection group and not in the control group [228], and in the end it only yielded mixed functional results [223, 229, 230].

Solid dECM are scaffolds that undergo a process of chemical, enzymatic and/or mechanical treatment to lyse or remove the cells while preserving the native structure and vasculature in their specific tissue location [205]. Because of this, they are good candidates for cardiac repair [121, 231]. dECM can be directly used in solid form, however, its implantation is more invasive and it poses more challenges as a drug-delivery material [205]. Solid dECM can be lyophilized, milled and solubilized through enzymatical digestion into a liquid solution that gels at physiological temperature [232]. This soluble dECM is more versatile than solid dECM, as it maintains the ECM composition but lacks the solid and structural constrains of solid dECM.

Hydrogels formed from soluble dECM have reported to reduce cardiac fibrosis and hypertrophy, increase angiogenesis, reduce CM apoptosis and recruit CPCs [233]. In a large model of MI, they attenuated cardiac remodeling, increased the EF, improved ventricular volumes and global wall motion index [234, 235]. These translated into one clinical trial were they also showed ability to reduce cardiac remodeling [227]. One of the main advantages of dECM hydrogels is that gelation is triggered by thermal stimuli. This makes them less harmful to cells, and external triggers such as UV radiation that may generate oxidative damage are not required [217]. However, their soft mechanical properties and relatively long gelation times are considered insufficiently robust to provide sustained mechanical support to the heart [205, 217].

Apart from their use as standalone therapies, hydrogels offer many perspectives as drug-delivery systems. Due to their high fluid content and their ability to exchange it with the surrounding medium, hydrogels can be used to administer cells, EVs and other drugs improving their retention at the target site and prolonging their survival and/or release [223]. Recent preclinical studies have shown that cell therapy can have a positive effect on cardiac function and that this effect was enhanced when administered in hydrogels [209, 210, 213, 236–247]. In addition, most of these studies report a synergistic effect of both the hydrogel and the cell therapy, improving overall efficacy [237, 240–243, 245]. Three clinical studies have been performed in the cardiac regenerative field combining cells and hydrogels (fibrin and collagen), all during coronary artery bypass graft [225, 248, 249]. The method proved to be safe although the study using fibrin hydrogel to deliver ESC progenitors reported alloimmunization [225]. The study by He et al. included a cell-only group, and their results provided evidence of enhanced benefit when administering the cells in an embedded hydrogel [249]. As cell therapy is moving towards the use of cell-free approaches such as EVs, injectable hydrogels have also been explored at *in vitro* and preclinical level as drug-delivery vehicles for EVs in MI [250–255]. Despite there are few studies comparing the characteristics and the efficacy of the different hydrogels *in vivo* (either alone, or for cell or EV delivery) [204], some may be more suitable for some applications than others [256]. For example, for the delivery of EVs or secretomes, hydrogels with smaller pore size are preferred [251].

Although hydrogels have shown promising applications in the field of cardiac regeneration as both standalone and drug-delivery systems, more progress is needed [121]. On the one hand, it is necessary to optimize the electrical, mechanical and gelation properties of injectable hydrogels while maintaining biodegradability, probably by the combination of both natural and synthetic hydrogels. On the other hand, it is necessary to further explore their potential as EV drug-delivery systems and confirm if the combined products do present enhanced retention and efficacy vs. hydrogels or EVs alone. The different cardiac regenerative therapies, including cells, EVs and hydrogels are illustrated in Figure 1.10.

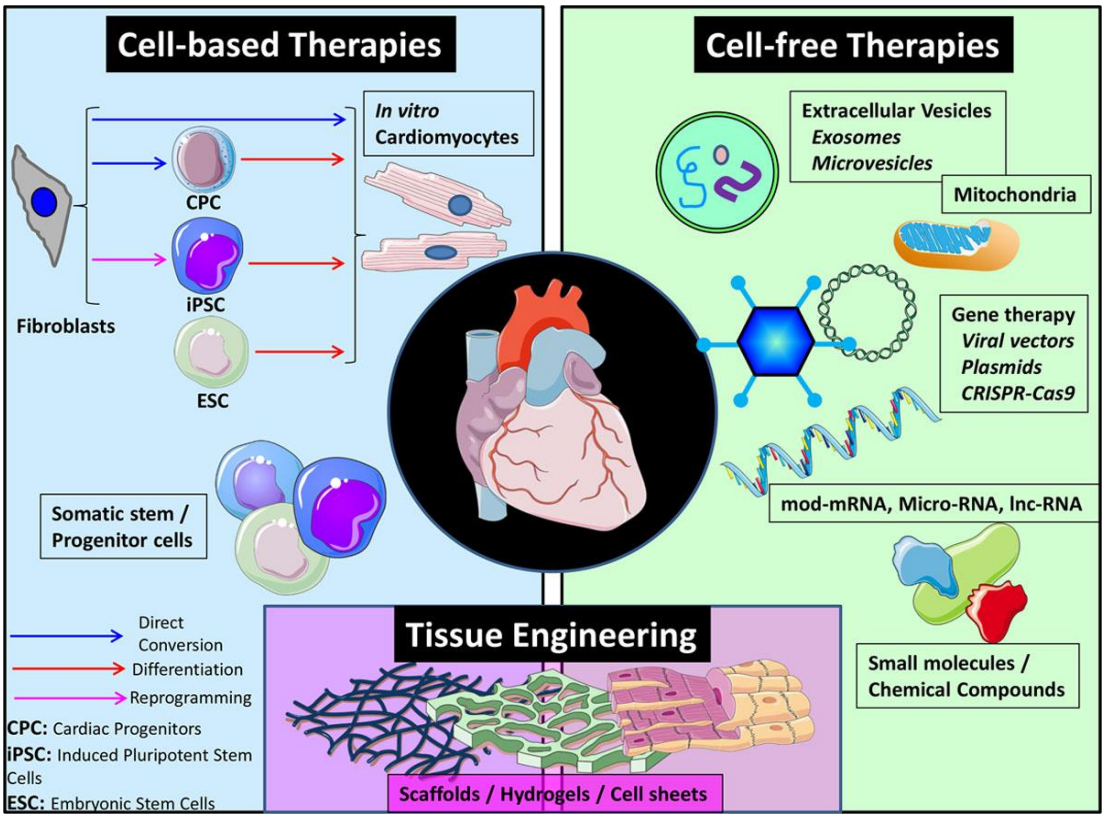

Figure 1.10. Regenerative therapies. Classification of the different type of therapies in cell-based, cell-free or tissue engineering is done mostly from an academic perspective. In reality many of them converge and the combined use of different strategies may lead to better results. CPC indicates cardiac progenitor cell; CRISPR-Cas9, clustered regularly interspaced short palindromic repeats-associated 9; ESC, embryonic stem cell; and iPSCs, induced pluripotent stem cell. Reproduced with permission [169]. Copyright © 2019 Wolters Kluwer Health, Inc.

1.3.4 Limitations and challenges for translation of cardiac regenerative and reparative products

Biological products such as stem cells, EVs and natural hydrogels present high therapeutic potential because of their ability to prevent and counteract different molecular, cellular and structural changes behind cardiac pathologies. However, their translation into the clinical scenario faces several problems that need to be addressed, at least partially, if we want them to succeed in clinical practice. Some of the most highlighted limitations are the lack of deep understanding of their MoA, their large variability and lack of standardization and their *in vivo* retention and biodistribution [115, 120, 121, 257].

One of the main reasons attributed to the failure of some clinical trials involving biological products (and stem cells in particular) is the lack of knowledge about their MoA [122]. Most of the clinical trials were initiated under the hypothesis that implanted stem cells will

differentiate into CMs and regenerate heart muscle or induce CM proliferation [122]. Despite the knowledge in recent years having enormously increased, with the paracrine hypothesis displacing this original hypothesis, there are still many unknowns regarding the specific molecules and signaling pathways involved [110, 122]. More specific knowledge could help in predicting success in humans and boosting efficacy. Therefore, strong efforts are, and should be further put, into elucidating these mechanisms. Nevertheless, full understanding of the MoA and pathways involved in the efficacy of biological products can be extremely difficult to achieve and may not be fully determinant for their use in the clinical practice [122]. As an example, the MoA of some pharmaceutical, everyday used drugs, such as statins, also remains elusive [122].

Another important challenge in therapeutical biological products is their standardization both regarding their source and manufacturing, release and delivery processes [258]. Differently to chemical or pharmaceutical compounds, biological products are more complex from the molecular and structural point of view and confirming their identity does not always extrapolate into confirmed efficacy [110]. Thus, when trying to standardize, there are many factors regarding their source that need to be considered: the tissue of origin, the cell type/identity and the source donor. ECM and cells isolated from different tissues present some common characteristics but also some differences that need to be controlled and taken into account when extrapolating the results [255, 259–263]. In general, using the same tissue source as the intended target has proven superior efficacy [203, 205, 264]. Even inside the same tissue, there may be similar but different cell types, and these slight differences may significantly influence the therapeutic properties [132]. Another key point in the use of biological therapies is whether the products should be obtained and expanded from the own donor (autologous) or from a generic one (allogenic) [265]. Autologous therapy was used in the first place in an attempt to avoid immune rejection. However, further studies showed that the immunogenic response with allogenic treatment was acceptable [265]. Advantages of allogenic treatment include immediate availability and higher product control [115, 265]. Even if from the same tissue and type, cells and tissues derived from different donors are not 100% identical, and this inherent variability can considerably alter their therapeutical properties. It has been demonstrated that cells of the same type but from different donors can yield different therapeutic potential [266–268]. Whether differences in the age, sex and associated pathologies of the donor determine their derived cells, tissue and EV therapeutic potential still remains unclarified [268–276]. Therefore, the use of previously selected highly potent allogenic products seems more convenient [121].

As biological products are sensitive to the environment, maintaining manufacturing conditions constant and developing adequate potency assays are essential factors for consistent and successful translation [110, 257]. The processes followed for biological product extraction, purification, and culture (in the case of cells) must be adequately described and maintained.

Factors such as culture time and number of passages may considerably affect senescence and cell therapeutic potential [87, 277]. In the case of dECM, the decellularization procedure (which can be more, or less aggressive) can also influence its composition, its physicochemical properties and its therapeutic efficacy [261, 278]. In EVs, differences in the characteristics of the parenteral cells, as well as the purification method used are also important to determine the EV population, the efficacy, and the ease of translation [176, 180, 279]. While high purification of exosome fractions from conditioned medium can be arduous and of doubtful translation, tangential flow filtration method allows for a less purified population of EV but is more suitable to comply with clinical manufacturing standards [202]. In addition, biological products may change their properties in time and depending on the environmental conditions. For example, inadequate or prolonged cryopreservation can affect biological tissue structure and degradation, and in the case of cells, it can affect viability and their therapeutic potential [110, 280]. In line with this, it becomes essential to develop adequate potency assays that allow discerning when a specific product is suitable for its use in the clinical scenario because it will be effective [110, 202, 257]. However, determining adequate quality criteria and optimum manufacturing and storing conditions requires devoted studies, which translate into significant time and resources. Unclear and multiple MoA, together with the lack of reference materials contribute to further complicate the task [110, 281].

It is also important to determine optimum parameters for delivery, such as best time to deliver the product [115] (which will also depend on the target pathology), the most suitable delivery route [120], and the adequate dose [202]. Regarding the time of delivery, for the treatment of cardiac aging short-term treatments applied later in life when the symptoms are initiated will be more translational and convenient than long-term or life-long treatments [17]. In the case of acute MI, it is important to bear in mind inflammation peaks in the target organism, as this can directly impact the survival of the transplanted cells [115]. Time of delivery will also depend on the expected MoA: if it prevents further damage (protective mechanism), it should be administered in early stages of the disease, while if it is capable of reverting the pathological changes it can be used in more advanced stages. The route of delivery plays a role in how the transplanted product biodistributes inside the organism [121, 161, 264]. Ideally, to maximize efficacy and minimize adverse events, the entire administered product is retained into the target organ (in this case the heart) and nothing reaches other organs. The different routes of delivery available (intravenous, intrapericardial, intracoronary and transendocardial) have different trade-offs [161]. On the one hand, the simpler, the less invasive, the most economical and therefore the most translational is the intravenous/systemic route. Nevertheless, it offers the less proportion of retention in the target tissue. On the other hand, the transendocardial route is more costly and invasive, but offers more localized administration and retention [161, 282]. The administration route and the retention are also important to determine the adequate dose. In cell therapy, different doses have been used in the clinical trials proving cell therapy to be save, but there is

still a lack of studies devoted to determining the best dose that optimizes efficacy but remains safe [110, 115, 120, 202].

One of the main challenges of cell and EV therapy is improving their retention [120]. It has been shown that implanted cells and EVs poorly engraft in the target region (even with the most invasive delivery routes). In addition, in the case of cells, even if they engraft, the hostile environment makes survival rates to be very low [121]. Such poor and short retention may be considerably limiting the observable therapeutic effect. To solve this, new approaches are looking at repeated dosing [122] and prolonged delivery. It seems unrealistic to think that with a single, short-lasting dose we will observe significant and long-lasting effects in diseases that currently lack adequate treatments. However, repeated dosing in the case of biological products may face translational problems as it is not practical and poses even further questions: the number of doses, their time interval, the amount of cells/EVs in each of the dose, etc. The modification and combination of biological products, such as cells or EVs with the use of biomaterials, is opening new perspectives [121, 169]. Apart from combining structural and biological support, both improved retention at the target site and more prolonged deliveries may be achieved [223].

Other factors that may have limited the translation of biological products into the clinical scenario are differences between the preclinical models and the target population of patients [258, 283]. First, there are significant differences in the cardiac regenerative capacities of rodents and humans, so results obtained in preclinical models may not necessarily translate to humans, especially if the cells or the EVs used as therapeutic product are of murine origin [120, 257]. Secondly, animals included in preclinical studies are usually young, and in some cases of only one gender. Preclinical studies should resemble as much as possible the target population of patients, where patients are usually aged, have other co-morbidities and have concomitant routine medications [115, 120, 169, 257].

It is also necessary to better refine the target pathology and population in clinical trials as well as the primary endpoints and how to measure them. While most of the clinical trials have focused on the treatment of HFrEF (of ischemic and non-ischemic origin), most biological products present benefits at molecular and structural levels common to several cardiac pathologies [120, 257]. Therefore, the potential of these biological products on cardiac diseases such as Duchenne muscular dystrophy (DMD) and HFpEF (associated to cardiac aging) should not be diminished and should be further explored [257]. In fact, most of the trials have focused on acute MI, where several more problems arise with respect to other pathologies [120]. First, the inflammation cascade is more dynamic and of higher scale than in other cardiac pathologies, what considerably limits implanted cell survival [284, 285]. Secondly, standard of care is now relatively good, so enormous amounts of patients will be required to demonstrate beneficial effects of cell-therapy on endpoints such as death [286]. Moreover, in most clinical trials, LV function,

commonly measured with the EF, was used as the primary endpoint. However, some clinical trials have reported benefits in the functional capacity, quality of life and reduced mortality and hospitalization [287–290]. In the end, clinical outcome is more relevant to patients than LV measurements, and because of the biological product's MoA, their benefits may not always translate into a direct improve in the EF [122, 257].

Finally, the field is also facing problems against legacy and resources obstacles. To ease translation, it is necessary to develop protocols and spaces that allow for the large-scale production of these products ensuring their standardization [110, 202]. In addition, due to the apparent contradictory results and some cases of academic misconduct, the field of cardiac cell therapy is facing lack of commercial interest. Commercial interest is required to move from proof-of-concept studies into larger clinical trials [110, 257]. In the end, well-designated phase III clinical trials are still needed to determine if these biological products are beneficial for patients [120, 122, 202, 257]. The priority concepts for solving these limitations in the cardiac regenerative and reparative field at different stages of product development and testing are summarized in Figure 1.11.

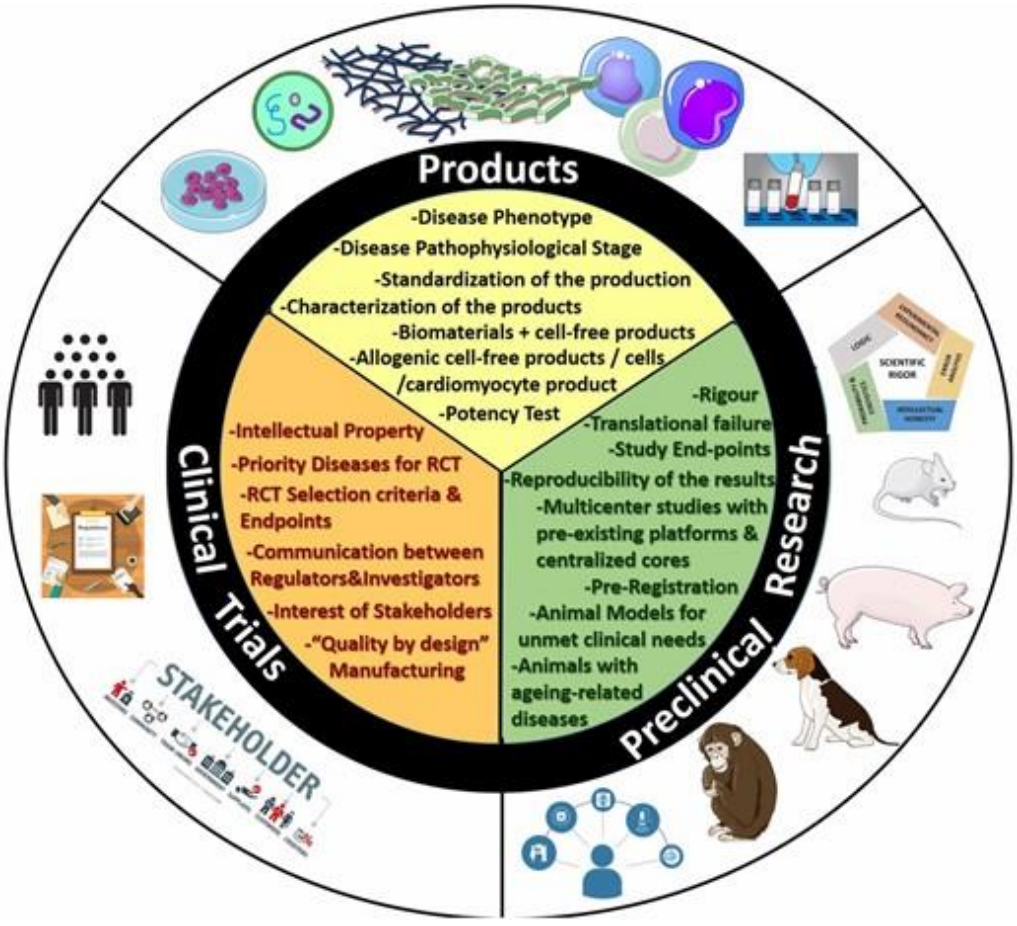

Figure 1.11. Priority concepts in cardiac regenerative and reparative medicine according to the field of research. Reproduced with permission [257]**.** Copyright © 2020, Oxford University Press.

Chapter 2

Motivation, objectives and thesis outline

2.1 Motivation

Cardiovascular diseases are the leading cause of disease burden and mortality in the world. They are also a major cause of disability and health care costs [1]. The main risk factor for the development of cardiovascular diseases is aging [16]. With the average lifespan of the human population continuously increasing, it is expected that the problem of cardiovascular diseases will only continue to grow in the following years [1]. Aging is particularly linked to an increase in the prevalence of heart-related pathologies such as heart failure (HF) and atrial fibrillation (AF) [16, 17].

Current pharmacological treatments for HF and AF, although dramatically changed the prognosis of these patients in the last decades, still present important efficacy and safety problems [2, 3] and are not regarded as definitive cures [4]. This makes it necessary to keep developing new treatment strategies that target the underlying fundamental molecular pathways and try to trigger endogenous reparative responses. In this context of limited therapeutic efficacy of the available medicines for some specific cardiac conditions considered as unmet medical needs, the use of advanced therapy medicinal products (ATMPs), including stem cell therapy, extracellular vesicles (EVs) and biomaterials such as hydrogels has emerged as a potential breakthrough [5]. Contrary to current treatments, biological products could have the potential to treat cardiac aging-associated pathologies from a more fundamental level [110], as they are able to improve cell survival and protection, cell-cell communication, angiogenesis, cardiomyogenesis, reduce inflammation and molecularly regulate proliferation and cell cycle [79].

Despite the promising potential of biological therapies, many challenges and unknowns remain to be solved before they can successfully reach the clinical scenario. Some of the most highlighted limitations are the lack of deep understanding of their mechanism of action (MoA), their large variability and lack of standardization (including inadequate potency tests), and in particular for cells and EVs, their low *in vivo* retention at the target site [115, 257].

2.2 Objectives

The main objective of this thesis is to develop, characterize and evaluate advanced therapies for the treatment of cardiac pathologies solving some of their current limitations to enhance their therapeutic potential. This aim is attained by addressing the following more specific objectives:

- To provide a practical guide for the development of potency assays for cell and cell-based cardiac reparative and regenerative products.
- To explore markers of anti-aging potency of cardiosphere-derived cell (CDCs) and their secreted EVs (CDC-EVs)
- To evaluate if the *in vitro* anti-senescent and pro-angiogenic activity of human CDC-EVs could be used as a predictor of their *in vivo* potency in an animal model of cardiac aging.
- To develop and characterize an optimized ATMP by combining solubilized cardiac extracellular matrix (cECM), polyethylene glycol (PEG), and EVs to yield an injectable hydrogel with short gelation time and improved retention of the EVs.
- To investigate and characterize the antiarrhythmic MoA of CDC-EVs in a suitable *in vitro* model of AF.

2.3 Thesis outline

This thesis begins with an introductory chapter (**Chapter 1**) that includes the state of the art of cardiac-aging related pathologies and the use of ATMPs such as cells, cell-derived EVs and hydrogels in the cardiac scenario. In **Chapter 2,** the motivation, the objectives, and the outline followed in this thesis are summarized. A practical guide for the development of cell-based potency assays in the cardiac field is provided in **Chapter 3.** The experimental work of the research is presented in **Chapters 4 to 7**. Finally, the discussion and main conclusions of this thesis are presented in **Chapter 8**. The detailed content of Chapters 3 to 8 is the following:

Chapter 3: The essential need for a validated potency assay for cell-based therapies in cardiac regenerative and reparative medicine. A practical approach to test development. In this chapter we describe the main characteristics and challenges for a cell therapy potency test focusing on the cardiovascular field. Moreover, we discuss different steps and types of assays that should be taken into consideration for an eventual potency test

development by tying together two fundamental concepts: target disease and expected MoA [291].

Chapter 4: Exploring the determinants of rejuvenating potency of cardiosphere-derived cells: chronological vs. biological age. In this chapter we evaluate if the chronological age of the donor, cell senescence and ability to form cardiospheres relate to CDC properties and the *in vitro* rejuvenating and pro-angiogenic potency of CDC-EVs.

Chapter 5: Anti-senescence *in vitro* potency of extracellular vesicles secreted by cardiosphere-derived cells predicts their rejuvenating effects in an aging rodent model. The purpose of this study is to evaluate if the *in vitro* anti-senescent and pro-angiogenic effect of the CDC-EVs, scored with a matrix assay, can be used to predict the *in vivo* potency of the CDC-EVs in a model of cardiac aging.

Chapter 6: Cardiac extracellular matrix hydrogel enriched with polyethylene glycol presents improved gelation time and increased on-target site retention of extracellular vesicles. In this chapter we develop an optimized product combining hydrogels from cECM, PEG and EVs to overcome their individual limitations: long gelation time of the cECM hydrogel and poor retention of the EVs. We characterize its gelation and mechanical properties, structure, biodegradation, bioactivity, and its EV release and on-site retention *in vivo* [292].

Chapter 7: Electrophysiological effects of extracellular vesicles secreted by cardiosphere-derived cells: unravelling the antiarrhythmic properties of cell therapy. The purpose of this study is to explore the electrophysiological modifications induced by CDC-EVs on arrhythmogenic tissue to better understand the mechanisms behind their antiarrhythmic effect [293].

Chapter 8: Discussion and conclusions. The results and main findings of this thesis are discussed, highlighting new directions for future work. Finally, the main conclusions are presented.

Chapter 3

The essential need for a validated potency assay for cell-based therapies in cardiac regenerative and reparative medicine. A practical approach to test development

3.1 Abstract

Biological treatments are one of the medical breakthroughs in the 21st century. The initial enthusiasm pushed the field towards indiscriminatory use of cell therapy regardless of the pathophysiological particularities of underlying conditions. In the reparative and regenerative cardiovascular field, the results of the over two decades of research in cell-based therapies, although promising, still could not be translated into clinical scenario. Now, when we identified possible deficiencies and try to rebuild its foundations rigorously on scientific evidence, development of potency assays for the potential therapeutic product is one of the steps which will bring our goal of clinical translation closer. Although, highly challenging, the potency tests for cell products are considered as a priority by the regulatory agencies. In this chapter, we describe the main characteristics and challenges for a cell therapy potency test focusing on the cardiovascular field. Moreover, we discuss different steps and types of assays that should be taken into consideration for an eventual potency test development by tying together two fundamental concepts: target disease and expected mechanism of action.

3.2 Introduction

Medical landscape is being dramatically changed by the introduction of cell-based therapies [120]. In the cardiovascular field, research in regenerative and reparative medicine made an enormous contribution to the understanding of profound pathophysiological processes underlying different diseases and biomolecular cellular organization and functioning. However, in clinical trials of the field, cell-based therapies have only shown modest efficacy. This has been

due in part to a lack of standardization, of comparability studies and of deep understanding of the mechanisms of actions (MoA) behind [115].

Development of adequate potency assays that reproducibly measure the ability of the cell-based ingredient to produce a given result (bioactivity), will be a step forward not only in industry, but also to overcome these limitations in academic research [257]. In fact, the International Council for Harmonisation of Technical Requirements for Pharmaceuticals for Human Use (ICH) recommends consideration of biological activity, alongside identity and purity among others, for determining product acceptance before intended use [294]. However, differently from small-molecule drugs (long dominating the pharmaceutic industry), cell-based therapeutics present higher inherent complexity and presumable several MoA that require a longer time to attain the clinical scenario and that complicate the development of adequate potency measurements. Key aspects are identifying critical quality attributes (CQAs) related to the MoA of the product, how to determine their acceptable ranges, and how to measure them reproducibly and feasibly on a routine basis.

In this chapter, we review the need and the requirements in developing potency assays for cell-based therapeutics in the cardiovascular field focusing on the recommendations by the ICH and those adopted by the U.S Food and Drug Administration (FDA) and the European Medicines Agency (EMA). Moreover, we discuss the specific challenges and the practical limitations of potency tests in the cardiovascular field not sufficiently commented in the regulatory papers. In addition to that, we elaborate on the link between the target cardiovascular disease and the expected MoA of the cell-based ingredient to propose potential candidates as *in vivo*, *in vitro* and surrogate measurements to evaluate potency of the product. The relationship between these processes discussed in this work are summarized in Figure 3.1.

3.3 Potency assay as regulatory recommendation to optimize research results

Potency has been defined as a quantitative measure of biological activity [294]. It can be considered equivalent to strength and defined as the therapeutic activity of the drug product [295, 296]. Therefore, a potency assay is a test or set of tests with the ability to confirm that the relevant biologic functions that correlate to the efficacy are present in the active ingredient and in the final product [297].

Product consistency is one of the pillars for the reproducibility of clinical effects and demonstrated efficacy. Identity, purity, stability, and quality, together with potency, need to be guaranteed to ensure this consistency. As a result, validated potency assays are necessary before

product release to support consistency in the strength of all released products. In fact, both the EMA [298] and the FDA [296] have pointed the need for measuring biological activity via a validated potency assay for qualification, validation and control of cell-based therapies [299]. In this regard, data demonstrating that the potency assay(s) measures an appropriate biological activity of the tested therapeutic agent is preferred when the material is ready for the first clinical trial [295].

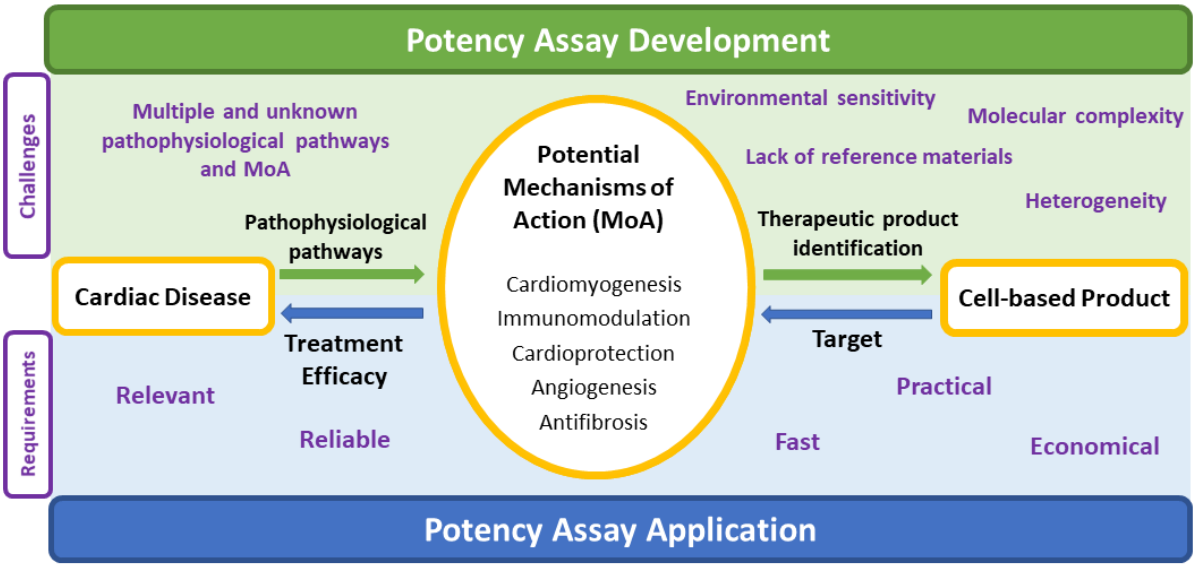

Figure 3.1. Development and challenges in potency assay development in the cardiovascular field. Development of potency assays for cell-based products consists in understanding the pathophysiology of the disease, identifying potential mechanisms of action (MoA) to counteract it and finding the most suitable cell-based product that exhibits these MoA. When applied, the potency assay needs to correlate bioactivity of the product, via a measurement related to the MoA, with treatment efficacy. Nevertheless, in the cardiovascular field, the process faces several challenges and high requirements.

However, cell-based therapies present several differences with respect to many classical pharmacological compounds (small molecular drugs). As "living products", cells present larger variability, more limited stability, and larger molecular and mechanistic complexity. Their biological activity and thus efficacy will strongly rely on their source, processing and/or storage. Viable cells may lose their biologic function during processing or storage [297], or change their properties in response to their environment with potentially significant functional and safety consequences [300]. As a result, merely confirming cell identity and viable cell number at the moment of product release does not necessarily correlate to biological activity measurements [298].

Solid potency tests are not only useful for ensuring that the final released product is consistent, effective, and high-quality manufactured. They also serve during the different stages of product development and manufacturing as part of product comparability, stability testing and quality evaluation [296, 298]. Adequate potency tests will allow the fair comparison of different products (different batches, different cell types or even different sources), and therefore the selection of the optimal one regarding a specific MoA. In addition to that, the potency assay may also be useful to assess stability by ensuring the strength of the product is maintained at the different stages of the manufacturing process and determining product shelf-life and optimum manufacturing and storage conditions. Investment in a solid potency assay from early stages of product development mitigates the risk of costly product failure in subsequent states [297].

3.4 Requirements of an "ideal" potency assay

An ideal potency assay should be relevant, practical, reliable and ideally quantify the biological activity related to the MoA [296, 298]. Although tolerant with the heterogeneity of the product, the assay must be able to detect meaningful changes potentially related to efficacy [296] and have predefined acceptance and rejection criteria [297] to conclude if the product is suitable for release, as well as its suitable dating periods. To be reliable, potency tests should have adequate reference materials: standards and/or controls to ensure interoperator and time-to-time consistency. Also, tests should report on accuracy, sensitivity, specificity and reproducibility to be amenable for validation and meet labelling requirements [296].

Figure 3.2 summarizes the steps to be followed in the process of a potency test development. When characterizing the product identity, it is important to appropriately control the mixture composition if several cell types are present in the product. Moreover, while identity, cell purity and proliferation will influence and may correlate to biological activity and potency, this must be demonstrated through qualified experiments.

3.5 Challenges in the development of potency assays for cell-based therapies

Development of a potency assay for cell-based products faces several challenges. One is the heterogeneity of the primary cells partially related with the particularities of their donors and the intention of use as an autologous or allogeneic treatment [296]. Allogeneic treatments have presented similar effect but several advantages over autologous treatments, such as larger availability and the possibility to select the most potent products [301]. Other factors such as cell

age and their previous exposure to risk factors can also determine potency and are more easily controlled in allogenic treatments. In cell-based products, and in particular in autologous treatments, tests requiring minimal amount would be preferred as the availability is considerably limited.

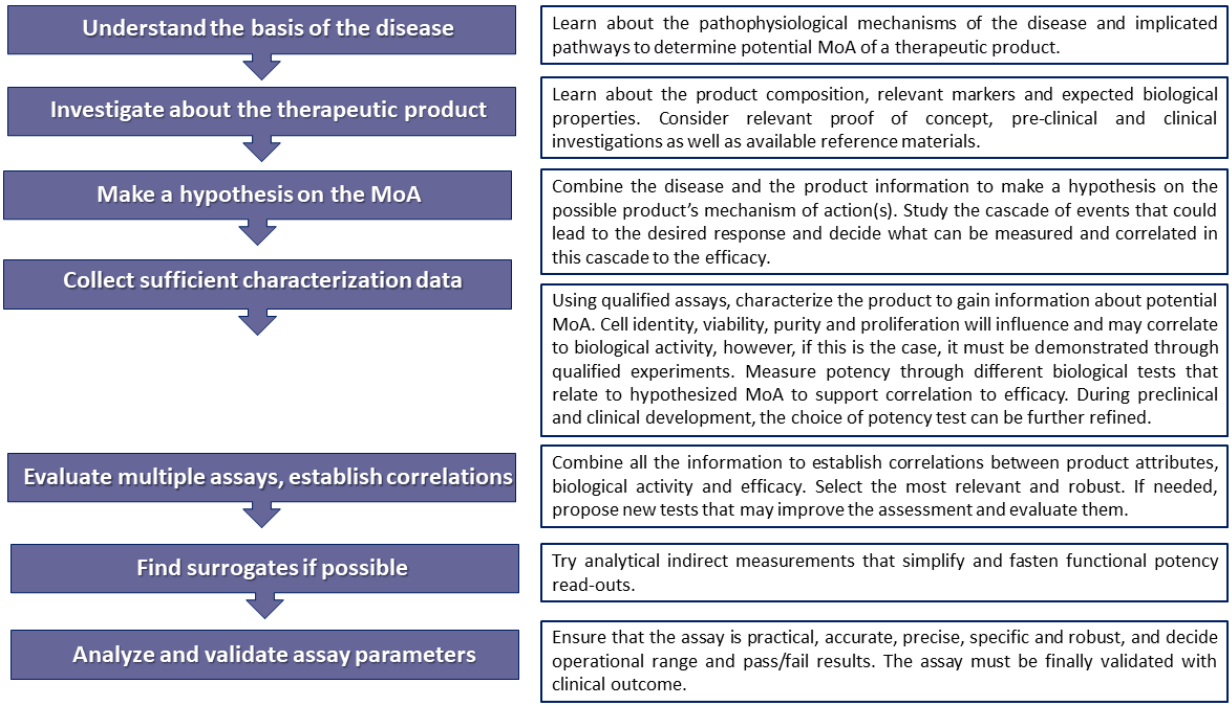

Figure 3.2. Steps in the development of a potency assay.

Furthermore, cell-based products present a high level of molecular complexity [298, 302], as well as multiple, and usually not fully-known MoA [303], entangling the selection of the most accurate potency test. Thus, as one single test may not be sufficient to fully represent several MoAs of the product, the final potency assay may be based on multiple complementary tests, the so called assay matrix [304]. Moreover, when cell-based product is administered *in vivo*, the biodistribution, as well as the retained amount of product in the target tissue are usually crucial for the efficacy but can be complex to model. This can considerably difficult establishing links between *in vitro* potency assays and the physiological MoA *in vivo* [305].

Cells are also very sensitive to environmental conditions, processing, storing, delivery, and administration, what affects their viability and quality attributes, and therefore, their stability and shelf-life [298]. So, despite potency should be measured on the final product, stability (referring to maintenance of its physiological and potency attributes in time) should also be demonstrated during the different phases of product's life. After the stability is confirmed at all the stages, potency measured at a given time-point can be used as indicative of product's quality [306].

Another important limitation is the lack of adequate reference materials and standards. To guarantee consistency, reference materials and standards must be highly characterized and be sufficiently homogenous and stable [307]. However, when attempting to quantify CQAs in biological materials, standardization becomes difficult as the tests commonly lack an existing certified reference material to use for comparison and often do not provide measurements in independent and internationally recognized units (for example, in International System of Units) [281]. The heterogeneity and complexity of living cells difficult the development of a reference cell line [305] or a "cell-ruler" [308] to normalize the potency measurement over several batches.

Determining acceptance and rejection criteria in cell-based products' potency assays is not always trivial. The acceptance criteria may be redefined as new knowledge about the product is gained *in vitro*, *in vivo*, and in the clinical scenario during the different stages of product and potency assay development. It is necessary to ensure that the final defined acceptance criteria consists in a numerical range that ensures biological activity and reflects clinical effectiveness [296].

The bioactivity of the product can be evaluated *in vitro* and/or *in vivo* [295]. Potency assays performed *in vivo* should include carefully defined controls, including sham and vehicle treatment groups, and take into consideration specific xenogeneic responses that might influence the induced effects. Main drawbacks of *in vivo* models for routine potency assessment are the costs and the time consumption [306]. Hence, *in vitro* models are generally preferred [309]. *In vivo* testing is commonly used to validate the *in vitro* predictability and to identify the pass/fail results for potency, as *in vitro* tests should correlate to the intended effect *in vivo* and assumed MoA.

In vitro functional assays, such as endothelial tube formation for angiogenesis or anti-inflammatory assessment are often not suitable for routine testing right before the product is administered since they present high variability and are time-consuming [298]. Therefore, when possible, the use of surrogate (non-direct) measurements that have previously demonstrated correlation with functional assays, such as for example specific gene expression or secretion of a factor, are preferred [295, 296].

3.6 Disease-targeted and mechanism of action-guided potency tests in cardiovascular regenerative medicine

Cell therapy products have been indistinguishably used for a wide range of cardiac diseases over the past two decades many times with just modest efficacy [120, 310]. However, the role of the pathophysiological pathways underlying each of the diseases should not be underestimated in the therapeutic response of a given cellular product and should be taken into

consideration for the right selection of the potency test. While a specific cell-product, with predominantly one MoA can be suitable for a particular condition, it may be inappropriate for a different disease. Moreover, the pathophysiological stage of the disease, acute or chronic, and the predominantly inflammatory or fibrotic underlying background, are also important factors to consider when opting for a particular product. Products with more immunomodulatory, anti-inflammatory and cardioprotective (anti-apoptotic) mechanisms of action may be preferred in early stages of the disease, while proangiogenic, anti-fibrotic and strategies targeting direct re-muscularization may be more beneficial in advanced stages of the disease.

Several MoA linked to cell-based therapies in cardiovascular regenerative medicine have been described [311]: cell survival and protection (cardioprotection), immunomodulatory, anti-inflammatory and anti-fibrotic effects, angiogenic and cardiomyogenic [79, 285]. To develop an adequate potency assay and successfully quantify the potential efficacy of a cell-based product, it is essential to identify the most relevant MoA of the therapeutic product and at least one of the disease-related significant pathophysiological pathways expected to be counteract by the former (Figure 3.3).

Some cell products have been characterized for their MoA, but a robust quantification of these effects to compare and identify the most potent cell type for a certain clinical condition, and/or from batch to batch is still lacking [115]. Today is accepted that the cells exert their therapeutic effects mostly through paracrine secretion of soluble factors and/or extracellular vesicles (EVs) [308, 180, 306, 293]. Indeed, EVs offer the potential to overcome the frailty of cell therapy by conserving their bioactivity regardless of the extremes of handling [200]. Moreover, the use of EVs, exosomes, or other cell-derived products ease standardization, costs and are more manageable to scale-up [310].

When the expected MoA is paracrine-mediated, the potency assay should initially focus on detection of secreted bioactive molecules or particles related to the process, such as cytokines, growth factors, miRNA, etc. and then, if possible, find surrogate markers [298]. These analytical assays can evaluate immunochemical, biochemical and/or molecular attributes such as cell surface markers, secretion factors, protein or gene expression patterns [309]. In case the intended effect is through tissue replacement (i.e. using pluripotent stem cells, PSCs), then cell retention, differentiation potential and maturity of the differentiated cardiomyocytes (CMs) should be considered for the potency assay.

3.7 Possible ways of measuring potency according to the expected mechanism of action

Once the potential MoA linked to the cell-based therapy product and the target cardiovascular pathology have been identified, it is important to determine the potential tests that could be used to quantify potency. In this section, different *in vivo*, *in vitro* and surrogate tests for the different potential MoA (cardiomyogenesis, electromechanical coupling, immunomodulation, cardioprotection, angiogenesis and anti-fibrosis) are reviewed (Figure 3.3).

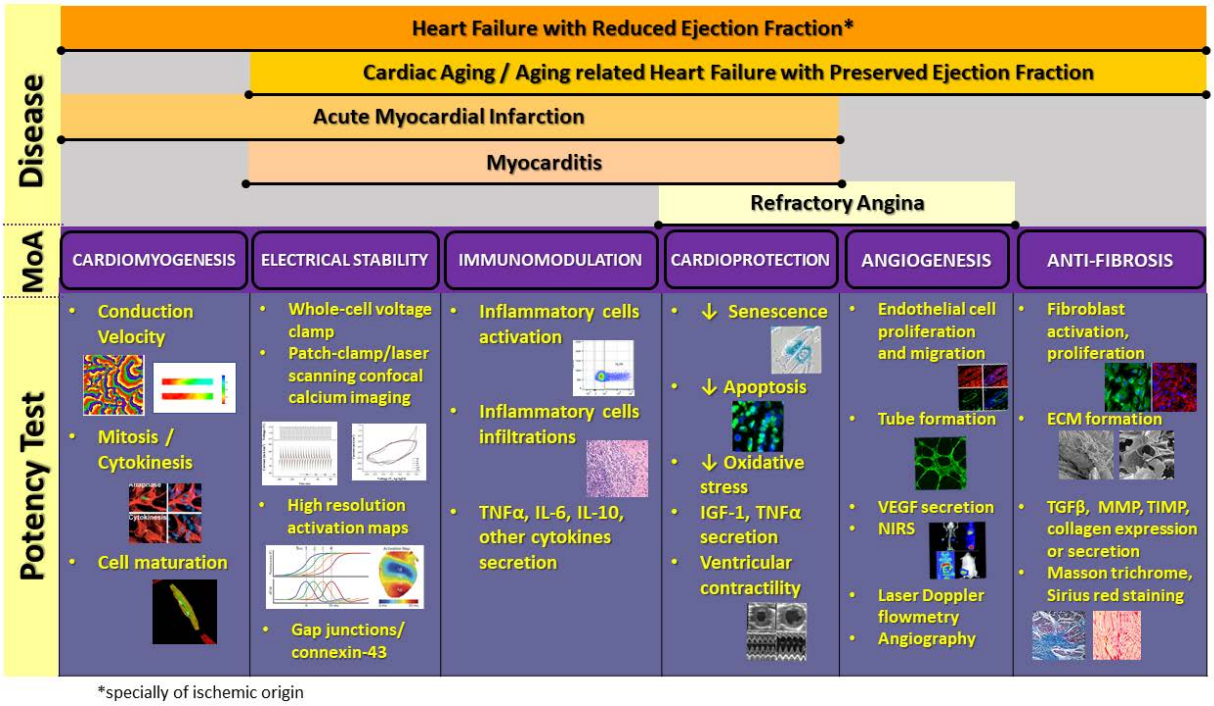

Figure 3.3. Potency tests based on the expected mechanism of action (MoA) for different cardiac diseases.

3.7.1 Cardiomyogenesis

Cardiomyogenesis refers to new CM formation that is now acknowledged to be rare in an adult human heart and still inefficiently achieved by different cell therapy modalities [169]. The newly formed CMs can result from direct differentiation of the implanted cells, from differentiation of endogenous cardiac stem cells, or from proliferation of pre-existing CMs. Cardiomyogenesis resulting from CM division can be confirmed *ex vivo* by using classical mitotic markers, such as Ki-67, phospho-histone 3 and thymidine analogs such as bromo-deoxyuridine in multinucleated CMs. However, these are not always indicative of true mitosis or cell division and require animals, which may difficult its use for routine testing. If still this is considered as the

MoA in a given condition, the combined use of different mitosis and cytokinesis markers (e.g. Aurora B kinase) could increase the efficiency of the potency test measured. Cardiomyogenesis arising from implanted cell differentiation can be assessed *in vitro* by quantifying their potential to differentiate into the myocyte lineage under specific conditions. Nonetheless, the potential to differentiate *in vitro* may differ *in vivo*, so adequate correlation between the *in vitro* differentiation, *in vivo* differentiation and *in vivo* efficacy must be previously demonstrated.

3.7.2 Electromechanical maturation and coupling

Exogenous or extrinsic replacement generally refers to implantation of CMs differentiated *in vitro* from embryonic stem cells (ESCs) or induced pluripotent stem cells (iPSCs). In these studies, electromechanical integration and maturity of transplanted cells into the injured heart is fundamental to achieve functional improvement [312] and should be considered for a potency assay. To evaluate electrophysiological maturity and avoid potential pro-arrhythmic effects [126], the final construct should be assessed for activation frequency, conduction velocity (CV) and action potential duration and morphology to be compared to native tissue electrophysiological characteristics. Electrophysiological studies are also crucial when the pursued target of the therapeutic product is the generation of biological pacemakers or an antiarrhythmic effect [313, 314].

In vitro cell automaticity (spontaneous activation) can be studied using whole-cell voltage clamp and simultaneous patch-clamp/laser scanning confocal calcium imaging. High resolution activation maps that characterize impulse initiation and propagation can reveal important information *in vitro* about the electrophysiology of the cells to be implanted and about temporal coupling between graft and host cells *ex vivo*. However, these tests are not practical for routine and massive testing because they are usually labor intensive and require highly specialized and costly equipment. Therefore, despite up to date there are no alternative or validated measurements on this regard, it is recommended to explore and attempt to validate alternative *in vitro* or surrogate markers for electrophysiological stability and maturity. For example, for functional integration to occur, the maturity of the electrical potential generated by differentiated cells is dependent on the amount and proportion of ion channels and the ability of the electrical potential to propagate to neighboring cells through gap junctions. Using protein and/or gene expression of ion channels and connexin-43 [315] in differentiated CMs, if validated, could be indicative of electrical maturity of the product. Evaluating modifications in these proteins *in vitro* in models of target cells or tissues under the presence of the therapeutic product could be indicative of electromechanical coupling and antiarrhythmic potential of the therapeutic agent.

3.7.3 Immunomodulation

Contrary to classical belief, inflammation is not necessarily an impediment to tissue regeneration. Some immune cells (monocytes and macrophages) are required for cardiac regeneration, and injury-induced CM proliferation is inhibited by immunosuppression [79]. Harnessing immune cells pro-reparative mechanism(s) to promote heart regeneration vs. their pro-inflammatory effect that exacerbates disease will still require better understanding. In fact, immunomodulation is gaining support as the main MoA behind cell therapies in the cardiovascular field [316]. Despite the challenges in establishing the mechanisms behind immunomodulation, mesenchymal stem cells (MSCs) and cardiac progenitor cells (CPCs) have shown to attenuate production of TNF-α and IL-6, to increase the expression of IL-10 [317], and to polarize an effector macrophage population [318]. Regarding potency assays, cell therapy effect on inflammatory response can be assessed *in vitro* by measuring macrophage activation and migration, and secretion of pro- and anti-inflammatory factors, such as TNF-α, IL-6, and IL-10.

3.7.4 Cardioprotection

Cardioprotection in terms of increased cellular resistance to internal or external stressors, is essential in limiting cardiac remodeling after injury, and therefore preserving cardiac function at a longer term. CM loss is probably the main issue related with the disease progression in ischemic heart disease and/or systolic heart failure (HF). These cells can be protected directly by means of antisenescence, antioxidative or antiapoptotic effects conferred by some therapeutic cells, or by stimulation of autophagy, among others [319]. Both MSCs and CPCs have shown to enhance cell survival, prevent apoptosis in CMs and prevent ischemic injury via paracrine mechanisms [320, 141, 176].

Ventricular contractility (i.e. left ventricular ejection fraction, EF) assessed by imaging techniques *in vivo* animals is accepted to translate underlying CMs survival and function. They can also contribute to the elucidation of the particular mechanisms and to identification of new potential markers. However, animal studies are more expensive and non-efficient as a frequent potency assay for batch release. Alternatively, if possible, *in vitro* functional tests once demonstrated to be correlated to *in vivo* expected efficacy could serve to evaluate and quantify cardioprotective efficacy of the therapeutic product. In this regard, evaluation of the effect of the cell-based products on CM apoptosis and/or senescence could be considered as potential *in vitro* potency assessments for validation. As example of further surrogate potency endpoints, the measurement of the secretion or expression of some cytokines (i.e. IGF-1, TNF-α [321, 322]) that have demonstrated to be associated with the inhibition of apoptosis and increased CM survival could be considered.

3.7.5 Angiogenesis

A continuous supply of nutrients, as well as routes for eliminating metabolic products, is essential for tissue health. In the absence of neovascularization following injury, the heart fails to repair and instead forms extensive fibrotic scar. Although the precise mechanisms of neovascularization are not well defined, endothelial cell proliferation and arrangement into tube-like structure finally leads to the formation of new vessels. Paracrine activity of MSCs and CPCs have shown to augment the pro-angiogenic activity of endothelial progenitor cells [323, 324, 132]. This effect has been linked to vascular endothelial growth factor (VEGF) secretion [323] and extracellular matrix metalloproteinase inducer (EMMPRIN) release.

In animal models, angiogenesis can be evaluated with angiography, laser Doppler flowmetry, near-infrared spectroscopy (NIRS), histology and immunohistochemistry [306]. *In vitro* proangiogenic potency can be analyzed by the ability of the therapeutic agent to induce endothelial cell proliferation and migration, or tube formation on Matrigel. However, due to the inherent variability of Matrigel, reference material should be used to ensure test reproducibility. Synthetic alternative materials presenting higher sensitivity and reproducibility could be alternatively considered [325]. While secretion of involved factors, such as VEGF could serve as a potential surrogate measurement, analyzing the combined secretion of different cytokines involved in angiogenesis instead of a single one, may increase the predictive value of the potency test [326].

3.7.6 Anti-fibrotic mechanism

Another key mechanism of progression of different types of cardiac injuries is fibrosis, an increased extracellular collagenous deposition. Transforming growth factor beta (TGF-β) is the main player for inducing fibroblast activation and proliferation, extracellular matrix formation, and endothelial to fibroblast transdifferentiation [43]. Different cell-based products, such as MSCs and CPCs have demonstrated to possess an anti-fibrotic effect by transcriptional downregulation of types I and II collagen synthesis [327] and by driving fibroblast to a more therapeutic profile (higher stroma-cell-derived factor 1, SDF-1, and VEGF secretion) [328].

Fibrosis can be easily visualized and quantified *ex vivo* with Masson trichrome or Sirius red staining. However, *in vitro* fibrosis can be non-directly inferred for example by evaluating fibroblasts TGF-β, matrix metalloproteinase (MMP) or tissue inhibitor of metalloproteinases (TIMP) secretion under the effect of the therapeutic product. TGF-β, MMP and TIMP secretion by the therapeutic cell product itself could be also indicative of fibroblast recruitment potential and serve as a surrogate endpoint.

3.8 Examples of potency assays for cell-based therapy products in the cardiovascular field

Among the most detailed potency assays for cell-based therapy products in the cardiovascular field are the one for Amorcyte, for MultiStem and for CardiAMP. Amorcyte, AMR001 is an autologous cell-therapy for the treatment of myocardial infarction (MI) based on CD34+CXCR4+cells. Several parameters were measured during phase I clinical, but only mobility in an SDF-1 gradient correlated to efficacy. Therefore, the MoA was thought to be product mobilization and migration to the damaged tissue along an SDF-1 gradient where administered cells facilitate tissue repair and vascular regeneration. As a result, an *in vitro* migration potency assay of CD34+CXCR4+cells in a defined SDF-1 gradient was used in later phases [297, 329]. MultiStem is another cell treatment for MI among other pathologies, but that uses allogeneic bone-marrow (BM) derived stromal cells. The main MoA is thought to be angiogenesis induction. The initial potency assay determined the minimum levels of VEGF, CXCL5 and IL-8 secreted by the cells that led to adequate tube formation, and finally secretion of these factors were replaced by their gene expression levels as surrogate markers [297, 329]. Recently, BioCardia has patented a new potency assay for their CardiAMP product, which consists in autologous bone marrow cells (BMCs) for the treatment of chronic myocardial ischemia or HF of ischemic origin. The potency assay, based on previous clinical trial results, defines a minimum number and proportion of CD19+, CD34+ and CD133+ cells in BMCs from the patient and before expansion to be related to efficacy [330]. Other potency assays and their corresponding validation have been investigated in the academy. One consists in a rapid cell invasion assay for identifying functional BMCs across Matrigel-coated transwells with an electric cell-substrate impedance sensing [331]. Other consists in an *in vitro* functional analysis for CPC-derived exosomes at GMP-Grade Manufacturing for evaluating their anti-apoptotic effect in CPC and HL-1 CMs and their pro-angiogenic activity through tube formation and amount of CD31 expression in endothelial cells [332].

3.9 Conclusions

The use of *in vivo* and some *in vitro* assays, although closer to the clinical scenario and more representative of the mechanism of action (MoA), commonly present high costs and are time consuming, making them unfeasible for mass production. The use of simple and easier to scale assays such as surrogates related to the specific MoA (i.e. as gene and protein expression or the secretion of specific factors) could be more practical. For cardiomyogenesis, potential to induce cardiomyocyte (CM) division or to differentiate into the CM lineage is proposed.

Expression of ion channels (sodium, calcium and potassium channels) and connexin 43 could be indicative of electromechanical maturation and coupling, whereas secretion of pro- and anti-inflammatory factors (TNF-α, IL-6 and IL-10) could determine immunomodulation. The anti-senescent and antiapoptotic potential of the product can be determined *in vitro* on CM and stromal cells, VEGF and specific cytokine secretion can be indicative of the angiogenic potential, and TGF-β, MMP and TIMP secretion of the antifibrotic potential. However, to develop these, or other scalable and accurate potency assays, further work is needed to validate that the potential surrogate measurements correlate to the efficacy of the product in patients.

Development of a potency assay for cell-based therapeutics in the cardiac field is now considered a priority by the regulatory agencies to optimize product efficacy in patients. Despite the challenges related with reference materials and the complexity of the biological treatments, all attempts should be made to develop robust and reproducible potency assays from early stages of product development. The potency assays should adequately reflect the product's relevant biological properties related to their expected MoA in the target cardiovascular disease.

Chapter 4

Exploring the determinants of rejuvenating potency of cardiosphere-derived cells: chronological vs. biological age

4.1 Abstract

Cardiosphere-derived cells (CDCs) have demonstrated to induce rejuvenation of the heart and to improve cardiac structure and diastolic function in old animals. However, the extent of the reparative effects of human CDCs seem to variate among different CDC-donors: younger donors are thought to generate more potent stem cells. While it is highly desirable to predict the *in vivo* efficacy at the early stages of product development to discard unsuitable donors, there is controversy on the relevance of donor and cell characteristics in determining cell potency. In this study we evaluated if the chronological age of the donor and/or cellular senescence of CDCs better predicts their potency. We focused specifically on the rejuvenating and pro-angiogenic potency and used CDC-derived extracellular vesicles (CDC-EVs) as therapeutic product. CDCs from 34 human donors (3 months to 81 years old, both sexes) were obtained and characterized. After CDC-EVs obtaining, we determined their rejuvenating and pro-angiogenic *in vitro* efficacy on different cell types relevant in heart physiology and pathology, and donor and CDC characteristics were correlated to their CDC-EVs potency. Ability to form cardiospheres and chronological age and sex of the donor did not relate to most CDC properties and did not determine CDC-EV rejuvenating and pro-angiogenic effect *in vitro*. CDC senescence related to other CDC bioactive properties, but this was insufficient to predict CDC-EV anti-senescence and pro-angiogenic *in vitro* potency. This study confirms that CDC-EVs have multiple rejuvenating and pro-angiogenic effects on different cell types involved in heart pathology and regeneration, but the extent is variable among donors and cannot be predicted by using chronological age of the donor or CDC senescence as surrogate markers. For determining cell potency, it is important to evaluate functionality relative to the expected mechanism of action, since merely cell identity and specific donor or cell characteristics may not translate into boosted efficacy for the treatment of a particular pathology.

4.2 Introduction

When moving stem cells as products from preclinical studies to the cardiac clinical scenario, hasty translation [283] led to underestimation of how cell heterogeneity and complexity could impact potency. Cell (and its derived products) potency has shown to depend on many other factors apart from cell identity, such as on the intended purpose and the expected MoA, the environment, the cell source, the age of the cells, the age of the donor and the intrinsic physiologically state of the tissue of origin [268, 276, 291, 333, 334]. Finding economic, feasible and efficient potency assays based on evidence of MoA for cell and cell-derived EVs still remains a challenge [110, 279, 291], and crucial for successful translation.

Despite most clinical trials used confirmation of cell identity as the single requirement right before product administration [291], the gold standard for cell potency assessment in cardiac applications is structural and functional recovery in a rodent model of myocardial infarction (MI) [268, 335]. However, this model is costly, time-consuming and of doubtful translation, hindering its use for routine testing [306]. *In vitro* functional assays do not reflect the complexity of living organisms, but they require less time and economic resources and can be representative of the MoA if properly validated. In fact, this type of assays is commonly used for elucidating mechanisms for cardiac repair behind cardiac stem cells and their derived EVs. Based on the expected MoA (pro-angiogenic and anti-senescent) feasible *in vitro* tests for CDCs and CDC-EVs for the treatment of cardiac aging could be their ability to induce tube formation and to prevent senescence in human cardiac stromal cells of different donors. Surrogates, usually referring to product characteristics, are further preferred to *in vitro* functional assays as they can be tested in early phases of product development and present less variability. Secretion of specific factors or miRNAs, or specific cell properties, are sometimes used as surrogate indicators of cell potency [291]. Nevertheless, little work exists to explore if these differences in cell characteristics or in secretome composition translate into enhanced functionality *in vitro* and *in vivo*.

Some of the explored CDC characteristics that seem relevant for their potency are: (i) the proportion of cells expressing specific surface markers, (ii) their ability to form cardiospheres, (iii) the chronological age of the donor and (iv) the cellular age. CDCs consistently express the stem factor CD105, and there are a variable proportion of cells expressing other surface markers: CD117+ (c-kit), CD90+ (Thy-1) and CD31+, while CD45+ remain minority as it is indicative of a cocktail of blood lineage markers [133]. CD105, CD117 and CD31+ are essential components of cardiospheres [134]. CD117 has been used as a marker of stem/progenitor cells in the heart [336] with regenerative potential, but there is controversy on whether it is related to other cell populations such as endothelial cells [337] or mast cells [338]. However, CDCs, with all the different subpopulations, have revealed superior paracrine function and improved functional

benefits vs. the CD117+ population and vs. the CD90+ populations alone. [132]. In addition, CD117 expression inside the CDC population seems not to be related to therapeutic efficacy in humans and depletion of CD117+ cells did not reduce the structural and functional benefits of CDCs in a mouse model of MI [339]. Nevertheless, CD90 expression seems to negatively correlate to CDC therapeutic efficacy in humans and its depletion to be beneficial for CDC potency *in vivo* [339]. The proportion of CD90+ has also been related to a reduced ability to form cardiospheres (less in number and in diameter), so cardiosphere number and size have also been associated with CDC potency in a mouse model of acute MI [334]. CD45+ cells, despite being residual in CDCs, have shown to be neither necessary nor sufficient for cardiosphere-formation. In fact, depletion of CD45+ cells increases the number of formed cardiospheres [340].

Whether chronological age of the donor is relevant to stem cell potency has been widely questioned in different scenarios. While some studies have concluded that chronological age was relevant to stem cell potency *in vitro* and *in vivo*, others have not observed significant differences. Stem-cell potency and aging considerably vary depending on the tissue source [341], the processing steps and the species used [342], therefore making extrapolation of results sometimes hard. In mesenchymal stem cells (MSCs) from murine origin, donor age has shown to be relevant in the angiogenic, regeneration and survival potential in a rodent hind limb ischemia model [343], in MSC proliferative and metabolism profiles [344], in the adipogenic, chondrogenic and osteogenic differentiation potential [345], and in their rejuvenating potential [173, 346]. These differences between chronologically young and aged MSCs in rodents seem to translate to their derived EVs cargo and potency [173, 346–352]. However, in MSCs from human origin, some studies concluded that age did not significantly affect MSCs properties and differentiation potential [269, 270], while others relate age with reduced therapeutic properties [271–273]. Regarding animal stem cells of cardiac origin, studies have reported differences in donor age potential. Cardiac explant-derived cells (EDCs) from old mice present increased cell senescence and secretion of senescence-associated cytokines and reduced cardiac repair potential [353]. Sca-1+CD31- subgroups from young mice presented higher differentiation into cardiac lineages and proliferation [354], reduced senescence and increased capacity to proliferate [355]. In CDCs from mice, the number of cells obtained, as well as the expression of CD117 and Sca-1 markers, proliferation, migration, clonogenicity and differentiation decreased with age [356]. In cardiac stem cells (CD117+) derived from human tissue, chronological age correlated to telomere dysfunction-induced foci and $p16^{INK4a}$ expression [357]. CD117+ Sca-1+ cells from donors over 70 years also have shown higher senescence-associated β-galactosidase (SA-β-gal), DNA damage γ-H2AX, senescence-associated secretory phenotype (SASP) and less ability to replicate and to differentiate [87]. CDCs from neonatal origin showed higher expression of ANG and VEGF, higher potential to differentiate into cardiomyocytes (CMs) and to improve left ventricular EF

(LVEF), reduce scar size and higher level of blood vessel preservation in infarcted rats [358]. Another more recent study showed that age did not significantly affect the quantity and quality of CDCs (in terms of SA-β-gal, the DNA damage marker γ-H2AX, the expression of VEGF, HGF, IGF-1, SDF-1, and TGF-β and *in vitro* angiogenesis) [274], but that SFRP1, a gene encoding a Wnt antagonist, was significantly up-regulated in CDCs from elderly patients (≥65 years old) and in CDCs whose senescent phenotype was induced [275].

Cellular aging is known to have a negative impact on cardiac function [359]. Cell senescence, as a way to measure cellular aging, alters negatively cell properties and secretome. Cellular senescence increases with the number of cell divisions. Therefore, it is affected by chronological age [342] and by the number of passages [333, 360]. Despite senescence being recommended as a cell quality marker for cell production [361], it is still not used on routinary analysis before cell product release [291]. Some studies have shown that senescence negatively impacts on cell reparative potency [87, 277] but it has been poorly explored as a marker of cell-derived EV potency. Highly senescent cells abundantly produce EVs [362–364]. In fact, the production of exosomes from MSCs increases by late passage cultures or senescent donors [364], probably through the p53/TSAP6 axis [365]. In addition, their cargo differs from non- (or less-) senescent cells [364, 366].

The objective of this study was to explore if the chronological age of the donor, cellular senescence of CDCs, the proportion of cells expressing specific surface markers or the ability to form cardiospheres could be used to predict CDC characteristics and CDC-EVs pro-angiogenic and rejuvenating potency *in vitro*.

4.3 Materials and Methods

4.3.1 CDCs and derived extracellular vesicle isolation

EVs were isolated from CDCs as described in detail by Smith et al. [133]. In brief, cardiac biopsies from patients undergoing cardiac surgery were processed through mechanical and enzymatic digestion to obtain explants of 1-2 mm size. The explants were cultured over fibronectin-coated plates in Iscove's Modified Dulbecco's Medium (IMDM) supplemented 20% with Fetal Bovine Serum (FBS). EDCs started leaving the explant and colonizing the plate after proximately 48 hours of culture, and they reached full confluency after approximately 16 days. Then, cells were transferred at a density of 25,000 cells/cm^2 to ultra-low-attachment Nunclon Plates (174932, Thermo Fisher Scientific, Waltham, MA, U.S.A) for 72 hours to allow them to form three-dimensional (3D) spheroids (cardiospheres), which are known to potentiate stemness and regenerative potential [133]. The cardiospheres were passaged to produce the CDCs and

their identity was confirmed by flow cytometry. When CDCs-P3 reached 80% confluence, the medium was changed to FBS-free IMDM, and left unchanged for 15 days to allow CDCs to secrete and concentrate EVs in the medium. Conditioned medium was filtrated using a 0.45-µm filter and ultraconcentrated using Centricon-Plus 70 Centrifugal Filter with 3-kDa cut-off frequency (Merck KGaA, Darmstadt, Germany). EVs were then analyzed by nano-particle tracking analysis (NTA, performed with NanoSight NS300 from Malvern Panalytical Ltd., Malvern, United Kingdom) and their protein content was determined with Bradford assay after EV lysis and protease inactivation. EVs were precipitated after incubation with 4% w/v polyethylene glycol (PEG) overnight at 4 ºC and centrifugation at 4 ºC at 1500x g for 30 min. For experiments, the precipitated EVs were resuspended in the corresponding medium at the specified dose.

4.3.2 Experimental protocol

With the aim of identifying markers that predict CDC potency, the experiments were divided in sections. First, CDCs from 34 human donors were obtained. During the obtainment, cells at the different stages (EDCs, cardiospheres and CDCs) were characterized. Finally, to match which characteristics determined *in vitro* potency, the efficacy of CDC-EVs of different donors was tested *in vitro* on different cell types relevant in heart physiology and pathology.

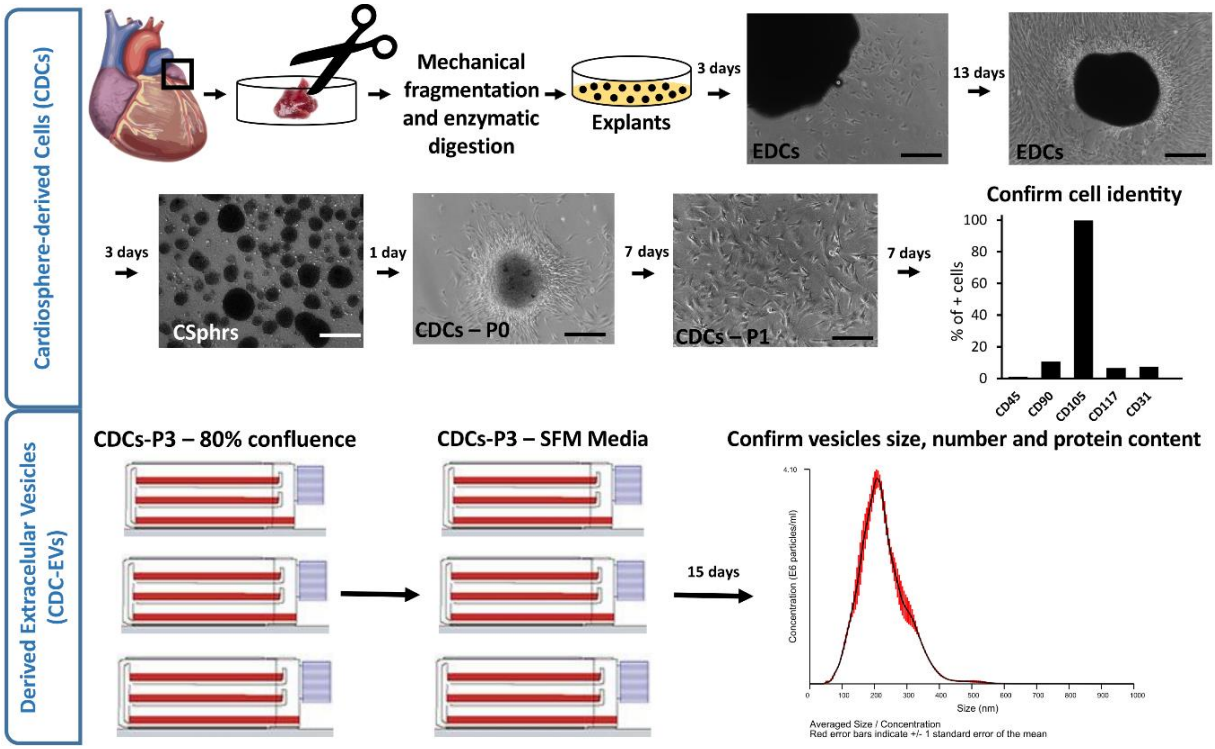

Figure 4.1. Methodology employed for cardiosphere-derived cell extracellular vesicle (CDC-EV) isolation. Cardiac biopsies from patients were immediately processed through mechanical and

enzymatic digestion to obtain explants of 1-2 mm. Explant-derived cells (EDCs) started leaving the explant and colonizing the plate after approximately 48 h of culture and reached full confluency after approximately 16 days. Then, the cells were transferred to ultra-low-attachment plates for 72 h to allow them to form three-dimensional (3D) spheroids (cardiospheres). Cardiospheres were passaged to produce the so-called cardiosphere-derived cells (CDCs-P0). Cell identity was confirmed by flow cytometry in CDCs-P1 cells. CDCs were further passaged until CDCs-P3 reached 80% confluence. At that point, the medium was changed to FBS-free IMDM, and left unchanged for 15 days to allow CDCs to secrete and concentrate EVs in the medium. Conditioned medium was filtrated and ultraconcentrated and EVs were precipitated and further resuspended. Quantification was performed through nanoparticle tracking analysis (NTA). Average particle size was 200 nm and maximum particle size 450 nm [293]. Scale bars correspond to 200 μm.

4.3.2.1 Product obtainment

Heart biopsies were collected from 34 patients who underwent cardiac surgery for other reasons. Patients of both sexes and different ages (including pediatric and adult) were included. Donor age and sex distribution are detailed in Table 4.1 and Figure 4.2. EDCs, cardiospheres, CDCs and CDC-EVs were subsequently obtained following the procedure described in section 4.3.1 (Figure 4.3).

	Males	Females	Total
PEDIATRIC (< 14 years)	8	6	14
ADULTS	9	11	20
TOTAL	17	17	**34**

Table 4.1. Cardiac biopsies donor distribution by age group and sex.

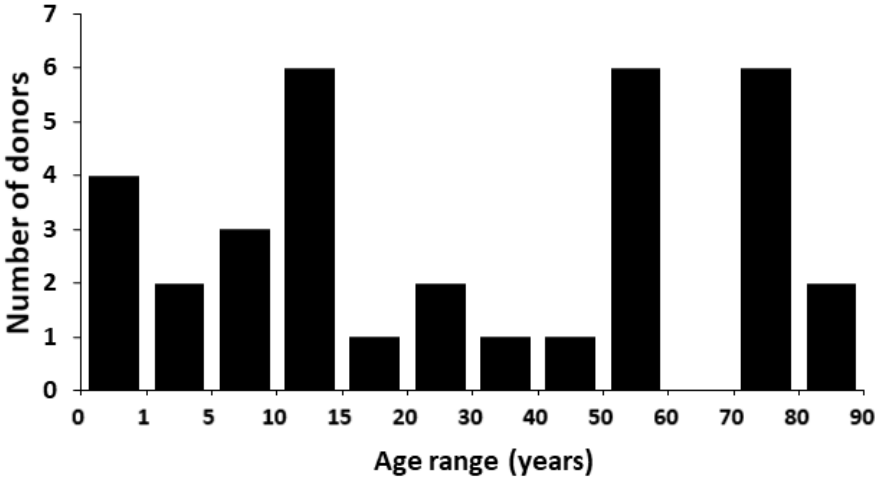

Figure 4.2. Cardiac biopsies donor distribution by age.

4.3.2.2 Product characterization

During the different stages of product (CDC-EVs) development, involved cells were characterized in terms of their genetic expression profile, their biological age and/or their activity. The characterization methods employed in the different stages of product development are summarized in Figure 4.3. In particular, cellular age in EDCs from passage 1 (from 18 patients) was measured by the percentage of senescent cells and the expression of some senescence-related genes (*CDKN1A, CDKN2A,* and *TP53*) as illustrated in Figure 4.3b. The expression of other genes related to stemness, fibrosis and the secretion of relevant factors for cardiac regeneration and repair was also investigated (*NANOG*, *hTERT*, *GATA4, MEF2C, TGFB1, VEGFA, IGF1, IGF1R, HGF, SOD1, SOD2*). The size of the 10 largest cardiospheres formed by the cells of the 34 patients was also recorded (Figure 4.3c). CDC-P2 identity was confirmed by expression of specific surface markers using flow cytometry (99.0 ± 0.2% CD105+ cells, 8.7 ± 1.6% CD117+ cells, 36.9 ± 3.8% CD90+ cells, 7.2 ± 1.5% CD31+ cells and 1.3 ± 0.2% CD45+ cells), and CDC-P2 biological age was characterized by the percent of senescent cells in all donors and by telomere length in 16 donors. Additional CDC-P2 characteristics explored in these 16 donors included proliferation, DNA synthesis, migration and VEGF-A secretion (Figure 4.3d). The protocols followed for each of the characterization tests are explained in detail in the following sections.

4.3.2.3 Product bioactivity evaluation

The reparative efficacy of the CDC-EVs derived from different donors with low senescent and highly senescent CDCs-P3 was evaluated *in vitro* on cardiac progenitor cells (CPCs, CDCs), CMs (HL-1), cardiac stromal cells (CSCs, EDCs) and endothelial cells (ECs, Human Umbilical Vein Endothelial Cells, HUVEC). CDC-EV anti-senescent potency was tested in the different cell types. While proliferation and DNA synthesis improvement induced by CDC-EVs was explored in CPCs and CSCs, CDC-EV ability to prevent apoptosis was studied in CMs and their pro-angiogenic potency was determined by the enhancement in endothelial tube formation and endothelial VEGF-A secretion. In addition, CDC-EV effects on preventing DNA damage and pro-inflammatory factor secretion (TNF-α) were investigated in CSCs. The scheme summarizing the explored CDC-EVs therapeutic effects in the different cell types is shown in Figure 4.4.

Bioactivity experiments using CDCs as targets were first used to confirm CDC reparative potency is exerted by paracrine activity (Figure 4.4a). CPCs, CDCs-P1 from three different donors with a moderate to high proportion of senescent cells were chosen as target cells and plated in complete medium at 13,000 cells/cm^2 in fibronectin pre-coated 12-well plates for senescence experiments and at 9,000 cells/cm^2 for proliferation and DNA synthesis experiments.

CDCs-P1 from four donors with a low to moderate proportion of senescent cells were chosen as treatment and seeded in 12-well ® (3460, Corning®) at 80,000 cells/cm^2 (for senescence experiments) and 35,500 cells/cm^2 (for proliferation and DNA synthesis experiments) as well as in standard 12-well plates at 13,000 cells/cm^2 for controls. After 24 hours, target CDCs were imaged, washed in Phosphate Buffered Saline (PBS), and cultured during 72 hours in FBS-free IMDM in the presence of the transwells seeded with the target cells from different donors or in absence of treatment cells (controls) as shown in Figure 4.4a. After these 72 hours of co-culture, target CDCs and treatment CDCs in the 12-well plates were imaged and fixed for senescence, proliferation and DNA synthesis quantification as explained in the following sections (sections 4.3.5.1, 4.3.9 and 4.3.5.2 respectively). Each condition was run in triplicate.

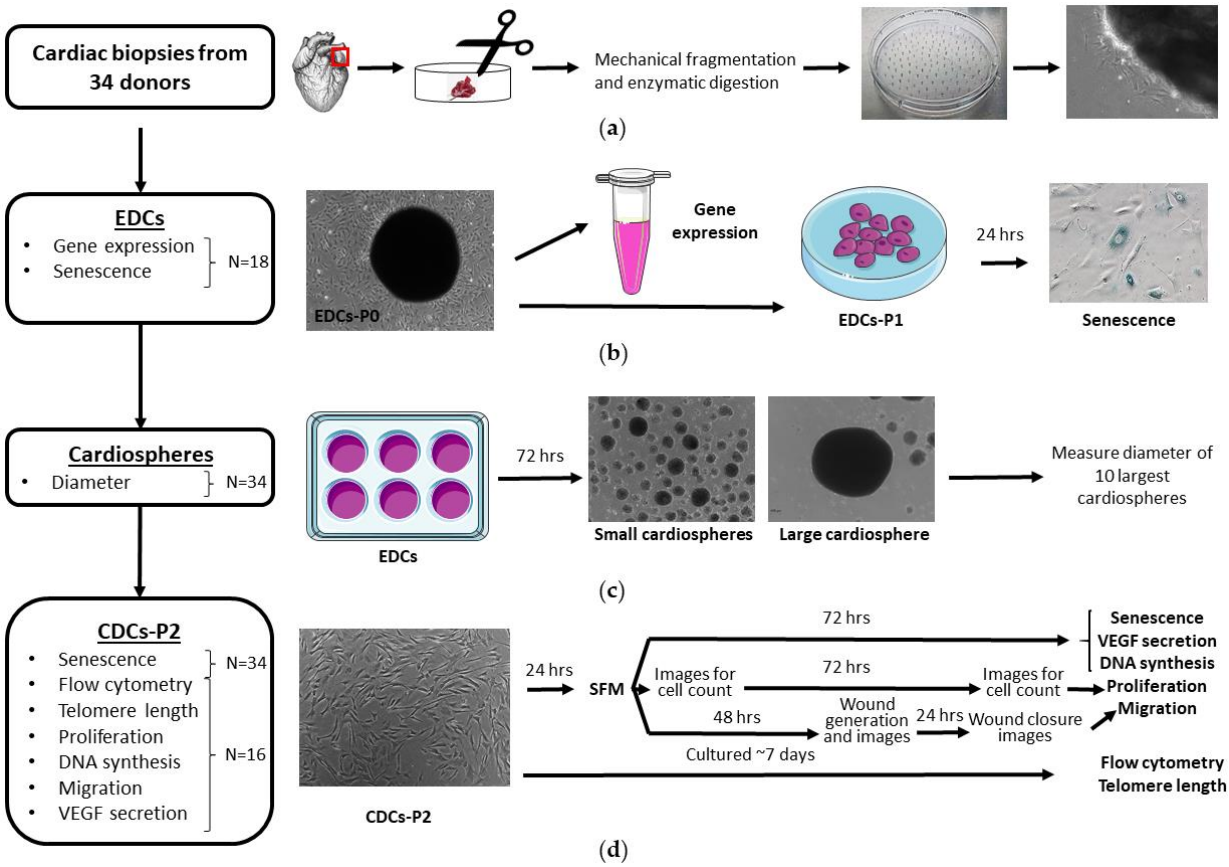

Figure 4.3. Procedure followed for explant-derived cells (EDCs), cardiosphere and cardiosphere-derived cells (CDCs) characterization. (**a**) Cardiac biopsies were collected from 34 patients who underwent cardiac surgery for other reasons. The biopsies were processed according to the protocol previously described (section 4.3.1) to obtain EDCs. (**b**) EDCs from 18 donors were characterized in terms of their relative gene expression (section 4.3.4) and senescence after 24 hours of culture (section 4.3.5.1). (**c**) Cardiospheres from the 34 donors formed after 72 hours were imaged and the diameter of the 10 largest measured (section 4.3.6). (**d**) CDCs were characterized in terms of their identity (flow cytometry, section 4.3.7), their biological age

(senescence, section 4.3.5.1, and telomere length, section 4.3.8), and proliferation (section 4.3.9), DNA synthesis (section 4.3.5.2), migration (section 4.3.10) and VEGF-A secretion (section 4.3.11.1).

CDC-EV anti-senescent and anti-apoptotic effects in CMs were studied *in vitro* on the HL-1 cell line (Figure 4.4b). HL-1 cells were plated in complete Claycomb medium at 10,500 cells/cm^2 in pre-coated 12-well plates and in triplicate for each of the apoptosis and senescence experiments. After 24 hours, HL-1 plates were washed in PBS and FBS-free Claycomb medium alone, or with CDC-EVs from two different donors at a dose of 300 μg/1·10^6 cells (42 μg/well), added. After another 24 hours, H_2O_2 was added to the HL-1 plates for a final concentration of 200 μM to induce apoptosis [367]. After 6 hours, the cells were fixed for senescence detection and apoptosis quantification as explained in the following sections (4.3.5.1 and 4.3.5.2).

The anti-senescent, pro-proliferative and DNA protective effect of CDC-EVs on CSCs was tested *in vitro* on EDCs-P2 from one donor with a moderate proportion of senescent cells (Figure 4.4d). EDCs-P1 were plated in complete IMDM medium at 13,000 cells/cm^2 in fibronectin pre-coated 12-well plates for senescence and DNA synthesis experiments, at 26,000 cells/cm^2 for DNA damage and TNF-α secretion, and at 4,200 cells/cm^2 in 6-well plates for proliferation experiments. After 24 hours, EDCs for the proliferation experiment were imaged and all EDCs were washed in PBS and cultured in FBS-free IMDM alone or with CDC-EVs from two different donors at a dose of 300 μg/1·10^6 cells. After another 24 hours, cells for DNA synthesis and TNF-α secretion studies were replaced with 500 μl of FBS-free IMDM and the rest were left untouched. After another 48 hours, EDCs for proliferation were imaged, media from EDCs for TNF-α secretion collected, and EDCs for senescence, DNA synthesis and DNA damage quantification fixed as explained in the following sections (4.3.11.2, 4.3.5.1 and 4.3.5.2). Each condition was run in triplicate.

HUVEC were used to test the CDC-EV anti-senescent and pro-angiogenic effect in ECs (Figure 4.4c). For senescence and VEGF-A secretion, HUVEC-P5 were plated at 21,000 cells/cm^2 in complete medium (M-200 supplemented with large vessel endothelial supplement, LVES) in 12-well plates and in triplicate for each condition. After 24 hours, the plates were washed in PBS and 500 μl of LVES-free M-200 alone or with CDC-EVs from two different donors (at a dose of 300 μg/1·10^6 cells, 25 μg/well) were added. After another 18 hours, the secretome was collected and analyzed with an VEGF-A ELISA as explained in section 4.3.11.1. The cells were fixed for senescence detection as later described (section 4.3.5.1). For endothelial tube formation, 87,500 HUVECs-P5 were resuspended in 500 μl of FBS-free M-200 (negative control), in M-200 with FBS (positive control) or in FBS-free M-200 with CDC-EVs from four different donors (two low senescent and two highly senescent) at 300 μg/1·10^6 cells and plated

on Geltrex-precoated 12-well plates in triplicate for each condition. After 15 hours of incubation, tube formation was imaged. Further details are provided on the 4.3.12 Tube formation section.

After exploring the effects of CDC-EVs from selected low senescent and highly senescent CDCs in the different cell types, the anti-senescent and pro-angiogenic potency of CDC-EVs from 18 donors was evaluated in CSCs and ECs to confirm if chronological age, cardiosphere size, EDC or CDC senescence could be used as surrogate markers of *in vitro* potency.

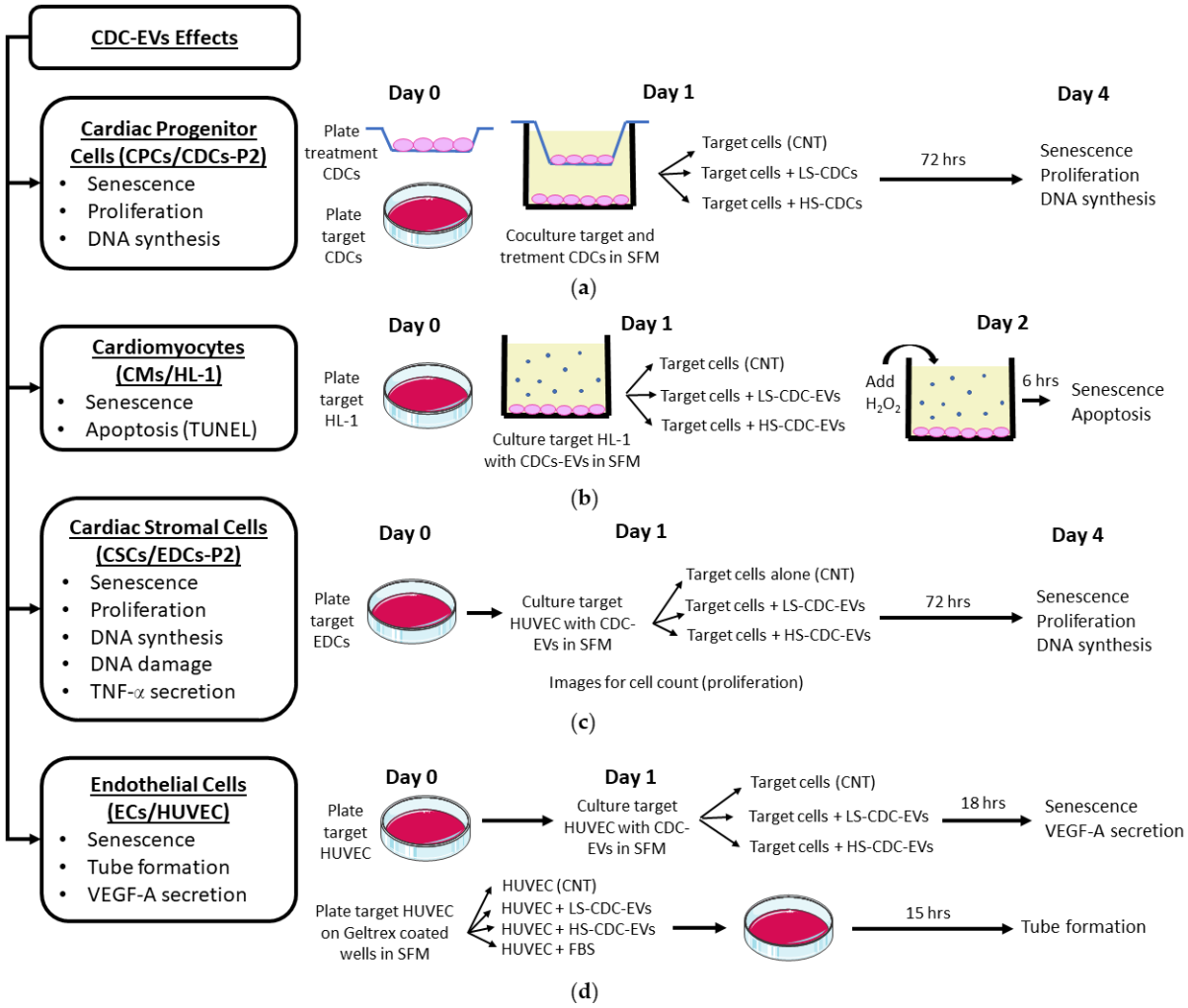

Figure 4.4. Procedure followed for evaluating the CDC-EV bioactivity in different cell types present in the heart. (**a**) Procedure followed for evaluating the anti-senescent and pro-proliferative potential of CDC-EVs on cardiac progenitor cells (CPCs). (**b**) Procedure followed for evaluating the anti-senescent and anti-apoptotic potency of CDC-EVs on cardiomyocytes (CMs). (**c**) Procedure followed for evaluating the anti-senescent, pro-proliferative and protective potency of CDC-EVs on cardiac stromal cells (CSCs). (**d**) Procedure followed for evaluating the anti-senescent and pro-angiogenic potency of CDC-EVs on endothelial cells (ECs).

4.3.3 Cell culture

All cell lines were cultured and passaged according to published manuals. Cultured cells were kept incubated at 37 °C, 5% CO_2, 21% O_2 and 90% humidity. When cells reached confluency, the cells were detached using TryPLE™ Select (12563, Gibco) instructions and replated in complete medium or frozen (on CryoStor®, C2894, Sigma-Aldrich, at -180 °C).

4.3.3.1 EDCs and CDCs

EDCs and CDCs were obtained and cultured following procedures previously published [133, 293]. When cultured and passaged, EDCs and CDCs were seeded over fibronectin coated plates (341631, Sigma-Aldrich, diluted to 12.5 μg/ml in PBS) at a density of 2,000 cells/cm^2 and maintained in IMDM (SH30228, Hyclone) supplemented 20% with Fetal Bovine Serum (FBS, F524, Sigma-Aldrich), 1% penicillin/streptomycin (PS, 15140, Gibco) and 0.1% 2-mercaptoetanol (31350, Gibco). EDCs and CDC cells reached confluency after approximately 7 days when cultured under these conditions. When doing experiments and obtaining CDC-EVs, the cells were cultured in FBS-free IMDM, keeping the other supplements (PS and 2-mercaptoetanol).

4.3.3.2 HL-1

HL-1 cells were passaged and cultured following procedures previously published [368]. HL-1 cells were seeded over gelatin/fibronectin coated plates (at 0.02%, G1393, Sigma-Aldrich and at 5 μg/ml in H_2Od, 341631, Sigma-Aldrich respectively) at a density of 15,000 cells/cm^2 and maintained in Claycomb Medium (51800C, Sigma-Aldrich) supplemented 10% with FBS (F524, Sigma-Aldrich), 1% PS and 1% GlutaMAX™ (35050, Gibco). HL-1 cells reached confluency after approximately 7 days when cultured under these conditions. When doing experiments in HL-1 with the CDC-EVs, the cells were cultured in FBS-free Claycomb, keeping the addition of the other supplements.

4.3.3.3 HUVEC

HUVEC (C0035C, Gibco) were passaged and cultured following supplier's instructions. HUVEC were plated over plates at a density of 2,500 cells/cm^2 and maintained in M-200 (Gibco) supplemented with Large Vessel Endothelial Supplement (LVES, A1460801, Gibco) or with the Low Serum Growth Supplement (LSGS) kit (S003K, Gibco). HUVEC reached 80% confluency after approximately 6 days when cultured under these conditions. When doing experiments in HUVEC with the CDC-EVs, the cells were cultured in FBS-free M-200 (unless specified), keeping the addition of the other supplements in the LSGS kit.

4.3.4 Gene expression analysis

EDCs-P0 from 18 donors were characterized in terms of the relative gene expression of specific genes involved in stemness, fibrosis, the secretion of relevant factors and senescence. The genes under study were: *NANOG*, *hTERT* and *GATA4, MEF2C, TGFB1, VEGF, IGF1, IGF1R, HGF, SOD1, SOD2, CDKN1A, CDKN2A,* and *TP53*. RNA from 300,000 pelleted EDCs-P0 was isolated using QIAzol Lysis Reagent instructions (QIAGEN, Venlo, The Netherlands) and relative gene expression quantification was performed with a two-step Real-Time Polymerase Chain Reaction (RT-PCR, in a MyCycler™ Thermal Cycler System, Bio-Rad Laboratories, Hercules, CA, U.S.A). One microgram of total RNA was reverse-transcribed into complementary DNA (cDNA) using the iScript™ cDNA Synthesis Kit (1708890, Bio-Rad Laboratories) and random hexamer primers in 20-µl reactions, following the manufacturer's instructions. cDNA obtained was diluted 1:20 and gene expression quantification was performed in a CFX RT-PCR Detection System (Bio-Rad Laboratories) using a 96-well plate and each sample was analyzed in triplicate. PCR amplifications were done with 2 µl of diluted cDNA using SYBR® Green chemistry (172-5124 Bio-Rad Laboratories) and specific primer pairs (Table 7.1) in a final volume of 20 µl. RT-qPCR efficiency for each assay was controlled using relative standard curves generated from a pool of cDNA. Ct data was collected and analyzed applying the $2^{-\Delta\Delta Ct}$ method for relative quantification using the sample with the highest expression as calibrator. Gene expression normalization factor was calculated for each sample based on the geometric mean of *GADPH* and *18S* reference genes in geNorm [369]. Specific primer pairs are detailed in Table 4.2.

Gene	Protein	Forward primer (5'-3')	Reverse primer (5'-3')	Exons	Protein Coding Transcript
NANOG	Homeobox protein NANOG	AATACCTCAGCCTCCAGCAGATGC	AGTAAAGGCTGGGGTAGGTAGGTGC	2-4 4-6	ENST00000229307.9 ENST00000541267.5
hTERT	Telomerase reverse transcriptase	GGTGGCACGGCTTTTGTTCAGATG	TTCAGCCGCAAGACCCCAAAGAG	11-12	ENST00000310581.10
GATA4	Transcription factor GATA-4	AGCAGCTTCTGCGCCTGTGG	TGGGGGCAGAAGACGGAGGG	2 3 2 3 3	ENST00000532059.6 ENST00000622443.3 ENST00000335135.8 ENST00000532977.1 ENST00000526974.1
MEF2C	Myocyte-specific enhancer factor 2C	TCCTGCAAATATGGCCCTAG	CCTGACACACCGGGATTGTT	12 11 11 11 11 12 11 11 10 11	ENST00000340208.9 ENST00000504921.7 ENST00000437473.6 ENST00000625585.2 ENST00000424173.6 ENST00000636998.1 ENST00000514028.5 ENST00000637732.1 ENST00000510942.5 ENST00000506554.5
TGFB1	Transforming growth factor beta-1 proprotein	AACCGGCCTTTCCTGCTTCTCA	TGCGTGTCCAGGCTCCAAATGTAG	5-7	ENST00000221930.6

VEGFA	Vascular endothelial growth factor A	TCTTCAAGCCATCCTGTGTG	TGCATTCACATTTGTTGTGC	3-4	ENST00000672860.2
				3-4	ENST00000372067.8
				3-4	ENST00000372064.9
				3-4	ENST00000372077.8
				3-4	ENST00000425836.7
				3-4	ENST00000372055.9
				3-4	ENST00000520948.5
				3-4	ENST00000413642.8
				3-4	ENST00000482630.7
				3-4	ENST00000417285.7
				3-4	ENST00000230480.10
				3-4	ENST00000324450.11
				3-4	ENST00000523950.5
				3-4	ENST00000523873.5
				3-4	ENST00000518689.5
				3-4	ENST00000518824.5
				3-4	ENST00000523125.5
				3-4	ENST00000457104.6
				3-4	ENST00000519767.5
IGF1	Insulin-like growth factor I	GCTGGTGGATGCTCTTCAGT	ACTCATCCACGATGCCTGTC	2-3	ENST00000307046.8
				3-4	ENST00000392904.5
				2-3	ENST00000392905.7
				2-3	ENST00000337514.11
				3-4	ENST00000644491.1
				2-3	ENST00000424202.6
IGF1R	Insulin-like growth factor 1 receptor	CTCATGCCTTGGTCTCCTTGTCCT	CGTCACTTCCTCCATGCGGTAAAT	5-6	ENST00000650285.1
				5-6	ENST00000649865.1
				4-5	ENST00000558898.1
HGF	Hepatocyte growth factor	AGCATGTCCTCCTGCATCTC	TGGTTTTTATCTTCAGTGCTGG	1-2	ENST00000222390.11
				1-2	ENST00000457544.7
				1-2	ENST00000444829.7
				1-2	ENST00000453411.6
				1-2	ENST00000423064.7
				1-2	ENST00000465234.2
				1-2	ENST00000354224.10
				1-2	ENST00000643024.1
				2-3	ENST00000412881.5
				2-3	ENST00000421558.1
SOD1	Superoxide dismutase [Cu-Zn]	CTAGCGAGTTATGGCGACGA	TAATGCTTCCCCACACCTTC	1-2	ENST00000270142.11
				1-2	ENST00000389995.4
SOD2	Superoxide dismutase [Mn], mitochondrial	CGTCACCGAGGAGAAGTACC	TGACCACCACCATTGAACTT	2-3	ENST00000538183.7
				2-3	ENST00000367055.8
				2-3	ENST00000545162.5
				2-3	ENST00000535561.5
				4-5	ENST00000546087.5
				2-3	ENST00000444946.6
				2-3	ENST00000537657.5
CDKN1A	Cyclin-dependent kinase inhibitor 1 (p21)	TCCAGCGACCTTCCTCATCCAC	TCCATAGCCTCTACTGCCACCATC	3	ENST00000244741.10
				3	ENST00000405375.5
				4	ENST00000448526.6
				3	ENST00000615513.4
CDKN2A	Cyclin-dependent kinase inhibitor 2A (p16)	CCCGTGGACCTGGCTGAG	TGATGATCTAAGTTTCCCGA	2-4	ENST00000498124.1
				2-3	ENST00000304494.10
				2-3	ENST00000579122.1
				2-3	ENST00000579755.2
				2-3	ENST00000530628.2
				3-4	ENST00000494262.5
				2-3	ENST00000498628.6
				1-2	ENST00000578845.2

TP53	Cellular tumor antigen p53	CTCCCCTGCCCTCAACAAGA	CCAACCTCAGGCGGCTCATA	5-7 5-7 4-6 5-7 5-7 5-7 4-6 5-7 5-7 5-7 4-6 1-3 1-3 1-3 1-3 2-4 1-3 1-3 4-6	ENST00000635293.1 ENST00000269305.9 ENST00000445888.6 ENST00000610292.4 ENST00000620739.4 ENST00000619485.4 ENST00000455263.6 ENST00000359597.8 ENST00000420246.6 ENST00000610538.4 ENST00000622645.4 ENST00000413465.6 ENST00000504937.5 ENST00000619186.4 ENST00000504290.5 ENST00000510385.5 ENST00000509690.5 ENST00000610623.4 ENST00000508793.5
GAPDH	Glyceraldehyde-3-phosphatase dehydrogenase	GTGGACCTGACCTGCCGTCT	GGAGGAGTGGGTGTCGCTGT	8 8 7 7 6 8	ENST00000229239.10 ENST00000396861.5 ENST00000396859.5 ENST00000396858.5 ENST00000619601.1 ENST00000396856.5
18S rRNA		CGGCGACGACCCATTCGAAC	GAATCGAACCCTGATTCCCCGTC		

Table 4.2. Primers used for RT-PCR in EDC characterization

4.3.5 Histochemistry

4.3.5.1 Senescence

Unless otherwise stated in the experimental protocol section, to estimate the percentage of senescent cells, cells were plated in complete medium at 13,000 cells/cm^2 in fibronectin pre-coated 12-well plates. After 24 hour-incubation, wells were washed and replaced with FBS-free medium (containing the resuspended CDC-EVs if applicable). After another 72 hour-incubation, the cells were fixed using Abcam's Senescence Detection Kit (ab65351, abcam, Cambridge, UK), which is used to detect SA-β-Gal activity in cultured cells. The samples were prepared, fixed and stained following the assay protocol (with overnight incubation). After staining, samples were washed and kept in 70% glycerol (G5516, Sigma-Aldrich) in PBS at 4 ºC. As SA-β-Gal positive cells develop a blue color, a total of around 10 images at 20x (around 650 cells) per well were taken with a Leica DMI3000B optical microscope and Leica DFC310 FX camera (Wetzlar, Germany), and manually classified as senescent (blue) or non-senescent using ImageJ Software.

4.3.5.2 Immunocytochemistry

Cell cultures for immunocytochemistry analysis were washed in PBS and fixed in 4% formaldehyde for at least 24 hours.

DNA synthesis

For analyzing DNA synthesis, fixed cells were washed three times in PBS and permeabilized with 0.1% Triton-X (X100, Sigma-Aldrich) in PBS for 30 min at room temperature (RT). They were later kept 1 hour at RT with Dako protein block (X0909, Dako), and overnight incubated in the Ki-67 primary antibody (ab15580, abcam) at a dilution of 1:400 in Dako protein block and 4 ºC in a humid chamber. After three 10 min washes, the samples were left in Alexa Fluor Goat anti-rabbit 488 nm antibody (10236882, Thermo Fisher Scientific, Waltham, MA, U.S.A) at 1:400 in Dako protein block 1 hour at RT, washed twice, incubated in DAPI (D8417, Sigma-Aldrich) at 1:5000 in PBS 10 min at RT, washed twice and kept in PBS at 4 ºC until imaging. Around 10 images at 10x per well (800-1200 cells) were acquired with the Leica DMI3000B optical microscope and Leica DFC310 FX camera (Wetzlar, Germany), and analyzed using ImageJ Software.

DNA damage

For analyzing DNA damage, fixed cells were processed and analyzed as indicated in the previous section (DNA synthesis) with some exceptions. The primary antibody used was the γ-H2AX (ab11174, abcam, Cambridge, U.K.) at 1:500 in Dako protein block for 1 hour at RT, while the secondary antibody was the Alexa Fluor Chicken anti-rabbit 594 nm (10759174, Thermo Fisher Scientific, Waltham, MA, U.S.A) at 1:400 in Dako protein block 1 hour at RT.

Apoptosis

Apoptosis was induced by incorporating H_2O_2 to the culture medium to a final concentration of 200 μM [132, 367]. After 6 hours, the cells were fixed and stained following the In situ Cell Death Detection Kit from Roche (11684795910, Basilea, Switzerland). The fixed samples were washed three times in PBS and permeabilized with 0.1% Triton-X in PBS for 30 min at RT. They were later kept 1 hour at RT with Dako protein block and incubated with the TUNEL reaction mixture in a humid chamber for 1 hour at 37 ºC. After two washes, the samples were incubated in DAPI at 1:5000 in PBS 10 min at RT, washed twice and kept in PBS at 4 ºC until imaging. Around 10 images at 20x per well (1200-1600 cells) were acquired with the Leica DMI3000B optical microscope and Leica DFC310 FX camera (Wetzlar, Germany), and manually analyzed using ImageJ Software.

4.3.6 Cardiosphere diameter

EDCs-P0 from 34 donors were transferred at a density of 25,000 cells/cm^2 to six ultra-low-attachment Nunclon Plate-wells for 72 hours to allow them to form 3D spheroids (cardiospheres). The 10 largest cardiospheres from each donor were imaged at 5x with the Leica

DMI3000B optical microscope and Leica DFC310 FX camera (Wetzlar, Germany), and their diameter measured using ImageJ Software.

4.3.7 Flow cytometry

For flow cytometry, 150,000 CDCs-P1 from 16 donors were plated in a 100 mm dish and cultured until full confluency (around one week) in complete medium. Cells were detached using TryPLE™ Select (12563, Gibco) instructions, counted (around 500,000) and resuspended in 500 µl of PBS. Corresponding antibodies (CD105 PE, CD117 APC, CD90 FITC, CD31 PerCP and CD45 Vioblue from Miltenyi Biotec) were added to the cell suspension and incubated during 15 min at RT in the absence of light. Immunofluorescence was quantified with a MACSQuant (Miltenyi-Biotech, Bergisch Gladbach) cytometer and data analyzed using Macs Quantify software. The average percentage of CDC-P2 from the different donors expressing each of the explored surface markers is summarized in Figure 4.5. 99.0 ± 0.2% CD105+ cells, 8.7 ± 1.6% CD117+ cells, 36.9 ± 3.8% CD90+ cells, 7.2 ± 1.5% CD31+ cells and 1.3 ± 0.2% CD45+ cells, in concordance to the population of CDCs described by other groups [133, 134, 370]. The markers expressed by each of the corresponding subpopulations in the CDC mixture are indicated in Table 4.3.

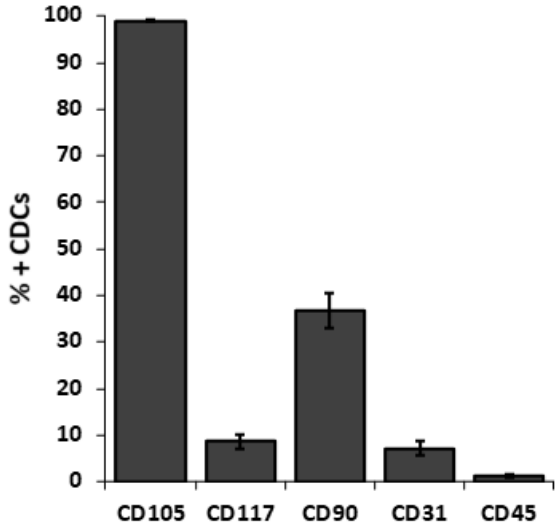

Figure 4.5. Percentage of CDCs expressing CD105, CD117, CD90, CD31 and CD45 by flow cytometry (*n* = 18 donors).

Surface Antigen	Expressed by
CD105	Regulatory component of the TGF- β receptor complex. Important in angiogenesis [371] and hematopoiesis [372]
CD117	Stem cell factor, c-kit
CD90	MSCs or cardiac fibroblasts, thy-1

CD31	Endothelial cells
CD45	Bone-marrow derived or endothelial progenitor stem cells. Hematopoietic progenitors

Table 4.3. Surface markers characteristic of each subpopulation of cells inside the CDC mixture.

4.3.8 Telomere length

CDC-P2 nucleus telomere length was analyzed with the Telomere PNA FISH Kit/Cy3 (K5326, Dako, Agilent, Santa Clara, CA, U.S.A). 150,000 CDCs-P1 from 16 donors were plated in a 100 mm dish and cultured until full confluency (around one week) in complete medium. Cells were detached using TryPLE™ Select (12563, Gibco) instructions, counted (250,000 - 500,000), pelleted and resuspended in 9 ml of KCl 75 mM in H_2Od. After 30 min incubation at 37 ºC, nuclei were fixed and washed in Carnoy's solution (methanol and acetic acid 3:1) and stored at 4 ºC until hybridation. Fixed nuclei were pre-treated, denatured and hybridized, washed and counterstained following the kit instructions and stored at -20 ºC until imaging. A minimum of 50 nuclei from each donor were imaged at 63.5x keeping the same image parameters with a confocal scanning inverted AOBS/SP2-microscope (Leica Microsystems, Wetzlar, Germany) and analyzed using ImageJ software. After background subtraction, nuclei were segmented in the corresponding DAPI image. The mean intensity value of each segmented nucleus was calculated in the Cy3 image, as the length of the telomeres is directly correlated to the fluorescence intensity of the spots [373].

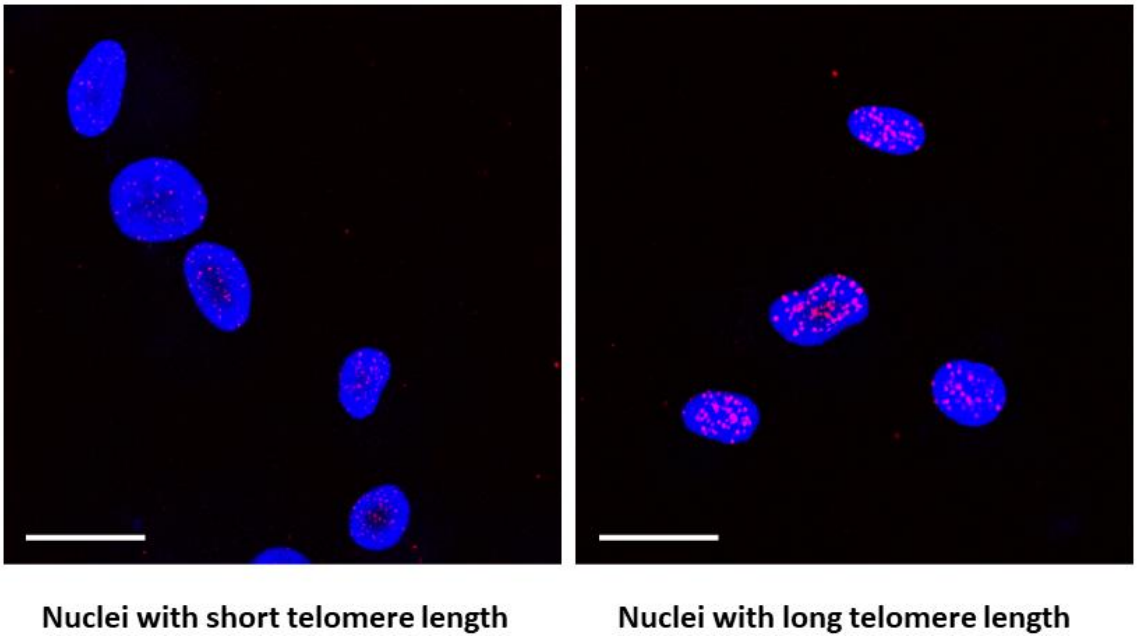

Figure 4.6. CDC nuclei from two different donors after merged DAPI and Telomere PNA FISH Kit/Cy3 staining. First image shows nuclei with shorter telomere length with respect to the

second image, as length of the telomeres is directly correlated to the fluorescence intensity of the red spots. Scale bar corresponds to 25 μm.

4.3.9 Proliferation

Target EDCs or CDCs-P1 from 16 donors were plated at 4,200 cells/cm^2 in 6-well plates (3 wells per condition/donor) in complete medium. After 24 hours (time 0), each well was washed with PBS, changed to FBS-free medium, an imaged at eight random locations previously marked at 5x with the Leica DMI3000B optical microscope and Leica DFC310 FX camera (Wetzlar, Germany). After another 72 hours, wells were imaged at the exact same locations with the same parameters. Cells in each image were manually counted using ImageJ, and Population Doubling Time (PDT) at each location was calculated according to Equation 1. Average PDT was obtained from the PDT at each of the 24 locations.

$$PDT = (t_2 - t_1) * \frac{\log(2)}{\log(q2) - \log(q1)}$$

Equation 1. Population Doubling Time. $t_2 - t_1$ is equal to the elapsed time, in this case 3 days. $q2$ is the final number of cells, in this case, after the 72 hours. $q1$ is the initial number of cells.

4.3.10 Migration

CDCs-P1 were plated at 57,000 cells/cm^2 in 12-well plates (3 wells per donor) in complete medium. After 24 hours, wells were washed, changed to FBS-free medium and incubated for 48 hours. Wounds were generated using a 1000 μl pipette tip, washed, and imaged at 5x in five different marked locations per well with the Leica DMI3000B optical microscope and Leica DFC310 FX camera (Wetzlar, Germany). After 24 hours, wounds were imaged at the same locations. Images were processed in ImageJ to determine the percentage of wound closure. First, the wound area at the time of wound generation (time 0) was determined. Then, cells in that same area were segmented in the image taken at the same location after 24 hours. The percentage of wound closure was calculated at each location as the area of the segmented cells divided by the total area of the wound. The average percentage of wound closure for CDCs of each donor was obtained by averaging the value in the 15 locations.

4.3.11 Factor secretion - ELISA

4.3.11.1 VEGF-A

To characterize CDC VEGF section, CDCs-P1 from 16 different donors were plated in triplicate at 28,500 cells/cm^2 in 12-well plates in complete medium. After 24 hours, each well was

washed with PBS and incubated with 600 µl of FBS-free media for 72 hours. After this time, the conditioned media was collected and the VEGF secretion analyzed following the VEGF enzyme-linked immunosorbent assay (ELISA) kit instructions from Enzo Life (156-0001, Enzo Life Sciences, Farmingdale, NY, U.S.A).

To study the effect of CDC-EVs on endothelial VEGF-A secretion, HUVEC-P5 were plated at 21,000 cells/cm^2 in complete medium in 12-well plates and in triplicate for each condition. After 24 hours, the plates were washed in PBS and 500 µl of FBS-free M-200 alone or with CDC-EVs from two different donors added. After another 18 hours, the secretome was collected and analyzed with an VEGF-A ELISA kit (ELH-VEGF kit, RayBiotech, Inc., Parkway Lane, GA, U.S.A).

4.3.11.2 TNF-α

EDCs-P1 were plated in complete medium at 26,000 cells/cm^2 in 12-well plates and in triplicate for each condition. After 24 hours, EDCs were washed in PBS and cultured in FBS-free IMDM alone or with CDC-EVs from two different donors. After another 24 hours, the medium was replaced by 500 µl of FBS-free IMDM. After 48 hours, conditioned media was collected, and TNF-α concentration determined using the TNF-α ELISA kit from Enzo Life (ADI-900-099, Enzo Life Sciences, Farmingdale, NY, U.S.A).

4.3.12 Tube formation

Ability of CDC-EVs to induce endothelial tube formation was tested on HUVECs-P5. 12-well plates were coated with 150 µl of Geltrex™ (A1413202, Thermo Fisher Scientific, Waltham, MA, U.S.A) and incubated at 37 ºC for 30 min. Later, 87,500 cells were resuspended in 500 µl of FBS-free M-200 (negative control), in M-200 with FBS (positive control) or in FBS-free M-200 with CDC-EVs from the different donors at 300 µg/1·10^6 cells and plated over the pre-coated plates in three wells per for each condition. After 15 hours of incubation, tube formation was imaged at 5x in 5-6 different locations in each well with the Leica DMI3000B optical microscope and Leica DFC310 FX camera (Wetzlar, Germany). 16-20 images per condition were analyzed and quantified automatically using the Angiogenesis Analyzer tool in ImageJ [374] and used to obtain the average total branching length.

4.3.13 Statistical analysis

Results are presented as mean ± standard error of the mean in the text and in figures. Continuous variables (proliferation, percentage of wound closure, factor secretion and total branching length) were compared under the different conditions using Student's t-tests.

Categorical variables (percentage of senescent cells, of Ki-67+cell, of γ-H2AX+ cells and of apoptotic cells) were compared using the Z-Score for two population proportions. Pearson tests were performed to study the correlation among the different parameters. All probability values reported are two-sided, with $p < 0.05$ considered significant.

4.4 Results

4.4.1 CDC's bioactivity is correlated to the cellular senescence status but not to the donor's chronological age

CDC senescence seems more determinant than chronological age in CDC proliferative and migrative capacities. An example of CDC properties from a chronologically aged donor (70 years old) but with low CDC senescence (9.1%) vs. a chronologically young donor (7 months old) but with high CDC senescence (14.8%) is shown in Figure 4.7a. The CDCs from the aged donor, but low senescent, are highly proliferative, with a higher proportion of Ki-67+ cells, and with a higher ability for wound closure compared to the CDCs from the young, but highly senescent donor.

Donor's chronological age or sex are unrelated to molecular markers of cellular aging in their derived EDCs and CDCs. Chronological age does not correlate to the genetic expression of *CDKN1A*, *CDK2A* and *TP53* in EDCs, nor any of the other genes explored ($R^2 < 0.15$, $p > 0.1$). No correlation was either observed between chronological age and EDC or CDC senescence (Figure 4.7), or to CDC telomere length. EDCs and CDCs from different gender did not present significant differences in the cellular aging markers explored. Donor's chronological age did not influence CDC proliferative capacity (PDT), DNA synthesis nor VEGF secretion ($R^2 < 0.15$, $p > 0.1$), but it negatively affected CDC migration ($R^2 = 0.33$, $p < 0.05$, Figure 4.7b).

Opposite to chronological age, EDC and CDC senescence related to the genetic expression of some aging-associated genes and to most CDC properties. The genetic expression of *CDK2A* in EDCs correlated significantly to CDC senescence ($R^2 = 0.22$, $p < 0.05$), and the expression of *CDKN1A* tended to correlate to EDC senescence ($R^2 = 0.17$, $p = 0.09$). Despite CDC senescence did not correlate to CDC telomere length or VEGF secretion ($R^2 < 0.15$, $p > 0.1$), it significantly affected CDC proliferation (PDT, $R^2 = 0.35$, $p < 0.05$), DNA synthesis ($R^2 = 0.34$, $p < 0.05$) and migration ($R^2 = 0.59$, $p < 0.001$) as shown in Figure 4.7c.

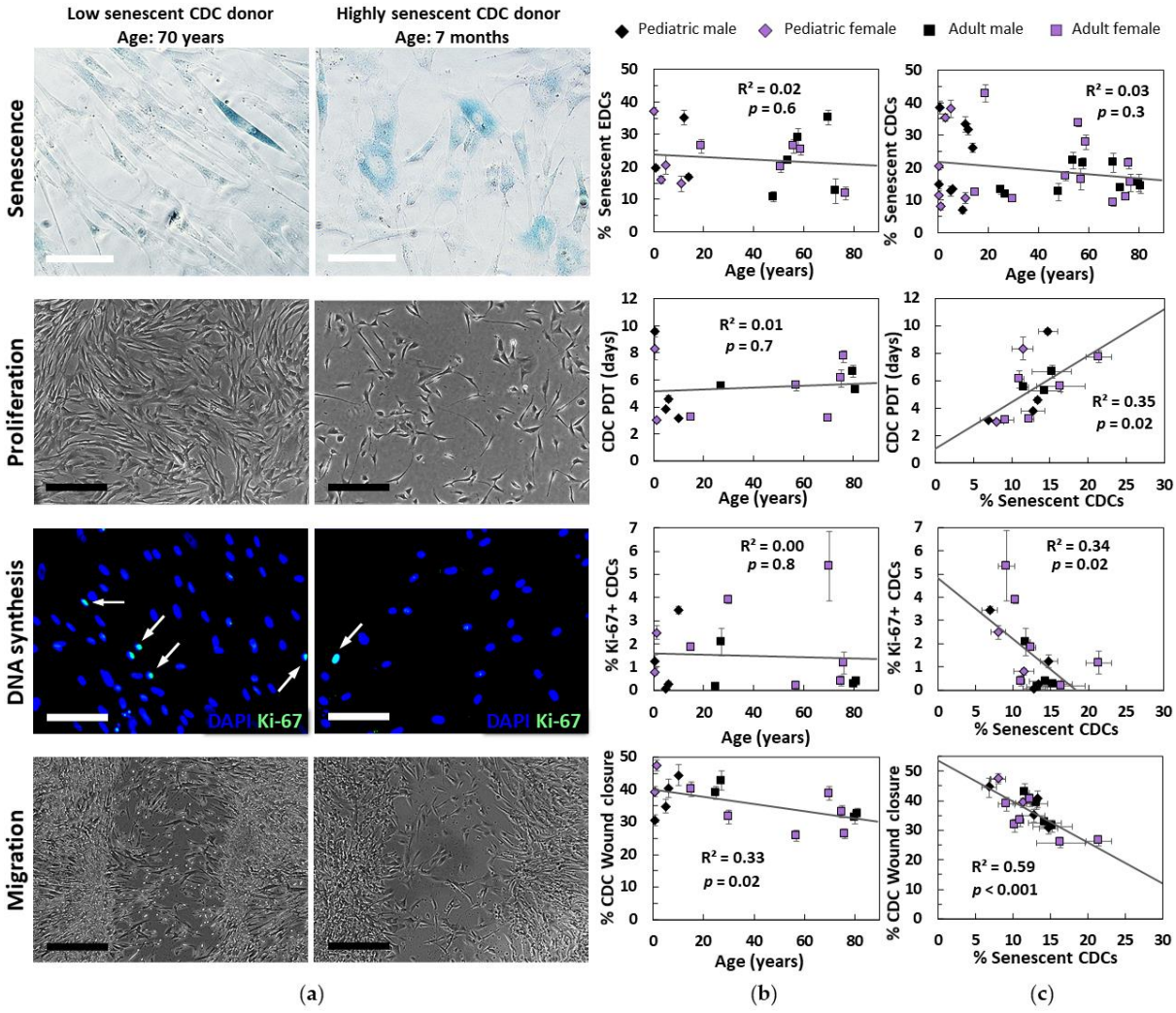

Figure 4.7. Donor chronological age vs. CDC biological age effect on different CDC properties. (**a**) Representative images from one chronologically aged donor (70 years old), but biologically young (9.1% of senescent CDCs) vs. one chronologically young donor (7 months old), but biologically aged (14.8% of senescent CDCs) after 72 hours of culture. (**b**) Chronological age is not significantly related to EDC or CDC senescence, population doubling time (PDT) or DNA synthesis capacity (% Ki-67+ CDCs) after 72 hours of culture. Chronological age significantly affects CDC migration capacity after 24 hours of wound generation. (**c**) CDC senescence however relates to PDT, DNA synthesis and migration capacity significantly and to a higher extent. Adult samples are represented with a square, while pediatric samples are represented with a diamond. Male samples are shown in black and female samples in purple. White scale bar corresponds to 100 μm, black scale bar to 400 μm.

4.4.2 Cardiosphere size and CDC surface markers relate to VEGF secretion, but not to other CDC properties

The genetic expression of *VEGFA*, *IGF1*, *CDKN2A* and *CDKN1A* in EDCs related to the size of the cardiospheres formed ($R^2 = 0.61$ and $p < 0.001$, $R^2 = 0.27$ and $p < 0.05$, $R^2 = 0.53$ and $p < 0.01$ and $R^2 = 0.17$ and $p = 0.08$ respectively). In this line, cardiosphere size correlated almost significantly to CDC VEGF secretion ($R^2 = 0.21$, $p = 0.08$), but it did not relate to chronological age of the donor or any of the CDC properties measured (senescence, telomere length, DNA synthesis, proliferation, migration), with $R^2 < 0.1$ and $p > 0.2$. The cardiosphere size also seemed significantly related to the percentage of CDC cells that were expressing certain surface markers. In particular, cardiosphere size related to the percentage of CD31+ CDCs ($R^2 = 0.24$, $p < 0.05$), to the percentage of CD45+ CDCs ($R^2 = 0.35$, $p < 0.01$) and to the percentage of CD117+ CDCs ($R^2 = 0.41$, $p < 0.01$). It did not significantly relate to the percentage of CD90+ CDCs ($R^2 = 0.11$, $p = 0.2$) nor the percentage of CD105+ CDCs ($R^2 = 0.01$, $p = 0.7$).

Regarding surface markers, only the percentage of CD117+ CDCs significantly related to CDC VEGF-A secretion ($R^2 = 0.28$, $p < 0.05$). The percentage of CD117+ CDCs did not significantly relate to chronological age and the other CDC properties explored: CDC senescence, telomere length, and DNA synthesis. Regarding proliferation and migration, higher proportion of CD117+ CDCs tended to have higher PDT and lower confluence at the wound area, but without reaching significance ($R^2 = 0.20$ and $p = 0.08$). The rest of the surface markers (%CD31+ CDCs, %CD45+ CDCs, %CD105+ CDCs and %CD90+ CDCs) did not correlate to VEGF-A secretion, to chronological age, nor to any of the other CDC properties explored ($R^2 < 0.15$, $p > 0.1$).

These results suggest that cardiosphere size and typical CDC surface markers, especially CD117, may be unrelated to CDC senescence, proliferation and migration, but they may relate to CDC VEGF-A secretion. The relationships found between VEGFA expression in EDCs, cardiosphere size, CDC composition and VEGF-A secretion are summarized in Figure 4.8.

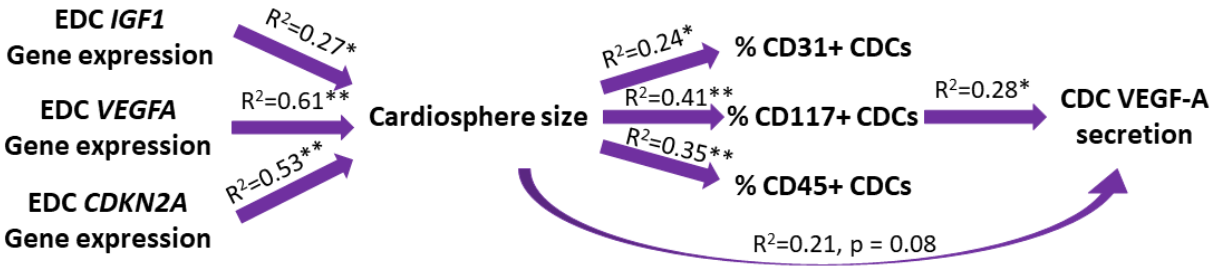

Figure 4.8. Cardiosphere size and surface markers relationship to VEGFA expression and secretion. * $p < 0.05$, ** $p < 0.01$. Gene expression and cardiosphere size relationship: $n = 18$. Cardiosphere size, surface markers and VEGF-A secretion relationship: $n = 16$.

4.4.3 CDC-EVs have an anti-senescent effect on different cell types in the heart

The anti-senescent effect of CDC-EVs derived from selected low senescent CDCs (LS-CDC-EVs) vs. highly senescent CDCs (HS-CDC-EVs) in CPCs, CMs, CSCs and ECs is shown in Figure 4.9. LS-CDC-EVs significantly reduced senescence in all the cell types explored: from 27.7±1.6 to 19.3±1.9 % of senescent CPCs ($p < 0.05$), from 16.7 ± 1.2 to 7.3 ± 0.7 % of senescent CMs ($p < 0.05$), from 33.3 ± 2.3 to 24.3 ± 1.9 % of senescent CSCs ($p < 0.05$) and from 23.7 ± 1.3 to 12.2 ± 1.0 % of senescent ECs ($p < 0.05$). However, HS-CDC-EVs only reduced senescence significantly, and similar to the LS-CDC-EVs, in CSCs (to 20.2 ± 1.7 $p < 0.05$) and in ECs (to 13.3 ± 1.0, $p < 0.05$). In CPCs and CMs, the presence of HS-CDC-EVs had not a significantly positive effect, and senescence was significantly worst vs. CPCs and CMs treated with the LS-CDC-EVs (26.2 ± 1.5% in CPCs and 20.5 ± 1.3% in CMs, $p < 0.05$).

4.4.4 CDC-EVs have other "pro-rejuvenating" and pro-angiogenic effects on different cell types in the heart

CDC-EVs also had other beneficial effects for the reparation of damaged or aged heart tissue (Figure 4.10). In CPCs, apart from reducing senescence, LS-CDC-EVs significantly increased DNA synthesis (0.4 ± 0.2 vs. 1.3 ± 0.4% Ki-67+ CDCs, $p < 0.05$) and proliferation (16 ± 3.4 vs. 29.6 ± 2.8 %, $p < 0.05$). However, these benefits were not observed when using HS-CDC-EVs. Apoptosis in CMs was significantly reduced by both LS- and HS-CDC-EVs, from 4.94 ± 0.6 in the control group to 2.29 ± 0.4 and 1.8 ± 0.4 % when treated with LS- and HS-CDC-EVs respectively, $p < 0.05$). In CSCs, proliferation was significantly improved when using LS-CDC-EVs (PDT decreased from 5.7 ± 0.6 to 4.1 ± 0.2 days, $p < 0.05$), but not when using HS-CDC-EVs (6.8 ± 0.9 days, $p > 0.1$ vs. control, $p < 0.05$ vs. LS-CDC-EVs). The same tendency was observed with CSC TNF-α secretion. LS-CDC-EVs reduced TNF-α secretion from 19.3 ± 3.4 to 12.3 ± 0.7 pg/million cells ($p = 0.07$ vs control), while HS-CDC-EVs did not (21.8 ± 1.6, $p < 0.05$ vs. LS-CDC-EVs). No significant differences were observed in CSCs when using LS-CDC-EVs or HS-CDC-EVs vs. control regarding DNA synthesis (percentage of Ki-67+ cells) and DNA damage (percentage of γ-H2AX+ cells).

CDC-EVs also showed pro-angiogenic effects in ECs. LS-CDC-EVS significantly increased total tubule length formed in ECs (from 9.2 ± 0.4 to 11.5 ± 0.5 $\cdot 10^3$ pixels, $p < 0.001$). HS-CDC-EVs increased tubule length, but not significantly (10.2 ± 0.5 10^3 pixels, $p = 0.1$ vs. control, $p = 0.01$ vs. LS-CDC-EVs). Despite both LS- and HS- CDC-EVs having a tendency to increase VEGF-A secretion in ECs, this was not significant ($p = 0.2$).

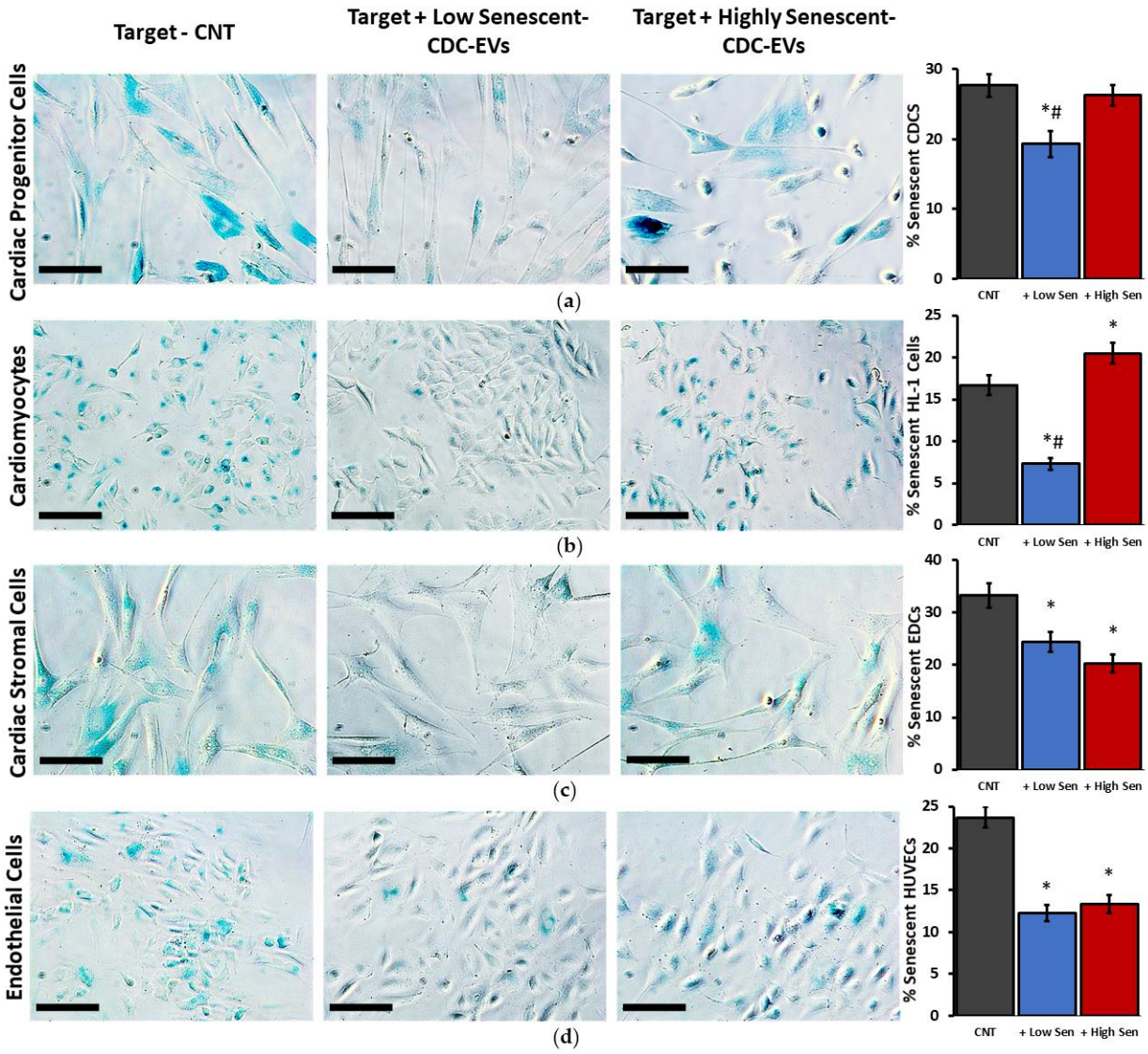

Figure 4.9. Anti-senescent effect of CDC-EVs from a low senescent CDC donor (Low Sen) and from a highly senescent CDC donor (High Sen) on different cell types in the heart. Senescent cells in blue. (**a**) CDC-EVs anti-senescent effect in cardiac progenitor cells (n = 862 ± 33 cells per group). (**b**) CDC-EVs anti-senescent effect in cardiomyocytes (n = 1122 ± 100 cells/group). (**c**) CDC-EVs anti-senescent effect in cardiac stromal cells (n = 487 ± 38 cells/group). (**d**) CDC-EVs anti-senescent effect in endothelial cells (n = 1125 ± 24 cells/group). * $p < 0.05$ vs. control (CNT). # $p < 0.05$ vs. treated with CDC-EVs from High Sen. Scale bar corresponds to 100 μm.

4.4.5 The extent of the CDC-EVs efficacy cannot be predicted by the cellular senescence status as surrogate marker

After observing CDC-EV variability in their anti-senescent and pro-angiogenic effect, CDC-EVs were obtained from 18 donors and evaluated in CSCs from two donors and in ECs. The CDC characterization parameters (chronological age and gender of the donor, EDC senescence,

cardiosphere size and CDC senescence) were correlated against the CDC-EVs capability to reduce CSCs senescence and to induce ECs tubule formation. Anti-senescent potency was tested in CSCs from two donors: one with moderate basal senescence (26.9 ± 1.4%) and one with high basal senescence (47.5 ± 1.28%). CDC-EVs reduced basal senescence of target 1 between -3.2 and -8.1%, being the reduction significant in 17/18 donors. In target 2, basal CSC senescence was reduced by all CDC-EVs as well (between -2.0 and -14.5%), being the reduction significant in 15/18. However, the anti-senescent effect of the CDC-EVs did not correlate to any of the CDC characterization parameters explored (Figure 4.11a). Regarding angiogenesis, all donors except one significantly improved endothelial branching length (between 15-47%). CDC-EVs pro-angiogenic effect did not correlate to their anti-senescent effect nor to any of the CDC characterization parameters explored (Figure 4.11b).

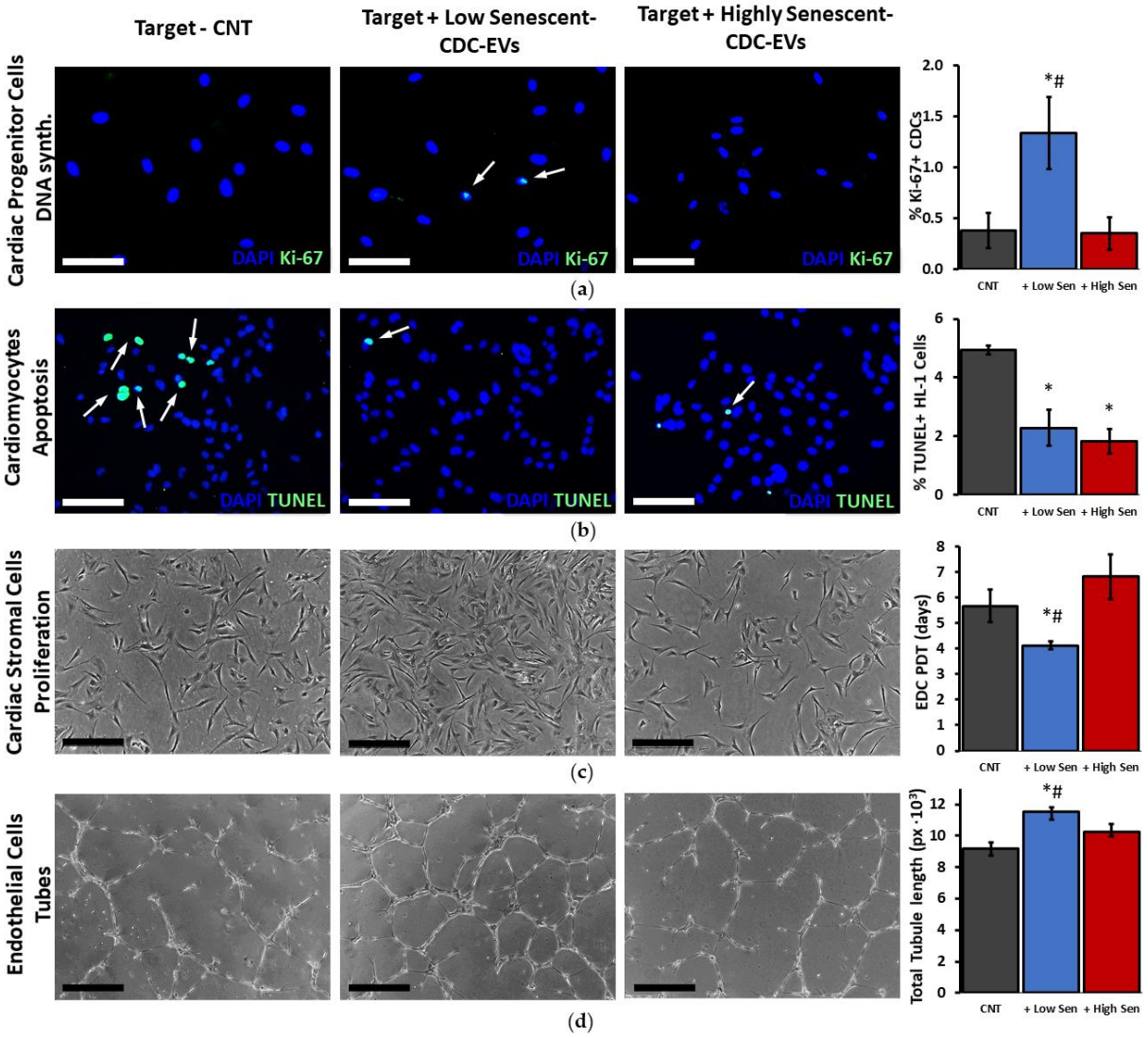

Figure 4.10. Other rejuvenating and pro-angiogenic effects of CDC-EVs from a low senescent CDC donor and from a highly senescent CDC donor on different cell types in the heart.. (**a**)

CDC-EVs effect on DNA synthesis in cardiac progenitor cells (n = 1263 ± 111 cells/group). (**b**) CDC-EVs anti-apoptotic effect in cardiomyocytes (n = 1368 ± 58 cells/group). (**c**) CDC-EVs effect on tube formation in endothelial cells (n = 19 ± 1 images/condition). (**d**) CDC-EVs proliferative effect in cardiac stromal cells (n = 21 ± 1 images/group). * $p < 0.05$ vs. CNT. # $p < 0.05$ vs. High Sen. White scale bar corresponds to 100 μm, black scale bar to 400 μm.

4.5 Discussion

The results of this work show that chronological age of the donor, cellular senescence and cardiosphere size are not determinant for CDC-EV anti-senescent and pro-angiogenic potency. While CDC-EVs from most human donors had significant (but variable) anti-senescent and pro-angiogenic effects, the extent of the effect was not affected by chronological age of the donor and by senescence of the cells. Chronological age of the donor did not relate to CDC characteristics such as senescence, telomere length, proliferative and DNA synthesis capacity, VEGF secretion and CDC-EV ability to reduce CSC senescence and induce EC tube formation. Although chronological age of the donor significantly related to CDC migration, wound closure capacity was more determined by CDC senescence than by chronological age of the donor. CDC senescence significantly determined CDC proliferative and DNA synthesis capacity as well. However, CDC senescence did not determine CDC-EV potential to reduce CSC senescence and induce EC tube formation. None of these CDC properties related to the percentage of cells expressing any of the typical surface markers used for CDC population characterization (CD45, CD90, CD117, CD105 and CD31). Therefore, despite CDCs from different donors meeting the identity requirements for being classified as CDCs, they presented variable degrees of senescence and of proliferative and migrative capacities.

A relationship between the cardiosphere size, specific CDC surface markers and VEGF-A secretion was observed. Cardiospheres from different donors varied largely in size: while the same number of cells in some donors produced fewer but larger cardiospheres, others produced a higher number of cardiospheres but smaller in size. VEGF-A gene expression in EDCs significantly correlated to cardiosphere size, which at the same time significantly correlated to the percentage of CD31+, CD117+ and CD45+ cells. Cardiospheres are known to have distinct layers with CD117+ cells at the core and CD105+ and CD31+ cells on the periphery [134]. Probably, larger cardiospheres form when the proportion of available CD117+ and CD31+ is higher as they can make the nucleus and the periphery of the cardiosphere grow. These larger cardiospheres then may yield higher proportions of CD117+ and CD31+ CDCs. On the contrary, when these populations are reduced, cardiospheres may tend to form smaller.

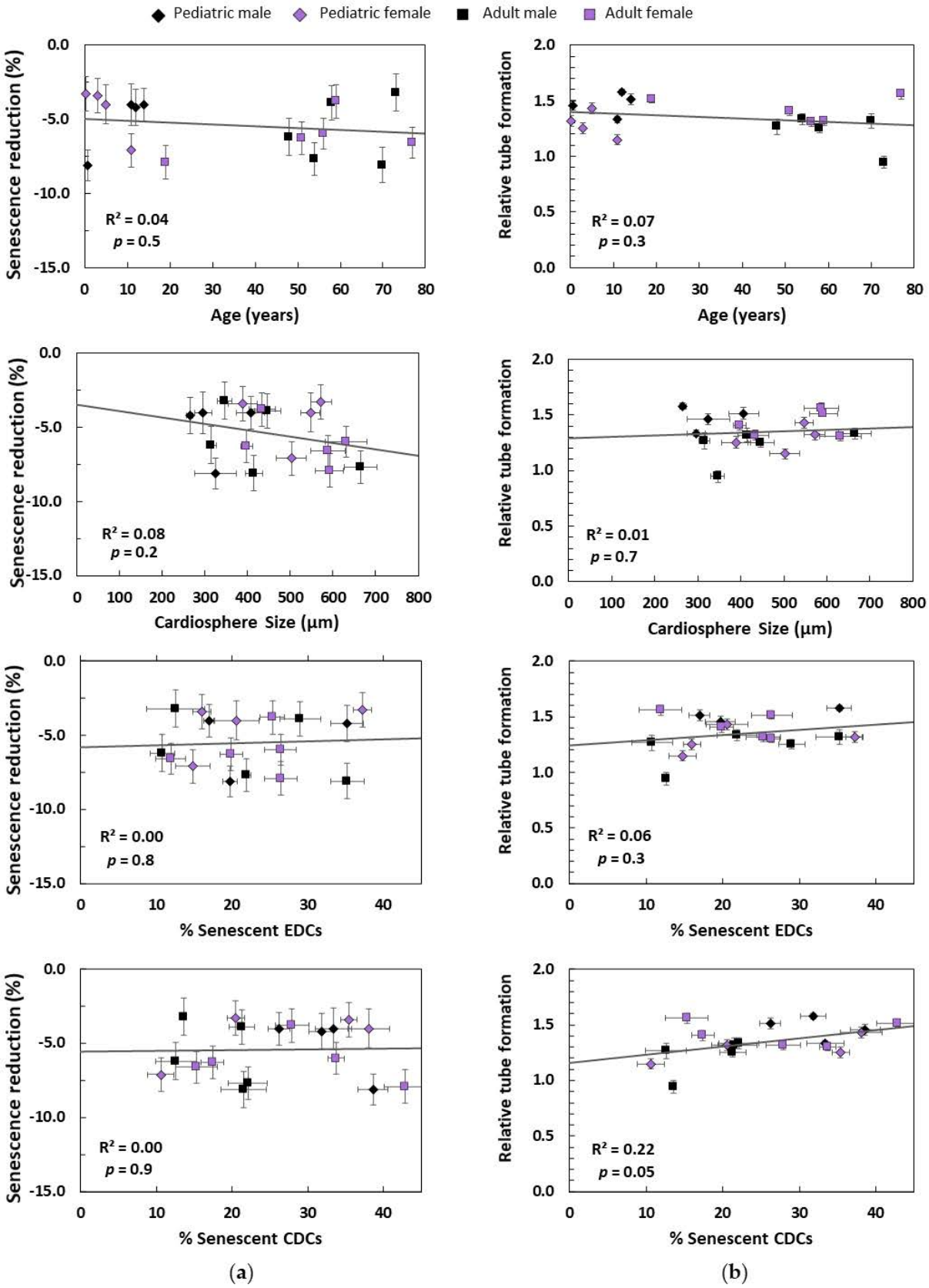

Figure 4.11. Correlation between the characteristics at different stages of product development and final CDC-EVs anti-senescent and pro-angiogenic potency *in vitro*. (**a**) Donor chronological

age, cardiosphere size, EDC senescence and CDC senescence vs. derived CDC-EVs anti-senescent potency in one of the CSC target donors (n = 1199 ± 27 cells/condition). (**b**) Donor chronological age, cardiosphere size, EDC senescence and CDC senescence vs. derived CDC-EVs pro-angiogenic potency in ECs (n = 19 ± 1 image/condition). Adult samples are represented with a square, while pediatric samples are represented with a diamond. Male samples are shown in black and female samples in purple.

Despite cardiosphere size also correlated to the percentage of CD45+ cells, these represent a minor amount of residual hematopoietic progenitors present in the CDC mixture, and they are not essential for cardiosphere formation [340]. In fact, in other studies, complete depletion of CD45+ cells has shown to increase the number of formed cardiospheres [340], which would be compatible with decreasing their size. The percentage of CD117+ CDCs (more abundant in the CDCs than CD31+ or CD45+ cells) positively correlated to CDC VEGF secretion. Regardless of the controversy on CD117+ cells identity, CD117 has been linked to angiogenesis and VEGF-A secretion [336, 375]. However, when comparing the VEGF-A secretion potential of isolated CD117+ cells from the CDC population vs. unsorted CDCs, unsorted-CDCs secreted more VEGF-A to the media [132]. Probably, the mesenchymal cell subpopulation is needed to provide physical or secretory support to the CD117+ subpopulation during CDC expansion [133], but if CD117+ proportions are too low, the VEGF-A secretion of the mixture diminishes. The percentage of CD90+ cells inside the CDC mixture has been negatively associated to CDC potency [132, 339]. Nevertheless, we have not observed that the percentage of CD90+ influenced in any of the CDC characteristics explored here. Differently to the work by Gamal-Eldin et. al [334] we did not observe a relationship between the expression of CD90+ cells and cardiosphere size. This is probably because their CDC population was immortalized and expressed CD90+ levels much higher than the ones of non-immortalized cardiospheres in this study. Although cardiosphere size and the percentage of CD117+ CDCs seemed to relate to CDC VEGF secretion, no relation was observed between cardiosphere size and CDC-EVs anti-senescent and pro-angiogenic potency, questioning its suitability as a potential potency marker.

The effect of chronological age of the donor on stem cell potential has been widely argued. However, most of the studies use stem cells from murine origin. While animal models are good for investigating mechanisms, the cardiac reparative potential and aging-related processes of neonatal and young rodents differ from human donors [120, 376–380]. Therefore, some of the differences observed in these studies may not necessarily translate into cardiac stem cells of human origin. In addition, several studies employing human cardiac stem cells compare characteristics of CDCs from donors with different profiles, but do not confirm if these differences in characterization translate into differences in CDC efficacy *in vitro* or *in vivo*. The

results from studies using extremely low numbers of samples for characterization and/or not including age as a continuous variable should also be taken cautiously.

If this work, chronological age of the donor did not affect the expression of surface markers in CDCs nor most of the CDC properties explored (only CDC migration). These results are similar to the work of Nakamura et al. [274], where characterization of CDCs from several donors did not reveal significant differences related to age of the donor. In this study, we further confirmed that the lack of different CDC characteristics associated with age translate into no differences in CDC-EVs anti-senescent and pro-angiogenic potency. On the contrary, another study by Simpson et. al [358] observed that CDCs from neonatal samples had higher potential to improve LVEF, reduce scar size and to preserve blood vessels in infarcted rats. However, this study does not clarify if for the *in vivo* experiment injected CDCs came from several neonates and adults or from single selected ones. As our study did not incorporate neonatal samples, if the enhanced potency they observed is only characteristic of neonates and not of young donors, these effects could not be observed in our study.

According to our results, advanced chronological age of the donor was not associated to significantly higher CDC senesce or reduced telomere length. Nevertheless, Cesselli et al. [357], observed that chronological age of CD117+ cells correlated to telomere dysfunction-induced foci and $p16^{INK4a}$ expression. Lewis-McDougall also reported similar results in CD117+ Sca-1+ cells from donors over 70 years, who showed higher SA-β-gal, DNA damage γ-H2AX, SASP and less ability to replicate and differentiate [87]. Despite the process of natural aging being associated to telomere shortening in cells *in vivo* [381], cellular aging, especially during *in vitro* culture, is heterogeneous as it depends on many other factors such as environmental factors, tissue origin, cell type and number of population doublings [345, 382–385]. Thus, chronological age of the donor is not always related to cellular age [386]. Moreover, it is important to note that most CSCs are obtained from cardiac biopsies of non-healthy patients. The cardiac pathology, as well as the stage, can also affect the stem cell potency and biological aging [268, 357, 387]. The influence of all these other factors, as well as the ability of cardiospheres to potentiate stemness, may translate differences in the chronological age of the donor into irrelevant for CDC telomere length and senescence.

Cellular age of the stem cells influences their properties, their secretome, and their EV cargo [347]. Therefore, it seems relevant to take cellular senescence into account for determining therapeutic potential. In fact, several studies have explored ways to rejuvenate cardiac stem cells to make them therapeutically more efficient [173, 353, 388, 389]. Even if some studies have suggested biomarkers of cellular senescence to determine cell potency [357], few work exists to confirm if these characterization differences translate into reduced efficacy and to promote

senescence as a measurement of product quality before product release for clinical trials. In this work, we observed how CDC senescence, despite not relating to chronological age of the donor, determined CDC proliferation and migration. These may be important in applications where CDCs are used directly as the therapeutic product (not CDC-derived products) and CDC engraftment, migration and proliferation are crucial to exert their mechanism of action (MoA). However, in this work we found that CDC senescence did not determine CDC-EVs pro-angiogenic and anti-senescent potency *in vitro*. Hence, the use of derived EVs as cell-free products may overcome the limitations and consequences of using cellular products with heterogeneous cellular ages.

In vitro functional assays are commonly used the explore the mechanisms of action and make comparisons between cellular products. They serve as an intermediate step between surrogates (usually product characteristics) and *in vivo* efficacy as they are more representative of the MoA than surrogates but require considerably less time and costs than *in vivo* efficacy experiments. Many studies exploring surrogate markers for potency confirm differences in cellular product characteristics but do not confirm if these differences translate into functional differences. Furthermore, when product differences are evaluated *in vivo*, continuous variables, such as chronological age of the donor, or cell senescence, are commonly transformed into discrete variables (e.g. "young" and "aged") because otherwise the costs will be not feasible. Nevertheless, when interpreting the results, it is not the same to use a pooled set of "young" and "old" donors widely characterized than to use single selected young and aged donors.

In this work, we chose to test the anti-senescent effect of CDC-EVs *in vitro* on different cell types, and in particular in human CSCs from two different donors. We also tested the rejuvenating ability of CDC-EVs from selected donors on proliferation and prevention of apoptosis in specific cell types including CMs. Finally, we evaluated the pro-angiogenic effect in a tube formation assay in endothelial cells. The reduction of *in vivo* senescence on the different cell types in the heart and the ability to induce new vessels has shown multiple therapeutical benefits associated with cardiac aging [87, 89, 359, 390]. Therefore, when targeting cardiac aging, evaluating the anti-senescent and the pro-angiogenic effect of CDC-EVs seem as reasonable *in vitro* functional assays. The results of this study allow concluding that in spite of the multiple beneficial effects of CDC-EVs on different cell types, when using cardio-sphere size, chronological age of the donor and cellular senescence as continuous variables, there is no relationship between these CDC characteristics and CDC-EVs efficacy *in vitro*, thus not recommending their use as surrogate potency markers. Morevoer, while CDC-EVs from certain donors exhibited large anti-senescent potency *in vitro*, they did not necessarily present large pro-angiogenic potency and vice versa. This highlights the need of performing adequate bioactivity

experiments specific for the expected MoA and the target pathology, as while one product may be highly potent for one specific purpose, it may not be for other.

However, this study presents some limitations that need to be considered when interpreting the results. Despite our results suggesting that cardiosphere size, chronological age, and cellular senescence are unrelated to CDC-EVs potency because no correlation was found with *in vitro* functionality, this conclusion should be further confirmed using an *in vivo* model, and studying, for example, correlation between *in vitro* and *in vivo* efficacy. In addition, although the number of donors included is not as small as in other studies (4-5) and the chronological age span is wide (3 months - 81 years old), larger number of donors, and inclusion of neonate samples, will make the study more robust. Finally, it will be worth exploring if other CDC and CDC-EVs characteristics previously related to potency determine anti-senescence and pro-angiogenic *in vitro* functionality. Some examples include SDF-1α secretion [110, 268, 391] and activation of the Heat Shock Response (HSR) [276], the expression of Mybl2 [353], activation of the Wnt/β-catening signaling pathway [275, 334, 335] or the mTOR pathway [392], and specific miRNA cargo in the CDC-EVs [196, 334, 393].

4.6 Conclusions

Extracellular vesicles derived from cardiosphere-derived cells (CDC-EVs) from most human donors present significant anti-senescent and pro-angiogenic potency, but the extent of the effect is variable and is not determined by the chronological age of the donor, CDC senescence or the ability to form cardiospheres. Since cell identity and specific donor or cell characteristics did not translate into boosted bioactivity of CDCs in this study, further evaluation of the *in vitro* functionality relative to the expected mechanism of action as determinant of therapeutic potency is warranted.

Chapter 5

Anti-senescence *in vitro* potency of extracellular vesicles secreted by cardiosphere-derived cells predicts their rejuvenating effects in an aging rodent model

5.1 Abstract

Cardiosphere-derived cells (CDCs) and their derived extracellular vesicles (CDC-EVs) have demonstrated to induce rejuvenation of the heart and to improve cardiac structure and function. However, the extent of the reparative effects of human CDCs seem to variate among different CDC-donors and there is a lack of robust potency markers to predict the *in vivo* efficacy at the early stages of product development. The purpose of this study was to evaluate if the *in vitro* anti-senescent and pro-angiogenic effect of the CDC-EVs could be used to predict their *in vivo* efficacy. CDC-EVs from 18 human donors were obtained and their anti-senescent and pro-angiogenic potency evaluated *in vitro* using a matrix assay with several markers. According to the performance in these tests, potency was scored and CDC-EVs with the highest and lower score were classified as potent (P-EVs) and non-potent (NP-EVs) respectively. The rejuvenating effect of both type of EVs were tested in an *in vivo* model of cardiac aging. In the heart of aged rats, P-EVs had the potential to significantly reduce the expression of the senescence-associated gene *GLB1* and to non-significantly reduce cardiac hypertrophy and *TGFB1* expression. On the contrary, NP- EVs did not significantly produce any effect and in fact significantly increased cardiac hypertrophy, cardiac fibrosis and reduced perfusion. At systemic level, while P-EVs significantly improved glucose metabolism and tended to drive total antioxidant capacity and hair growth to a healthier profile, NP-EVs did not significantly improve any of the explored parameters and even significantly increased total antioxidant capacity. After further validation, the matrix assay proposed here could be used as an *in vitro* potency test to evaluate EV suitability as an allogenic product before its use in the treatment of cardiac aging.

5.2 Introduction

Cellular, structural and functional changes associated with age are largely responsible for heart diseases such as heart failure with preserved ejection fraction (HFpEF) and atrial fibrillation (AF) [22]. Cardiac aging is associated to increased cell senescence [394], compromised myocardial perfusion [395], and increased fibrosis [396] among others. While finding effective treatments remains as an unmet clinical need, cardio-sphere derived cells (CDCs) and their derived extracellular vesicles (CDC-EVs) present promising characteristics for reverting some of these age-associated pathological changes [140], such as increasing microvessel formation, [136], attenuating cardiomyocyte (CM) apoptosis and hypertrophy, reducing regional fibrosis [137, 138] and acting as immunomodulators [137, 139]. However, cell and cell-derived products present an inherent complexity that translates into a variable potency hard to predict [268, 276, 291, 333, 334].

These variations in potency, together with the lack of knowledge about the specific mechanisms of actions, could justify why similar studies end with apparent contradictory results [133, 140, 397–399], or why results in the clinical scenario have not been as successful as expected. Despite being known that potency depends on many parameters apart from cell identity [268, 276, 291, 333, 334], identity is commonly used as a synonym of potency for cell use in clinical trials [291]. Yet, the standard model for testing cell and cell-derived product potency before its use in the clinical scenario are *in vivo* models of myocardial infarction (MI) [268, 335]. Nevertheless, this potency test is costly, time-consuming, and does not allow for product classification at early stages [306]. Using characteristics of the donor (such as age and sex), and specific CDC characteristics (such as cardiosphere size and senescence) as surrogate markers, as shown in the previous chapter, may not be optimum to predict CDC-EVs functionality. Finding economic, feasible and efficient potency assays based on evidence of mechanism of action (MoA) for cell and cell-derived EVs still remains a challenge [110, 279, 291], and crucial for successful translation. Therefore, *in vitro* functional assays, which are more representative of the MoA than surrogates, but more manageable than *in vivo* assays, seem like an alternative worth exploring.

One of the main interesting mechanisms of action of CDC and CDC-EVs to treat aging-related pathologies is their anti-senescent effect [140]. Senescence is related to molecular changes and can be assessed using several biomarkers such as senescence-associated β-galactosidase (SA-β-Gal), p53/p21 and p16 expression, and telomere shortening [400]. However, in some cases, telomere length might be an unreliable measure of senescence [361]. Other factors, such as TGF-β, are also related to cardiac aging-related pathology such as increased fibrosis [401], senescence [402] and inflammation [403]. CDC-EVs also have the ability to increase IL-6 levels in plasma [404] and to induce IL-6 secretion by CSC and by macrophages [405]. Although IL-6 is

associated with the senescence associated secretory phenotype (SASP) [406], acute IL-6 response can activate immune cells, initiate a protective response in tissue, and trigger wound healing [407]. Ability to induce new vessel formation (angiogenesis) by activation of endogenous endothelial cells also seems as an important MoA of CDCs and CDC-EVs [180, 195, 196]. One common method to compare angiogenic potency *in vitro* is to evaluate the capacity of the product to induce tube formation in Human Umbilical Vein Endothelial Cells (HUVEC) [408].

Considering the related mechanisms by which CDC-EVs may exert beneficial effects for the treatment of cardiac aging and ways to measure them, we proposed using the CDC-EV anti-senescent and pro-angiogenic potency *in vitro* as functional *in vitro* assays to predict CDC-EV potency *in vivo*. For achieving this purpose, we designed a matrix assay consisting in evaluating the anti-senescent potency on cardiac stromal cells (CSCs) from human origin of two different donors and the pro-angiogenic effect on human endothelial cells. The anti-senescent effect was evaluated using several markers: (i) the percentage of CSC expressing SA-β-gal, (ii) the amount of CSC secreted IL-6 and (iii) the CSC relative gene expression of senescence and fibrosis-related genes (*CDKN1A*, *TGFB1*, *CDKN2A* and *TP53*). The pro-angiogenic effect was evaluated according to the CDC-EV potency to induce tube formation on endothelial cells. The performance in each of the different tests was scored and added to obtain a final potency score. As a result, selected CDC-EVs as potent according to this score had the highest anti-senescent and pro-angiogenic potency *in vitro* while selected CDC-EVs as non-potent had the lowest *in vitro* anti-senescent and pro-angiogenic potency. Then, rejuvenating and pro-angiogenic activity of potent (P-EVs) vs. non-potent (NP-EVs) CDC-EVs were tested in an *in vivo* model of D-galactose (D-gal) induced cardiac aging.

5.3 Materials and Methods

5.3.1 Experimental protocol

CDC-EVs were obtained from 18 donors (3 months to 81 years old, both sexes) as previously described in section 4.3.1. Their rejuvenating and pro-angiogenic potency was evaluated *in vitro* and the ones exhibiting the largest effect were classified as "potent" (P-EVs) and the ones with the lowest effect as "non-potent" (NP-EVs). Selected P- and NP-EV rejuvenating potency was later evaluated in an *in vivo* model of cardiac aging.

5.3.1.1 Potent and non-potent CDC-EV selection

The CDC-EV rejuvenating and pro-angiogenic potency was tested *in vitro* on human CSCs and human endothelial cells (ECs) with a custom designed matrix-assay (Figure 5.1a).

Explant-derived cells (EDCs) from passage 3 and from two different human donors were obtained as explained in section 4.3.1 and used as the target CSC population as they contain a variety of cell types important in heart physiology and pathology [133, 134]. EDCs-P3 from donor 1 (54 years old, male) were moderately senescent (25.6 ± 1.4 %), and EDCs-P3 from donor 2 (56 years old, female) were highly senescent (47.5 ± 1.3 %). The rejuvenating potency of CDC-EVs was determined as their ability to reduce CSC senescence, to induce CSC IL-6 secretion and to reduce the expression of *CDKN1A* (p21), *TGFB1* (TGF-β), *CDKN2A* (p16) and *TP53* (p53) senescence and fibrosis-related genes in CSCs. CDC-EVs pro-angiogenic potency was determined as their ability to induce tube formation of HUVEC.

EDCs-P2 from the two donors were plated in complete Iscove's Modified Dulbecco's Medium (IMDM) at 13,000 cells/cm^2 in fibronectin pre-coated 12-well plates. After 24 hours, EDCs were washed in Phosphate Buffered Saline (PBS) and cultured in Fetal Bovine Serum (FBS)-free IMDM alone or with CDC-EVs from the 18 CDC-EV donors at a dose of 300 μg/1·10^6 cells. After another 72 hours, media from EDCs for IL-6 secretion was collected, and EDCs for senescence or gene expression analyses were fixed and analyzed as explained in the following section (5.3.2). Each condition was run in triplicate.

For endothelial tube formation, as explained in section 4.3.2.3, 87,500 HUVECs-P5 were resuspended in 500 μl of FBS-free M-200 (negative control), in M-200 with FBS (positive control) or in FBS-free M-200 with CDC-EVs from the eighteen different donors at 300 μg/1·10^6 cells and plated on Geltrex-precoated 12-well plates in triplicate for each condition. After 15 hours of incubation, tube formation was imaged and quantified. Further details are provided on the 5.3.2.4 section. Each condition was run in triplicate.

With the results from the different tests in the matrix-assay, we observed that there were not CDC-EVs with the most and least rejuvenating and pro-angiogenic potency in all the considered tests. Therefore, we decided to score the performance (or potency) of each of the CDC-EVs in each of the tests in the matrix-assay and add them to calculate a final potency score. The score in each of the different tests was assigned as shown in Table 5.1. In each test, the CDC-EVs were divided in three groups: the ones showing superior performance (6/18, first tercile), the ones showing average performance (second tercile) and the ones showing the worst performance (third tercile). The CDC-EVs with the highest total score were selected as potent and the CDC-EVs with the total lowest score were selected as non-potent. The maximum possible score was 18 if CDC-EVs showed superior performance in all the tests in the matrix-assay.

Test	Target	CDC-EV score if in first tercile	CDC-EV score if in second tercile	CDC-EV score if in third tercile
Senescence reduction	CSCs from donor 1	2	1	0
	CSCs from donor 2	2	1	0
Increase in IL-6 secretion	CSCs from donor 1	2	1	0
	CSCs from donor 2	2	1	0
CDKN1A expression reduction	CSCs from donor 1	1	0.5	0
	CSCs from donor 2	1	0.5	0
TGFB1 expression reduction	CSCs from donor 1	1	0.5	0
	CSCs from donor 2	1	0.5	0
CDKN2A expression reduction	CSCs from donor 1	1	0.5	0
	CSCs from donor 2	1	0.5	0
TP53 expression reduction	CSC from donor 1	1	0.5	0
	CSC from donor 2	1	0.5	0
Increase in tube formation	HUVEC	2	1	0

Table 5.1. CDC-EV score assigned according to the extent of the beneficial effect in each of the different tests in the matrix-assay. The final potency score was calculated as the sum of all of them.

5.3.1.2 *In vivo* study

To see if the *in vitro* matrix-assay could predict the potency of the CDC-EVs *in vivo*, we tested the rejuvenating effects of the *in vitro* selected potent (P-) and non-potent (NP-) EVs in a rodent model of induced cardiac aging. The experimental procedure is illustrated in Figure 5.1b. Thirty-six 12-week-old Sprague-Dawley rats (30% females) were randomly allocated into four groups: healthy controls (n = 11), cardiac aged controls (sham group, D-gal, n = 12), cardiac aged treated with potent CDC-EVs (D-gal + P-EVs, n = 7) and cardiac aged treated with non-potent CDC-EVs (D-gal + NP-EVs, n = 6). To induce cardiac aging, animals in the cardiac aged groups received during 13 weeks daily sterile intraperitoneal (IP) injections of 600 mg/kg of D-galactose (D-gal, G53688, Sigma Aldrich in PBS, at 300 mg/ml) as described [409]. For 13 weeks, animals in the healthy control group received daily IP injections of PBS. After this time, the animals received IP the corresponding treatment according to their group allocation: either PBS alone (healthy controls and cardiac aging sham group), or PBS with P-EVs or NP-EVs at a dose of 7.5 mg/kg. During the seven following weeks, the animals received twice a week an IP injection of PBS or D-gal according to their group allocation. At the endpoint, the animals underwent a hemodynamic study, blood sample collection and were euthanized.

The effect of inducing aging with D-gal and the rejuvenating benefits of P- and NP-EVs were explored at cardiac and systemic level. At functional level in the heart, we explored

hemodynamic performance and cardiac perfusion (using Single Photon Emission Computer Tomography, SPECT). After sacrifice, we determined cardiac hypertrophy and fibrosis, and the genetic expression of senescence and fibrosis-related genes (*GLB1*, *TGFB1*, *CDKN2A* and *TP53*). At systemic level, we recorded differences in body weight, glucose tolerance test, hair regrowth and serum total antioxidant capacity. Cardiac perfusion, glucose tolerance and hair regrowth were recorded both before and after treatment administration. The timeline indicating the moment at which each of the tests was performed is included in Figure 5.1b. Further details about the different tests are included in the next section (5.3.3).

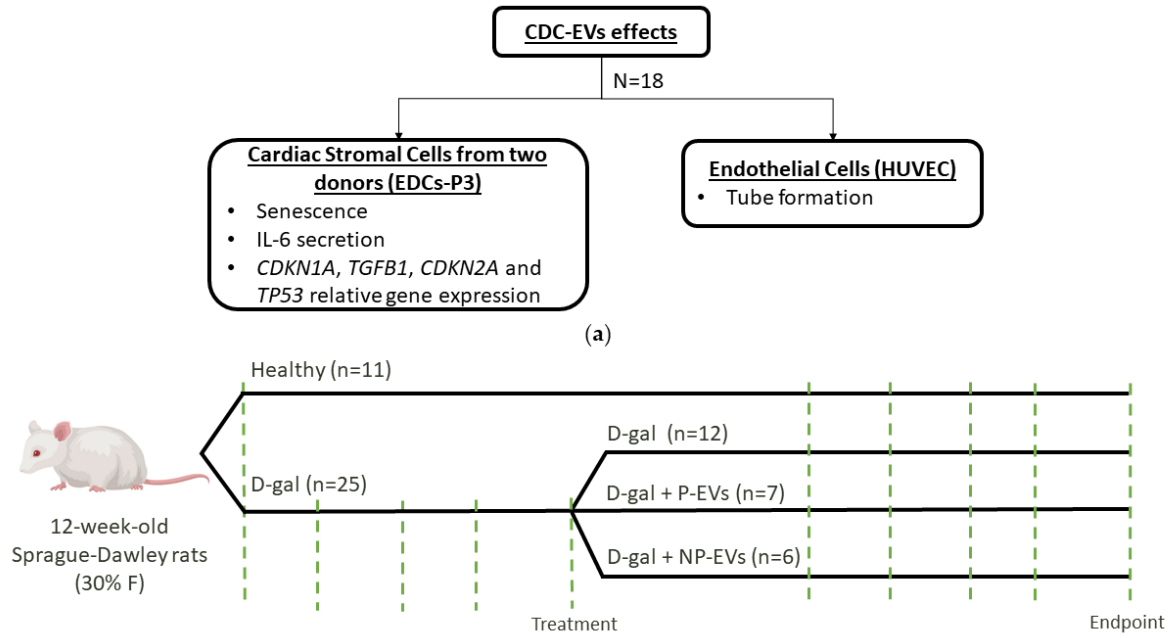

Age of the rat (weeks)	12	20-23	24	25	26		26.5	27-29	31	32	33-35
Test		Hair regrowth	SPECT	Glucose test			Glucose test	Hair regrowth	SPECT		Hemodynamic study
Product administration	Premature aging with daily D-gal (600 mg/kg/day) IP injections				PBS/EVs	Twice a week D-gal (600 mg/kg/day) IP injections					

(b)

Figure 5.1. Experimental protocol. (**a**) Extracellular vesicles obtained from cardiosphere-derived cells (CDC-EVs) from cardiac biopsies from 18 different donors were obtained and their anti-senescent and pro-angiogenic effect evaluated *in vitro* with a panel of different tests. According to the results, CDC-EVs were classified as potent (P-EVs) and non-potent (NP-EVs). (**b**) P-EVs and NP-EVs rejuvenating and pro-angiogenic potency was tested in a rodent model of cardiac aging. Timeline including group distribution, product administration and tests performed. F: Female. D-gal: D-galactose. P: potent. NP: non-potent. SPECT: Single Photon Emission Computer Tomography. IP: Intraperitoneal.

5.3.2 *In vitro* characterization and classification

5.3.2.1 Anti-senescent effect

As in section 4.3.5.1, CSCs were plated in complete medium at 13,000 cells/cm^2 in fibronectin pre-coated 12-well plates. After 24 hour-incubation, wells were washed and replaced with Fetal Bovine Serum (FBS)-free medium (blank or containing the resuspended CDC-EVs). After another 72 hour-incubation, the cells were fixed using Abcam's Senescence Detection Kit (ab65351, abcam, Cambridge, UK), which is used to detect SA-β-Gal activity in cultured cells. The samples were prepared, fixed and stained following the assay protocol (with overnight incubation). After staining, samples were washed and kept in 70% glycerol (G5516, Sigma-Aldrich) in PBS at 4 ºC. As SA-β-Gal positive cells develop a blue color, a total of around 10 images at 20x (around 1000-1500 cells) per well were taken with a Leica DMI3000B optical microscope and Leica DFC310 FX camera (Wetzlar, Germany), and manually classified as senescent (blue) or non-senescent using ImageJ Software. All samples were run in triplicate. Senescence reduction of CDC-EVs from each donor was calculated as senescence of EDCs-P3 from donor 1 (25.6 ± 1.4 %) or donor 2 (47.5 ± 1.3 %) minus the senescence of the EDCs-P3 of the same donor when treated with the corresponding CDC-EVs.

5.3.2.2 IL-6 secretion

CSCs were plated in complete medium at 13,000 cells/cm^2 in fibronectin pre-coated 12-well plates. After 24 hour-incubation, wells were washed and replaced with 600 µl of FBS-free medium (blank or containing the resuspended CDC-EVs). After another 72 hour-incubation, the conditioned media was collected, diluted 1:25, and IL-6 levels determined following the kit instructions from Enzo Life (ADI-900-033, Enzo Life Sciences, Farmingdale, NY, U.S.A). All samples were run in triplicate. Increment in IL-6 secretion caused by CDC-EVs was calculated as IL-6 secretion of EDCs-P3 from donor 1 or donor 2 under the effect of the different CDC-EVs minus the IL-6 secreted by the untreated EDCs (140 ± 6.6 pg/pl in donor 1 and 291 ± 26 pg/pl in donor 2).

5.3.2.3 Gene expression analysis

The gene expression of senescence and fibrosis-related genes in target CSCs under control conditions or treated with the CDC-EVs from the eighteen different donors were analyzed. The genes under study were: *CDKN1A* (p21), *TGFB1* (TGF-β), *CDKN2A* (p16) and *TP53* (p53). CSCs were plated in complete medium at 13,000 cells/cm^2 in fibronectin pre-coated 12-well plates. After 24 hour-incubation, wells were washed and replaced with FBS-free medium (blank or containing the resuspended CDC-EVs). After another 72 hour-incubation, RNA was isolated, reverse-transcribed into cDNA, PCR amplified and the gene expression quantified as

described in section 4.3.4. Specific primer pairs were detailed in Table 4.2. All samples were run in triplicate. The relative expression of each gene in the CSCs under the effect of the different CDC-EVs was normalized by the expression of the same gene in the untreated CSCs.

5.3.2.4 Pro-angiogenic effect

The pro-angiogenic effect of the different CDC-EVs was tested as their ability to induce tube formation. The procedure was as described in section 4.3.12. 12-well plates were coated with 150 µl of Geltrex™ (A1413202, Thermo Fisher Scientific, Waltham, MA, U.S.A) and incubated at 37 ºC for 30 min. Later, 87,500 HUVEC-P5 were resuspended in 500 µl of FBS-free M-200 (negative control), in M-200 with FBS (positive control) or in FBS-free M-200 with the CDC-EVs at 300 µg/1·10^6 cells and plated over the pre-coated plates in three wells per for each condition. After 15 hours of incubation, tube formation was imaged at 5x in 5-6 different locations in each well with the Leica DMI3000B optical microscope and Leica DFC310 FX camera (Wetzlar, Germany). 16-20 images per condition were analyzed and quantified automatically using the Angiogenesis Analyzer tool in ImageJ [374] and used to obtain the average total branching length. The relative tube formation of HUVEC treated with the different CDC-EVs was obtained by normalizing the total branching length by the total branching length of HUVEC with FBS-free-medium (and without any CDC-EVs).

5.3.3 *In vivo* evaluation

5.3.3.1 Hemodynamic study and sacrifice

The hemodynamic study was conducted following the Sciscience PV surgical protocol for rat left ventricle (LV) acute pressure-volume measurement (open chest approach). Briefly, the rats were anesthetized using 3% sevofluorane and kept mechanically ventilated through a tracheotomy. A lateral thoracotomy was performed to expose the heart, and the catheter FTH-1918B-E218 with the ADV500 system from Transonic used to record pressure-volume inside the LV. After the procedure, blood was collected, and the animals euthanized with a cardiac injection of 5 ml of 10 mEq KCl. The heart was extracted, cleaned in cold PBS, and later weighted and fixed for analysis as described in next sections.

The pressure and volume signals were analyzed with custom software developed in MATLAB. Regarding the pressure wave, we compared the maximum, the minimum, the end-diastolic (EDP) and the pressure range (maximum - minimum). Also, the maximum derivative of pressure, the minimum derivative of pressure and the isovolumic relaxation constant (tau). Tau was obtained by fitting a first order exponential (of the form Ae^{bx}) in the pressure wave between the time of the maximum of the derivative and the time of the minimum of the pressure. Tau was calculated as -1/b. All the parameters were calculated by averaging at least four beats in each

animal. The number of animals in each group that underwent the hemodynamic study were: healthy: n = 7, D-gal: n = 7, D-gal + P-EVs: n = 7, D-gal + NP-EVs: n = 6.

5.3.3.2 Gene expression analysis

The gene expression of senescence and fibrosis-related genes in the cardiac tissue of the rats in the different groups was analyzed. The genes under study were *GLB1* (β-galactosidase), *TGFB1* (TGF-β), *CDKN2A* (p16) and *TP53* (p53). A small portion of the apex was homogenized, and RNA was isolated, reverse-transcribed into cDNA and PCR amplified. The gene expression was quantified as described in section 4.3.4, but using *ACTB* as reference gene for gene expression normalization. Specific primer pairs are detailed in Table 5.2. The number of animals in each group that underwent the cardiac gene expression analysis were: healthy: n = 6, D-gal: n = 11, D-gal + P-EVs: n = 7, D-gal + NP-EVs: n = 6.

Gene	Protein	Forward primer (5'-3')	Reverse primer (5'-3')	Exons	Transcript
GLB1	β-galactosidase	AGAACGGAGGGCCCATCATAACC	TCCTGCAGGGTCCCACACTTGA	5-6	ENSRNOT00000013632.6
				5-6	ENSRNOT00000095071.1
				5-6	ENSRNOT00000112983.1
TGFB1	TGF-β	GGCTGAACCAAGGAGACGGAATA	GTGGCCATGAGGAGCAGGAAG	3-5	ENSRNOT00000028051.5
CDKN2A	p16	CGAACTGCGAGGACCCCACCAC	CGTTCCCAGCGGAGGAGAGTA GATACC	3-4	ENSRNOT00000084293.1
				3-4	ENSRNOT00000079251.1
				2	ENSRNOT00000103638.1
TP53	p53	AGCATCGAGCTCCCTCTGAGTCA	AGGGCTTCCTCTGGGCCTTCTA AC	1-3	ENSRNOT00000104927.1
				2-4	ENSRNOT00000046490.4
				1-3	ENSRNOT00000114382.1
				2-4	ENSRNOT00000083458.2
				2-4	ENSRNOT00000085115.2
				2-3	ENSRNOT00000102405.1
				1-2	ENSRNOT00000080584.2
				1-2	ENSRNOT00000091216.2
ACTB	β-actin	GGCCGTCTTCCCCTCCA	CAGTTGGTGACAATGCCGTG	2-3	ENSRNOT00000080216.2
				1-2	ENSRNOT00000042459.5
				2-3	ENSRNOT00000105242.1

Table 5.2. Primers used for RT-PCR in heart samples from rat experiments.

5.3.3.3 Cardiac hypertrophy

Cardiac hypertrophy was determined at the endpoint by calculating the ratio between the heart weight and the body weight. For determining heart weight, hearts were carefully cleaned and washed from major vessels, blood, and clots in PBS. The hearts were weighted after removing excess fluid. The number of animals in each group that were included in the cardiac hypertrophy measurement were: healthy: n = 8, D-gal: n = 12, D-gal + P-EVs: n = 7, D-gal + NP-EVs: n = 6.

5.3.3.4 Cardiac fibrosis

Excised hearts were fixed in 4% formaldehyde at least for one month and a tissue portion in the medium region of the ventricles dehydrated and embedded in paraffin blocks. This was done with a Myr STP120 (Tarragona, Spain) tissue processor with the following program: (i) 3 times, 1 hour each, in 96% ethanol (ii) 3 times, 1 hour each, in 100% ethanol (iii) 3 times, 1 hour each, in isoparaffin, and (iv) twice, 2 hours each, in paraffin, followed by inclusion with a Myr EC350-1 modular tissue embedding center. The blocks were cut into 3 μm slices with a microtome (Microm HM325, Thermo Scientific), mounted, and fixed to the glass slide with heat (90º C for 1 hour followed by 60ºC for 2 hours). The slices were later deparaffined (embedding in isoparaffin during 60 s while shaking) and hydrated (embedding in 100% ethanol during 60 s while shaking, the same procedure in 96% ethanol, and in distilled water). The slices were finally stained with Masson's Trichrome staining using the reagents and the procedure from Bio-Optica. The slides were mounted and imaged with a Leica DM 1000 LED microscope (8 random images per heart, in interstitial sites, at 20x) and manually segmented for estimating the percentage of fibrotic area (in blue) using ImageJ. The number of animals in each group that were included in the cardiac fibrosis measurement were: healthy: n = 4, D-gal: n = 12, D-gal + P-EVs: n = 7, D-gal + NP-EVs: n = 6.

5.3.3.5 Cardiac perfusion

ECG-gated SPECT images were performed with a small-animal scanner (μSPECT, MILabs, the Netherlands) 60 minutes after the intravenous administration of 65.7 ± 11.9 ^{99m}Tc-sestamibi. The SPECT acquisition parameters were an isotropic voxel size of 0.4 mm and 1 hour of acquisition time, images were reconstructed using two-dimensional ordered subset expectation maximization (OSEM-2D) with 16 subsets and 1 iteration. For manual analysis, Multimodality Workstation software (MMWKS) [410] was used to define LV myocardium by a single expert to get the mean, maximum and minimum of ^{99m}Tc-sestamibi uptake values. The number of animals in each group that underwent the cardiac perfusion study before receiving the treatment were: D-gal + P-EVs: n = 4, D-gal + NP-EVs: n = 2. The number of animals in each group that underwent the cardiac perfusion study at the endpoint were: healthy: n = 4, D-gal: n = 4, D-gal + P-EVs: n = 6, D-gal + NP-EVs: n = 4. To prepare the images for Figure 5.4d, intensity of representative raw SPECT images was normalized by the injected dose, by the animal weight and by the acquisition time using ImageJ to allow for comparison. From the normalized 3-dimensional (3D) image, a slide in the middle of the LV was chosen and displayed using the physics look up table with the same window and level in the images of the different animals.

5.3.3.6 Total antioxidant capacity

Blood collected at the endpoint on serum tubes was left at room temperature (RT) during 30 min and then centrifuged at 2000× g at 4° C for 15 minutes. Serum was stored at -80º C until used. After 1:500 dilution, total antioxidant capacity was determined following the kit's instructions (MAK187, Sigma-Aldrich). The total antioxidant capacity values were normalized by the total protein concentration in the same serum samples, determined with Bradford assay. Total antioxidant capacity was estimated in the following number of animals in each group: healthy: n = 6, D-gal: n = 12, D-gal + P-EVs: n = 7, D-gal + NP-EVs: n = 6.

5.3.3.7 Glucose tolerance test

Animals were deprived from food 8 hours before performing the glucose test. Basal glucose level was measured with a FreeStyle Optimum Neo H (Abbott, Chicago, IL, U.S.A) glucometer, and then a 10% glucose solution (100 mg/ml in PBS) was IP injected at 10 ml/kg. Blood glucose levels were recorded 30 min, 60 min, 90 min and 120 min post-injection. To analyze the results, data were fitted to a 4th order polynomial (in a least-squares sense), and the total area under the curve, the recovery time, the increment in the area under the curve until the recovery time, and the maximum and minimum glucose levels were obtained. Figure 5.2 shows an example of glucose level evolution during the tolerance test, the fitting, and the illustration of the corresponding parameters obtained. The glucose tolerance test was performed in the following number of animals in each group: healthy: n = 7, D-gal: n = 7, D-gal + P-EVs: n = 7, D-gal + NP-EVs: n = 6.

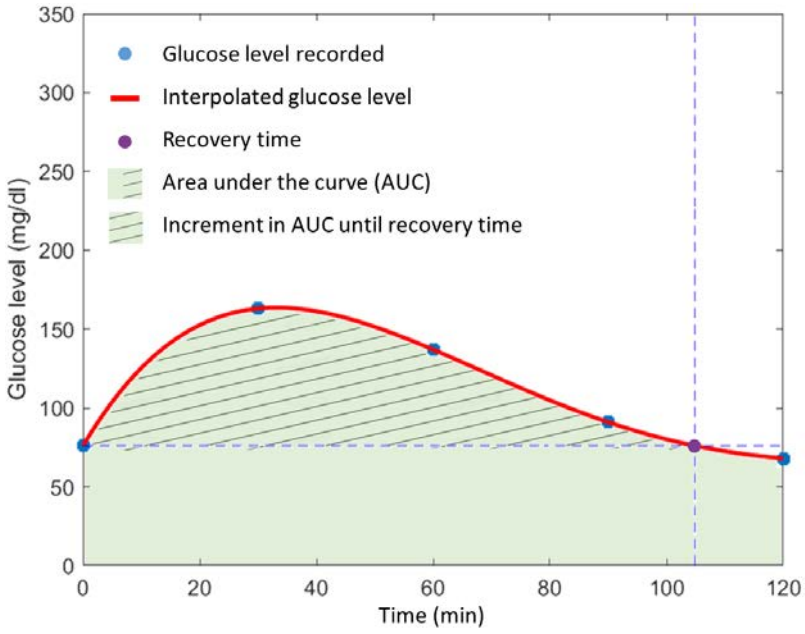

Figure 5.2. Glucose level changes in time and the corresponding parameters measured. At time 0, after basal glucose level recording, 10% glucose solution was injected intraperitoneally at 10

ml/kg. Glucose level values recorded are in blue. Glucose level curve resulting from interpolating the glucose values recorded is in red. Point at which the basal glucose level is recovered is in purple (recovery time). Total area under the curve (AUC) is in green. Increment in AUC until recovery time is with diagonal lines.

5.3.3.8 Hair regrowth

A 2 x 2 cm approximate area was shaved in the chest of the rats. The area was imaged after shaving, after 7 days and after 17 days to monitor hair regrowth. The images were manually segmented using ImageJ to determine the area of hair regrowth. Hair regrowth was explored in the following number of animals in each group: healthy: n = 8, D-gal: n = 12, D-gal + P-EVs: n = 7, D-gal + NP-EVs: n = 6.

5.3.4 Statistical analysis

Results are presented as mean ± standard error of the mean in the text and in figures. Continuous variables were compared using Student's t-tests. Categorical variables (percentage of senescent cells) were compared using the Z-Score for two population proportions. All probability values reported are two-sided, with $p < 0.05$ considered significant.

5.4 Results

5.4.1 CDC-EVs present variable anti-senescent and pro-angiogenic potency *in vitro*, which allows their classification as potent (P-EVs) and non-potent (NP-EVs)

The CDC-EVs obtained from the 18 different donors presented variable anti-senescent and pro-angiogenic potency (Figure 5.3). Regarding their anti-senescent effect, (i) most CDC-EVs significantly reduced human CSC senescence from two different donors (Figure 5.3b), (ii) all CDC-EVs significantly increased CSC IL-6 secretion (Figure 5.3c) and (iii) most CDC-EVs reduced CSC *CDKN1A* (Figure 5.3d) and *CDKN2A* (Figure 5.3g) expression but only a few CDC-EVs reduced *TGFB1* (Figure 5.3e) and *TP53* (Figure 5.3f) expression. All CDC-EVs except from one donor (number 18) significantly increased tube formation on endothelial cells (Figure 5.3h).

Figure 5.3a shows the total potency score obtained by the CDC-EVs from different donors used to classify them as potent (green, total score between 11 and 14), mild-potent (white, total score between 7.5 and 8.5) and non-potent (red, between 5 and 7). The CDC-EVs with the highest potency (1 and 2, with 14 and 12.5 points in the potency score over 18 possible

respectively), were among the 33% best CDC-EVs in most of the potency tests in the assay matrix. On the other hand, the least potent donor (18, with 5 points in the potency score), was among the worst 33% CDC-EVs in most of the potency tests in the assay matrix, not showing a significant beneficial effect in most of the *in vitro* tests. The performance of each of the different CDC-EVs on the different tests of the potency matrix assay is shown in Figure 5.3b-h.

For example, in Figure 5.3b we can see how CDC-EVs from donor 5, classified as potent, had the highest average reduction in CSC senescence: 8.1 ± 1.05% in CSCs from the first donor (from 25.6 in control conditions to 17.5% when treated, $p < 0.001$) and 11.0 ± 1.25% in CSCs from the second donor (from 47.5 to 36.5% when treated, $p < 0.001$). However, reduction in CSC senesce with CDC-EVs from donor 16, selected as non-potent, were considerably lower: 4.0 ± 1.4% ($p = 0.04$) in CSCs from the first donor, and -3.2 ± 1.24 ($p > 0.05$) in CSCs from the second donor. The reduction in senescence induced by CDC-EVs was in general higher in CSCs from the second donor, as the basal senescence was higher.

According to these results, CDC-EVs from donors 1 (14 years old, male) and 2 (77 years old, female) were selected as the most potent and used for treating animals assigned to the potent EVs group (P-EVs) *in vivo*. CDC-EVs from donor 18 (73 years old, male) were considered as the least potent and were used for treating the animals assigned to the non-potent EVs group (NP-EVs).

5.4.2 P-EVs have more rejuvenating cardiac effect *in vivo* than NP-EVs

Potent and non-potent CDC-EVs selected according to their potency score in the matrix assay were tested in an *in vivo* model of induced cardiac aging. Administration of daily D-gal had several cardiac-aging related effects at cardiac genetic, tissue, organ and functional level (Figure 5.4). The administration of P-EVs was able to revert some of these cardiac-aging associated effects, while the administration of NP-EVs had a minor effect or even contributed more negatively to cardiac aging (Figure 5.4).

Senescence in the cardiac tissue, measured at genetic level with the relative expression of the *GLB1* gene, was significantly increased with the daily administration of D-gal (1.56 ± 0.17 vs. 1.00 ± 0.1 in the healthy group, $p < 0.05$) as shown in Figure 5.4a. The use of P-EVs reversed this effect, as relative *GLB1* expression was significantly lower vs. the D-gal group (0.93 ± 0.19, $p < 0.05$) and non-significantly different vs. the healthy group. The use of NP-EVs, despite also showed a tendency to reverse this effect (1.10 ± 0.20), did not significantly reduce *GLB1* expression vs. the D-gal group. The relative expression levels of the other senescence-associated genes explored (*CDKN2A* and *TP53*) presented no differences between groups (data not shown).

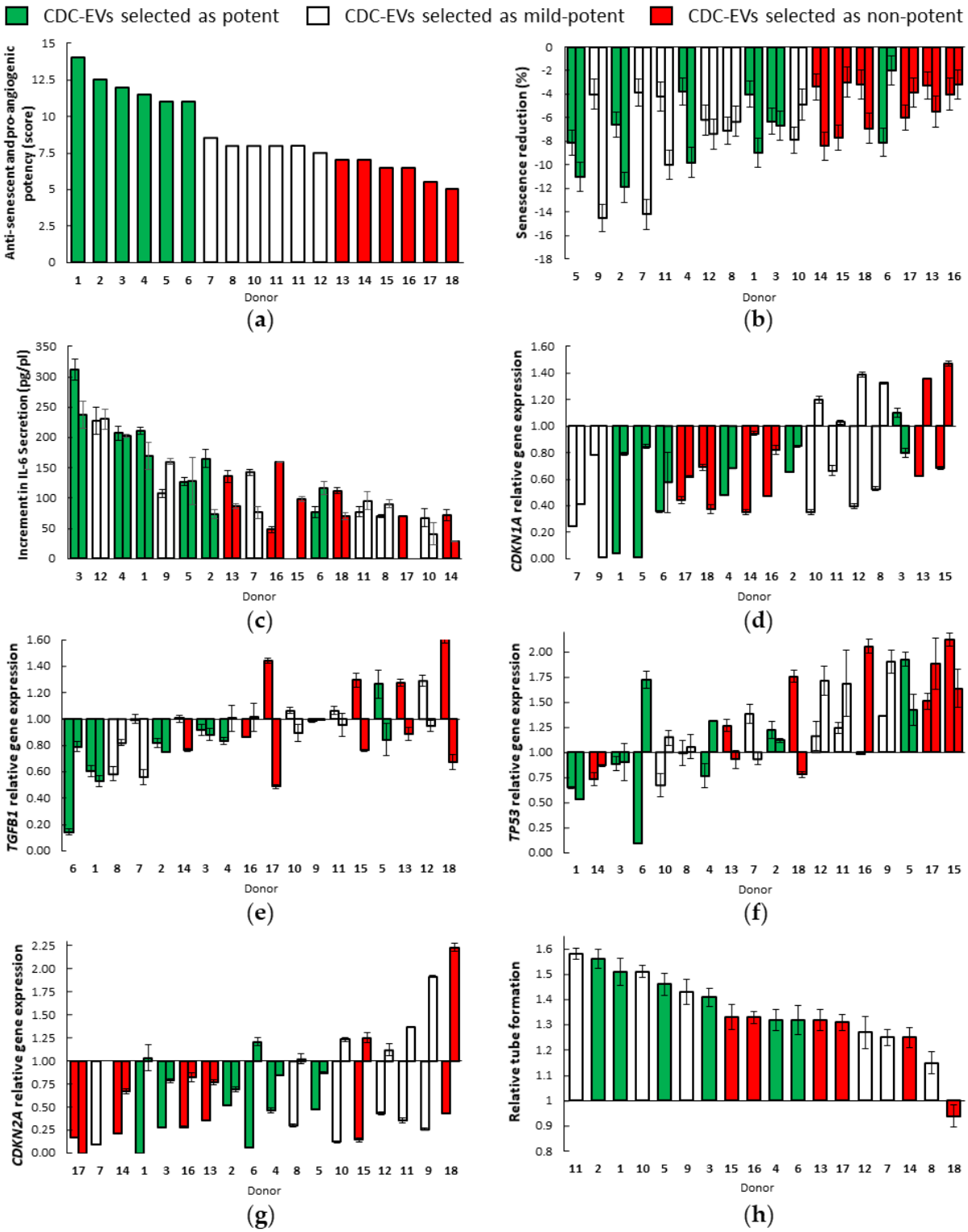

Figure 5.3. Performance of CDC-EVs from the different donors in the different tests in the potency matrix-assay. (**a**) Total score obtained in the potency matrix-assay, used for the classification of potent CDC-EVs, mild-potent CDC-EVs and non-potent CDC-EVs. (**b**) Reduction in CSC senescence (in two target donors) induced by the different CDC-EVs (n = 1199 ± 27 cells/condition in target donor 1 and n = 1520 ± 18 cells/condition in target donor 2).

(**c**) Increment in CSC IL-6 secretion (in two target donors) induced by the different CDC-EVs (n = 3 samples/condition). (**d**) *CDKN1A* relative expression in CSC (from two target donors) under the effect of the different CDC-EVs (n = 3 samples/condition). (**e**) *TGFB1* relative expression in CSC (from two target donors) under the effect of the different CDC-EVs (n = 3 samples/condition). (**f**) *TP53* relative expression in CSC (from two target donors) under the effect of the different CDC-EVs (n = 3 samples/condition). (**g**) *CDKN2A* relative expression in CSC (from two target donors) under the effect of the different CDC-EVs (n = 3 samples/condition). (**h**) Relative tube formation in endothelial cells under the effect of the different CDC-EVs. All data are with respect to untreated CSCs or endothelial cells (n = 19 ± 1 images/condition).

Cardiac hypertrophy, measured as the ratio between the heart weight and the body weight, tended to be increased by daily administration of D-gal (2.6 ± 0.09 vs. 2.5 ± 0.1 g/kg in the healthy group, Figure 5.4b). Despite the same tendency being observed in animals of both sexes, due to the large variability in the ratio between males and females and to the smaller number of females, the difference was only significant in the male group (2.5 ± 0.05 vs. 2.2 ± 0.1 g/kg, $p < 0.01$). When using P-EVs, cardiac hypertrophy was slightly reduced vs. the D-gal group, but without reaching significance (2.4 ± 0.1 g/kg, $p > 0.05$ vs. D-gal and vs. healthy). When using NP-EVs, cardiac hypertrophy was significantly higher (2.9 ± 0.11 g/kg) both vs. the healthy group and the P-EVs groups ($p < 0.05$). When considering only males, this difference was also significant vs. the D-gal group ($p < 0.05$).

D-gal and EV administration also had significant effects in cardiac fibrosis (Figure 5.4c). At genetic level, D-gal administration significantly increased relative *TGFB1* expression (1.77 ± 0.17 vs. 1.00 ± 0.1, $p = 0.01$). This expression was reduced by P-EVs (1.5 ± 0.23) to the point of not being significantly different to the healthy group ($p > 0.05$), but this reduction did not achieve significance vs. the D-gal group. NP-EVs also reduced relative *TGFB1* expression, but to a lesser extent (1.6 ± 0.35, $p > 0.05$ vs. all groups). At cardiac tissue level, the percentage of interstitial fibrosis was significantly increased by D-gal (from 1.42 ± 0.17 to 2.02 ± 0.11%, $p < 0.05$). Animals in the P-EVs group presented a similar average cardiac fibrosis (2.01 ± 0.18%), but without significant differences vs. the healthy group ($p = 0.06$). However, animals in the NP-EVs group presented a significantly higher cardiac fibrosis than healthy animals (2.10 ± 0.15, $p < 0.05$ vs. healthy). Representative images of cardiac fibrosis in animals in the different groups are shown in Figure 5.4c.

At functional level, D-gal administration did not significantly worse cardiac perfusion nor cardiac hemodynamic performance. Cardiac perfusion measured by SPECT mean activity at the endpoint was similar in the healthy, D-gal and P-EVs groups (262 ± 7, 264 ± 13 and 252 ± 12

cps respectively, all differences not significant, $p > 0.05$, Figure 5.4d). Nevertheless, cardiac perfusion of animals treated with NP-EVs was considerably worse than animals in healthy and D-gal groups (220 ± 7 cps, $p < 0.05$ vs. healthy and D-gal). Minimum and maximum activity values were not significantly different among all groups, confirming that mean values differences are only due to cardiac perfusion differences. As the SPECT images from some animals at pre-treatment was available, we compared the evolution in cardiac perfusion in some animals before and after receiving P- or NP-EVs. While animals receiving P-EVs tended to improve their cardiac perfusion (Δ 12 ± 19 cps), administration of NP-EVs tended to worse their cardiac perfusion (Δ -3 ± 16 cps). However, due to the small number of animals with this data available, the difference was not significant. Representative images of SPECT activity in animals in all groups at endpoint and the corresponding image of the P-EV and NP-EV animals before receiving the EVs are shown in Figure 5.4d. Regarding hemodynamic performance, animals in the D-gal group did not record increases in maximum, end-diastolic and minimum ventricular pressure and did not show differences in their maximum and minimum derivatives of pressure and the isovolumic relaxation constant (tau) (data not shown). Therefore, there were no margin for observing beneficial effects of EV administration.

5.4.3 P-EVs have more beneficial systemic effects *in vivo* than NP-EVs

Apart from the cardiac effects, daily D-gal administration also had other aging-related systemic effects, some of which were partly overcome by P-EVs (Figure 5.5). D-gal daily administration reduced the increment in body weight (Figure 5.5a), so at week 32, the animals in the D-gal group had a considerably lower body weight (546 ± 40 g) vs. the healthy animals (676 ± 60 g). The difference was not significant ($p = 0.08$) due to the large differences in body weight between males and females. However, when analyzing both sexes separately, the difference was significant ($p < 0.05$) in the male group and had the same tendency in the female group. Animals in the P- and NP- group had body weights similar to the D-gal group (535 ± 51 and 511 ± 55, $p > 0.05$ vs. all other groups).

Regarding total antioxidant capacity (Figure 5.5b), D-gal administration tended to increase it vs. the healthy group, but without reaching significance (1.51 ± 0.07 vs. 1.38 ± 0.02, $p > 0.05$). P-EVs tended to slightly compensate the increase (1.46 ± 0.08), while NP-EVs even further accentuated it (1.54 ± 0.11), but these small differences did not reach significance. When looking at total antioxidant capacity differences by gender, while the general tendencies previously described were mainly observed in males (were in fact higher total antioxidant capacity in the NP-EV group reached significance with respect to the healthy group, $p < 0.05$), in females all groups had very similar total antioxidant capacity.

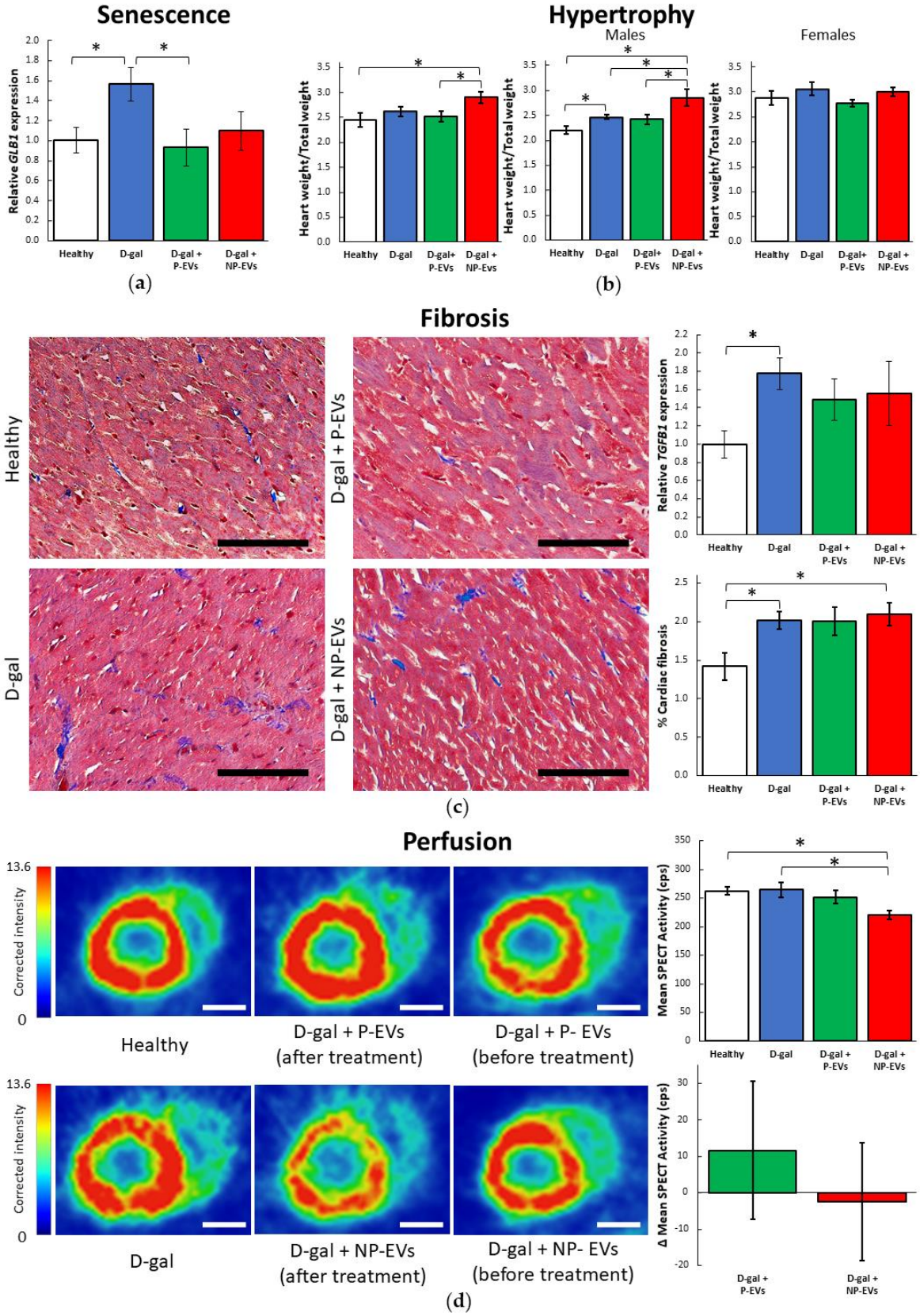

Figure 5.4. Cardiac effects of D-gal and P- and NP-EV administration. (**a**) Effects on cardiac senescence at genetic level (healthy: *n* = 6, D-gal: *n* = 11, D-gal + P-EVs: *n* = 7, D-gal + NP-

EVs: n = 6). (**b**) Effects on cardiac hypertrophy on the whole population (healthy: n = 8, D-gal: n = 12, D-gal + P-EVs: n = 7, D-gal + NP-EVs: n = 6), on males (healthy: n = 5, D-gal: n = 9, D-gal + P-EVs: n = 5, D-gal + NP-EVs: n = 4) and on females (healthy: n = 3, D-gal: n = 3, D-gal + P-EVs: n = 2, D-gal + NP-EVs: n = 2). (**c**) Effects on cardiac fibrosis at genetic (healthy: n = 6, D-gal: n = 11, D-gal + P-EVs: n = 7, D-gal + NP-EVs: n = 6) and tissue level (healthy: n = 4, D-gal: n = 12, D-gal + P-EVs: n = 7, D-gal + NP-EVs: n = 6). Representative images of interstitial fibrosis in animals in each group. (**d**) Effects on cardiac perfusion (healthy: n = 4, D-gal: n = 4, D-gal + P-EVs: n = 6, D-gal + NP-EVs: n = 4) and the evolution in cardiac perfusion (D-gal + P-EVs: n = 4, D-gal + NP-EVs: n = 2). Representative images of Single Photon Emission Computer Tomography (SPECT) intensity corrected by injected activity, animal weight and acquisition time in animals in the different groups. Also shown images of animals in the P- and NP-EVs groups before receiving the EVs to illustrate the effect of the treatment administration. D-gal: D-galactose. EVs: Extracellular vesicles. P: potent. NP: non-potent. Black scale bar corresponds to 100 μm. White scale bar corresponds to 5 mm. * $p < 0.05$.

Daily administration of D-gal also seemed to influence in glucose metabolism (Figure 5.5c). Both the total AUC and the increment in the AUC until the recovery time were significantly lower in the D-gal vs. the healthy group ($p < 0.05$). P-EVs, contrary to NP-EVs, partially compensated the D-gal effect: AUC was closer in the P-EVs to the healthy than to the D-gal group ($p > 0.05$ vs. both groups) and increment in the AUC until the recovery time was significantly higher in the P-EVs than in the D-gal group ($p < 0.05$).

D-gal administration also seem to negatively impact on hair regrowth (Figure 5.5d). After 7 days, animals in the D-gal group only had a 16 ± 3% of hair regrowth, while healthy animals had 37.1 ± 7.0% ($p < 0.05$). Both P- and NP- EVs improved hair regrowth vs. D-gal (30.6 ± 11.6 and 29.1 ± 11.3 respectively, $p > 0.05$ both vs. D-gal and healthy groups). No significant differences were observed in hair regrowth between any of the groups after 17 days. Representative images of the differences in hair regrowth after 7 days in animals belonging to the different groups are shown in Figure 5.5e.

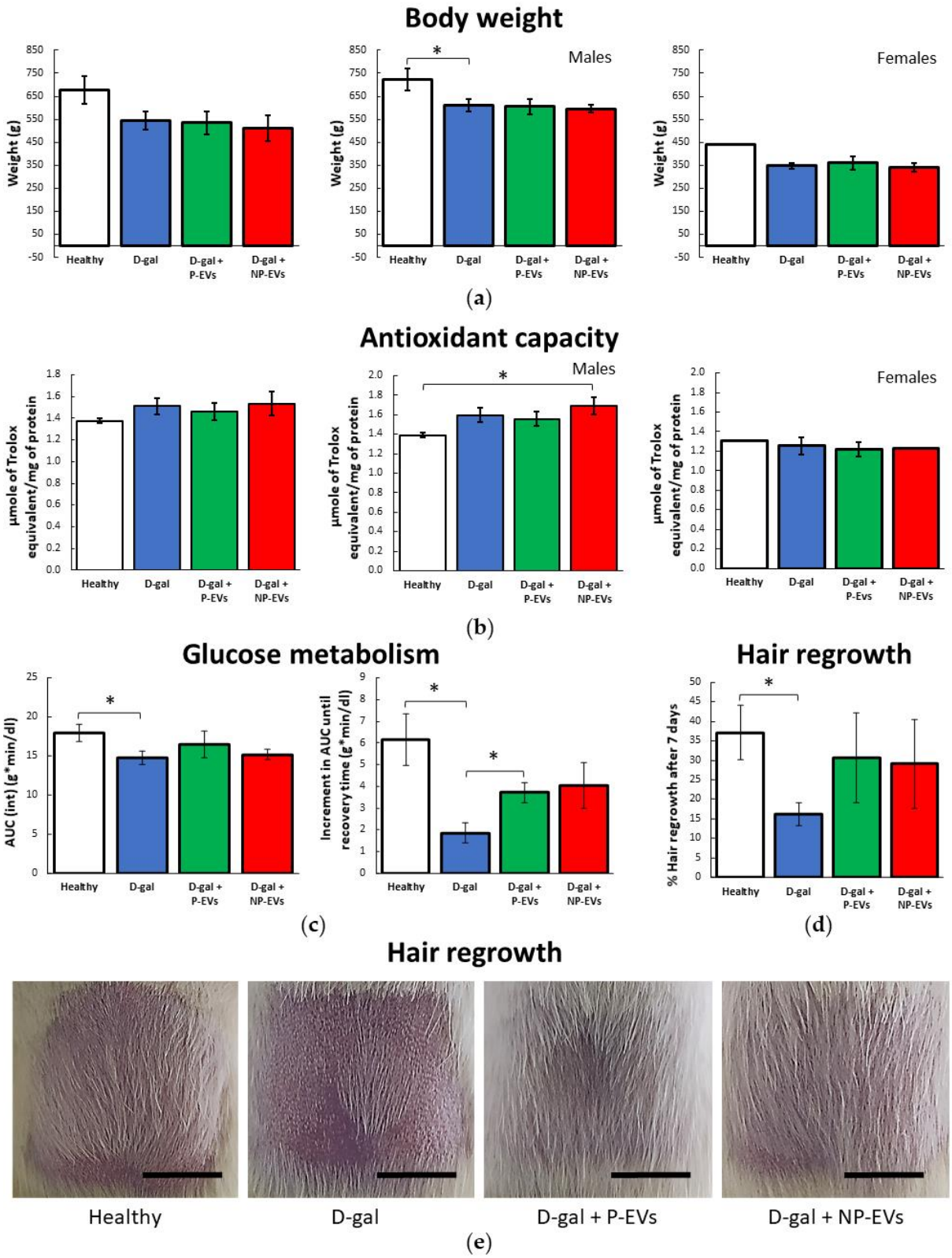

Figure 5.5. Systemic effects induced by D-gal and by P- and NP-EVs in the rodent model. (**a**) Body weight in week 32 in all animals (healthy: n = 6, D-gal: n = 12, D-gal + P-EVs: n = 7, D-gal + NP-EVs: n = 6), in males (healthy: n = 5, D-gal: n = 9, D-gal + P-EVs: n = 5, D-gal + NP-

EVs: *n* = 4), and in females (healthy: *n* = 1, D-gal: *n* = 3, D-gal + P-EVs: *n* = 2, D-gal + NP-EVs: *n* = 2). (**b**) Total antioxidant capacity in serum in all animals (healthy: *n* = 6, D-gal: *n* = 12, D-gal + P-EVs: *n* = 7, D-gal + NP-EVs: *n* = 6), in males (healthy: *n* = 5, D-gal: *n* = 9, D-gal + P-EVs: *n* = 5, D-gal + NP-EVs: *n* = 4), and in females (healthy: *n* = 1, D-gal: *n* = 3, D-gal + P-EVs: *n* = 2, D-gal + NP-EVs: *n* = 2). (**c**) Area under the curve (AUC) and increment in AUC until recovery time from the glucose tolerance test (healthy: *n* = 7, D-gal: *n* = 7, D-gal + P-EVs: *n* = 7, D-gal + NP-EVs: *n* = 6). (**d**) Percentage of hair regrowth 7 days after shaving (healthy: *n* = 8, D-gal: *n* = 12, D-gal + P-EVs: *n* = 7, D-gal + NP-EVs: *n* = 6). (**e**) Representative images of hair regrowth in the animals in the different groups 7 days after shaving. D-gal: D-galactose. EVs: Extracellular vesicles. P: potent. NP: non-potent.

5.5 Discussion

The results of this study show that senescence and angiogenesis-related *in vitro* functional assays can be used as predictors of CDC-EV *in vivo* potency for cardiac aging. The matrix assay proposed here evaluates and scores *in vitro* the anti-senescent potency on CSCs and the pro-angiogenic potency on endothelial cells using several markers. According to the results in the matrix assay, the EVs can be classified as potent, mild-potent and non-potent. These differences in the therapeutic potential *in vitro* seem to translate to the *in vivo* model, as EVs selected as potent had higher rejuvenating potential than EVs selected as non-potent in a rodent model of induced cardiac aging.

To quantify the effect of the *in vitro* potency, we decided to design a matrix assay that evaluated and scored the anti-senescent potency on CSCs from human origin of two different donors and the pro-angiogenic effect on human endothelial cells. The anti-senescent effect was evaluated using SA-β-gal expression, IL-6 secretion and *CDKN1A*, *TGFB1*, *CDKN2A* and *TP53* expression. The pro-angiogenic effect was evaluated according to the CDC-EV potential to induce tube formation on HUVEC. The performance in each of the different tests was scored and added to obtain a final potency score, so that selected CDC-EVs as potent according to this score had the highest anti-senescent and pro-angiogenic potency *in vitro* while selected CDC-EVs as non-potent had the lowest *in vitro* anti-senescent and pro-angiogenic potency.

EVs classified as potent (P-EVs) with the *in vitro* matrix assay had higher cardiac rejuvenating potency *in vivo* than EVs classified as non-potent (NP-EVs). While P-EVs had the potential to significantly reduce the expression of the senescence-associated gene *GLB1* in D-gal age-induced-animals and to non-significantly reduce cardiac hypertrophy and *TGFB1* expression, NP-EVs did not significantly produce any effect and in fact significantly increased cardiac hypertrophy, cardiac fibrosis and reduce perfusion. These results are in accordance with the

effects observed in the *in vitro* functional assay. While P-EVs (from donors 1 and 2) had significant beneficial effects in most *in vitro* effects explored (reducing CSC senescence, increasing CSC IL-6 secretion, reducing the genetic expression of senescence-associated genes and improving angiogenesis), NP-EVs (from donor 18) only significantly improved CSC senescence in one of the two target donors, increased CSC IL-6 secretion and reduced *CDKN2A* expression. In addition, NP-EVs even tended to worse *TGFB1*, *TP53* and *CDKN2A* expression in CSCs and reduced endothelial tube formation. *In vivo*, P-EVs also presented a higher tendency to induce rejuvenation at systemic level than NP-EVs. While P-EVs significantly improved the increment in the AUC until recovery time in the glucose test and tended to drive total antioxidant capacity and hair growth to a healthier profile, NP-EVs did not significantly improve any of the explored parameters and even significantly increased total antioxidant capacity.

Although the results go in the direction of our hypothesis and clearly show differences between the changes induced by P- and NP-EVs, the benefits exerted by P-EVs are still not as remarkable as those in other studies [140], probably because of the limitations of the cardiac aging model used. Administration of daily D-gal for several weeks is described to drive age-related physiological changes in different tissues, particularly in the heart, but we were not able to replicate all these effects despite using higher D-gal doses and for considerably longer than described in the reference articles. D-gal injections have been related to increased senescence [409] (by increasing SA-β-gal, p21 and p53 expression and increasing AGE protein levels [411]) and to decreased cardiac function (increased cardiac hypertrophy, CM cross-sectional area and decreased EF and fractional shortening (FS) [412]. At systemic level, D-gal is also described to decrease antioxidant and total antioxidant capacity levels [413]. However, in this study, D-gal only induced moderate changes at cardiac and systemic level: for example, no differences were observed between healthy and D-gal animals at hemodynamic and cardiac perfusion level and only moderate changes in *GLB1* expression, hypertrophy and cardiac fibrosis were observed, being the values and differences still far from those of naturally aged of pathological animals [140, 414–416]. Therefore, as D-gal did not induce large damage at cellular, structural, and functional level, we cannot consider these animals as truly aged or pathological, giving little room for the P-EVs to exert any significant benefits. While the number of animals included in this study was not very high, the deviation was, becoming hard to find significance in the small differences caused either by the model or by P-EVs in these relatively healthy animals.

Despite the results here suggesting that *in vitro* EV potency seems to predict efficacy *in vivo*, future experiments should be addressed to confirm the rejuvenating efficacy of P vs. NP-EVs in naturally aged animals, as well as to validate if the potency score developed here correlates with *in vivo*, and later clinical, efficacy. To do so, CDC-EVs from large numbers of donors should be assessed for the potency score and then tested *in vivo*. These would also help defining pass and

fail quantitative ranges, as the potency score proposed here depends on whether the CDC-EVs are among the best, the middle, or the worst tercile, and not on quantitative values.

In spite of all the limitations, the results highlight the importance of performing adequate potency tests before using biological products in the clinical scenario, as the use of non-potent or suboptimal products may lead to unforeseen results. Accordingly, we propose a potency matrix assay with tests that are relatively fast, easy, and economic to implement and show that it is capable of predicting *in vivo* outcome. After further validation, this matrix assay could eventually replace *in vivo* potency assays (more resource- and time-consuming) before clinical translation.

5.6 Conclusions

Differences in the *in vitro* anti-senescent and pro-angiogenic potency of extracellular vesicles derived from cardiosphere-derived cells (CDC-EV) can be used to predict CDC-EV *in vivo* efficacy in a model of cardiac aging. We suggest as a potency test an *in vitro* matrix assay consisting in scoring the CDC-EVs potential to reduce senescence-associated β-galactosidase (SA-β-gal), *CDKN1A*, *TGFB1*, *CDKN2A* and *TP53* expression and to increase IL-6 secretion on cardiac stromal cells, together with CDC-EV ability to induce endothelial tube formation. According to the results in the different *in vitro* tests, CDC-EVs can be classified as potent (P-EVs), mild-potent and non-potent (NP-EVs). EVs classified *in vitro* as potent showed more rejuvenating potential in an *in vivo* model of induced cardiac aging than EVs classified as non-potent. After further validation, the matrix assay proposed here could be a suitable *in vitro* potency test for discerning suitable biological products for their allogenic use in the cardiac aging clinical scenario.

Chapter 6

Cardiac extracellular matrix hydrogel enriched with polyethylene glycol presents improved gelation time and increased on-target site retention of extracellular vesicles

6.1 Abstract

Stem-cell-derived extracellular vesicles (EVs) have demonstrated multiple beneficial effects in preclinical models of cardiac diseases. However, poor retention at the target site may limit their therapeutic efficacy. Cardiac extracellular matrix hydrogels (cECMH) seem promising as drug-delivery materials and could improve the retention of EVs, but may be limited by their long gelation time and soft mechanical properties. Our objective was to develop and characterize an optimized product combining cECMH, polyethylene glycol (PEG), and EVs (EVs–PEG–cECMH) in an attempt to overcome their individual limitations: long gelation time of the cECMH and poor retention of the EVs. The new combined product presented improved physicochemical properties (60% reduction in half gelation time, $t_{1/2}$, $p < 0.001$, and threefold increase in storage modulus, $p < 0.01$, vs. cECMH alone), while preserving injectability and biodegradability. It also maintained *in vitro* bioactivity of its individual components (55% reduction in cellular senescence vs. serum-free medium, $p < 0.001$, similar to EVs and cECMH alone) and increased on-site retention *in vivo* (fourfold increase vs. EVs alone, $p < 0.05$). In conclusion, the combination of EVs–PEG–cECMH is a potential multipronged product with improved gelation time and mechanical properties, increased on-site retention, and maintained bioactivity that, all together, may translate into boosted therapeutic efficacy.

6.2 Introduction

Regenerative and reparative therapies, although they seem promising in different cardiovascular diseases, present demanding requirements that are difficult to achieve and that

limit their translation into the clinical scenario [283]. Regenerative products must be biocompatible and bioactive, preferably injectable in a unique dose, and adequately retained and degraded at the site of interest.

The main problems of cell products derive from their large variability and their lack of stability and standardization [115]. Some of the challenges seemed to be solved once it was clarified that most of their beneficial effects are caused by paracrine mediators, such as extracellular vesicles (EVs), which possess meaningful advantages as therapeutics vs. their parenteral cells [180, 417]. In particular, EVs derived from cardiosphere-derived cells (CDCs) have shown potential to improve cardiac function in infarcted [181] and aged hearts [140], as well as antiarrhythmic effects [293]. However, EV retention at the target site remains as one of their main challenges [418].

The use of injectable biomaterials for cardiac regeneration, such as hydrogels, has also been explored. Those derived from cardiac extracellular matrix (cECMH) mimic the biophysical and topographical properties of the ECM and gel at physiological temperature. In addition, they improve cardiac function in preclinical models [235] and have shown safety in a phase I clinical trial [222]. Nevertheless, slow gelation time, rapid degradation, and poor mechanical properties [217] are some of their physicochemical limitations. The combination of naturally derived hydrogels with synthetic materials, such as polyethylene glycol (PEG), seems promising [217] to make cECMH more suitable for therapeutic use.

Apart from providing structural support and favorable bioactivity on surrounding tissue, biomaterials can also be used for the delivery of small particles and/or cells to improve their retention at the injection site [419]. The combination of hydrogels with other bioactive products may solve some of the current limitations they possess individually, and enhance the therapeutic response with a synergistic effect [204]. However, specific designs for specific purposes will probably be needed.

The aim of this work was to develop, characterize, and evaluate *in vitro* and *in vivo* the suitability of a new product composed by EVs derived from CDCs embedded in a PEG–cECM hydrogel (EVs–PEG–cECMH) for its use as a regenerative product. Firstly, we explored the different physicochemical properties of the combined product (EVs–PEG–cECMH) vs. the cECMH alone, and how PEG, which can also be used as a purification method of EVs from conditioned medium, influenced the gelation time and the mechanical properties. Secondly, we confirmed that product combination into the EVs–PEG–cECMH did not negatively affect the bioactivity of the individual components and served to improve EV retention at the injection site compared to EV administration in the standard delivery vehicle.

6.3 Materials and methods

6.3.1 EDCs, CDCs, and derived extracellular vesicle isolation

EVs used as therapeutic product were isolated from human CDCs, as previously described in section 4.3.1. The mean EV size obtained by the nanoparticle tracking analysis (NTA) software was 170 nm ± 20 nm, with a maximum particle size of 450 nm. For experiments, EVs were incubated overnight at 4 °C in 4% *w/v* polyethylene glycol (PEG), precipitated by centrifugation at 1500× g for 30 min, and resuspended in the corresponding medium (SFM or cECMH) at a concentration of 5 mg/ml, unless otherwise stated. Considering the 4% *w/v* PEG concentration in the conditioned medium, the size of the pellet containing the EVs (150–250 μl) and the volume of cECM in which the pellet was resuspended (1 ml), the estimated PEG concentration in the combined product of EVs–PEG–cECM solution was 8 ± 2 mg/ml.

6.3.2 Porcine myocardial matrix decellularization, lyophilization, and characterization

Porcine myocardial matrix was decellularized with slight modifications from a previous protocol from our group [420]. The heart from six euthanized minipigs (6.5 months old on average, three males) were immediately extracted, cleaned from fat, valves, and fibrotic regions, and the myocardium was cut into thin slices (1 mm thick) as shown in Figure 6.1a. The slices were individually decellularized in a distilled water solution at 1% *w/v* of sodium dodecyl sulfate (SDS) under constant shaking for 48–72 hours, and then washed in distilled water for another 72 hours. All the solutions were changed daily. The slices were then disinfected for 30 min in peracetic acid at 1% and kept in phosphate-buffered saline (PBS) with 1% penicillin/streptomycin (Gibco) at 4 °C until lyophilization (Figure 6.1b). Three slices from different animals (decellularized and non-decellularized) were frozen in Tissue O.C.T., cut into 4 μm slices, and stained with DAPI to confirm decellularization. This decellularization protocol has been previously shown in our group to yield less than 50 ng of DNA content per mg of tissue [420]. The lyophilized samples (in a Telstar, Lioalfa-6 lyophilizer, Munich, Germany, Figure 6.1c) were later cut into small pieces (around 1mm size), mixed, and stored at -20 °C until used for hydrogel preparation (Figure 6.1d). Sulfated glycosaminoglycan (sGAG) content (total and O-sulfated) and proteins present in the lyophilized matrix were confirmed in 3 samples by using the Blyscan assay (Biocolor Ltd, Carrickfergus, U.K.) and by Liquid chromatography–tandem mass spectrometry (LC–MS/MS, in a Triple TOF 6600, Sciex, Old Connecticut Path Framingham, MA, U.S.A), respectively.

The LC–MS/MS analysis was made using a previously standardized method by our group [421, 422]. An equal amount of protein from the samples was loaded on a 10% SDS-PAGE gel. The run was stopped as soon as the front had penetrated 3 mm into the resolving gel [423, 424]. The protein band was visualized by Sypro Ruby fluorescent staining (Lonza, Basel, Switzerland), excised, and subjected to in-gel, manual tryptic digestion following the protocol described previously by our group [421, 422]. Peptides were extracted by performing three 20-min incubations in 40 µl of 60% acetonitrile dissolved in 0.5% HCOOH. The resulting peptide extracts were pooled, concentrated in a SpeedVac, and stored at -20 °C.

Digested peptides were separated using reverse phase chromatography. Gradient was developed using a micro liquid chromatography system (Eksigent Technologies nanoLC 400, Sciex, Framingham, MA, U.S.A) coupled to a high-speed Triple TOF 6600 mass spectrometer (Sciex, Framingham, MA, U.S.A) with a micro flow source. The analytical column used was a silica-based reversed phase column YMC-TRIART C18 150 × 0.30 mm, with a 3 mm particle size, and 120 Å pore size (YMC Technologies, Teknokroma, Sciex, Framingham, MA, U.S.A). The trap column was a YMC-TRIART C18 (YMC Technologies, Teknokroma, Sciex, Framingham, MA, U.S.A) with a 3 mm particle size and 120 Å pore size, switched on-line with the analytical column. The loading pump delivered a solution of 0.1% formic acid in water at 10 µl/min. The micro-pump provided a flow rate of 5 µl/min and was operated under gradient elution conditions, using 0.1% formic acid in water as mobile phase A, and 0.1% formic acid in acetonitrile as mobile phase B. Peptides were separated using a 90-minute gradient ranging from 2% to 90% mobile phase B (mobile phase A: 2% acetonitrile, 0.1% formic acid; mobile phase B: 100% acetonitrile, 0.1% formic acid). Injection volume was 4 µl.

Data acquisition was carried out in a TripleTOF 6600 System (Sciex, Framingham, MA, U.S.A) using a data-dependent workflow. Source and interface conditions were as follows: ion spray voltage floating (ISVF) 5500 V, curtain gas (CUR) 25, collision energy (CE) 10, and ion source gas 1 (GS1) 25. The instrument was operated with Analyst TF 1.7.1 software (Sciex, Framingham, MA, U.S.A). Switching criteria were set to ions greater than the mass to charge ratio (m/z) 350 and smaller than m/z 1400, with charge state of 2–5, mass tolerance 250 ppm, and an abundance threshold of more than 200 counts (cps). Former target ions were excluded for 15 s. The instrument was automatically calibrated every 4 hours using as external calibrant tryptic peptides from pep Cal Mix (Sciex, Framingham, MA, U.S.A).

After MS/MS analysis, data files were processed using ProteinPilotTM 5.0.1 software from Sciex, which uses the algorithm ParagonTM for database search and ProgroupTM for data grouping. Data were searched using a Sus Scrofa specific Uniprot database. False discovery rate was performed using a non-lineal fitting method, displaying only those results that reported a 1% global false discovery rate or better [425, 426]. For the plot in Figure 6.3, relative abundance of

each protein was determined from the number of peptides identified, corrected by the size of the protein (in KDa, from Uniprot).

6.3.3 Cardiac extracellular matrix hydrogel (cECMH) synthesis

Hydrogels from the lyophilized decellularized cECM were prepared fresh for each experiment, with slight modifications from previous protocols [232]. The lyophilized myocardial matrix was solubilized with pepsin (P6887, Sigma-Aldrich, at 1 mg/10 mg of lyophilized matrix) in 0.01 M HCl (1 ml/10 mg of matrix) under constant stirring for 72 hours, at which point no solid particles were visible (Figure 6.1e). The solubilized cardiac matrix solution was placed on ice and adjusted to pH 7.4 by progressive addition of 0.1 M NaOH, and to physiological salt concentration (PBS 1x) by addition of 1/9 of the volume of PBS 10x. For hydrogel formulations incorporating PEG, (molecular weight = 8000, P5414, Sigma-Aldrich, at 3, 6, 12, or 16 mg/ml in the final solution), the corresponding amount of polymer was dissolved in the PBS 10x, sterile filtered, and added to the solution. All formulations were brought to a final concentration of 8 mg of solubilized cardiac matrix per ml of solution with the addition of PBS 1x. The solution was centrifuged at 4000 rpm and 4 °C for 5 min to remove any remaining insoluble particles (if any) and kept at 4 °C until used (maximum 24 hours). The solution was used for the characterization experiments, injected or gelled at 37 °C as detailed in the next sections (Figure 6.1f-g).

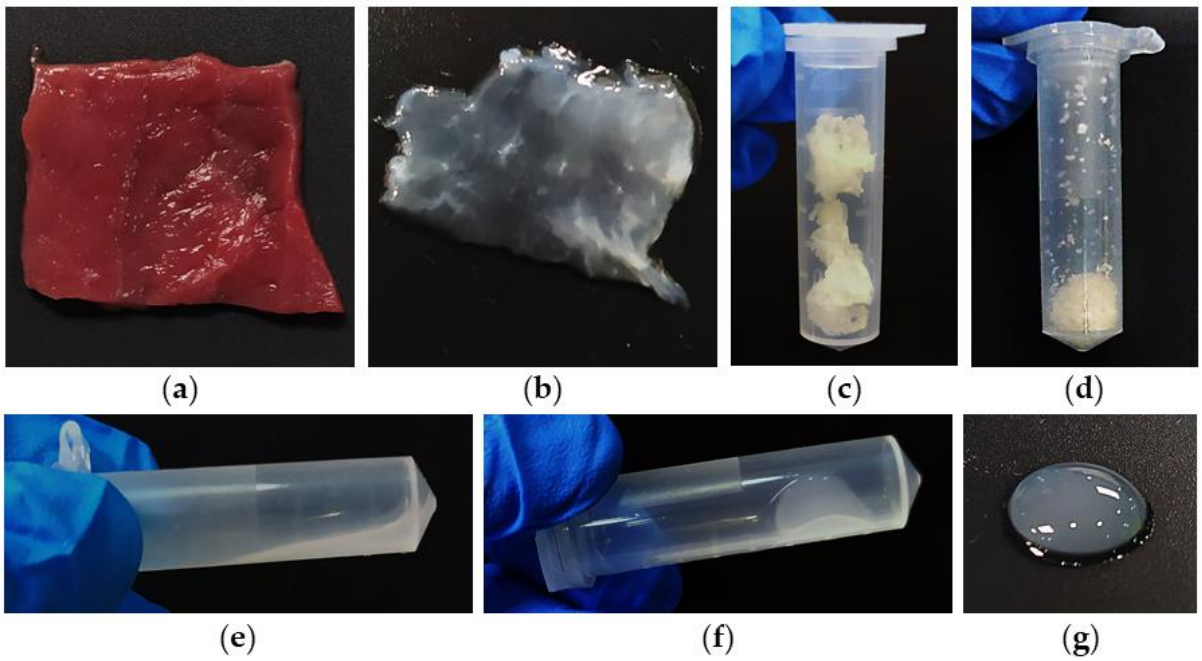

Figure 6.1. Procedure followed for the preparation of the cardiac extracellular matrix hydrogel (cECMH). (**a**) Porcine cardiac tissue cut into small, thin slides. (**b**) Decellularized cECM slides. (**c**) Lyophilized cECM. (**d**) Milled cECM. (**e**) Solubilized cECM. (**f-g**) Gelled cECM (cECMH).

6.3.4 Gelation kinetics

Gelation kinetics from three different batches of the control hydrogels, with PEG at 3, 6, 12, and 16 mg/ml, and with EVs prepared as described above, were studied by turbidimetry as previously published [427, 428]. A total of 100 µl of each solution in triplicate were placed in a 96-well plate, and the optical density (OD) at 405 nm and 37 °C was measured every 15 seconds with a SynergyTM HTX Multi-Mode Microplate Reader (BioteK, Winooski, VT, U.S.A.) during 90 min (when a plateau in all samples had been reached). OD values were averaged and normalized for each group. From the normalized plot, the half gelation time ($t_{1/2}$, at which normalized OD was 0.5), the lag phase (t_{lag}, at which the linear fit in the linear region of the plot was zero), and the speed of gelation (S, slope of the linear fit) were compared among the different groups.

6.3.5 Scanning electron microscopy

To study the effect of PEG and EVs on the hydrogel structure and fiber diameter, Scanning Electron Microscopy (SEM) images from hydrogels of two different batches at the different conditions (cECMH, cECMH with PEG at 3, 6, and 12 mg/ml, and EVs–PEG–cECMH) were taken. The solubilized matrix (800 µl) was gelled at 37 °C for 24 hours, and then dehydrated with a series of ethanol washes (2 hours at 20%, 2 hours at 40%, overnight at 60%, 2 hours at 80%, 2 hours at 100%, and overnight at 100%). The dehydrated samples were dried in a Thar R100W reactor by using supercritical CO_2, as previously described [427], and then were immersed in liquid nitrogen before sectioning. Sectioned samples were mounted, and sputter coated for 75 s with gold using Leica EM ACE600 (Wetzlar, Germany) to prepare them for imaging with a Philips XL30 SEM (Eindhoven, The Netherlands). Four random images at 24,000x were taken for each sample, and the widths of 20 distinguishable fibers per image (160 fibers per condition) were measured using ImageJ Software.

6.3.6 Rheometry and injectability

Viscosity and rheology measurements were performed in a TA Instruments AR-G2 rheometer (New Castle, DE, U.S.A) on samples with the different conditions (cECMH, and cECMH with PEG at 3, 6, and 12 mg/ml, and with EVs) as shown in Figure 6.2a-c. Viscosity was measured with a 40 mm diameter aluminum Peltier plate at the different conditions (from three different batches, each sample in triplicate). The rheometer was maintained at 25 °C and viscosity was measured between 0.1 and 500 Hz. For storage (G') and loss modulus (G") measurements, 1500 µl of hydrogel solution was gelled for 24 hours at 37 °C on 25 mm diameter disc-shaped molds. The linear viscoelastic region was determined in 3 samples, applying an

oscillatory strain sweep with amplitudes from 0.01% to 200% at a frequency of 1 Hz using a 25 mm diameter sand-blasted Peltier plate. In 4 samples of each condition (from two different batches), the dynamic frequency sweep at a fixed strain within the viscoelastic region (0.15%) was performed from 0.01 to 2 Hz at 37 °C. G' and G" at 1 rad/s (0.16 Hz) were plotted.

Injection forces are also important parameters for shear-thinning hydrogel characterization [429]. Injectability of the different preparations was confirmed through a commercially available Myostar injection catheter equipped with a 27 G needle at the tip (Biosense Webster, Irvine, CA, U.S.A.). The force required for injecting the different solutions with a 1 ml Luer-lock syringe connected to the Myostar catheter was measured at an injection speed of 500 µl/min using a QTest 1L Elite System (MTS, Artisan Technology Group, Champaign, IL, U.S.A., Figure 6.2d-e) and recorded using TestWorks Software. Measurements were performed at room temperature (RT) in 3 samples for each group (PBS, cECMH, cECMH with PEG at the different concentrations, and EVs–PEG–cECMH).

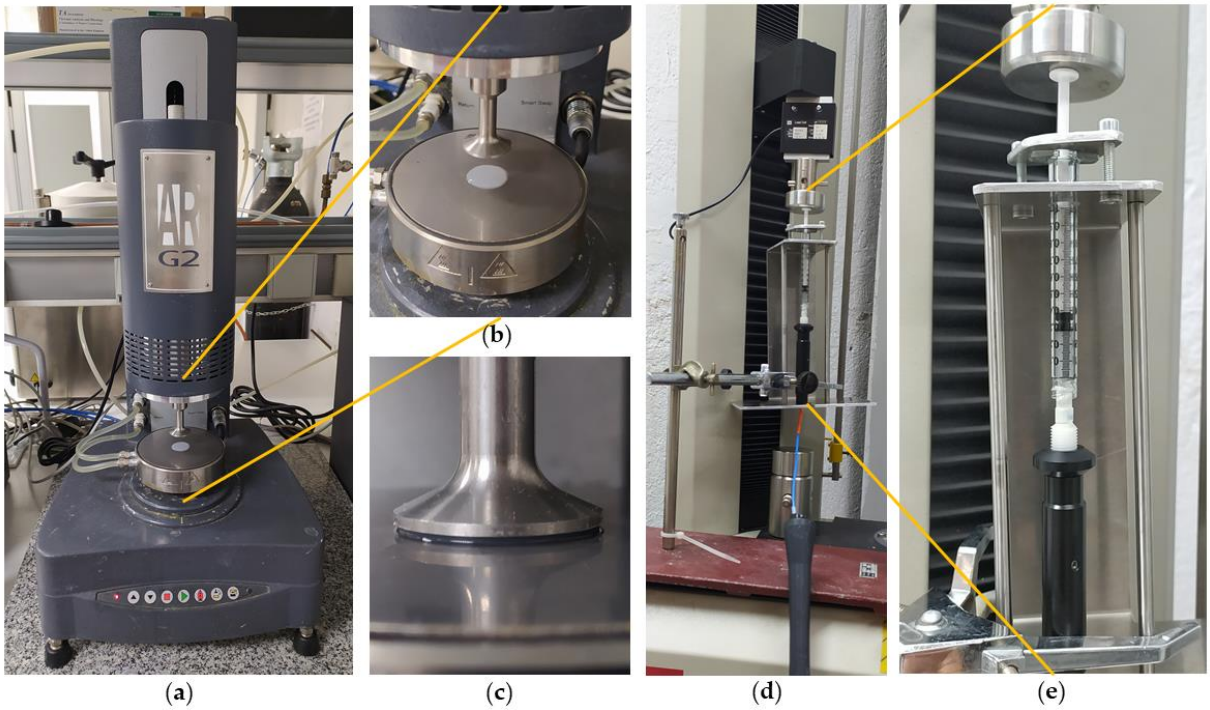

Figure 6.2. Set up for the rheometry and injectability tests. (**a**) TA Instruments AR-G2 rheometer set up with a cECMH. (**b**) Geometry and cECMH sample aligned in the AR-G2 rheometer. (**c**) Geometry correctly placed over the cECMH sample ready for storage and loss modulus measurements. (**d**) QTest 1L Elite System, Luer-lock syringe and Myostar catheter set up for measuring the injection force. (**e**) Luer-lock syringe and Myostar catheter positioning during the injection force measurement in the QTest 1L Elite System.

6.3.7 Enzymatic degradation assay

The degradation assay of the hydrogels from six samples (coming from three different batches) at the different conditions (cECMH, and cECMH with PEG at 3, 6, and 12 mg/ml) was performed as previously described, with slight modifications [430]. Briefly, the solubilized matrix (20 µl) was gelled at 37 °C for 24 hours in a 1.5 ml Eppendorf. A total of 20 µl of collagenase type II (200 units/ml, LS004176, Worthington) dissolved in 0.1 M Trizma base buffer (T1503, Sigma-Aldrich) pH 7.4 and 0.25M $CaCl_2$ were added, and the samples were further incubated at 37 °C for 5, 24, and 48 hours. A total of 20 µl of collagenase in 20 µl of PBS was used as blanks. Following incubation, the samples were centrifuged at 15,000 rpm for 5 min, and 10 µl of the supernatant was mixed with an equal volume of 2% ninhydrin reagent solution (N7285, Sigma-Aldrich). The samples were boiled at 10 min in a water bath, and then 380 µl of distilled water was added. In total, 100 µl (in triplicate) was transferred into a 96-well plate and the OD at 570 nm was measured using an EMax® Plus Microplate Reader (BioteK, Winooski, VT, U.S.A). With the ninhydrin assay, a higher OD at 570 nm is indicative of more soluble amines.

6.3.8 EV bioactivity — anti-senescent effect

The bioactivity of the EVs, the cECMH, and the PEG–cECMH with the encapsulated EVs (EVs–PEG–cECMH) was tested by investigating their anti-senescent effect in EDCs coming from two patients different from the EVs used as treatment. In triplicate, 250 µl samples of EVs (at 0.56 mg/ml) in SFM, cECM alone, or EVs in PEG–cECM were incubated for gelation during 24 hours at 37 °C in 12-well Transwells® (3460, Corning®). EDCs from passage 3 were seeded at a concentration of 15,000 cells/cm^2 in fibronectin precoated 12-well plates. The cells were left for 24 hours to attach, and then the medium was changed to SFM (2 ml/well), and the Transwells® with SFM (controls), EVs in SFM, cECMH, or EVs–PEG–cECMH were added. After 72 hours, the Transwells® were removed and the cells fixed and stained with the senescence-associated beta-galactosidase (SA-β-gal) assay, following the manufacturer's instructions (ab65351 Senescence Detection Kit, abcam®). A total of 14 images at 20x (around 650 cells) per well were taken with a Leica DMI3000B optical microscope and Leica DFC310 FX camera (Wetzlar, Germany), and analyzed using ImageJ Software. Cells were classified as senescent or non-senescent depending on whether they presented a blue color, and the percentage of senescent cells was calculated.

6.3.9 EV release from cECMH

Three samples of 100 µl of solubilized cECM and with the EVs resuspended in PEG–cECM were incubated for gelation during 24 hours at 37 °C in 24-well Transwells® (3422,

Corning®). EVs resuspended in SFM were used as controls. The samples were later placed in 24-well plates, where 600 μl of SFM was added to each well. The medium was collected daily and replaced, and the number of particles released was measured in triplicate by NTA using a Nanosight NS300 instrument and Nanosight NTA 3.4. software (Malvern Paranalytical, Malvern, U.K.) [431]. The samples were injected at RT into the sample chamber using a syringe pump, and, for each sample, three videos of 60 s were recorded with screen gain 1 and camera level at 11.

6.3.10 EV *in vivo* retention

6.3.10.1 EV labeling

Radioactive labeling of the isolated EVs was carried out with the Single-Photon Emission Computed Tomography (SPECT) radionuclide ^{99m}Tc based on previous protocols of exosome radiolabeling [432]. Briefly, 9–12 mCi of commercial [^{99m}Tc] $NaTcO_4$ (Curium Pharma, Madrid, Spain) was reduced in the presence of 0.01M $SnCl_2$ in HAc (10%). The reaction was performed for 5 min at 37 °C and 700 rpm, under N_2 atmosphere. Then, the mixture was neutralized (pH = 7) with 2.8 N NaOH. EVs (3 mg, 400 μl) were added to the ^{99m}Tc (IV) solution and incubated and shacked for 30 min at 37 °C and 700 rpm. Radiolabeled EVs were purified by centrifuging with 10 KDa Amicon filters (Merck Life Science, Darmstadt, Germany) and resuspended in 400 μl of PBS or PEG–cECM solution. Radiochemical purity of the recovered product was established by radio-thin-layer chromatography (iTLC) using a miniGita Single system (Elisa-Raytest, Angleur, Belgium).

6.3.10.2 EV tracking by SPECT-CT imaging

Multimodality imaging was performed with a small-animal SPECT scanner (μSPECT, MILabs, Houten, the Netherlands) and a preclinical Computer Tomography (CT) system (Super Argus, SEDECAL, Algete, Spain). SPECT and CT images were acquired 15 min and 24 hours after subcutaneous administration of an average 300 μCi dose (no significant differences between groups) of radiolabeled EVs (3 mg of protein, 400 μl of PBS or PEG–cECM solution). Six Balb/C, 15-week-old female mice of 23.3 ± 1.8 g were divided in two groups; half of them (n = 3) received EVs in PBS and the rest EVs in PEG–cECM. To co-register the SPECT and CT images, each animal was placed on an in-house multimodal bed surrounded by three noncoplanar capillaries filled with a mixture of ^{99m}Tc and Iopamiro (Bracco Imaging S.p.A, Milan, Italy), which was visible in both modalities. The SPECT acquisition parameters were an isotropic voxel size of 0.75 mm and an acquisition time of 15 min and 1.25 hours. SPECT images were reconstructed using two-dimensional ordered subset expectation maximization (OSEM-2D) with 16 subsets and 1 iteration. The CT was obtained immediately after completion of SPECT imaging. CT study

was acquired using an X-ray beam current of 240 mA and a tube voltage of 40 kVp, and reconstructed using an FDK algorithm [433]. SPECT-CT images were co-registered following the method of García-Vazquez V. [434].

6.3.10.3 Image analysis

The area of radioactivity was segmented on the SPECT images using a threshold at 50% of the maximum using ImageJ 1.49i. The area was compared between the animals that had been injected with the radioactively labeled EVs resuspended in PBS vs. EVs resuspended in the PEG–cECM.

6.3.11 Statistical analysis

Results are presented as mean ± standard deviation in the text and in figures. Continuous variables were compared using Student's *t*-tests. Pearson tests were performed to study the correlation between the PEG concentration and the different parameters in the cECMH. All probability values reported are two-sided, with $p < 0.05$ considered significant.

6.4 Results

6.4.1 Lyophylized cECM retained native ECM proteins and sGAGs.

Decellularization of the myocardial matrix was confirmed by the absence of visible nuclei after DAPI staining. Blyscan assay on the lyophilized samples revealed a retained sGAG content of 6.1 ± 0.4 μg/mg of lyophilized cECM, of which 1.7 ± 0.6 μg/mg was O-sulfated. LC–MS/MS confirmed the presence of around 140 different proteins related to ECM and cardiac tissue. Figure 6.3 shows some of the most abundant proteins identified. Collagens of different types (I, VI, III, IV, and V) compose most of the cECM, but other relevant proteins involved in providing structure and promoting cell attachment and migration, such as fibrinogen, lumican, elastin, laminin, and fibronectin, are also present.

6.4.2 cECM hydrogels incorporating EVs and PEG have shorter gelation times, larger fiber diameter, and improved mechanical properties while remaining injectable and biodegradable

6.4.2.1 Gelation kinetics

Turbidimetry measurements at 37 °C showed an increase in OD as the solutions gelled. After 90 min, OD had reached a plateau in all the samples. The incorporation of PEG to the cECM solution significantly reduced the amount of time needed to reach the plateau, and,

therefore, the gelation time (Figure 6.4a). While $t_{1/2}$ was 42 ± 2 min for the control condition, when PEG was incorporated at concentrations of 3, 6, and 12 mg/ml, the $t_{1/2}$ was reduced to 34 ± 4, 20 ± 5, and 9 ± 2 min, respectively (R^2 = 0.96, p = 0.02). The reduction in $t_{1/2}$ with the incorporation of PEG was achieved due to a faster initiation of polymerization (shorter lag phase, t_{lag}, R^2 = 0.99, p < 0.01) and to an increased speed of gelation (slope of the OD change, R^2 = 0.83, p = 0.08). The relationship of $t_{1/2}$, t_{lag}, and the slope of gelation with the PEG concentration is summarized in Figure 6.4b. As PEG concentration was increased, the turbidity of the gels (final OD value without normalization) also increased (data not shown). For PEG concentrations higher than shown (16 mg/ml), no significant change in OD was observed during the 90 min, and the solution did not polymerize, even after 24 hours of incubation at 37 °C. This suggested that higher PEG concentrations impede adequate gelation.

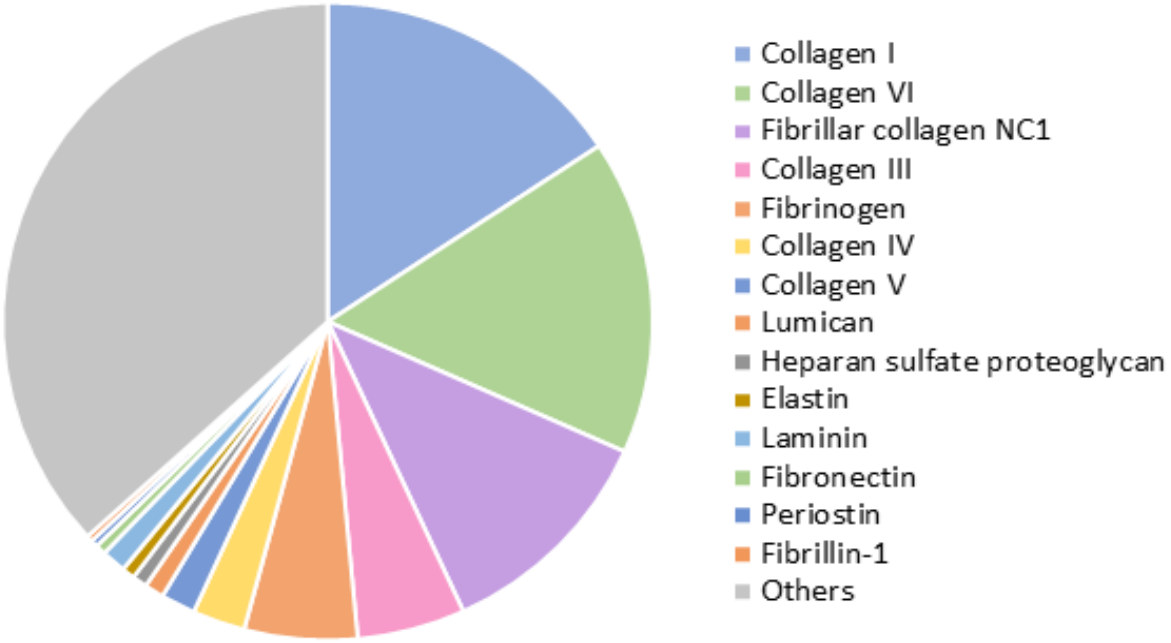

Figure 6.3. Proteins identified by liquid chromatography–tandem mass spectrometry (LC–MS/MS) in the lyophilized cardiac extracellular matrix (cECM) (n = 3).

For the combined product, EVs isolated from conditioned medium [140, 293] were incorporated into the hydrogels (EVs–PEG–cECMH), observing similar gelation kinetics to hydrogels with PEG (Figure 6.4a). They also presented reduced lag and gelation time ($t_{1/2}$ = 13 ± 3 min) and a higher speed of gelation (slope = 0.022 ± 0.009). The estimated PEG concentration in the combined EVs–PEG–cECMH product was 8 ± 2 mg of PEG per 1 ml of cECM solution.

6.4.2.2 Fiber diameter

Hydrogel formulations incorporating PEG and EVs formed the characteristic nanofibrous structure with an increase in average fiber diameter, as shown and quantified in SEM

images (Figure 6.4c). Fiber density was not homogeneous across the gels, and the fibers tended to be randomly oriented in all the samples. However, fiber diameter was strongly correlated to the amount of PEG in the hydrogel (R^2 = 0.72, p < 0.01). EVs–PEG–cECMH also presented an increased fiber diameter with respect to standard hydrogels (100 ± 20 nm vs. 60 ± 20 nm, p < 0.001).

6.4.2.3 Injectability, viscosity, storage, and loss modulus

All the formulations prepared remained injectable and with a viscosity suitable for their application through a Myostar injection catheter. In all the samples, the viscosity decreased as shear rate increased, as is characteristic of shear-thinning behavior (Figure 6.5a). This property is important for injectability, as well as for improved retention [429]. The formulation with the highest PEG concentration (12 mg/ml) presented inconsistent viscosity values (data not shown). These results seemed not to be reliable, since the very short gelation time of the samples with this concentration of PEG did not allow it to remain in soluble form during the viscosity measurement. For the remaining PEG concentrations (3 and 6 mg/ml), the amount of PEG present did not relate with a change in the viscosity of the solutions at 0.16 Hz (R^2 = 0.1, p > 0.05), and the EVs-PEG–cECM did not present significant viscosity differences with respect to cECM alone (Figure 6.5b). Injection force measurements revealed that no additional force is required for the injection of cECM solutions incorporating PEG or the EVs–PEG–cECM compared to the injection of cECM solution alone (Figure 6.5c). However, the force required to inject any of the cECM solutions was significantly higher than the one required to inject the standard vehicle (p < 0.001, PBS).

The mechanical properties of the different hydrogel formulations are summarized in Figure 6.5d-e. The amount of incorporated PEG was directly related to an increase in the storage modulus of the derived hydrogels (R^2 = 0.79, p < 0.001). While higher PEG concentrations also lead to a significantly higher loss modulus, the correlation was weaker in comparison to the storage modulus (R^2 = 0.39, p < 0.01). EVs–PEG–cECMH also presented a higher storage modulus than cECMH (15 ± 5 vs. 4.5 ± 0.9 Pa, p < 0.01), and a slightly higher loss modulus (1.5 ± 0.5 vs. 1.1 ± 0.2, p > 0.05).

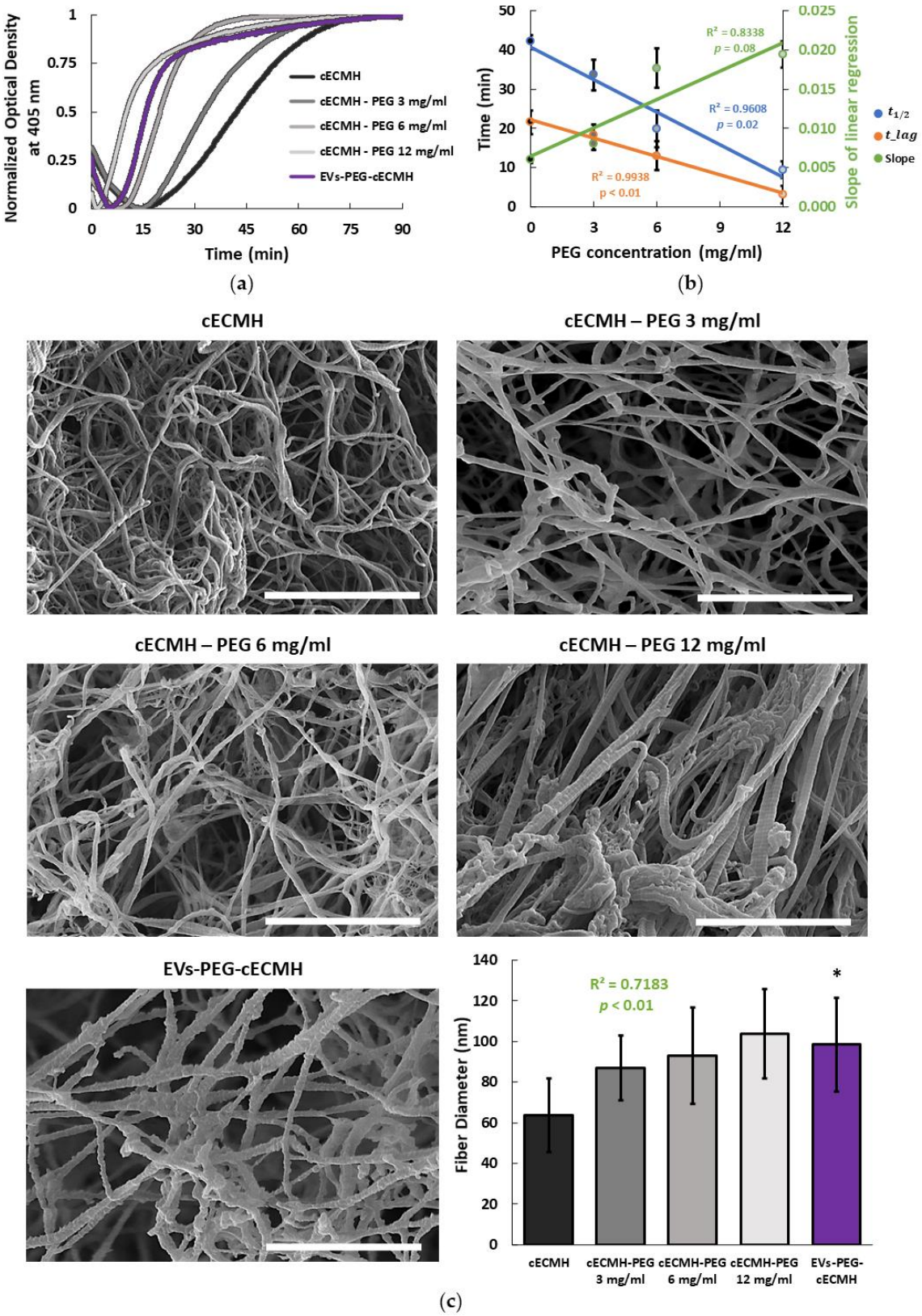

Figure 6.4. Gelation kinetics and fiber diameter. (**a**) Turbidimetric average results over time, with optical density (OD) normalized at 405 nm for the different formulations (n = 3, each in triplicate, for each condition). (**b**) Correlation between the PEG concentration and the half

gelation time ($t_{1/2}$), the lag time (t_{lag}), and the slope of the linear regression (speed of gelation) obtained from turbidimetry (n = 3, each in triplicate, for each condition). (**c**) Scanning electron microscopy (SEM) images of the different hydrogel formulations and their average fiber diameter (n = 160 fibers for each condition). Scale bars correspond to 2 μm. Squared Pearson's correlation coefficient for PEG concentration vs. fiber diameter and its significance ($p < 0.01$). * $p < 0.001$ vs. cECMH. cECMH, cardiac extracellular matrix hydrogel; PEG, polyethylene glycol; EVs, extracellular vesicles.

6.4.2.4 Degradation

The ninhydrin assay (indicative of the amount of soluble amines) showed that PEG incorporation into the hydrogels did not affect their degradation rate, as there were no significant differences in OD at 570 nm between any of the formulations at the same time point ($p > 0.05$, Figure 6.5f). All the samples presented significantly higher degradation after being incubated for 48 hours with collagenase compared to 5 hours of incubation ($p < 0.05$, paired Student's t-tests). The combined product (EVs–PEG–cECMH) presented the highest value of OD (0.454 ± 0.08 after 5 hours, 0.654 ± 0.16 after 24 hours, and 0.673 ± 0.17 after 48 hours) in the ninhydrin test. However, we did not consider this sample for comparison with the others because of the interference of the residual amines of the conditioned medium of the EVs in the ninhydrin test.

6.4.3 The combined product of EVs–PEG–cECMH maintains the bioactivity of the individual components

The bioactivity and potential beneficial effect of the PEG–cECMH with the embedded EVs was confirmed by evaluating the reduction in cardiac stromal cell (EDCs) senescence from two different donors in culture (this property of EVs derived from CDCs was proved in other studies [140]). As control groups for EVs–PEG–cECMH, we used EDCs incubated with serum-free media (SFM), EVs alone, or cECMH alone (Figure 6.6a-b). EVs and cECMH significantly reduced basal senescence (by around 40%, $p < 0.01$) in the EDCs derived from both patients. No significant differences were detected between the EVs and the cECMH used alone. When using the combined product (EVs–PEG–cECMH), basal senescence was further reduced (by ~55%, $p < 0.001$). This difference was also significant with respect to using EVs alone in one of the patients ($p < 0.05$). Images taken with optical microscopy in EDCs from patient 1 show a higher proportion of senescent EDCs (in blue) under basal conditions (SFM) than when exposed to EVs alone or cECMH alone, and a lower proportion of senescent cells when exposed to EVs–PEG–cECMH (Figure 6.6c).

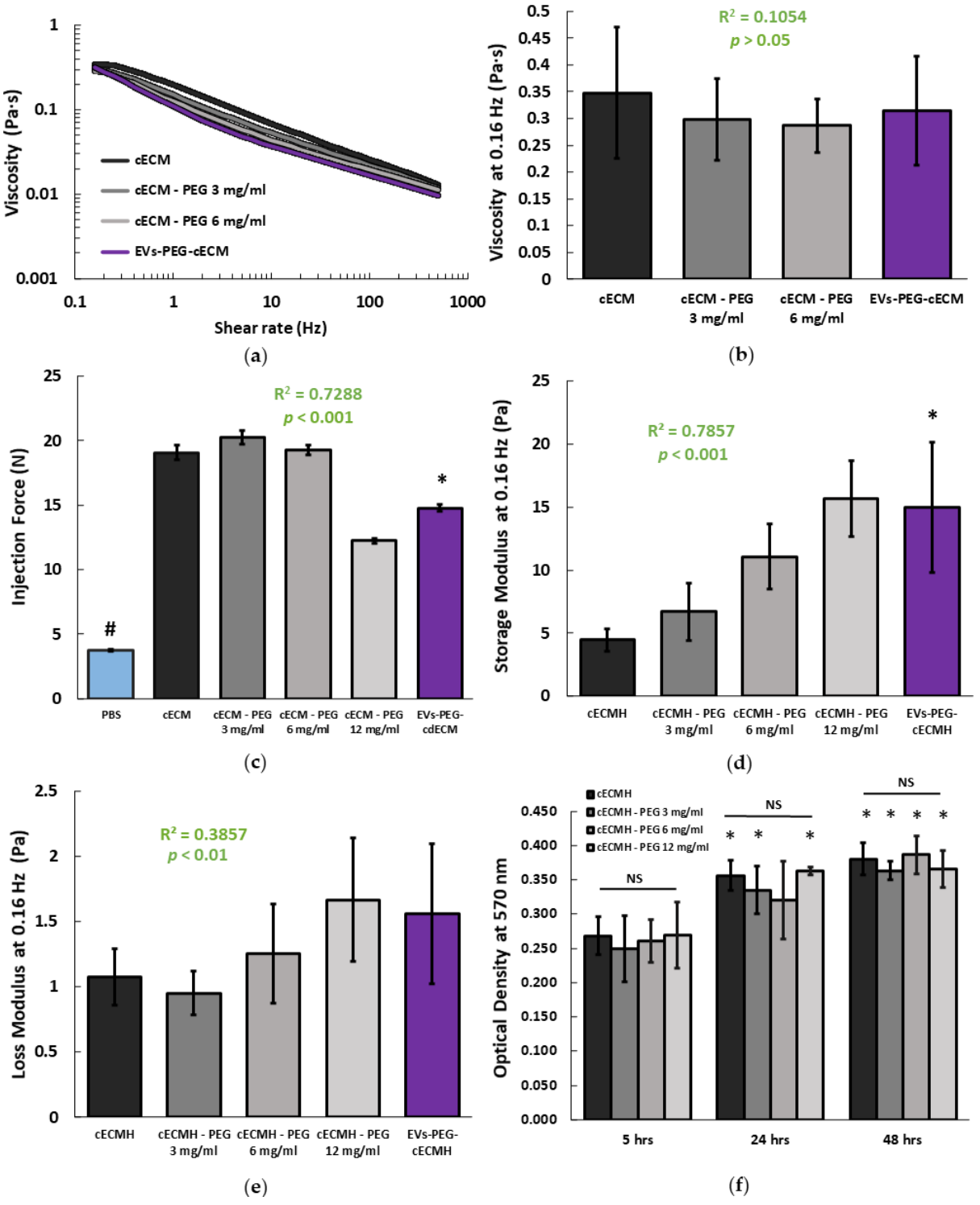

Figure 6.5. Mechanical properties and degradation of the cECMH alone, with PEG, and with PEG-isolated EVs. (**a**) Average viscosity of the different hydrogel solution formulations (n = 3 for each condition, each in triplicate). (**b**) Viscosity at 0.16 Hz (n = 3). Squared Pearson's correlation coefficient for PEG concentration in the cECMH vs. viscosity at 0.16 Hz and its significance (p > 0.05). (**c**) Force required for injection (n = 3). Squared Pearson's correlation

coefficient for PEG concentration in the cECMH vs. injection force and its significance (p < 0.001). * p < 0.001 vs. cECMH. # p < 0.001 vs. all other groups. (**d**) Storage modulus at 0.16 Hz (n = 4). Squared Pearson's correlation coefficient for PEG concentration in the cECMH vs. storage modulus and its significance (p < 0.001). * p < 0.01 vs. cECMH. (**e**) Loss modulus at 0.16 Hz (n = 4). Squared Pearson's correlation coefficient for PEG concentration in the cECMH vs. loss modulus and its significance (p < 0.01) (**f**) Enzymatic degradation (soluble amines, n = 6, each in triplicate). * p < 0.05 with respect to their same group at 5 hours. cECMH, cardiac extracellular matrix hydrogel; PEG, polyethylene glycol; EVs, extracellular vesicles.

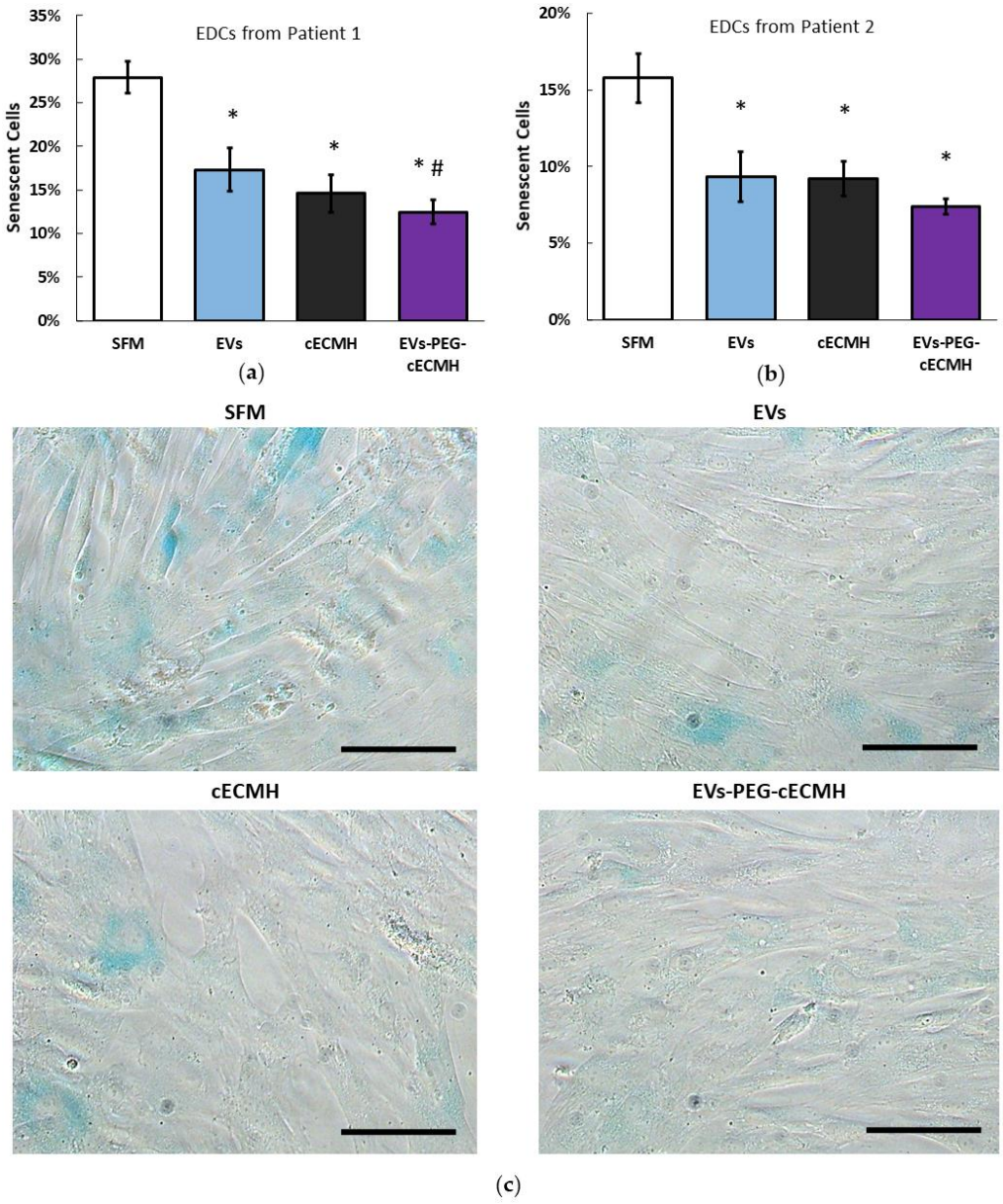

Figure 6.6. Bioactivity of EVs alone, cECMH, and EVs–PEG–cECMH, measured as anti-senescent effect. (**a**) Percentage of senescent explant-derived cells (EDCs) from patient 1 under basal conditions and under exposure to EVs alone, cECMH alone, or EVs–PEG–cECMH (n =

3). (**b**) Percentage of senescent EDCs from patient 2 under the different conditions (n = 3). (**c**) Optical microscopy images from EDCs (senescent cells in blue) from patient 1 under the different conditions. * $p < 0.01$ with respect to serum-free media (SFM). # $p < 0.05$ with respect to the EVs group. Scale bars correspond to 100 μm. cECMH, cardiac extracellular matrix hydrogel; PEG, polyethylene glycol; EVs, extracellular vesicles.

6.4.4 The combined product of EVs–PEG–cECMH shows a higher local EV retention *in vivo*

6.4.4.1 EV Release

Most EVs incorporated into the PEG–cECMH were cumulatively released during the first 48 hours (Figure 6.7a). After this time, there were no significant differences ($p > 0.05$) between the particles detected in control samples (EVs resuspended in SFM) and the cumulative number of particles released by the EVs–PEG–cECMH. During days 3 and 4, some particles continued to be released, but in considerably lower amounts. The number of particles detected in SFM alone (without EVs) or in medium exposed to cECMH or PEG–cECMH alone (without EVs embedded) was insignificant, confirming that particles detected in control samples and in samples from EVs–PEG–cECMH did correspond to the added EVs.

6.4.4.2 *In vivo* retention

SPECT–CT images of mice revealed a larger area of ^{99m}Tc radioactively labeled EVs at the subcutaneous injection site when administered embedded in the PEG–cECMH compared to their administration resuspended in PBS (Figure 6.7b-c). The area of EVs was four times larger ($p < 0.05$) after 15 min post-injection when using the PEG–cECMH to deliver them. After 24 hours, the average area of concentrated EVs was twice as large when applied with the PEG–cECMH, but the difference was not significant ($p = 0.1$).

6.5 Discussion

According to our results, the combination of EVs–PEG–cECMH optimizes the features of its individual bioactive components and makes it more suitable in different therapeutical applications. EVs–PEG–cECMH maintained or significantly improved the physicochemical properties (particularly the gelation time), while not hindering injectability and degradation vs. cECMH alone. PEG at low concentrations, which, in fact, can be used to isolate EVs from conditioned medium, was responsible for these differences. In addition, the EVs are progressively released from the EVs–PEG–cECMH and are better retained at the injection site *in vivo* when administered in the EVs–PEG–cECMH compared to EVs administered in the

standard vehicle (PBS). The combination of the products reduces cellular senescence, maintaining the bioactive properties of cECMH and EVs alone.

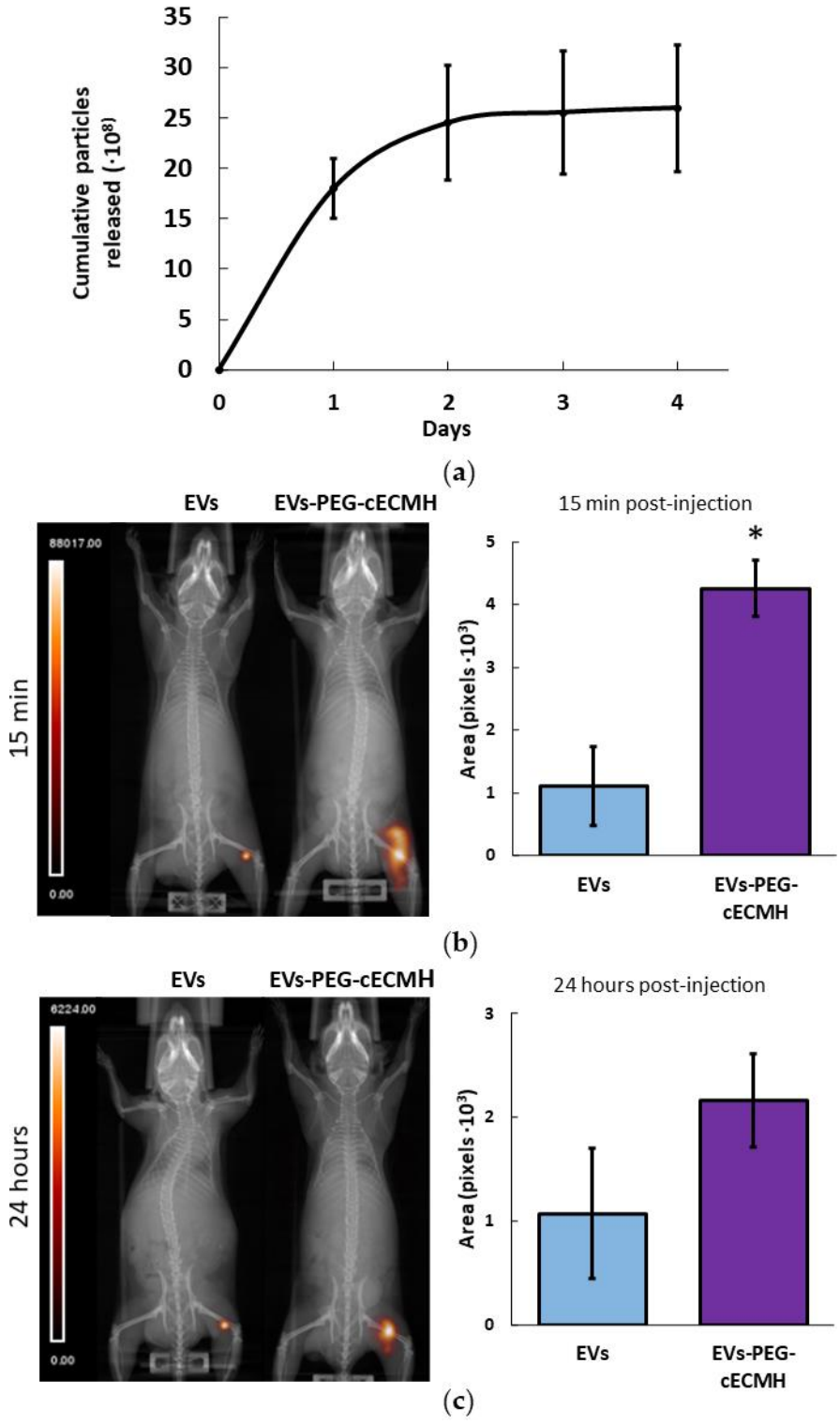

Figure 6.7. EV release from the EVs–PEG–cECMH and EV *in vivo* retention. (**a**) Number of cumulative EVs released into the medium from EVs–PEG–cECMH for 4 days (n = 3, each run in triplicate), evaluated using nanoparticle tracking analysis (NTA). The error bars were obtained

by the standard deviation of the three different samples. After 48 hours there were no significant differences ($p > 0.05$) with the number of particles detected in control samples. (**b**) Representative single-photon emission computed tomography–computed tomography (SPECT–CT) images and area of radioactively labeled EVs ($n = 3$) after *in vivo* injection of EVs resuspended in phosphate buffered saline (PBS) or in PEG–cECM (EVs–PEG–cECM) 15 min and (**c**) 24 hours post-injection. * $p < 0.05$. cECMH, cardiac extracellular matrix hydrogel; PEG, polyethylene glycol; EVs, extracellular vesicles.

Although the incorporation of low-molecular-weight PEG up to a certain concentration (12 mg/ml) proportionally improved the gelation properties of the cECMH, higher PEG concentrations impeded gelation. cECMH have collagen as their main component, so they share some similarities in the gelation kinetics with collagen hydrogels [428]. During the lag phase, collagen nucleation occurs by forming triple helices. Later, during the gelation phase, these assemble into ordered structures to form fibrils [435]. The addition of PEG seems to speed up the nucleation phase and favor collagen fibril formation during gelation. This more rapid formation could be responsible for the larger fiber diameter [430] and the higher turbidity of the gels [435]. Larger fiber diameter could also result from PEG entangled in collagen fibers, similar to hyaluronic acid chains incorporated into a collagen network without crosslinking [436]. Other studies have incorporated PEG into cECM or collagen hydrogels to tailor their material properties [430, 437]. However, these studies incorporate multi-armed PEG with functionalized groups that crosslink with the collagen network or modified PEGs that require external triggers for polymerization, such as UV light. The addition of functionalized multi-armed PEGs at high concentrations (12-24 mg/ml) still allows the formation of gels at 37 °C without external triggers and the tuning of mechanical properties and degradation, but they do not improve the gelation time [430]. Slow gelation times, which can increase tissue necrosis, have been highlighted as a main drawback of ECM hydrogels [217].

Mechanical properties of the ECM hydrogels are also improved with the incorporation of PEG, while injectability and biodegradation are maintained. The mechanical properties of cECMH alone are considered insufficiently robust for providing prolonged mechanical support in the injured heart, where they are subjected to significant strain and contraction [217]. In addition, these properties influence cell fate [438] and migration [439]. PEG–cECMH or EVs–PEG–cECMH present a significantly higher storage modulus, making them more suitable for cardiac applications than cECMH alone. The reduction in the gelation time and the increase in the elasticity of the cECMH after gelation did not negatively affect the viscosity of the liquid form and their injectability through the Myostar catheter. Even the solutions with reduced gelation time could be uniformly injected and did not clog the catheter, an essential property for cardiac applications [440]. In fact, when adding the EVs, the force required for injection was

considerably lower. Moreover, the incorporation of PEG with the method presented here (linear PEG without functionalized groups that react with amines in collagen) does not influence the cECMH biodegradation rate, which *in vivo* studies have shown to completely degrade within 14–28 days post-injection [235].

Hydrogels as vehicles to deliver EVs have already shown potential for improved *in vivo* retention and boosted cardiac function [251, 253, 441]. Applications where fast gelation time becomes especially important (e.g., to retain bioactive molecules at the site of injection [217], embed cells, or create three-dimensional (3D) tissue-like structures [442]) while maintaining injectability and natural tissue environment may potentially benefit from the improved physicochemical properties of PEG incorporation into ECM hydrogels. The combined product presented here (EVs–PEG–cECMH), with an estimated PEG concentration of 8 ± 2 mg, (matching the results obtained in the physicochemical analysis, in which the combined product presented average values between the cECMH with PEG at 6 and 12 mg/ml), benefits from these improved physicochemical properties.

EVs administered *in vivo* in the PEG–cECM solution also achieved the goal of improved retention at the target site when compared to EVs administered with the standard vehicle (PBS). This is probably because the fast gelation time of the combined product prevents the rapid absorption of the subcutaneously injected EVs into the bloodstream right after the injection. According to NTA measurements, EVs encapsulated in the PEG–cECMH are mostly released during the first 48 hours, which is in line with other studies [255]. In addition, SEM images of the EVs–PEG–cECMH show rougher collagen fibers with respect to cECMH or PEG–cECMH alone. This phenomenon has also been observed in other studies, where this roughness has been related to embedded proteins and vesicles [427]. After several days of soaking the hydrogels, as the particles were released to the medium, the fibers started to look smoother. Accordingly, our *in vivo* experiment showed that, although a high proportion of the EVs are probably released from the PEG–cECMH during the first day, a large amount of EVs still remain encapsulated at the injection site after 24-hours.

Both the cECMH [235] and the EVs [181] individually have shown favorable effects for the treatment of cardiac pathologies in preclinical models. While EVs have been shown to halt proinflammatory and profibrotic pathways and induce angiogenesis [181], the ECM hydrogels provide mechanical support and an environment with a structure and protein composition close to the native cardiac tissue [235]. Moreover, ECM hydrogels promote cellular influx and their degradation products favor cellular migration, proliferation [443], and angiogenesis [444]. In this study, despite EVs and the cECMH individually showing significant (and similar) anti-senescent properties in cardiac stromal cells (CSCs) from different human donors, this effect tended to be

enhanced when both products were used together, indicating a possible synergistic effect of both products.

Even if the EVs embedded in PEG–cECMH showed promising characteristics for its use in cardiac regenerative applications, future studies should confirm if the improved physicochemical properties of the combined product (provided by the PEG), the bioactivity, and the enhanced *in vivo* EV retention vs. the use of the individual components alone translate into improved functionality in an animal model. Furthermore, mechanical properties of the PEG–cECMH, although improved with the addition of PEG, are still far from mimicking that of the native ECM. In this study, EVs were tracked *in vivo* only for 24 hours, and our *in vitro* tests demonstrated that most particles are released during the first 48 hours. Presumably, a longer liberation time of the EVs from the PEG–cECMH could increase the efficacy of the product, mimicking repeated dosing. Labeling the EVs with other molecular methods (such as with optical probes), would allow *in vivo* tracking of the EVs for longer. This could help determine for how long the EVs can remain at the target site after being injected in the PEG–cECMH. To further improve and optimize these properties, it becomes necessary to explore modifications in the hydrogel composition. For example, modifying the ECM concentration and incorporating additional synthetic materials could contribute to the tailoring of mechanical and degradation properties [428, 430], as well as pore size [445] and EV release rate.

Regardless of the limitations cited above, here we show that the delivery of EVs isolated with PEG and embedded in cECMH offer a minimally invasive, injectable therapeutical product with a fast thermosensitive response at physiological temperature. The product can provide an environment with proteins naturally present in the myocardium and with mechanical and structural support, while it enables the retention and release of the EVs at the target site. The combined product (EVs–PEG–cECMH) presents bioactivity and is biodegradable. As EVs–PEG–cECMH solves some of the current limitations of this type of biological therapy, it can potentially be used in different regenerative medicine applications.

6.6 Conclusions

Hydrogels derived from cardiac extracellular matrix (cECMH) incorporating polyethylene glycol (PEG) present promising characteristics for the delivery of extracellular vesicles (EVs) for different regenerative applications. Once injected into the target tissue, the product rapidly gels at physiological temperature. The incorporation of EVs with PEG to the cECMH improves the mechanical properties while maintaining the injectability and the biodegradability. In addition, the combined product showed bioactivity similar to its individual components. With the EVs–PEG–

cECMH, the EVs are better retained *in vivo* on-site. These improved properties of the combined product solve some of the current limitations of the individual use of these regenerative components, which may be translated into an increased therapeutic efficacy.

Chapter 7

Electrophysiological effects of extracellular vesicles secreted by cardiosphere-derived cells: unraveling the antiarrhythmic properties of cell therapies

7.1 Abstract

Although cell-based therapies have shown potential antiarrhythmic effects that could be mediated by their paracrine action, the mechanisms and the extent of these effects were not deeply explored. We investigated the antiarrhythmic mechanisms of extracellular vesicles secreted by cardiosphere-derived cells (CDC-EVs) on the electrophysiological properties and gene expression profile of HL-1 cardiomyocytes (CMs). HL-1 cultures were primed with CDC-EVs or serum-free media alone for 48 hours, followed by optical mapping and gene expression analysis. In optical mapping recordings, CDC-EVs reduced the activation complexity of the CMs by 40%, increased rotor meandering and reduced rotor curvature, as well as induced an 80% increase in conduction velocity (CV). HL-1 cells primed with CDC-EVs presented higher expression of *SCN5A*, *CACNA1C* and *GJA1*, coding for proteins involved in I_{Na}, I_{CaL} and Cx43 respectively. Our results suggest that CDC-EVs reduce the activation complexity by increasing CV and modifying rotor dynamics, which could be driven by an increase in expression of *SCN5A* and *CACNA1C* genes, respectively. Our results provide new insights into the antiarrhythmic mechanisms of cell therapies, which should be further validated using other models.

7.2 Introduction

Tachyarrhythmias are variations that increase the normal heart rate (HR) without a physiological justification [446], and they are classified into supraventricular and ventricular arrhythmias according to their origin [447]. They affect over 2.2% population [448] and are one of the main causes of morbidity and mortality worldwide [449]. Clinically they can manifest as heart failure (HF), chest pain, weakness, syncope, cardiomyopathy and even cardiac arrest and

death [450]. In spite of their high prevalence and impact, current treatments are still suboptimal [449].

To improve treatment efficacy, an understanding of the physiological mechanisms behind the tachyarrhythmias becomes essential [451]. The two main pointed mechanisms are enhanced impulse formation and conduction disturbances. Contrary to impulse formation, conduction disturbances produce so-called reentrant arrhythmias, in which the arrhythmia is commonly both initiated and sustained [446]. Rotors (spiral wave reentries that rotate around anatomical points) can occur around anatomical or functional obstacles, such as fibrotic regions, but their initiation and maintenance success is tightly related to low conduction velocity (CV) [446, 452] and short action potential duration [453].

Despite some studies reducing arrhythmogenicity by improving CV [454, 455], antiarrhythmic drugs used in the clinic do not currently act through this mechanism [456, 457]. CV in the cardiac tissue is mainly determined by the presence of gap junctions and by the late sodium current (I_{Na}). Gap junctions play an important role in action potential propagation between cardiomyocytes (CMs) [315, 455], as they allow the passage of ions between different cells [458].

Shortening of the action potential duration is associated with shorter refractory periods and larger rotor stability [459]. Low L-type calcium current (I_{CaL}, determined by the presence of voltage-dependent L-type calcium channels coded by the *CACNA* family), is related to shorter action potential durations [460] and decreased meandering [461], leading to more rotor stability. Decreased meandering and an increase in rotor curvature reduce the probability of collision with other rotors and reduce the area needed for the rotor to self-sustain, increasing the number of possible simultaneous rotors in a certain area. These rotor dynamics related to shorter action potentials and low conduction velocities allow for a larger number of reentries in the cardiac tissue, leading to a larger activation complexity [462]. This increase in complexity, as a more arrhythmogenic profile, is related to longer arrhythmia sustainment and lower ablation success [463].

Most pharmacologic therapies act by modulating or blocking ion channels, but do not correct the underlying causes [464]. On the other hand, ablation therapy produces irreversible changes in the cardiac substrate that limit its long-term success and its use in complex activation cases [465]. The efficacy of ablation and pharmacological therapies for tachyarrhythmias could be eventually optimized by emerging biological therapies, capable of modifying the pathophysiological substrate [464]. Some studies showed the antiarrhythmic properties of mesenchymal stem cells (MSCs) [466–470] or cardiosphere-derived cells (CDCs) [471, 472], while others demonstrated pro-arrhythmic effects [473, 474]. While the topic is still controversial, most

of this proarrhythmicity is associated to stem cell engraftment itself and the alteration of the overall tissue excitability, as these effects are not observed or seem to be opposite when their paracrine factors are used instead [469, 473]. Extracellular vesicles (EVs) are the main paracrine mediators of the stem cells [475, 476] and their use as therapeutics may have advantages compared to their parenteral cells [180, 417]. It was demonstrated that blocking production of EVs renders CDCs ineffective, whereas extracellular vesicles secreted by human CDCs (CDC-EVs) reproduce the benefits of the parent CDCs [180, 476], as well as cardiac progenitor cells with broad-ranging bioactivity in preclinical and clinical studies [140, 141].

Therefore, a deeper understanding and exploration of the mechanisms behind the potential antiarrhythmic effects of EVs secreted by cardiac stem cells and whether these are comparable to antiarrhythmic drugs could contribute to the development of more effective antiarrhythmic therapeutics. The objective of this study was to investigate the antiarrhythmic effects of human CDC-EVs on the cardiomyocyte monolayer presenting spontaneous arrhythmogenic activity and to elucidate the underlying antiarrhythmic mechanisms.

7.3 Materials and methods

7.3.1 CDCs and derived extracellular vesicle isolation

EVs used as treatment were isolated from CDCs from two different human donors as explained in section 4.3.1. CDC identity was confirmed by flow cytometry (0.9% CD45+ cells, 10.6% CD90+ cells, 6.6% CD117+ cells, 99.8% CD105+ cells, and 7.4% CD31+ cells). Half of the CDC-EVs plates were treated with EVs from one donor, and the other half were treated with CDC-EVs from the other donor. No significant differences in proliferation, electrophysiological properties (i.e. activation complexity, dominant frequency, rotor dynamics and CV) and gene expression profile were observed between the two donors. For experiments, the precipitated EVs were resuspended in Claycomb medium without Fetal Bovine Serum (FBS) at 100 μg/ml.

7.3.2 Experimental protocol

The overall experimental protocol is summarized in Figure 7.1a. After CDC-EV isolation and quantification, HL-1 cells were plated in 35-mm-diameter petri dishes at a density of 26,000 cells/cm^2 and maintained according to the protocol established by Claycomb et al. [368]. Spontaneous beating activity was observed during cell expansion. When cultures reached a confluency of 80% (two days after plating), the culture medium was changed to serum-free medium, resulting in a control group and an EV group (with EVs resuspended in the serum-free

medium). Fully confluent cultures were analyzed with the optical mapping (OM) technique, obtaining recordings of 20 s (n = 12 in control and n =12 in CDC-EVs group). After OM, cells were lysed and kept for further gene expression analysis in order to contrast the electrophysiological results with cardiac remodeling at the molecular level.

7.3.3 Optical mapping recordings

Cell cultures were stained with rhod-2 AM (Ca^{2+}-sensitive probe) fluorescent dye prior to the calcium transient (CaT) imaging so that the propagation patterns could be recorded. HL-1 cells were incubated in serum-free media with rhod-2 (AAT Bioquest) at 3.3 μM (from 1mM aliquots in dimethyl sulfoxide, DMSO) and Probenecid (AAT Bioquest) at 1.75 mM (from 265 mM aliquots in Tyrode solution) for 30 min at 37 ºC and 5% CO_2 level. After dye loading, the serum-free medium was changed to fresh Tyrode solution (containing, in mM: NaCl 130, $NaHCO_3$ 24, NaH_2PO_4-H_2O 1.2, $MgCl_2$ 1, KCl 4, glucose 5.6, $CaCl_2$ 2.3) at physiological temperature.

To excite rhod-2, cultures were illuminated with a green light-emitting diode light source with a plano-convex lens and a green excitation filter. Fluorescence was recorded with an electron-multiplying charge-coupled device with a custom emission filter and a high-speed camera lens as described in reference [477]. Basal recordings of fluorescence were acquired at 50 frames/s and a field of view of ~2 x 2 cm^2. To facilitate linear propagation for velocity measurement, cell cultures were delimited in rectangular areas and stimulated with pulses of 40 V amplitude, 4 ms width and 1 Hz pacing period.

7.3.4 Calcium image processing

Electrophysiological properties of cell cultures were analyzed by processing CaT recordings as illustrated in Figure 7.1b. with custom software written in MATLAB, quantifying dominant frequency (DF), complexity, curvature, rotor meandering and CV as described by Climent et al. [477, 478].

7.3.4.1 Spectral analysis

Power spectra were obtained using a Welch periodogram (2-s Hamming window overlap). DF for each pixel was defined as the frequency with the largest peak in the power spectrum, and DF for each culture was calculated as its maximum DF value.

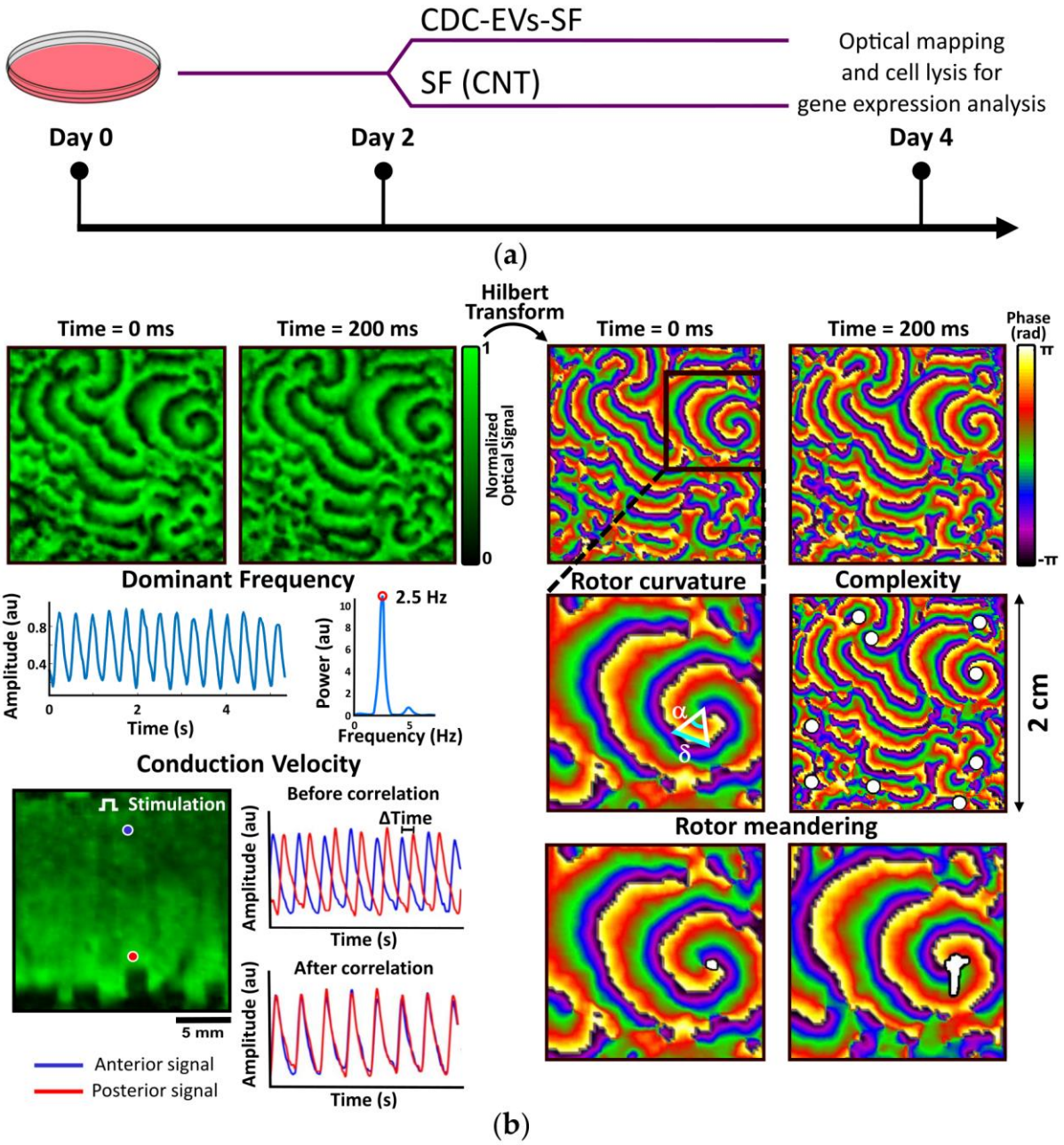

Figure 7.1. Experimental protocol and methodology employed for calcium transient (CaT) recording analysis. (**a**) Experimental set up consisting of cell seeding at day 0, Claycomb medium without FBS (serum-free (SF)), and with addition of extracellular vesicles (EVs) in CDC-EV group at day 2, and optical mapping and cell lysis for later RNA extraction at day 4; (**b**) Example of optical mapping recording analysis. Two snapshots of optical mapping recordings are shown at 0 and 200 ms (upper left), as well as their phase maps, obtained by applying Hilbert Transform (upper right). Example of the optical mapping signal for a specific pixel, and its corresponding power spectrum, with the peak marking the dominant frequency, are shown (middle left). For conduction velocity (CV) (lower left), the culture is divided into delimited areas and two pixels are selected (with their corresponding optical mapping signals). Correlation of these signals gives

the time elapsed (Δt) between the activation of the two points. CV is calculated as the ratio between the physical distance between the two points and the time elapsed. Rotor curvature, complexity and meandering calculated from phase maps are represented. Rotor curvature was determined from the derivative of the relative angle (α) over the relative distance (δ) in lines from the rotor tip to 2π (middle right). For complexity, phase singularities (PSs) were identified and quantified in a certain area (middle right). In rotor meandering, from the phase map, the path followed by the tip was traced and quantified (lower right).

7.3.4.2 Phase singularities and rotor dynamics

Phase maps were obtained by applying Hilbert transform to CaT signals, defining phase singularities (PSs) as points surrounded by phases from 0 to 2π monotonically changing. Complexity was defined as the mean number of simultaneous functional reentries in a certain area (PS/cm^2).

For curvature measuring, lines connecting phase transitions from 0 to 2π were traced from the rotor tip to the periphery. The curvature of the rotor was the mean of the curvatures at each point, which were calculated as the derivative of the relative angle (α) over the relative distance (δ).

Rotor meandering was defined as the distance covered by the rotor tip over PS duration (cm/s). From the phase map, the path followed by the tip was traced and quantified. Meandering in each cell culture was calculated as the mean value of the meandering of all the PS.

7.3.4.3 Conduction velocity

CV was defined as the distance traveled by the linear propagation front (cm/s) in areas that only allowed unidirectional propagation. CaT signals from pixels at a known spatial distance were correlated to obtain time elapsed between their activations (Δt). CV was calculated as the distance between the pixels divided by the elapsed time. For each culture, mean CV was computed with a minimum of eight delimitated areas.

7.3.5 Gene expression analysis

The procedure followed for RNA isolation from the cell cultures, its reverse-transcription into cDNA and PCR amplification and gene expression quantification was as described in section 4.3.4, but using *ACTB* and *36B4* as reference genes in geNorm for gene expression normalization. The genes under study - *SCN5A*, *CACNA1C* and *GJA1* - encode for proteins related to cardiac impulse propagation and involved in different ion currents and channels: voltage-activated sodium current (I_{Na}), L-type calcium current (I_{CaL}) and connexin 43 (Cx43), respectively.

Gene	Protein	Forward primer (5'-3')	Reverse primer (5'-3')	Exons	Transcript
SCN5A	Nav1.5	CACCTTCACCGCCATCTACA	AAGGTGCGTAAGGCTGAGAC	4-5	ENSMUST00000065196.13
				5-6	ENSMUST00000120420.2
CACNA1C	Cav1.2	CCTCGAAGCTGGGAGAACAG	TGTGTGGGAGTCAATGGAGC	27-28	ENSMUST00000112793.10
				27-28	ENSMUST00000190285.2
				27-28	ENSMUST00000187317.7
				26-27	ENSMUST00000186889.7
				26-27	ENSMUST00000187940.7
				26-27	ENSMUST00000187474.7
				26-27	ENSMUST00000189389.7
				27-28	ENSMUST00000188522.7
				27-28	ENSMUST00000185345.7
				26-27	ENSMUST00000189520.7
				27-28	ENSMUST00000188106.7
				26-27	ENSMUST00000078320.14
				26-27	ENSMUST00000112790.9
				26-27	ENSMUST00000075591.13
				26-27	ENSMUST00000188078.7
				26-27	ENSMUST00000188865.7
				27-28	ENSMUST00000187386.7
				24-25	ENSMUST00000220022.2
				24-25	ENSMUST00000219833.2
				23-24	ENSMUST00000219018.2
				23-24	ENSMUST00000219223.2
				22-23	ENSMUST00000112825.9
GJA1	Cx43	CCGGTTGTGAAAATGTCTGCT	CGTGAGCCAAGTACAGGAGT	2	ENSMUST00000220069.2
				2	ENSMUST00000068581.9
ACTB	Beta-actin	TGCTCTAGACTTCGAGCAG	AAGAGCCTCAGGGCATCGG	4	ENSMUST00000100497.11
				3	ENSMUST00000167721.8
				3	ENSMUST00000171419.8
36B4	Acidic ribosomal phosphoprotein P0	GCGACCTGGAAGTCCAACTA	ATCTGCTGCATCTGCTTGG	2-3	ENSMUST00000086519.12
				2-3	ENSMUST00000156359.2
				1-2	ENSMUST00000152976.2

Table 7.1. Primers used for RT-PCR in HL-1 cells

7.3.6 Statistical analysis

Results are presented as mean ± standard deviation in the text and ± standard error of the mean in figures. Continuous variables were compared using Student's t-tests. Pearson tests were performed to study the correlation among the different electrophysiological parameters and between gene expression. All probability values reported are two-sided, with $p < 0.05$ considered significant.

7.4 Results

CDC-EVs seem to drive HL-1 cells to a less arrhythmogenic profile. Figure 7.3 shows the comparison of the complexity, the dominant frequency, rotor dynamics and CV for control vs. treated with CDC-EV HL-1 cell monolayers to illustrate the differences in their electrophysiological properties. The corresponding graphs summarizing the results, as well as

representative images of culture wells in both groups, are also shown. The plates were fully confluent during optical mapping recordings (plates in both groups reached confluency simultaneously) and there were no significant differences in the cell density between the control and the active treatment arms (0.42 ± 0.03 x 10^6 cells/cm^2 vs. 0.45 ± 0.05 x 10^6 cells/cm^2, p > 0.05, Figure 7.2).

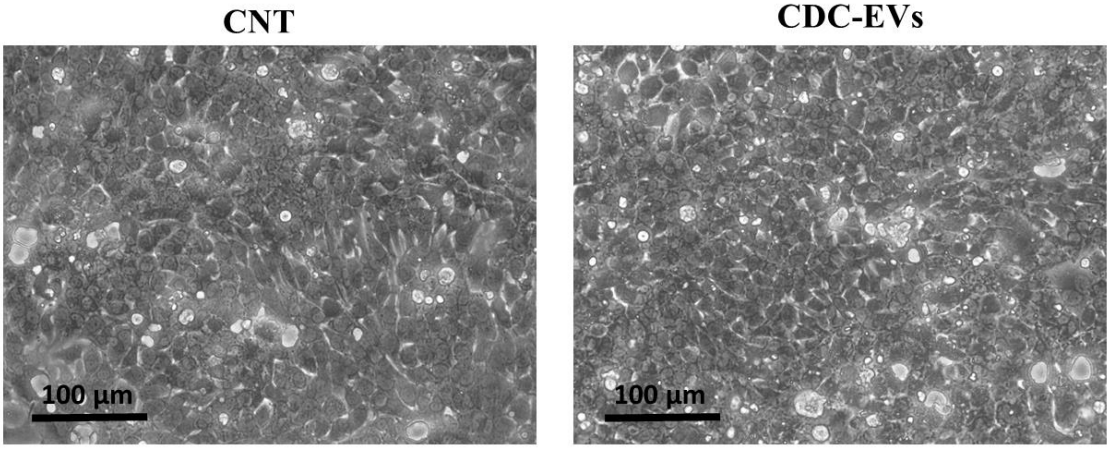

Figure 7.2. Representative images of the HL-1 culture at 100% confluency on day 4 of the experiment in control and CDC-EVs group. Cell count was 0.42 ± 0.03 * 10^6 cells/cm^2 in control plates and 0.45 ± 0.05 * 10^6 cells/cm^2 in CDC-EVs plates, p > 0.05. CNT: control. CDC-EVs: extracellular vesicles obtained from cardiosphere-derived cells.

7.4.1 Effects of extracellular vesicles derived from CDCs on activation dominant frequency, complexity and rotor dynamics

In order to study the electrophysiological modifications of EVs-CDCs on baseline arrhythmogenic substrate (spontaneously activating), dominant frequency, activation complexity and rotor dynamics were analyzed (Figure 7.3). We observed a significant reduction of ~40% in the activation complexity of the CDC-EV treated group (number of phase singularity points per square centimeter, 2.60 ± 0.57 vs. 1.54 ± 0.20 PS/cm^2, p < 0.01, Figure 7.3a). It can be noticed how, in the control group, there were abundant wavebreaks and secondary rotors, while, in the CDC-EV treated group, there were fewer and larger rotors, with one main rotor covering most of the dish, indicative of simpler activation patterns (Figure 7.3a). However, regarding spectral characteristics, both control and treated groups presented no significant differences in their activation rate, which was around a frequency of 4 Hz. (3.61 ± 1.44 vs. 4.69 ± 2.15 Hz; p = ns. Figure 7.3b). CDC-EVs also induced significant differences in rotor dynamics. In particular, HL-1 monolayers treated with CDC-EVs presented significant larger spatial rotor instability in contrast to control plates, as rotors tended not to remain at fixed positions in the CDC-EV treated group. As a result, rotor meandering was significantly higher (1.45 ± 0.7 vs. 4.48 ± 1.95

cm/s, $p < 0.01$, Figure 7.3c) and presented smaller curvatures (1.95 ± 0.45 vs. 0.92 ± 0.23 rad/cm, $p < 0.01$, Figure 7.3c).

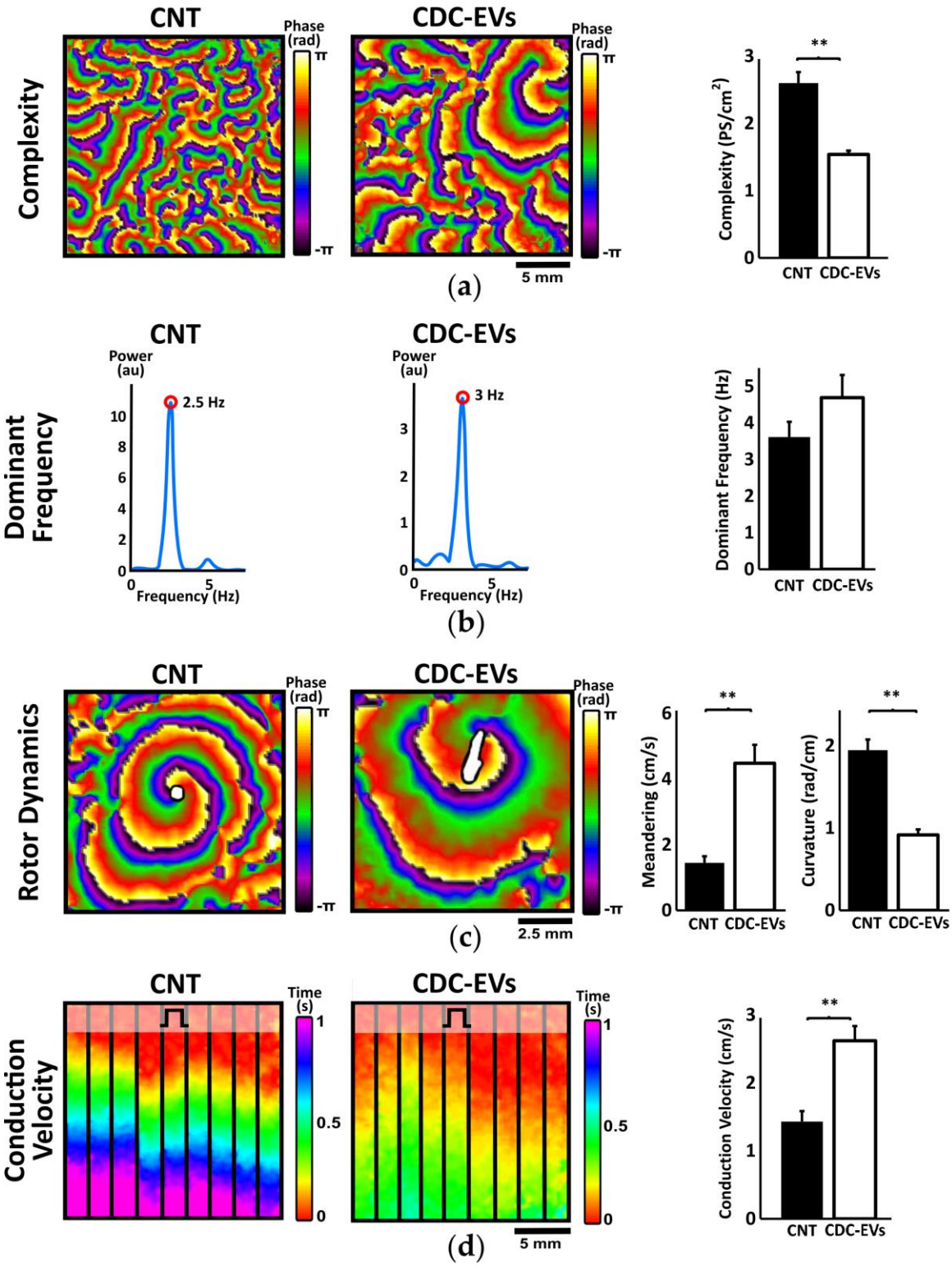

Figure 7.3. Electrophysiological characteristics comparison (n = 12 in each group) and representative examples of control (CNT) and CDC-EV treated cultures. Examples of

complexity, dominant frequency, rotor dynamics and conduction velocity are illustrated for both groups. (**a**) Complexity was higher in the CNT vs the CDC-EV group (** $p < 0.01$). (**b**) Average dominant frequency was not significantly different among both groups (* $p > 0.05$). (**c**) Rotor meandering was larger in the CDC-EV group vs CNT (** $p < 0.01$), while curvature was smaller (** $p < 0.01$). (d) Conduction velocity was higher in the CDC-EV group (** $p < 0.01$). The isochrone map shows how the impulse took less time to travel the same distance in the CD-EV group (500 ms) vs. the CNT group (1000 ms).

7.4.2 Extracellular vesicles derived from CDCs increase conduction velocity in arrhythmogenic substrate and increase ion channel expression

CV was assessed in HL-1 cell monocultures in linear propagations at a controlled stimulation rate of 1 Hz in absence of spontaneous activity. CV significantly increased by 80% in cultures treated with CDC-EVs (from 1.43 ± 0.53 cm/s in the control group to 2.62 ± 0.75 cm/s in the CDC-EV treated group, Figure 7.3d). As shown in the representative isochrone map in Figure 7.3d, the electrical impulse propagated over 1.5 cm of cell culture in ~1000 ms in the control group, while the propagation in the CDC-EV treated group was ~500 ms.

The analysis of the relative gene expression of genes associated to relevant proteins in electrophysiological remodeling revealed a significantly higher gene expression of *SCN5A*, *CACNA1C* and *GJA1* (coding for proteins involved in the regulation of I_{Na}, I_{CaL} and Cx43 respectively) in the treated group (Figure 7.4).

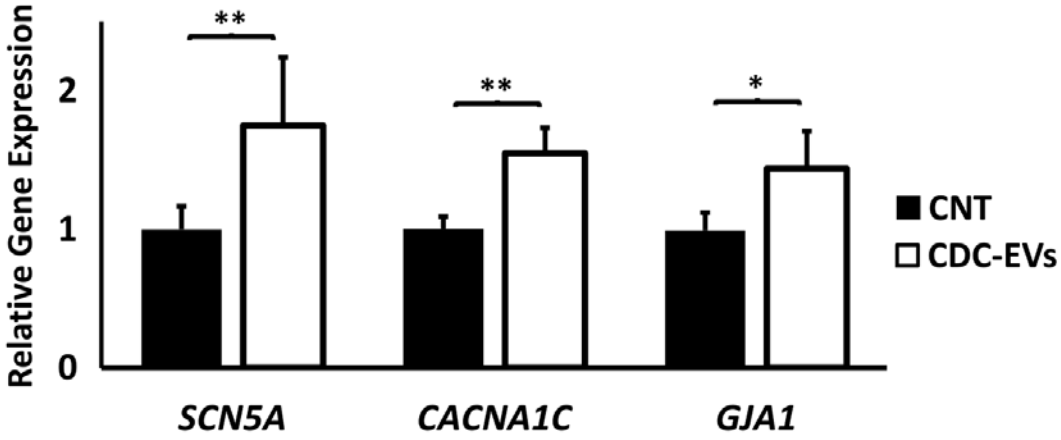

Figure 7.4. Relative gene expression results ($n = 9$ in each group) normalized to *ACTB* and *36B4* housekeeping genes. Relative gene expression of *SCN5A* (** $p < 0.01$), *CACNA1C* (** $p < 0.01$) and *GJA1* (* $p < 0.05$) was significantly higher in the CDC-EV treated group.

To investigate the mechanism behind the reduction in complexity and the increase in CV in treated plates, gene expression of *SCN5A*, *CACNA1C* and *GJA1* were correlated to the electrophysiological parameters measured (Figure 7.5a). While *GJA1* did not show a significant

relationship, an increase in *SCN5A* and *CACNA1C* expression significantly correlated with CV ($R^2 = 0.26$, $p < 0.05$ and $R^2 = 0.57$, $p < 0.01$ respectively), meandering ($R^2 = 0.61$, $p < 0.01$ and $R^2 = 0.72$, $p < 0.01$) and reduction in complexity ($R^2 = 0.45$, $p < 0.01$ and $R^2 = 0.63$, $p < 0.01$).

7.4.3 Activation complexity electrophysiological mechanisms

To analyze the electrophysiological mechanisms driving the reduction in the activation complexity of the arrhythmogenic substrate under CDC-EV treatment, we analyzed mean dominant frequency, rotor curvature, rotor meandering and CV in relation to complexity (Figure 7.5b). Changes in complexity showed a significant correlation to dominant frequency ($R^2 = 0.19$, $p < 0.05$), CV ($R^2 = 0.56$, $p < 0.01$), meandering ($R^2 = 0.46$, $p < 0.01$) and curvature ($R^2 = 0.18$, $p < 0.05$). Higher conduction velocities, higher rotor meandering, and lower curvatures found in CDC-EV treated plates are responsible for the reduction in the overall activation complexity. Changes in rotor movement in CDC-EV treated plates (larger meandering) are associated to a decrease in their curvature, which probably results in a larger area needed for a rotor to self-maintain. This may result in a reduction of the possible number of active rotors in a given area and, therefore, reduce the activation complexity. This higher CV and rotor meandering found in treated plates correlates with the higher expression of *SCN5A* and *CACNA1*. This suggests that the antiarrhythmic properties of EVs are mediated by the increased expression of these genes, which modifies rotor dynamics and CV, leading to a reduction of the overall complexity of activation.

7.5 Discussion

The main finding of this study is that CDC-EVs reduce the spontaneous activation complexity of HL-1 CMs. Our results suggest that this simplification to a less arrhythmogenic profile may be driven by two mechanisms: the increase in the CV and the modification of rotor dynamics, correlated to a higher *SCN5A* and *CACNA1C* expression.

Low and heterogeneous CV of cardiac tissue has been related to higher irregular reentry formation and probability of arrhythmic episodes [452]. Despite the fact that improving CV can reduce arrhythmogenicity under certain scenarios [454, 455], no chemical drugs have shown strong antiarrhythmic effects through this mechanism to date [456, 457]. Therefore, if confirmed in other cellular models, CDC-EVs may act as novel therapeutic CV modulators.

CDC-EVs seem to enhance the gene expression of *SCN5A*, coding for a protein directly related to I_{Na} and *GJA1*, coding for Cx43. An increase in I_{Na} conductance is related to a faster depolarization and hence to a higher CV of the excitable tissue [452]. The higher CV in CDC-EV

treated plates may be caused by the higher expression of *SCN5A*. In contrast, Cx43, also known to play an important role in action potential propagation between CMs and strongly linked to CV and antiarrhythmogenicity [315, 455], showed a significantly higher expression in treated plates but did not correlate significantly with CV measurements. This suggests that *SCN5A* may play a dominant role in the modifications of CV in our cell model.

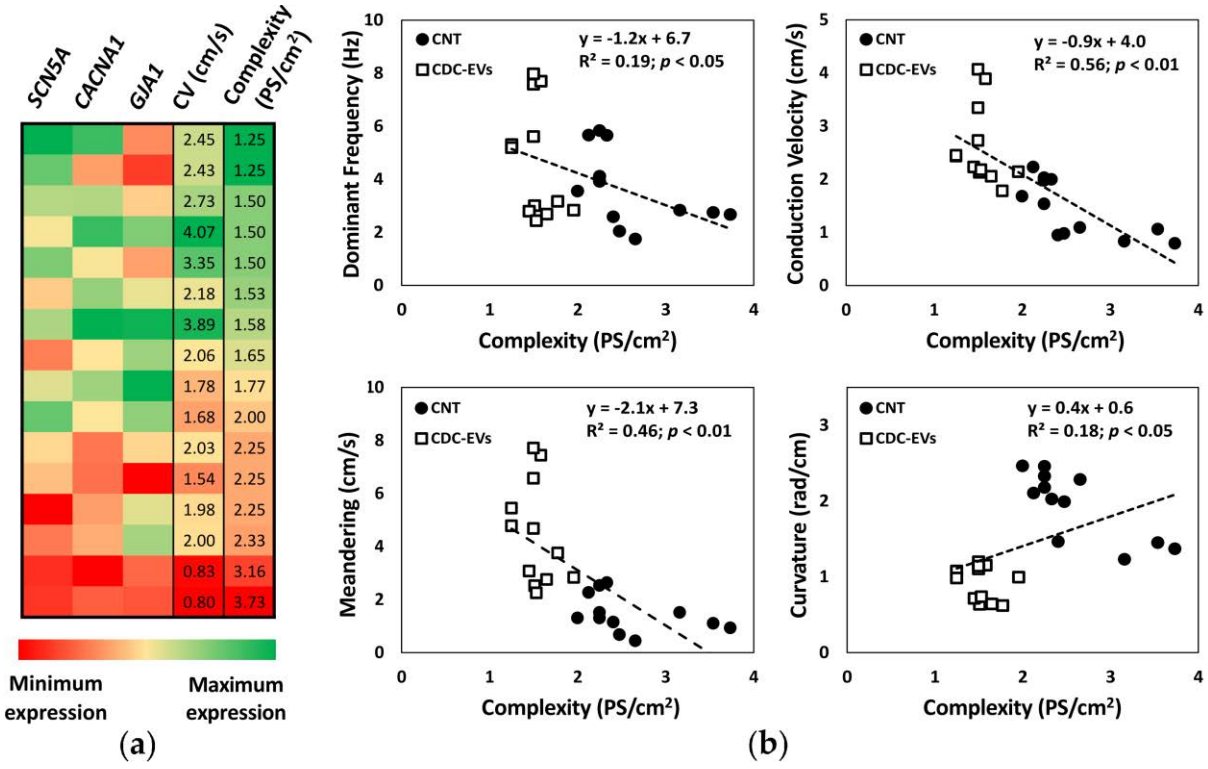

Figure 7.5. Relative gene expression relationship with CV and complexity, and relationship of the different electrophysiological parameters with activation complexity. (**a**) Relative gene expression of *SCN5A*, *CACNA1C* and *GJA1* in each sample and its associated CV and complexity. While *SCN5A* and *CACNA1C* higher expression correlated significantly with higher CV and lower complexity measurements, *GJA1* expression did not. (**b**) Dominant frequency ($p < 0.05$), CV ($p < 0.01$), meandering ($p < 0.01$) and curvature ($p < 0.05$) correlated significantly to activation complexity.

The second mechanism via which CDC-EVs could reduce activation complexity is by acting over rotor dynamics. Lengthening of the action potential and the refractory period is commonly associated with an increase in rotor meandering and reduction in curvature [459]. This promotes rotor instability, increasing the likelihood of collision with other rotors and enlarging the area needed for the rotor to self-maintain. As a result, the number of possible simultaneous rotors in a certain area and, therefore, the complexity decrease. A higher increase in I_{CaL} is related to larger action potential durations [460] (p. 187) and larger meandering [461]. Treated plates showed a significant higher expression of *CACNA1C* (codes for a protein related to I_{CaL}) that

correlated significantly to rotor meandering. A higher expression of *CACNA1C* could lead to a higher conductance of calcium channels and increase in I_{CaL}, which could explain the higher rotor meandering found in CDC-EV treated plates.

Recently, Cho et al. [471] demonstrated the antiarrhythmic effects of CDCs in rats with HF and preserved ejection fraction (HFpEF) explained by the upregulation of I_{to}, homogenization of the action potential duration, and fibrosis decrease. Our results are complementary to their findings and illustrate that the antiarrhythmic effect of CDC-EVs are mediated both by an increase in CV and by modification of rotor dynamics. Our results open new perspectives into the unraveling of the antiarrhythmic properties of the CDCs.

This study used HL-1 CM monolayers as models of arrhythmic substrate. Despite being an *in vitro* cell line capable of presenting a mature cardiac phenotype and being widely used to study cardiac electrophysiology and arrhythmias [477–486], their use has several limitations that must be taken into account. HL-1 cells, although being mature, are of murine origin and present important electrophysiological differences with adult human cardiac tissue. In fact, the expression of genes related to potassium currents (such as I_{K1}) could not be analyzed in our study due to the extremely low expression. Monolayers also represent an *in vitro* two-dimensional (2D) scenario that aims to represent a more complex three-dimensional (3D) *in vivo* environment. In addition to that, since HL-1 cultures present spontaneous arrhythmogenic activity, it is not possible to observe the complete elimination of spontaneous activations under the effect of EVs. Although gene expression patterns were used to investigate potential mechanisms of actions, we should not consider gene expression as a surrogate of protein expression, since they do not necessarily correlate under all circumstances.

Considering these limitations, future studies should be directed towards validation of the increase in CV, rotor meandering, and reduction in complexity of CDC-EVs in other cell models and human samples. Protein expression should also be investigated to support the possible mechanism of action (MoA) behind the influence of CDC-EVs on the electrophysiological properties of CMs.

7.6 Conclusions

Extracellular vesicles derived from cardiosphere-derived cells (CDC-EVs) reduce spontaneous activation complexity and increase conduction velocity of the HL-1 cardiomyocytes leading to a less arrhythmogenic profile. If validated in other cellular models, CDC-EVs may be used specifically as antiarrhythmic agents in a wide range of cardiac pathologies.

Chapter 8

Discussion and conclusions

8.1 Main findings

The use of advanced therapies, including stem cell therapy, extracellular vesicles (EVs) and biomaterials such as hydrogels emerged as a potential breakthrough for the treatment of cardiac pathologies [5] because contrary to current treatments, they have the potential to treat cardiac aging-associated pathologies from a more fundamental level [110]. They are able to improve cell survival and protection, cell-cell communication, angiogenesis, cardiomyogenesis, reduce inflammation and molecularly regulate proliferation and cell cycle [79]. However, they still pose many problems and questions that need to be solved before they can successfully reach the clinical scenario. Some of the most highlighted limitations are the lack of deep understanding of their mechanism of action (MoA), their large variability and lack of standardization (including inadequate potency tests), and in particular for cells and EVs, their low *in vivo* retention at the target site [115, 257].

In this context, this thesis aimed to explore, develop and evaluate new strategies to solve some of these current limitations for cardiosphere-derived cell secreted extracellular vesicles (CDC-EVs). Specific goals included (i) to ease the development of adequate potency assays, (ii) explore if specific donor and cell characteristics could be used to predict the potency of cardiosphere-derived cells-secreted EVs (CDC-EV), (iii) propose a specific potency test for the treatment of cardiac-aging associated pathologies based on CDC-EV expected MoA, (iv) develop a new product that enhances EV *in vivo* retention on-site and (v) explore the electrophysiological mechanisms by which EVs exert antiarrhythmic properties.

Regarding the first specific goal, we developed a guide for the development of potency tests in the cardiac field. We proposed several potency tests depending on the target pathology and the specific MoA of the biological product. When cardiomyogenesis is the expected MoA, we proposed as a potency assay to quantify cardiomyocyte (CM) division induction and ability of the cells to differentiate into the CM lineage. To evaluate electromechanical maturation and coupling, the expression of ion channels (sodium, calcium and potassium channels) and connexin 43 could be used as indicators. Secretion of pro- and anti-inflammatory factors (TNF-α, IL-6 and

IL-10) is recommended to determine immunomodulation. The anti-senescent and anti-apoptotic potency of the product can be determined *in vitro* on CM and stromal cells, while angiogenic potency can be assessed by VEGF and specific cytokine secretion. Regarding antifibrotic potency, transforming growth factor-β (TGF-β), MMP and TIMP secretion of either the therapeutic product or the target cells are suggested.

According to this, we decided to explore specifically whether if donor and CDC characteristics were determinant for CDC-EVs anti-aging potency. The results showed that chronological age of the donor, cellular senescence and cardiosphere size are not determinant for CDC-EV anti-senescent and pro-angiogenic potency. While CDC-EVs from most human donors had significant (but variable) anti-senescent and pro-angiogenic effects, the extent of the effect was not affected by chronological age of the donor and by senescence of the parenteral cells. We then decided to test if the *in vitro* antisenescent and pro-angiogenic potency could be used to predict the *in vivo* potency in the treatment of cardiac aging. We proposed a matrix assay that evaluated and scored *in vitro* the anti-senescent potency on cardiac stromal cells (CSCs) and the pro-angiogenic potency on endothelial cells (ECs) using several markers. According to the results in the matrix assay, the EVs were classified as potent and non-potent. These differences in the therapeutic potential *in vitro* have been translated to the *in vivo* model of induced cardiac aging.

We then thought that a method to improve CDC-EVs retention and enhance therapeutic efficacy *in vivo* was to deliver the EVs embedded in a hydrogel. We considered hydrogels from cardiac extracellular matrix (cECMH) as the most appropriate as they have already been tested successfully in clinical trials [227] and better mimic the structure and composition of the cardiac tissue. However, cECMH present mechanical properties considerably distant from native cardiac tissue and have long gelation times [205, 217]. Therefore, to optimize their features, we further combined the cECMH with polyethylene glycol (PEG). According to our results, the combination of PEG–cECMH improved the physicochemical properties (particularly the gelation time), while not hindering injectability and degradation vs. cECMH alone. In addition, the embedded EVs in the PEG-cECMH were progressively released and were better retained at the injection site *in vivo* when administered with the combined hydrogel compared to EVs administered in the standard vehicle (saline). Moreover, the combined product maintained the bioactive properties of cECMH and EVs alone, as it reduced senescence of CSCs.

Finally, we investigated the electrophysiological changes induced by CDC-EVs to better understand and highlight their poorly explored antiarrhythmic effects. The main finding of this study was that CDC-EVs reduced the spontaneous activation complexity of HL-1 CMs. Our results suggested that this simplification to a less arrhythmogenic profile may be driven by two mechanisms: the increase in the conduction velocity (CV) and the modification of rotor dynamics, correlated to a higher *SCN5A* and *CACNA1C* expression.

In summary, these findings together propose solutions to some of the current limitations of CDC-EVs and new ways to understand and enhance their therapeutic efficacy in the field of cardiac-aging related pathologies. Regarding standardization and potency assays, we provide insights and guides into the development of potency assays in the cardiovascular field, we discard the chronological age of the donor, cardiosphere size and CDC senescence as markers of CDC-EV potency and we propose as a potency test a matrix assay assessing the anti-senescent and pro-angiogenic potency *in vitro* illustrating its utility in a model of cardiac aging. To mitigate the limitation of poor EV retention, we develop a new product combining natural and synthetic materials that exhibits improved mechanical properties and faster gelation and show that when used to deliver EVs, it improves EV retention on-site. Regarding the MoA behind the antiarrhythmic effects, we show that EVs reduce the activation complexity and increase CV, opening new perspectives worth exploring for the treatment of cardiac arrhythmias.

8.2 Comparison with previous studies

The contributions of this work propose new strategies to enhance CDC-EV therapeutic efficacy and to overcome some of their current limitations for translation. Potency assays are a requirement by the regulatory agencies to determine product acceptance before intended use [294] and are essential to guarantee successful clinical translation, especially in biological products were variability can considerably affect the efficacy [110, 202, 257]. However, existing guides for the development of potency assays for biological products are general [294–298, 306] and none is specifically covering the challenges and limitations regarding the development of potency assays for cardiovascular diseases. To our knowledge, the work developed in Chapter 3 is the first to discuss specifically potency tests for cell-based products in the cardiovascular field and to elaborate on the link between the target cardiovascular disease and the expected MoA of the cell-based ingredient. Accordingly, we propose potential candidates as *in vivo*, *in vitro* and surrogate measurements to evaluate potency of the product.

Using the proposed guide developed in Chapter 3, we investigated if specific surrogate markers, such as chronological age of the cell donor, cell senescence or cardiosphere size could be used as markers of CDC and CDC-EVs potency in the context of cardiac aging. Previous studies had reported differences in cardiac progenitor cells (CPCs) according to chronological age of the donor, but most of them used cells of animal origin [353–356]. In this regard, it is important to highlight that laboratory animals are exposed to controlled environments and commonly share the same genotype, making probably the chronological age a more relevant factor influencing the biological conditions of the donated cells. In the case of cells from human origin, some studies did report age-related differences while others did not [87, 274, 275, 357,

358]. In addition, most of these studies compare characteristics of CPCs from donors with different profiles, but do not confirm if these differences in characterization translate into differences in CDC efficacy *in vitro* or *in vivo*. In our work, we found that chronological age of the donor did not affect the expression of surface markers in CDCs nor most of the CDC properties explored (only CDC migration). These results are similar to the work of Nakamura et al. [274], where characterization of CDCs from several donors did not reveal significant differences related to age of the donor. Regarding cellular senescence as a biomarker of cell and cell-derived EV potency, it has been previously proposed in some studies [357], but few work exists to confirm the relationship between cellular senescence and reduced therapeutic efficacy. We did confirm that CDC senescence determined other CDC characteristics more than chronological age, but these differences did not relate to impaired or enhanced anti-senescent and pro-angiogenic potency of their derived CDC-EVs.

After discarding these donor and cell characteristics as surrogate markers of CDC-EV potency, we explored if CDC-EV *in vitro* anti-senescent and pro-angiogenic potency could be used to predict the *in vivo* functionality in a model of cardiac aging. Another study had proposed an *in vitro* functional analysis for CPC-derived exosomes by evaluating their anti-apoptotic effect in CPC and HL-1 CMs and their pro-angiogenic activity through tube formation and amount of CD31 expression in endothelial cells [332]. However, the purpose of this study was to develop a standardized production method for large-scale and good manufacturing practice-exosomes, and not to validate if the potency assay could effectively differentiate potent from non-potent EVs. Despite future work being needed for appropriate validation, the results of our study show that differences in the *in vitro* anti-senescent and pro-angiogenic potency can be quantified and hold the potential to predict *in vivo* efficacy in the treatment of cardiac aging.

Hydrogels as vehicles to deliver EVs have already shown potential for improved *in vivo* retention and boosted cardiac function in previous studies [251, 253, 441]. Nevertheless, cECM hydrogels, which have additionally show that are safe in a phase I clinical trial [222], present some physicochemical limitations as slow gelation time, rapid degradation, and poor mechanical properties [217]. While other studies have attempted to tailor their material properties with the incorporation of PEG [430, 437], these studies incorporate multi-armed PEG with functionalized groups that crosslink with the collagen network or modified PEGs that require external triggers for polymerization, such as UV light. The addition of functionalized multi-armed PEGs at high concentrations still allows the formation of gels at 37 °C without external triggers and the tuning of their mechanical properties and degradation, but they do not improve the gelation time [430]. Our results show that the delivery of EVs isolated with PEG and embedded in cECMH offer a minimally invasive, injectable therapeutical product with a faster thermosensitive response at physiological temperature while maintaining the bioactivity of the individual components and the

biodegradability. Furthermore, this system allows an improved EV retention and gradual release at the site of interest.

With respect to the antiarrhythmic properties of CDC-EVs, these have been poorly explored as most of the regenerative and reparative therapies have been studied in the context of heart failure (HF) and more in particular in myocardial infarction (MI) [122]. Recently, Cho et al. [471] demonstrated the antiarrhythmic effects of CDCs in rats with HF and preserved ejection fraction (HFpEF) explained by the upregulation of I_{to}, homogenization of the action potential duration, and fibrosis decrease. Our results are complementary to their findings and illustrate that the antiarrhythmic effect of CDC-EVs are mediated both by an increase in CV and by modification of rotor dynamics. Our results open new perspectives into the unraveling of the antiarrhythmic properties of the CDCs and potential new treatments, as despite improving CV can reduce arrhythmogenicity under certain scenarios [454, 455], no chemical drugs have shown strong antiarrhythmic effects through this mechanism to date [456, 457].

8.3 Limitations

The results in this work, although promising, present some limitations that need to be taken into account when extrapolating the results. The most significant limitation of this work is that it is mainly performed *in vitro,* with only part of the results validated *in vivo*. *In vitro* experiments are convenient because they allow testing higher numbers of samples, exploring mechanisms and discarding hypothesis. However, mammals are complex multisystemic organisms and sometimes the results observed in simple *in vitro* models do not translate *in vivo*. Moreover, even if validated *in vivo*, animal models (and small animal models in particular) present important differences with respect to the target population. Therefore, while positive *in vivo* results do not necessarily imply clinical positive results, *in vivo* and *in vitro* models allow exploring mechanisms and are necessary to validate new hypothesis worth further exploring. Despite the limitations of the *in vitro* models, all the work developed in these studies uses as therapeutic product cells and EVs obtained from human samples to ease translation. The effects explored *in vitro*, except those explored on CMs, are also studied over cells of human origin.

In this regard, limitations with respect to the potency tests suggested in Chapter 3 and the matrix assay developed in Chapter 5 (or any other potentially scalable and accurate potency assay) are that they will always require final validation by confirming that the potential measurements do correlate to the efficacy of the product in patients. In addition, although the results go in the direction of our hypothesis and show differences between the changes induced by EVs classified as potent and non-potent *in vivo*, the cardiac aging model used also presents some limitations. In particular, we only observed moderate differences between healthy and D-gal (aged) animals at

molecular and structural level, and none at functional level, being the values and differences still far from those of naturally aged of pathological animals [140, 414–416]. This, together with the relatively low number of animals included in this study, make it difficult to see the potential small differences caused either by the model or by the potent EVs.

With respect to the combined product consisting in EVs, cECMH and PEG, despite showing improved properties and retention, we did not assess if these improvements translate into enhanced functionality in an animal model. Furthermore, mechanical properties of the PEG–cECMH, even if improved with the addition of PEG, are still far from mimicking that of the native ECM. Moreover, EVs were only tracked *in vivo* for 24 hours. Longer *in vivo* tracking could help determine for how long the EVs can remain at the target site after being injected.

The main limitation of the study in Chapter 7 is the CM model. HL-1 cells are mature, but of murine origin and present important electrophysiological differences with adult human cardiac tissue. Furthermore, monolayers represent an *in vitro* two-dimensional (2D) scenario that aims to represent a more complex three-dimensional (3D) *in vivo* environment. However, an adequate *in vitro* model of adult, mature human CMs is still lacking [487].

8.4 Future work

The results of these studies illustrate the potential of CDC-EVs and their *in vitro* characterization and potency assessment for the successful treatment of cardiac pathologies. Nevertheless, future work is needed to further validate these results both at preclinical and clinical level.

Regarding the proposed potency assay for CDC-EV evaluation in the treatment of cardiac aging, further work should be directed towards validating if the matrix assay developed correlates with efficacy in naturally aged animals and in the clinical scenario. To do so, first, CDC-EVs from large numbers of donors should be assessed for the potency score and then tested *in vivo*. These would also help defining pass and fail quantitative ranges, as the potency score proposed here depends on whether the CDC-EVs are among the best, the middle, or the worst tercile, and not on quantitative values. In addition, although the number of donors included is not small (n = 18) and the chronological age span is wide (3 months - 81 years old), larger number of donors, and inclusion of neonate samples, will make the study more robust. It will also be worth exploring if other CDC and CDC-EVs characteristics, apart from chronological age of the donor, CDC senescence, cardiosphere size and the expression of specific gene and surface markers, significantly related to potency and could serve as surrogate markers of anti-senescence and pro-angiogenic *in vitro* functionality. Some examples could

include CDC SDF-1α secretion [110, 268, 391], activation of the Heat Shock Response (HSR) [276], CDC expression of Mybl2 [353], activation of the Wnt/β-catening signaling pathway [275, 334, 335] or the mTOR pathway [392], and specific miRNA cargo in the CDC-EVs [196, 334, 393].

In the work in Chapter 6, we confirmed the improved properties and EV retention of the EVs embedded in a PEG–cECM hydrogel. To further improve and optimize these properties, it becomes necessary to explore further modifications in the hydrogel composition. For example, modifying the ECM concentration and incorporating additional synthetic materials could contribute to the tailoring of mechanical and degradation properties [428, 430], as well as pore size [445] and EV release rate. Moreover, labeling the EVs with other molecular methods (such as with optical probes), would allow *in vivo* tracking of the EVs for longer than 24 hours to determine for how long the EVs can remain at the target site after being injected in the PEG–cECM solution. It is also important to confirm if these improved mechanical properties, gelation time and EV retention of the combined product do translate into enhanced efficacy in an *in vivo* (large animal) model of heart failure. In fact, our group is currently assessing if the intramyocardial administration of EVs embedded in the PEG–cECM hydrogel better improves cardiac function and structure in a porcine model of chronic MI vs. the injection of saline (sham), PEG–cECM hydrogel alone, or EVs alone.

We are also currently working on validation of our main findings in Chapter 7 (CDC-EVs increase CV, rotor meandering, and reduce in complexity in arrhythmogenic tissue) in other *in vitro* models using CMs derived from human induced pluripotent stem cells (iPSC-CM). In these experiments, we are also investigating possible protein changes that may further elucidate the MoA behind the benefits of CDC-EVs on the electrophysiological properties of CMs.

8.5 Conclusions

This thesis provides new insights into mechanisms to enhance the therapeutic potential of advanced therapies in the cardiac field. In particular, the following conclusions can be drawn:

- Despite the challenges and the complexity of the biological treatments, attempts should be made to develop robust and reproducible potency assays to predict therapeutic efficacy. We provide a guide that suggests some potency assays based on the product's expected mechanism of action (MoA) and the target cardiovascular disease.

- The therapeutic efficacy of human extracellular vesicles derived from cardiosphere-derived cells (CDC-EVs) is variable and is not determined by the chronological age of

the donor or CDC senescence status. It is important to evaluate functionality relative to the expected MoA when determining cell potency, as cell identity and specific donor or cell characteristics may not translate into boosted efficacy for the treatment of a particular pathology.

- Differences in CDC-EV *in vitro* anti-senescent and pro-angiogenic potency can be used to predict CDC-EV *in vivo* efficacy in a model of cardiac aging. We suggest as a potency test an *in vitro* matrix assay consisting in scoring the CDC-EVs potential to reduce senescence-associated markers on cardiac stromal cells and to induce endothelial tube formation. EVs classified *in vitro* as potent with the matrix assay showed to be more protective in an *in vivo* model of induced cardiac aging than EVs classified as non-potent. After further validation, the matrix assay proposed here could be a suitable *in vitro* potency test for discerning suitable allogenic biological products in the cardiac aging clinical scenario.

- Hydrogels derived from cardiac extracellular matrix incorporating polyethylene glycol present promising characteristics for the delivery of EVs for different regenerative applications. The combined product rapidly gels at physiological temperature and presents improved mechanical properties while maintaining the injectability, the biodegradability, and the bioactivity of its individual components. In addition, the EVs are better retained *in vivo* on-site.

- CDC-EVs reduce spontaneous activation complexity and increase conduction velocity (CV) of cardiomyocytes (CMs) leading to a less arrhythmogenic profile. If validated in other cellular models, CDC-EVs may be used specifically as antiarrhythmic agents in a wide range of cardiac pathologies.

CDC-EVs therapeutic translation may have been limited by their lack of standardization, their poor retention, and the lack of knowledge about their specific mechanisms of actions. To ease standardization, successful potency assays based on the product's expected MoA and the target cardiovascular disease should be developed. Human CDC-EVs exhibit potential for the treatment of cardiac aging-associated pathologies as they present anti-senescent and pro-angiogenic effects. However, here we showed that the extent of the therapeutic potential is variable among donors and cannot be adequately predicted by using simple characteristics of the donor or their parenteral cells. Accordingly, we propose as a potency test an *in vitro* matrix assay that classifies the CDC-EVs according to their anti-senescent and pro-angiogenic efficacy and illustrate its potential to predict their therapeutic benefit in cardiac aging. To solve the limitation of low EVs retention at the site of interest, we developed and optimized a new drug-delivery advanced therapeutic medicinal product. This product combines natural and synthetic

biomaterials for the intramyocardial delivery of CDC-EVs. Finally, we looked *in vitro* at the electrophysiological changes induced by CDC-EVs on CMs to shed light on the mechanisms by which they exert their poorly explored antiarrhythmic properties. Our findings indicate that EV increase the CV of the arrhythmogenic substrate and reduce its activation complexity, probably by inducing a higher expression of connexins and Na^+ and Ca^{2+} ion channels. Despite future work being still needed, these findings together propose solutions to some of the limitations of CDC-EVs and new ways to understand and enhance their therapeutic efficacy in the field of cardiac-aging related pathologies.

References

[1] Roth GA, Mensah GA, Johnson CO, et al. Global burden of cardiovascular diseases and risk factors, 1990–2019: update from the GBD 2019 study. *J Am Coll Cardiol* 2020; 76: 2982–3021.

[2] Kaplinsky E, Mallarkey G. Cardiac myosin activators for heart failure therapy: focus on omecamtiv mecarbil. *Drugs Context* 2018; 7: 212518.

[3] Kraft M, Büscher A, Wiedmann F, et al. Current drug treatment strategies for atrial fibrillation and TASK-1 inhibition as an emerging novel therapy option. *Front Pharmacol* 2021; 12: 638445.

[4] Tenreiro MF, Louro AF, Alves PM, et al. Next generation of heart regenerative therapies: progress and promise of cardiac tissue engineering. *npj Regen Med* 2021; 6: 1–17.

[5] Soni M, Ferrell B, Wikholm C, et al. Stem cell therapies and treatment advances for heart failure with preserved ejection fraction. *Georgetown Medical Review* 2020; 4: 12344.

[6] SMART. *Servier Medical Art*, https://smart.servier.com/ (accessed 22 February 2022).

[7] Tortora GJ, Derrickson BH. *Principles of anatomy and physiology*. John Wiley & Sons, 2008.

[8] Doll S, Dreßen M, Geyer PE, et al. Region and cell-type resolved quantitative proteomic map of the human heart. *Nat Commun* 2017; 8: 1469.

[9] Litviňuková M, Talavera-López C, Maatz H, et al. Cells of the adult human heart. *Nature* 2020; 588: 466–472.

[10] Bergmann O, Zdunek S, Felker A, et al. Dynamics of cell generation and turnover in the human heart. *Cell* 2015; 161: 1566–1575.

[11] Geevarghese A, Herman IM. Pericyte-endothelial cross-talk: implications and opportunities for advanced cellular therapies. *Transl Res* 2014; 163: 296–306.

[12] Iozzo P. Myocardial, perivascular, and epicardial fat. *Diabetes Care* 2011; 34: S371–S379.

[13] Wada AM, Smith TK, Osler ME, et al. Epicardial/mesothelial cell line retains vasculogenic potential of embryonic epicardium. *Circ Res* 2003; 92: 525–531.

[14] Steffens S, Nahrendorf M, Madonna R. Immune cells in cardiac homeostasis and disease: emerging insights from novel technologies. *Eur Heart J* 2021; ehab842.

[15] Zhou B. Sinoatrial node pacemaker cells: cardiomyocyte- or neuron-like cells? *Protein Cell* 2021; 12: 518–519.

[16] Lakatta EG, Levy D. Arterial and cardiac aging: major shareholders in cardiovascular disease enterprises: Part II: the aging heart in health: links to heart disease. *Circulation* 2003; 107: 346–354.

[17] Chiao YA, Rabinovitch PS. The aging heart. *Cold Spring Harb Perspect Med* 2015; 5: a025148.

[18] Lam CSP, Donal E, Kraigher-Krainer E, et al. Epidemiology and clinical course of heart failure with preserved ejection fraction. *Eur J Heart Fail* 2011; 13: 18–28.

[19] Brouwers FP, Hillege HL, van Gilst WH, et al. Comparing new onset heart failure with reduced ejection fraction and new onset heart failure with preserved ejection fraction: an epidemiologic perspective. *Curr Heart Fail Rep* 2012; 9: 363–368.

[20] Oktay AA, Rich JD, Shah SJ. The emerging epidemic of heart failure with preserved ejection fraction. *Curr Heart Fail Rep* 2013; 10: 401–410.

[21] Sharma K, Kass DA. Heart failure with preserved ejection fraction: mechanisms, clinical features, and therapies. *Circ Res* 2014; 115: 79–96.

[22] Steenman M, Lande G. Cardiac aging and heart disease in humans. *Biophys Rev* 2017; 9: 131–137.

[23] Lakatta EG. Age-associated cardiovascular changes in health: Impact on cardiovascular disease in older persons. *Heart Fail Rev* 2002; 7: 29–49.

[24] Jones SA. Ageing to arrhythmias: conundrums of connections in the ageing heart. *J Pharm Pharmacol* 2006; 58: 1571–1576.

[25] Bergmann O, Bhardwaj RD, Bernard S, et al. Evidence for cardiomyocyte renewal in humans. *Science* 2009; 324: 98–102.

[26] Olivetti G, Melissari M, Capasso JM, et al. Cardiomyopathy of the aging human heart. Myocyte loss and reactive cellular hypertrophy. *Circ Res* 1991; 68: 1560–1568.

[27] Katz AM, Rolett EL. Heart failure: when form fails to follow function. *Eur Heart J* 2016; 37: 449–454.

[28] DeQuach JA, Mezzano V, Miglani A, et al. Simple and high yielding method for preparing tissue specific extracellular matrix coatings for cell culture. *PLOS ONE* 2010; 5: e13039.

[29] Meschiari CA, Ero OK, Pan H, et al. The impact of aging on cardiac extracellular matrix. *GeroScience* 2017; 39: 7–18.

[30] Ouzounian M, Lee DS, Liu PP. Diastolic heart failure: mechanisms and controversies. *Nat Rev Cardiol* 2008; 5: 375–386.

[31] Fahrenbach JP, Mejia-Alvarez R, Banach K. The relevance of non-excitable cells for cardiac pacemaker function. *J Physiol* 2007; 585: 565–578.

[32] Talman V, Ruskoaho H. Cardiac fibrosis in myocardial infarction—from repair and remodeling to regeneration. *Cell Tissue Res* 2016; 365: 563–581.

[33] Campisi J, d'Adda di Fagagna F. Cellular senescence: when bad things happen to good cells. *Nat Rev Mol Cell Biol* 2007; 8: 729–740.

[34] McHugh D, Gil J. Senescence and aging: Causes, consequences, and therapeutic avenues. *J Cell Biol* 2018; 217: 65–77.

[35] Campisi J. Aging, cellular senescence, and cancer. *Annu Rev Physiol* 2013; 75: 685–705.

[36] Muñoz-Espín D, Serrano M. Cellular senescence: from physiology to pathology. *Nat Rev Mol Cell Biol* 2014; 15: 482–496.

[37] Almeida AJPO de, Ribeiro TP, Medeiros IA de. Aging: molecular pathways and implications on the cardiovascular system. *Oxid Med Cell Longev* 2017; 2017: e7941563.

[38] Shimizu I, Minamino T. Cellular senescence in cardiac diseases. *J Cardiol* 2019; 74: 313–319.

[39] Goffart S, von Kleist-Retzow J-C, Wiesner RJ. Regulation of mitochondrial proliferation in the heart: power-plant failure contributes to cardiac failure in hypertrophy. *Cardiovasc Res* 2004; 64: 198–207.

[40] Kang R, Li R, Dai P, et al. Deoxynivalenol induced apoptosis and inflammation of IPEC-J2 cells by promoting ROS production. *Environ Pollut* 2019; 251: 689–698.

[41] Purnomo Y, Piccart Y, Coenen T, et al. Oxidative stress and transforming growth factor-β1-induced cardiac fibrosis. *Cardiovasc Hematol Disord Drug Targets* 2013; 13: 165–172.

[42] Ochoa CD, Wu RF, Terada LS. ROS signaling and ER stress in cardiovascular disease. *Mol Aspects Med* 2018; 63: 18–29.

[43] Bujak M, Frangogiannis NG. The role of TGF-beta signaling in myocardial infarction and cardiac remodeling. *Cardiovasc Res* 2007; 74: 184–195.

[44] Lyu G, Guan Y, Zhang C, et al. TGF-β signaling alters H4K20me3 status via miR-29 and contributes to cellular senescence and cardiac aging. *Nat Commun* 2018; 9: 2560.

[45] Yan M, Sun S, Xu K, et al. Cardiac aging: from basic research to therapeutics. *Oxid Med Cell Longev* 2021; 2021: e9570325.

[46] Denzel MS, Storm NJ, Gutschmidt A, et al. Hexosamine pathway metabolites enhance protein quality control and prolong life. *Cell* 2014; 156: 1167–1178.

[47] Tocchi A, Quarles EK, Basisty N, et al. Mitochondrial dysfunction in cardiac aging. *Biochimica et Biophysica Acta (BBA) - Bioenergetics* 2015; 1847: 1424–1433.

[48] Nakou ES, Parthenakis FI, Kallergis EM, et al. Healthy aging and myocardium: A complicated process with various effects in cardiac structure and physiology. *Int J Cardiol* 2016; 209: 167–175.

[49] Martín-Fernández B, Gredilla R. Mitochondria and oxidative stress in heart aging. *Age (Dordr)* 2016; 38: 225–238.

[50] Neuman RB, Bloom HL, Shukrullah I, et al. Oxidative stress markers are associated with persistent atrial fibrillation. *Clin Chem* 2007; 53: 1652–1657.

[51] Verjans R, van Bilsen M, Schroen B. MiRNA deregulation in cardiac aging and associated disorders. *Int Rev Cell Mol Biol* 2017; 334: 207–263.

[52] van Almen GC, Verhesen W, van Leeuwen REW, et al. MicroRNA-18 and microRNA-19 regulate CTGF and TSP-1 expression in age-related heart failure. *Aging Cell* 2011; 10: 769–779.

[53] Jazbutyte V, Fiedler J, Kneitz S, et al. MicroRNA-22 increases senescence and activates cardiac fibroblasts in the aging heart. *Age (Dordr)* 2013; 35: 747–762.

[54] Boon RA, Iekushi K, Lechner S, et al. MicroRNA-34a regulates cardiac ageing and function. *Nature* 2013; 495: 107–110.

[55] Nagpal V, Rai R, Place AT, et al. MiR-125b is critical for fibroblast-to-myofibroblast transition and cardiac fibrosis. *Circulation* 2016; 133: 291–301.

[56] Xiao Y, Zhao J, Tuazon JP, et al. MicroRNA-133a and myocardial infarction. *Cell Transplant* 2019; 28: 831–838.

[57] Yuan J, Liu H, Gao W, et al. MicroRNA-378 suppresses myocardial fibrosis through a paracrine mechanism at the early stage of cardiac hypertrophy following mechanical stress. *Theranostics* 2018; 8: 2565–2582.

[58] Miyamoto S. Autophagy and cardiac aging. *Cell Death Differ* 2019; 26: 653–664.

[59] Delbridge LMD, Mellor KM, Taylor DJ, et al. Myocardial stress and autophagy: mechanisms and potential therapies. *Nat Rev Cardiol* 2017; 14: 412–425.

[60] Zile MR, Brutsaert DL. New concepts in diastolic dysfunction and diastolic heart failure: Part II: causal mechanisms and treatment. *Circulation* 2002; 105: 1503–1508.

[61] Kass DA, Bronzwaer JGF, Paulus WJ. What mechanisms underlie diastolic dysfunction in heart failure? *Circ Res* 2004; 94: 1533–1542.

[62] Gu J, Zhao F, Wang Y, et al. The molecular mechanism of diastolic heart failure. *IMI* 2015; 2: 143–148.

[63] Josephson IR, Guia A, Stern MD, et al. Alterations in properties of L-type Ca channels in aging rat heart. *J Mol Cell Cardiol* 2002; 34: 297–308.

[64] Janczewski AM, Spurgeon HA, Lakatta EG. Action potential prolongation in cardiac myocytes of old rats is an adaptation to sustain youthful intracellular Ca2+ regulation. *J Mol Cell Cardiol* 2002; 34: 641–648.

[65] Feridooni HA, Dibb KM, Howlett SE. How cardiomyocyte excitation, calcium release and contraction become altered with age. *J Mol Cell Cardiol* 2015; 83: 62–72.

[66] Van Wagoner DR, Pond AL, Lamorgese M, et al. Atrial L-type Ca2+ currents and human atrial fibrillation. *Circ Res* 1999; 85: 428–436.

[67] Broglio F, Fubini A, Morello M, et al. Activity of GH/IGF-I axis in patients with dilated cardiomyopathy. *Clin Endocrinol (Oxf)* 1999; 50: 417–430.

[68] Khan AS, Sane DC, Wannenburg T, et al. Growth hormone, insulin-like growth factor-1 and the aging cardiovascular system. *Cardiovasc Res* 2002; 54: 25–35.

[69] Groban L, Pailes NA, Bennett CDL, et al. Growth hormone replacement attenuates diastolic dysfunction and cardiac angiotensin II expression in senescent rats. *J Gerontol A Biol Sci Med Sci* 2006; 61: 28–35.

[70] Ock S, Ham W, Kang CW, et al. IGF-1 protects against angiotensin II-induced cardiac fibrosis by targeting αSMA. *Cell Death Dis* 2021; 12: 688.

[71] Corpas E, Harman SM, Blackman MR. Human growth hormone and human aging. *Endocr Rev* 1993; 14: 20–39.

[72] Vasan RS, Sullivan LM, D'Agostino RB, et al. Serum insulin-like growth factor I and risk for heart failure in elderly individuals without a previous myocardial infarction: the Framingham Heart Study. *Ann Intern Med* 2003; 139: 642–648.

[73] Rodriguez-Perez AI, Borrajo A, Diaz-Ruiz C, et al. Crosstalk between insulin-like growth factor-1 and angiotensin-II in dopaminergic neurons and glial cells: role in neuroinflammation and aging. *Oncotarget* 2016; 7: 30049–30067.

[74] Domenighetti AA, Wang Q, Egger M, et al. Angiotensin II-mediated phenotypic cardiomyocyte remodeling leads to age-dependent cardiac dysfunction and failure. *Hypertension* 2005; 46: 426–432.

[75] Dai D-F, Chen T, Johnson SC, et al. Cardiac aging: from molecular mechanisms to significance in human health and disease. *Antioxid Redox Signal* 2012; 16: 1492–1526.

[76] Iravanian S, Dudley SC. The renin-angiotensin-aldosterone system (RAAS) and cardiac arrhythmias. *Heart Rhythm* 2008; 5: S12-17.

[77] Najafi A, Sequeira V, Kuster DWD, et al. β-adrenergic receptor signalling and its functional consequences in the diseased heart. *Eur J Clin Invest* 2016; 46: 362–374.

[78] Yan L, Vatner DE, O'Connor JP, et al. Type 5 adenylyl cyclase disruption increases longevity and protects against stress. *Cell* 2007; 130: 247–258.

[79] Broughton KM, Wang BJ, Firouzi F, et al. Mechanisms of cardiac repair and regeneration. *Circ Res* 2018; 122: 1151–1163.

[80] McDonagh TA, Metra M, Adamo M, et al. 2021 ESC Guidelines for the diagnosis and treatment of acute and chronic heart failure: Developed by the Task Force for the diagnosis and treatment of acute and chronic heart failure of the European Society of Cardiology (ESC) With the special contribution of the Heart Failure Association (HFA) of the ESC. *Eur Heart J* 2021; 42: 3599–3726.

[81] Xu D, Chandler O, Wee C, et al. Sodium-Glucose Cotransporter-2 Inhibitor (SGLT2i) as a Primary Preventative Agent in the Healthy Individual: A Need of a Future Randomised Clinical Trial? *Front Med* 2021; 8: 712671.

[82] Huynh K. Novel sGC stimulator improves outcomes in patients with HFrEF. *Nat Rev Cardiol* 2020; 17: 320–321.

[83] Teerlink JR, Diaz R, Felker GM, et al. Cardiac myosin activation with omecamtiv mecarbil in systolic heart failure. *N Eng J Med* 2021; 384: 105–116.

[84] Hindricks G, Potpara T, Dagres N, et al. 2020 ESC Guidelines for the diagnosis and management of atrial fibrillation developed in collaboration with the European Association for Cardio-Thoracic Surgery (EACTS): The Task Force for the diagnosis and management

of atrial fibrillation of the European Society of Cardiology (ESC) Developed with the special contribution of the European Heart Rhythm Association (EHRA) of the ESC. *Eur Heart J* 2021; 42: 373–498.

[85] Baar MP, Brandt RMC, Putavet DA, et al. Targeted apoptosis of senescent cells restores tissue homeostasis in response to chemotoxicity and aging. *Cell* 2017; 169: 132-147.e16.

[86] Zhu Y, Tchkonia T, Pirtskhalava T, et al. The Achilles' heel of senescent cells: from transcriptome to senolytic drugs. *Aging Cell* 2015; 14: 644–658.

[87] Lewis-McDougall FC, Ruchaya PJ, Domenjo-Vila E, et al. Aged-senescent cells contribute to impaired heart regeneration. *Aging Cell* 2019; 18: e12931.

[88] Anderson R, Lagnado A, Maggiorani D, et al. Length-independent telomere damage drives post-mitotic cardiomyocyte senescence. *EMBO J* 2019; 38: e100492.

[89] Walaszczyk A, Dookun E, Redgrave R, et al. Pharmacological clearance of senescent cells improves survival and recovery in aged mice following acute myocardial infarction. *Aging Cell* 2019; 18: e12945.

[90] Kirkland JL, Tchkonia T, Zhu Y, et al. The clinical potential of senolytic drugs. *J Am Geriatr Soc* 2017; 65: 2297–2301.

[91] Owens WA, Walaszczyk A, Spyridopoulos I, et al. Senescence and senolytics in cardiovascular disease: Promise and potential pitfalls. *Mech Ageing Dev* 2021; 198: 111540.

[92] Chiao YA, Zhang H, Sweetwyne M, et al. Late-life restoration of mitochondrial function reverses cardiac dysfunction in old mice. *eLife*; 9: e55513.

[93] Dai D-F, Hsieh EJ, Chen T, et al. Global proteomics and pathway analysis of pressure-overload–induced heart failure and its attenuation by mitochondrial-targeted peptides. *Circ Heart Fail* 2013; 6: 1067–1076.

[94] Poznyak AV, Ivanova EA, Sobenin IA, et al. The role of mitochondria in cardiovascular diseases. *Biology (Basel)* 2020; 9: 137.

[95] Cruzen C, Colman RJ. Effects of caloric restriction on cardiovascular aging in non-human primates and humans. *Clin Geriatr Med* 2009; 25: 733–743.

[96] Sheng Y, Lv S, Huang M, et al. Opposing effects on cardiac function by calorie restriction in different-aged mice. *Aging Cell* 2017; 16: 1155–1167.

[97] López-Lluch G, Hunt N, Jones B, et al. Calorie restriction induces mitochondrial biogenesis and bioenergetic efficiency. *Proc Natl Acad Sci U S A* 2006; 103: 1768–1773.

[98] Nisoli E, Tonello C, Cardile A, et al. Calorie restriction promotes mitochondrial biogenesis by inducing the expression of eNOS. *Science* 2005; 310: 314–317.

[99] Wahl D, Solon-Biet SM, Wang Q-P, et al. Comparing the effects of low-protein and high-carbohydrate diets and caloric restriction on brain aging in mice. *Cell Rep* 2018; 25: 2234-2243.e6.

[100] Luck C, DeMarco VG, Mahmood A, et al. Differential regulation of cardiac function and intracardiac cytokines by rapamycin in healthy and diabetic rats. *Oxid Med Cell Longev* 2017; 2017: 5724046.

[101] Urfer SR, Kaeberlein TL, Mailheau S, et al. A randomized controlled trial to establish effects of short-term rapamycin treatment in 24 middle-aged companion dogs. *GeroScience* 2017; 39: 117–127.

[102] Quarles E, Basisty N, Chiao YA, et al. Rapamycin persistently improves cardiac function in aged, male and female mice, even following cessation of treatment. *Aging Cell* 2020; 19: e13086.

[103] Dai D-F, Karunadharma PP, Chiao YA, et al. Altered proteome turnover and remodeling by short-term caloric restriction or rapamycin rejuvenate the aging heart. *Aging Cell* 2014; 13: 529–539.

[104] Stallone G, Infante B, Grandaliano G, et al. Management of side effects of sirolimus therapy. *Transplantation* 2009; 87: S23-26.

[105] Selvarani R, Mohammed S, Richardson A. Effect of rapamycin on aging and age-related diseases—past and future. *GeroScience* 2021; 43: 1135–1158.

[106] Puche JE, García-Fernández M, Muntané J, et al. Low doses of insulin-like growth factor-I induce mitochondrial protection in aging rats. *Endocrinology* 2008; 149: 2620–2627.

[107] Ma Y, Liu Y, Han F, et al. Growth differentiation factor 11: a "rejuvenation factor" involved in regulation of age-related diseases? *Aging* 2021; 13: 12258–12272.

[108] Hammers DW, Merscham-Banda M, Hsiao JY, et al. Supraphysiological levels of GDF11 induce striated muscle atrophy. *EMBO Mol Med* 2017; 9: 531–544.

[109] Zimmers TA, Jiang Y, Wang M, et al. Exogenous GDF11 induces cardiac and skeletal muscle dysfunction and wasting. *Basic Res Cardiol* 2017; 112: 48.

[110] Marbán E. A mechanistic roadmap for the clinical application of cardiac cell therapies. *Nat Biomed Eng* 2018; 2: 353–361.

[111] EMA. Advanced therapy medicinal products: Overview. *European Medicines Agency*, https://www.ema.europa.eu/en/human-regulatory/overview/advanced-therapy-medicinal-products-overview (2018, accessed 14 February 2022).

[112] Iglesias-Lopez C, Agustí A, Vallano A, et al. Current landscape of clinical development and approval of advanced therapies. *Mol Ther Methods Clin Dev* 2021; 23: 606–618.

[113] Iglesias-López C, Agustí A, Obach M, et al. Regulatory framework for advanced therapy medicinal products in europe and united states. *Front Pharmacol* 2019; 10: 921.

[114] Leri A, Rota M, Hosoda T, et al. Cardiac stem cell niches. *Stem Cell Res* 2014; 13: 631–646.

[115] Madonna R, Van Laake LW, Davidson SM, et al. Position Paper of the European Society of Cardiology Working Group Cellular Biology of the Heart: cell-based therapies for myocardial repair and regeneration in ischemic heart disease and heart failure. *Eur Heart J* 2016; 37: 1789–1798.

[116] Goichberg P, Chang J, Liao R, et al. Cardiac stem cells: biology and clinical applications. *Antioxid Redox Signal* 2014; 21: 2002–2017.

[117] Sanz-Ruiz R, Climent AM, Fernández-Santos ME, et al. Call to action from the cardiovascular reparative medicine community: A Report of the Sixteenth International Symposium on Cardiovascular Regeneration and Repair. *Eur Heart J* 2019; 40: 2661–2662.

[118] Torán JL, López JA, Gomes-Alves P, et al. Definition of a cell surface signature for human cardiac progenitor cells after comprehensive comparative transcriptomic and proteomic characterization. *Sci Rep* 2019; 9: 4647.

[119] Boland MJ, Nazor KL, Loring JF. Epigenetic regulation of pluripotency and differentiation. *Circ Res* 2014; 115: 311–324.

[120] Fernández-Avilés F, Sanz-Ruiz R, Climent AM, et al. Global position paper on cardiovascular regenerative medicine. *Eur Heart J* 2017; 38: 2532–2546.

[121] Madonna R, Van Laake LW, Botker HE, et al. ESC Working Group on Cellular Biology of the Heart: position paper for Cardiovascular Research: tissue engineering strategies combined with cell therapies for cardiac repair in ischaemic heart disease and heart failure. *Cardiovasc Res* 2019; 115: 488–500.

[122] Bolli R, Solankhi M, Tang X-L, et al. Cell therapy in patients with heart failure: a comprehensive review and emerging concepts. *Cardiovasc Res* 2021; cvab135.

[123] Cuende N, Rico L, Herrera C. Concise review: bone marrow mononuclear cells for the treatment of ischemic syndromes: medicinal product or cell transplantation? *Stem Cells Transl Med* 2012; 1: 403–408.

[124] Dominici M, Le Blanc K, Mueller I, et al. Minimal criteria for defining multipotent mesenchymal stromal cells. The International Society for Cellular Therapy position statement. *Cytotherapy* 2006; 8: 315–317.

[125] Wysoczynski M, Bolli R. A realistic appraisal of the use of embryonic stem cell-based therapies for cardiac repair. *Eur Heart J* 2020; 41: 2397–2404.

[126] Romagnuolo R, Masoudpour H, Porta-Sánchez A, et al. Human embryonic stem cell-derived cardiomyocytes regenerate the infarcted pig heart but induce ventricular tachyarrhythmias. *Stem Cell Reports* 2019; 12: 967–981.

[127] Liu Y-W, Chen B, Yang X, et al. Human embryonic stem cell-derived cardiomyocytes restore function in infarcted hearts of non-human primates. *Nat Biotechnol* 2018; 36: 597–605.

[128] Machiraju P, Greenway SC. Current methods for the maturation of induced pluripotent stem cell-derived cardiomyocytes. *World J Stem Cells* 2019; 11: 33–43.

[129] Chong JJH, Yang X, Don CW, et al. Human embryonic-stem-cell-derived cardiomyocytes regenerate non-human primate hearts. *Nature* 2014; 510: 273–277.

[130] Shiba Y, Gomibuchi T, Seto T, et al. Allogeneic transplantation of iPS cell-derived cardiomyocytes regenerates primate hearts. *Nature* 2016; 538: 388–391.

[131] Zhu K, Wu Q, Ni C, et al. Lack of remuscularization following transplantation of human embryonic stem cell-derived cardiovascular progenitor cells in infarcted nonhuman primates. *Circ Res* 2018; 122: 958–969.

[132] Li T-S, Cheng K, Malliaras K, et al. Direct comparison of different stem cell types and subpopulations reveals superior paracrine potency and myocardial repair efficacy with cardiosphere-derived cells. *J Am Coll Cardiol* 2012; 59: 942–953.

[133] Smith RR, Barile L, Cho HC, et al. Regenerative potential of cardiosphere-derived cells expanded from percutaneous endomyocardial biopsy specimens. *Circulation* 2007; 115: 896–908.

[134] Davis DR, Zhang Y, Smith RR, et al. Validation of the cardiosphere method to culture cardiac progenitor cells from myocardial tissue. *PLOS ONE* 2009; 4: e7195.

[135] Kreke M, Smith RR, Marbán L, et al. Cardiospheres and cardiosphere-derived cells as therapeutic agents following myocardial infarction. *Expert Rev Cardiovasc Ther* 2012; 10: 1185–1194.

[136] Malliaras K, Ibrahim A, Tseliou E, et al. Stimulation of endogenous cardioblasts by exogenous cell therapy after myocardial infarction. *EMBO Mol Med* 2014; 6: 760–777.

[137] Tseliou E, Couto G de, Terrovitis J, et al. Angiogenesis, cardiomyocyte proliferation and anti-fibrotic effects underlie structural preservation post-infarction by intramyocardially-injected cardiospheres. *PLOS ONE* 2014; 9: e88590.

[138] Chimenti I, Smith RR, Li T-S, et al. Relative roles of direct regeneration versus paracrine effects of human cardiosphere-derived cells transplanted into infarcted mice. *Circ Res* 2010; 106: 971–980.

[139] López E, Marinaro F, de Pedro M de LÁ, et al. The Immunomodulatory Signature of Extracellular Vesicles From Cardiosphere-Derived Cells: A Proteomic and miRNA Profiling. *Front Cell Dev Biol* 2020; 8: 321.

[140] Grigorian-Shamagian L, Liu W, Fereydooni S, et al. Cardiac and systemic rejuvenation after cardiosphere-derived cell therapy in senescent rats. *Eur Heart J* 2017; 38: 2957–2967.

[141] Makkar RR, Smith RR, Cheng K, et al. Intracoronary cardiosphere-derived cells for heart regeneration after myocardial infarction (CADUCEUS): a prospective, randomised phase 1 trial. *Lancet* 2012; 379: 895–904.

[142] Malliaras K, Makkar RR, Smith RR, et al. Intracoronary cardiosphere-derived cells after myocardial infarction: evidence of therapeutic regeneration in the final 1-year results of the CADUCEUS trial (CArdiosphere-Derived aUtologous stem CElls to reverse ventricULar dySfunction). *J Am Coll Cardiol* 2014; 63: 110–122.

[143] Chakravarty T, Makkar RR, Ascheim DD, et al. ALLogeneic heart STem cells to Achieve myocardial Regeneration (ALLSTAR) trial: rationale and design. *Cell Transplant* 2017; 26: 205–214.

[144] Makkar RR, Kereiakes DJ, Aguirre F, et al. Intracoronary ALLogeneic heart STem cells to Achieve myocardial Regeneration (ALLSTAR): a randomized, placebo-controlled, double-blinded trial. *Eur Heart J* 2020; 41: 3451–3458.

[145] Ostovaneh MR, Makkar RR, Ambale-Venkatesh B, et al. Effect of cardiosphere-derived cells on segmental myocardial function after myocardial infarction: ALLSTAR randomised clinical trial. *Open Heart* 2021; 8: e001614.

[146] Taylor M, Jefferies J, Byrne B, et al. Cardiac and skeletal muscle effects in the randomized HOPE-Duchenne trial. *Neurology* 2019; 92: e866–e878.

[147] Marban L, Rogy S, McDonald C, et al. Late breaking news e-poster presentation: LBP 5 HOPE-2 one-year results show clinically relevant improvements in upper limb & cardiac function in patients with later stage Duchenne Muscular Dystrophy. *Neuromuscul Disord* 2020; 30: S168–S169.

[148] Capricor Inc. *A phase 2, randomized, double-blind, placebo-controlled trial evaluating the safety and efficacy of intravenous delivery of allogeneic cardiosphere-derived cells in subjects with Duchenne muscular dystrophy*. Clinical Trial Registration NCT03406780, clinicaltrials.gov, https://clinicaltrials.gov/ct2/show/NCT03406780 (3 June 2020, accessed 14 February 2022).

[149] Chakravarty T, Henry TD, Kittleson M, et al. Allogeneic cardiosphere-derived cells for the treatment of heart failure with reduced ejection fraction: the Dilated cardiomYopathy iNtervention with Allogeneic MyocardIally-regenerative Cells (DYNAMIC) trial. *EuroIntervention* 2020; 16: e293–e300.

[150] Ishigami S, Ohtsuki S, Tarui S, et al. Intracoronary autologous cardiac progenitor cell transfer in patients with hypoplastic left heart syndrome: the TICAP prospective phase 1 controlled trial. *Circ Res* 2015; 116: 653–664.

[151] Tarui S, Ishigami S, Ousaka D, et al. Transcoronary infusion of cardiac progenitor cells in hypoplastic left heart syndrome: Three-year follow-up of the Transcoronary Infusion of Cardiac Progenitor Cells in Patients With Single-Ventricle Physiology (TICAP) trial. *J Thorac Cardiovasc Surg* 2015; 150: 1198–1207, 1208.e1–2.

[152] Ishigami S, Ohtsuki S, Eitoku T, et al. Intracoronary cardiac progenitor cells in single ventricle physiology. *Circ Res* 2017; 120: 1162–1173.

[153] Marbán E. *Regress-HFPEF: Regression of fibrosis & reversal of diastolic dysfunction in HFPEF patients treated with allogeneic CDCs*. Clinical Trial Registration NCT02941705, clinicaltrials.gov, https://clinicaltrials.gov/ct2/show/NCT02941705 (16 March 2021, accessed 14 February 2022).

[154] Lewis MI, Shapiro S, Hage A, et al. Abstract 14949: Allogeneic CDCs for pulmonary arterial hypertension therapy (ALPHA Study): Phase 1A data. *Circulation* 2018; 138: A14949–A14949.

[155] Marban E. *A phase I study of the safety and feasibility of central intravenous delivery of allogeneic human cardiosphere-derived stem cells in patients with pulmonary arterial hypertension ALPHA trial*. Clinical

Trial Registration NCT03145298, clinicaltrials.gov, https://clinicaltrials.gov/ct2/show/NCT03145298 (16 March 2021, accessed 14 February 2022).

[156] Capricor Inc. *CAP-1002 treatment in patients with severe COVID-19 and in critical condition as indicated by life support measurements*. Clinical Trial Registration NCT04338347, clinicaltrials.gov, https://clinicaltrials.gov/ct2/show/NCT04338347 (29 November 2020, accessed 14 February 2022).

[157] Singh S, Chakravarty T, Chen P, et al. Allogeneic cardiosphere-derived cells (CAP-1002) in critically ill COVID-19 patients: compassionate-use case series. *Basic Res Cardiol* 2020; 115: 36.

[158] Hong KU, Guo Y, Li Q-H, et al. c-kit+ Cardiac stem cells alleviate post-myocardial infarction left ventricular dysfunction despite poor engraftment and negligible retention in the recipient heart. *PLOS ONE* 2014; 9: e96725.

[159] Tang X-L, Li Q, Rokosh G, et al. Long-term outcome of administration of c-kit(POS) cardiac progenitor cells after acute myocardial infarction: transplanted cells do not become cardiomyocytes, but structural and functional improvement and proliferation of endogenous cells persist for at least one year. *Circ Res* 2016; 118: 1091–1105.

[160] Tang X-L, Nakamura S, Li Q, et al. Repeated administrations of cardiac progenitor cells are superior to a single administration of an equivalent cumulative dose. *J Am Heart Assoc* 2018; 7: e007400.

[161] Li J, Hu S, Zhu D, et al. All roads lead to Rome (the heart): cell retention and outcomes from various delivery routes of cell therapy products to the heart. *J Am Heart Assoc* 2021; 10: e020402.

[162] Malliaras K, Li T-S, Luthringer D, et al. Safety and efficacy of allogeneic cell therapy in infarcted rats transplanted with mismatched cardiosphere-derived cells. *Circulation* 2012; 125: 100–112.

[163] Wysoczynski M, Guo Y, Moore JB, et al. Myocardial reparative properties of cardiac mesenchymal cells isolated on the basis of adherence. *J Am Coll Cardiol* 2017; 69: 1824–1838.

[164] Guo Y, Nong Y, Li Q, et al. Comparison of one and three intraventricular injections of cardiac progenitor cells in a murine model of chronic ischemic cardiomyopathy. *Stem Cell Rev Rep* 2021; 17: 604–615.

[165] Sanz-Ruiz R, Fernández-Avilés F. Cardiovascular reparative and regenerative medicine: state-of-the-art. *REC: Interventional Cardiology (English Ed)* 2020; 2: 71–73.

[166] Mirotsou M, Jayawardena TM, Schmeckpeper J, et al. Paracrine mechanisms of stem cell reparative and regenerative actions in the heart. *J Mol Cell Cardiol* 2011; 50: 280–289.

[167] Gnecchi M, Zhang Z, Ni A, et al. Paracrine mechanisms in adult stem cell signaling and therapy. *Circ Res* 2008; 103: 1204–1219.

[168] Hodgkinson CP, Bareja A, Gomez JA, et al. Emerging concepts in paracrine mechanisms in regenerative cardiovascular medicine and biology. *Circ Res* 2016; 118: 95–107.

[169] Grigorian Shamagian L, Madonna R, Taylor D, et al. Perspectives on directions and priorities for future preclinical studies in regenerative medicine. *Circ Res* 2019; 124: 938–951.

[170] Phinney DG, Pittenger MF. Concise review: MSC-derived exosomes for cell-free therapy. *Stem Cells* 2017; 35: 851–858.

[171] Suzuki E, Fujita D, Takahashi M, et al. Therapeutic effects of mesenchymal stem cell-derived exosomes in cardiovascular disease. *Adv Exp Med Biol* 2017; 998: 179–185.

[172] Kervadec A, Bellamy V, Harane NE, et al. Cardiovascular progenitor–derived extracellular vesicles recapitulate the beneficial effects of their parent cells in the treatment of chronic heart failure. *J Heart Lung Transplant* 2016; 35: 795–807.

[173] Wang L, Wei J, Da FFA, et al. Rejuvenation of senescent endothelial progenitor cells by extracellular vesicles derived from mesenchymal stromal cells. *JACC Basic Transl Sci* 2020; 5: 1127–1141.

[174] Aminzadeh MA, Rogers RG, Fournier M, et al. Exosome-mediated benefits of cell therapy in mouse and human models of Duchenne muscular dystrophy. *Stem Cell Reports* 2018; 10: 942–955.

[175] El Harane N, Kervadec A, Bellamy V, et al. Acellular therapeutic approach for heart failure: in vitro production of extracellular vesicles from human cardiovascular progenitors. *Eur Heart J* 2018; 39: 1835–1847.

[176] Barile L, Lionetti V, Cervio E, et al. Extracellular vesicles from human cardiac progenitor cells inhibit cardiomyocyte apoptosis and improve cardiac function after myocardial infarction. *Cardiovasc Res* 2014; 103: 530–541.

[177] Bian S, Zhang L, Duan L, et al. Extracellular vesicles derived from human bone marrow mesenchymal stem cells promote angiogenesis in a rat myocardial infarction model. *J Mol Med (Berl)* 2014; 92: 387–397.

[178] Shao L, Zhang Y, Lan B, et al. MiRNA-sequence indicates that mesenchymal stem cells and exosomes have similar mechanism to enhance cardiac repair. *Biomed Res Int* 2017; 2017: 4150705.

[179] Khan M, Nickoloff E, Abramova T, et al. Embryonic stem cell-derived exosomes promote endogenous repair mechanisms and enhance cardiac function following myocardial infarction. *Circ Res* 2015; 117: 52–64.

[180] Ibrahim AG-E, Cheng K, Marbán E. Exosomes as critical agents of cardiac regeneration triggered by cell therapy. *Stem Cell Reports* 2014; 2: 606–619.

[181] Gallet R, Dawkins J, Valle J, et al. Exosomes secreted by cardiosphere-derived cells reduce scarring, attenuate adverse remodelling, and improve function in acute and chronic porcine myocardial infarction. *Eur Heart J* 2017; 38: 201–211.

[182] Potz BA, Scrimgeour LA, Pavlov VI, et al. Extracellular vesicle injection improves myocardial function and increases angiogenesis in a swine model of chronic ischemia. *J Am Heart Assoc* 2018; 7: e008344.

[183] Timmers L, Lim SK, Arslan F, et al. Reduction of myocardial infarct size by human mesenchymal stem cell conditioned medium. *Stem Cell Res* 2007; 1: 129–137.

[184] Arslan F, Lai RC, Smeets MB, et al. Mesenchymal stem cell-derived exosomes increase ATP levels, decrease oxidative stress and activate PI3K/Akt pathway to enhance myocardial viability and prevent adverse remodeling after myocardial ischemia/reperfusion injury. *Stem Cell Res* 2013; 10: 301–312.

[185] Ciullo A, Biemmi V, Milano G, et al. Exosomal expression of CXCR4 targets cardioprotective vesicles to myocardial infarction and improves outcome after systemic administration. *Int J Mol Sci* 2019; 20: E468.

[186] Milano G, Biemmi V, Lazzarini E, et al. Intravenous administration of cardiac progenitor cell-derived exosomes protects against doxorubicin/trastuzumab-induced cardiac toxicity. *Cardiovasc Res* 2020; 116: 383–392.

[187] Vandergriff AC, de Andrade JBM, Tang J, et al. Intravenous cardiac stem cell-derived exosomes ameliorate cardiac dysfunction in doxorubicin induced dilated cardiomyopathy. *Stem Cells Int* 2015; 2015: e960926.

[188] Singla DK, Ahmed A, Singla R, et al. Embryonic stem cells improve cardiac function in Doxorubicin-induced cardiomyopathy mediated through multiple mechanisms. *Cell Transplant* 2012; 21: 1919–1930.

[189] Rogers RG, Fournier M, Sanchez L, et al. Disease-modifying bioactivity of intravenous cardiosphere-derived cells and exosomes in mdx mice. *JCI Insight* 2019; 4: 130202.

[190] Fu S, Zhang Y, Li Y, et al. Extracellular vesicles in cardiovascular diseases. *Cell Death Discov* 2020; 6: 1–9.

[191] van Niel G, D'Angelo G, Raposo G. Shedding light on the cell biology of extracellular vesicles. *Nat Rev Mol Cell Biol* 2018; 19: 213–228.

[192] Barile L, Cervio E, Lionetti V, et al. Cardioprotection by cardiac progenitor cell-secreted exosomes: role of pregnancy-associated plasma protein-A. *Cardiovasc Res* 2018; 114: 992–1005.

[193] Walravens A-S, Smolgovsky S, Li L, et al. Mechanistic and therapeutic distinctions between cardiosphere-derived cell and mesenchymal stem cell extracellular vesicle non-coding RNA. *Sci Rep* 2021; 11: 8666.

[194] Walravens A, Peck K, Smolgovsky S, et al. Extracellular vesicles from cardiosphere-derived cells and from mesenchymal stem cells show different immunomodulatory capabilities and distinct RNA Cargo. *Cytotherapy* 2018; 20: S24.

[195] Lang JK, Young RF, Ashraf H, et al. Inhibiting extracellular vesicle release from human cardiosphere derived cells with lentiviral knockdown of nSMase2 differentially effects

proliferation and apoptosis in cardiomyocytes, fibroblasts and endothelial cells in vitro. *PLOS ONE* 2016; 11: e0165926.

[196] Namazi H, Mohit E, Namazi I, et al. Exosomes secreted by hypoxic cardiosphere-derived cells enhance tube formation and increase pro-angiogenic miRNA. *J Cell Biochem* 2018; 119: 4150–4160.

[197] Zhu D, Cheng K. Cardiac cell therapy for heart repair: should the cells be left out? *Cells* 2021; 10: 641.

[198] de Couto G, Gallet R, Cambier L, et al. Exosomal microrna transfer into macrophages mediates cellular postconditioning. *Circulation* 2017; 136: 200–214.

[199] Cambier L, de Couto G, Ibrahim A, et al. Y RNA fragment in extracellular vesicles confers cardioprotection via modulation of IL-10 expression and secretion. *EMBO Mol Med* 2017; 9: 337–352.

[200] Akers JC, Ramakrishnan V, Yang I, et al. Optimizing preservation of extracellular vesicular miRNAs derived from clinical cerebrospinal fluid. *Cancer Biomark* 2016; 17: 125–132.

[201] Bosch S, de Beaurepaire L, Allard M, et al. Trehalose prevents aggregation of exosomes and cryodamage. *Sci Rep* 2016; 6: 36162.

[202] Zhang J, Bolli R, Garry DJ, et al. Basic and translational research in cardiac repair and regeneration. *J Am Coll Cardiol* 2021; 78: 2092–2105.

[203] Menasché P. Cell therapy with human esc-derived cardiac cells: clinical perspectives. *Front Bioeng Biotechnol* 2020; 8: 601560.

[204] Hoeeg C, Dolatshahi-Pirouz A, Follin B. Injectable hydrogels for improving cardiac cell therapy—in vivo evidence and translational challenges. *Gels* 2021; 7: 7.

[205] Bejleri D, Davis ME. Decellularized extracellular matrix materials for cardiac repair and regeneration. *Adv Healthc Mater* 2019; 8: e1801217.

[206] Sun H, Zhou J, Huang Z, et al. Carbon nanotube-incorporated collagen hydrogels improve cell alignment and the performance of cardiac constructs. *IJN* 2017; 12: 3109–3120.

[207] Stoppel WL, Gao AE, Greaney AM, et al. Elastic, silk-cardiac extracellular matrix hydrogels exhibit time-dependent stiffening that modulates cardiac fibroblast response. *J Biomed Mater Res A* 2016; 104: 3058–3072.

[208] Kambe Y, Yamaoka T. Biodegradation of injectable silk fibroin hydrogel prevents negative left ventricular remodeling after myocardial infarction. *Biomater Sci* 2019; 7: 4153–4165.

[209] Xu B, Li Y, Deng B, et al. Chitosan hydrogel improves mesenchymal stem cell transplant survival and cardiac function following myocardial infarction in rats. *Exp Ther Med* 2017; 13: 588–594.

[210] Liu Y, Li P, Qiao C, et al. Chitosan hydrogel enhances the therapeutic efficacy of bone marrow-derived mesenchymal stem cells for myocardial infarction by alleviating vascular endothelial cell pyroptosis. *J Cardiovasc Pharmacol* 2020; 75: 75–83.

[211] He Y, Hou H, Wang S, et al. From waste of marine culture to natural patch in cardiac tissue engineering. *Bioact Mater* 2021; 6: 2000–2010.

[212] Follin B, Ghotbi AA, Clemmensen AE, et al. Retention and functional effect of adipose-derived stromal cells administered in alginate hydrogel in a rat model of acute myocardial infarction. *Stem Cells Int* 2018; 2018: 7821461.

[213] Ghanta RK, Aghlara-Fotovat S, Pugazenthi A, et al. Immune-modulatory alginate protects mesenchymal stem cells for sustained delivery of reparative factors to ischemic myocardium. *Biomater Sci* 2020; 8: 5061–5070.

[214] McCain ML, Agarwal A, Nesmith HW, et al. Micromolded gelatin hydrogels for extended culture of engineered cardiac tissues. *Biomaterials* 2014; 35: 5462–5471.

[215] Bonafè F, Govoni M, Giordano E, et al. Hyaluronan and cardiac regeneration. *J Biomed Sci* 2014; 21: 100.

[216] O'Brien FJ. Biomaterials & scaffolds for tissue engineering. *Mater Today* 2011; 14: 88–95.

[217] Peña B, Laughter M, Jett S, et al. Injectable hydrogels for cardiac tissue engineering. *Macromol Biosci* 2018; 18: e1800079.

[218] Millon LE, Mohammadi H, Wan WK. Anisotropic polyvinyl alcohol hydrogel for cardiovascular applications. *J Biomed Mater Res B Appl Biomater* 2006; 79: 305–311.

[219] Navaei A, Truong D, Heffernan J, et al. PNIPAAm-based biohybrid injectable hydrogel for cardiac tissue engineering. *Acta Biomater* 2016; 32: 10–23.

[220] Jongpaiboonkit L, King WJ, Lyons GE, et al. An adaptable hydrogel array format for 3-dimensional cell culture and analysis. *Biomaterials* 2008; 29: 3346–3356.

[221] Han M, Yildiz E, Kaleli HN, et al. Tissue-like optoelectronic neural interface enabled by PEDOT:PSS hydrogel for cardiac and neural stimulation. *Adv Healthc Mater* 2021; e2102160.

[222] Hernandez MJ, Christman KL. Designing acellular injectable biomaterial therapeutics for treating myocardial infarction and peripheral artery disease. *JACC Basic Transl Sci* 2017; 2: 212–226.

[223] Pezzana C, Agnely F, Bochot A, et al. Extracellular vesicles and biomaterial design: new therapies for cardiac repair. *Trends in Mol Med* 2021; 27: 231–247.

[224] Chi JS, Kloner RA. Stress and myocardial infarction. *Heart* 2003; 89: 475–476.

[225] Menasché P, Vanneaux V, Hagège A, et al. Transplantation of human embryonic stem cell–derived cardiovascular progenitors for severe ischemic left ventricular dysfunction. *J Am Coll Cardiol* 2018; 71: 429–438.

[226] Frey N, Linke A, Süselbeck T, et al. Intracoronary delivery of injectable bioabsorbable scaffold (IK-5001) to treat left ventricular remodeling after ST-elevation myocardial infarction: a first-in-man study. *Circ Cardiovasc Interv* 2014; 7: 806–812.

[227] Traverse JH, Henry TD, Dib N, et al. First-in-man study of a cardiac extracellular matrix hydrogel in early and late myocardial infarction patients. *JACC Basic Transl Sci* 2019; 4: 659–669.

[228] Anker SD, Coats AJS, Cristian G, et al. A prospective comparison of alginate-hydrogel with standard medical therapy to determine impact on functional capacity and clinical outcomes in patients with advanced heart failure (AUGMENT-HF trial). *Eur Heart J* 2015; 36: 2297–2309.

[229] Sabbah HN, Wang M, Gupta RC, et al. Augmentation of left ventricular wall thickness with alginate hydrogel implants improves left ventricular function and prevents progressive remodeling in dogs with chronic heart failure. *JACC Heart Fail* 2013; 1: 252–258.

[230] Mann DL, Lee RJ, Coats AJS, et al. One-year follow-up results from AUGMENT-HF: a multicentre randomized controlled clinical trial of the efficacy of left ventricular augmentation with Algisyl in the treatment of heart failure. *Eur J Heart Fail* 2016; 18: 314–325.

[231] Chen F-M, Liu X. Advancing biomaterials of human origin for tissue engineering. *Prog Polym Sci* 2016; 53: 86–168.

[232] Singelyn JM, DeQuach JA, Seif-Naraghi SB, et al. Naturally derived myocardial matrix as an injectable scaffold for cardiac tissue engineering. *Biomaterials* 2009; 30: 5409–5416.

[233] Wassenaar JW, Gaetani R, Garcia JJ, et al. Evidence for mechanisms underlying the functional benefits of a myocardial matrix hydrogel for post-MI treatment. *J Am Coll Cardiol* 2016; 67: 1074–1086.

[234] Singelyn JM, Sundaramurthy P, Johnson TD, et al. Catheter-deliverable hydrogel derived from decellularized ventricular extracellular matrix increases endogenous cardiomyocytes and preserves cardiac function post-myocardial infarction. *J Am Coll Cardiol* 2012; 59: 751–763.

[235] Seif-Naraghi SB, Singelyn JM, Salvatore MA, et al. Safety and efficacy of an injectable extracellular matrix hydrogel for treating myocardial infarction. *Sci Transl Med* 2013; 5: 173ra25.

[236] Tang J, Cui X, Caranasos TG, et al. Heart repair using nanogel-encapsulated human cardiac stem cells in mice and pigs with myocardial infarction. *ACS Nano* 2017; 11: 9738–9749.

[237] Gao X-R, Xu H-J, Wang L-F, et al. Mesenchymal stem cell transplantation carried in SVVYGLR modified self-assembling peptide promoted cardiac repair and angiogenesis after myocardial infarction. *Biochem Biophys Res Commun* 2017; 491: 112–118.

[238] Bhutani S, Nachlas ALY, Brown ME, et al. Evaluation of hydrogels presenting extracellular matrix-derived adhesion peptides and encapsulating cardiac progenitor cells for cardiac repair. *ACS Biomater Sci Eng* 2018; 4: 200–210.

[239] Kanda P, Alarcon EI, Yeuchyk T, et al. Deterministic encapsulation of human cardiac stem cells in variable composition nanoporous gel cocoons to enhance therapeutic repair of injured myocardium. *ACS Nano* 2018; 12: 4338–4350.

[240] Li H, Gao J, Shang Y, et al. Folic acid derived hydrogel enhances the survival and promotes therapeutic efficacy of iPS cells for acute myocardial infarction. *ACS Appl Mater Interfaces* 2018; 10: 24459–24468.

[241] Qiao L, Kong Y, Shi Y, et al. Synergistic effects of adipose-derived stem cells combined with decellularized myocardial matrix on the treatment of myocardial infarction in rats. *Life Sci* 2019; 239: 116891.

[242] Bai R, Tian L, Li Y, et al. Combining ECM hydrogels of cardiac bioactivity with stem cells of high cardiomyogenic potential for myocardial repair. *Stem Cells Int* 2019; 2019: e6708435.

[243] Chen Y, Li C, Li C, et al. Tailorable hydrogel improves retention and cardioprotection of intramyocardial transplanted mesenchymal stem cells for the treatment of acute myocardial infarction in mice. *J Am Heart Assoc* 2020; 9: e013784.

[244] Yao Y, Yang L, Feng L, et al. IGF-1C domain–modified hydrogel enhanced the efficacy of stem cells in the treatment of AMI. *Stem Cell Res Ther* 2020; 11: 136.

[245] Gerbin KA, Mitzelfelt KA, Guan X, et al. Delta-1 functionalized hydrogel promotes hESC-cardiomyocyte graft proliferation and maintains heart function post-injury. *Mol Ther Methods Clin Dev* 2020; 17: 986–998.

[246] Firoozi S, Pahlavan S, Ghanian M-H, et al. A cell-rree SDKP-conjugated self-assembling peptide hydrogel sufficient for improvement of myocardial infarction. *Biomolecules* 2020; 10: 205.

[247] Wang Q, He X, Wang B, et al. Injectable collagen scaffold promotes swine myocardial infarction recovery by long-term local retention of transplanted human umbilical cord mesenchymal stem cells. *Sci China Life Sci* 2021; 64: 269–281.

[248] Chachques JC, Trainini JC, Lago N, et al. Myocardial assistance by grafting a new bioartificial upgraded myocardium (MAGNUM clinical trial): one year follow-up. *Cell Transplant* 2007; 16: 927–934.

[249] He X, Wang Q, Zhao Y, et al. Effect of intramyocardial grafting collagen scaffold with mesenchymal stromal cells in patients with chronic ischemic heart disease: a randomized clinical trial. *JAMA Network Open* 2020; 3: e2016236.

[250] Lv K, Li Q, Zhang L, et al. Incorporation of small extracellular vesicles in sodium alginate hydrogel as a novel therapeutic strategy for myocardial infarction. *Theranostics* 2019; 9: 7403–7416.

[251] Han C, Zhou J, Liang C, et al. Human umbilical cord mesenchymal stem cell derived exosomes encapsulated in functional peptide hydrogels promote cardiac repair. *Biomater Sci* 2019; 7: 2920–2933.

[252] Liu B, Lee BW, Nakanishi K, et al. Cardiac recovery via extended cell-free delivery of extracellular vesicles secreted by cardiomyocytes derived from induced pluripotent stem cells. *Nat Biomed Eng* 2018; 2: 293–303.

[253] Waters R, Alam P, Pacelli S, et al. Stem cell-inspired secretome-rich injectable hydrogel to repair injured cardiac tissue. *Acta Biomater* 2018; 69: 95–106.

[254] Yoon SJ, Fang YH, Lim CH, et al. Regeneration of ischemic heart using hyaluronic acid-based injectable hydrogel. *J Biomed Mater Res B Appl Biomater* 2009; 91: 163–171.

[255] Hernandez MJ, Gaetani R, Pieters VM, et al. Decellularized extracellular matrix hydrogels as a delivery platform for microRNA and extracellular vesicle therapeutics. *Adv Ther* 2018; 1: 1800032.

[256] Tan Y, Wang L, Chen G, et al. Hyaluronate supports hESC-cardiomyocyte cell therapy for cardiac regeneration after acute myocardial infarction. *Cell Prolif* 2020; 53: e12942.

[257] Grigorian-Shamagian L, Sanz-Ruiz R, Climent A, et al. Insights into therapeutic products, preclinical research models, and clinical trials in cardiac regenerative and reparative medicine: where are we now and the way ahead. Current opinion paper of the ESC Working Group on Cardiovascular Regenerative and Reparative Medicine. *Cardiovas Res* 2021; 117: 1428–1433.

[258] Chamuleau SAJ, van der Naald M, Climent AM, et al. Translational research in cardiovascular repair. *Circ Res* 2018; 122: 310–318.

[259] Hass R, Kasper C, Böhm S, et al. Different populations and sources of human mesenchymal stem cells (MSC): A comparison of adult and neonatal tissue-derived MSC. *Cell Commun Signal* 2011; 9: 12.

[260] Mahon OR, Browe DC, Diaz-Payno PJ, et al. Extracellular matrix scaffolds derived from different musculoskeletal tissues drive distinct macrophage phenotypes and direct tissue-specific cellular differentiation. *J Immunol Regen Med* 2021; 12: 100041.

[261] Fernández-Pérez J, Ahearne M. The impact of decellularization methods on extracellular matrix derived hydrogels. *Sci Rep* 2019; 9: 14933.

[262] Williams C, Quinn KP, Georgakoudi I, et al. Young developmental age cardiac extracellular matrix promotes the expansion of neonatal cardiomyocytes in vitro. *Acta Biomater* 2014; 10: 194–204.

[263] Silva AC, Rodrigues SC, Caldeira J, et al. Three-dimensional scaffolds of fetal decellularized hearts exhibit enhanced potential to support cardiac cells in comparison to the adult. *Biomaterials* 2016; 104: 52–64.

[264] Wiklander OPB, Nordin JZ, O'Loughlin A, et al. Extracellular vesicle in vivo biodistribution is determined by cell source, route of administration and targeting. *J Extracell Vesicles* 2015; 4: 26316.

[265] Sanz-Ruiz R, Fernández-Avilés F. Autologous and allogeneic cardiac stem cell therapy for cardiovascular diseases. *Pharmacol Res* 2018; 127: 92–100.

[266] Assoni A, Coatti G, Valadares MC, et al. Different donors mesenchymal stromal cells secretomes reveal heterogeneous profile of relevance for therapeutic use. *Stem Cells Dev* 2017; 26: 206–214.

[267] Zhang C, Zhou L, Wang Z, et al. Eradication of specific donor-dependent variations of mesenchymal stem cells in immunomodulation to enhance therapeutic values. *Cell Death Dis* 2021; 12: 1–11.

[268] Cheng K, Malliaras K, Smith RR, et al. Human cardiosphere-derived cells from advanced heart failure patients exhibit augmented functional potency in myocardial repair. *JACC Heart Fail* 2014; 2: 49–61.

[269] Prall WC, Saller MM, Scheumaier A, et al. Proliferative and osteogenic differentiation capacity of mesenchymal stromal cells: Influence of harvesting site and donor age. *Injury* 2018; 49: 1504–1512.

[270] Prager P, Kunz M, Ebert R, et al. Mesenchymal stem cells isolated from the anterior cruciate ligament: characterization and comparison of cells from young and old donors. *Knee Surg Relat Res* 2018; 30: 193–205.

[271] Liu M, Lei H, Dong P, et al. Adipose-derived mesenchymal stem cells from the elderly exhibit decreased migration and differentiation abilities with senescent properties. *Cell Transplant* 2017; 26: 1505–1519.

[272] Choudhery MS, Badowski M, Muise A, et al. Donor age negatively impacts adipose tissue-derived mesenchymal stem cell expansion and differentiation. *J Transl Med* 2014; 12: 8.

[273] Yamaguchi S, Horie N, Satoh K, et al. Age of donor of human mesenchymal stem cells affects structural and functional recovery after cell therapy following ischaemic stroke. *J Cereb Blood Flow Metab* 2018; 38: 1199–1212.

[274] Nakamura T, Hosoyama T, Kawamura D, et al. Influence of aging on the quantity and quality of human cardiac stem cells. *Sci Rep* 2016; 6: 22781.

[275] Nakamura T, Hosoyama T, Murakami J, et al. Age-related increase in Wnt inhibitor causes a senescence-like phenotype in human cardiac stem cells. *Biochem Biophys Res Commun* 2017; 487: 653–659.

[276] Sharma S, Mishra R, Simpson D, et al. Cardiosphere-derived cells from pediatric end-stage heart failure patients have enhanced functional activity due to the heat shock response regulating the secretome. *Stem Cells* 2015; 33: 1213–1229.

[277] Sepúlveda JC, Tomé M, Fernández ME, et al. Cell senescence abrogates the therapeutic potential of human mesenchymal stem cells in the lethal endotoxemia model. *Stem Cells* 2014; 32: 1865–1877.

[278] Taylor DA, Sampaio LC, Ferdous Z, et al. Decellularized matrices in regenerative medicine. *Acta Biomater* 2018; 74: 74–89.

[279] Willis GR, Kourembanas S, Mitsialis SA. Toward exosome-based therapeutics: isolation, heterogeneity, and fit-for-purpose potency. *Front Cardiovasc Med* 2017; 4: 63.

[280] Hoogduijn MJ, de Witte SFH, Luk F, et al. Effects of freeze-thawing and intravenous infusion on mesenchymal stromal cell gene expression. *Stem Cells Dev* 2016; 25: 586–597.

[281] Bravery CA, French A. Reference materials for cellular therapeutics. *Cytotherapy* 2014; 16: 1187–1196.

[282] Kanelidis AJ, Premer C, Lopez J, et al. Route of delivery modulates the efficacy of mesenchymal stem cell therapy for myocardial infarction: a meta-analysis of preclinical studies and clinical trials. *Circ Res* 2017; 120: 1139–1150.

[283] Povsic TJ, Sanz-Ruiz R, Climent AM, et al. Reparative cell therapy for the heart: critical internal appraisal of the field in response to recent controversies. *ESC Heart Fail* 2021; 8: 2306–2309.

[284] Golpanian S, Wolf A, Hatzistergos KE, et al. Rebuilding the damaged heart: mesenchymal stem cells, cell-based therapy, and engineered heart tissue. *Physiol Rev* 2016; 96: 1127–1168.

[285] Sanz-Ruiz R, Fernández-Avilés F. Cardiovascular regenerative and reparative medicine: is myocardial infarction the model? *Eur Heart J* 2020; 41: 3459–3461.

[286] Mathur A, Fernández-Avilés F, Bartunek J, et al. The effect of intracoronary infusion of bone marrow-derived mononuclear cells on all-cause mortality in acute myocardial infarction: the BAMI trial. *Eur Heart J* 2020; 41: 3702–3710.

[287] Heldman AW, DiFede DL, Fishman JE, et al. Transendocardial mesenchymal stem cells and mononuclear bone marrow cells for ischemic cardiomyopathy: the TAC-HFT randomized trial. *JAMA* 2014; 311: 62–73.

[288] Henry TD, Pepine CJ, Lambert CR, et al. The Athena trials: Autologous adipose-derived regenerative cells for refractory chronic myocardial ischemia with left ventricular dysfunction. *Catheter Cardiovasc Interv* 2017; 89: 169–177.

[289] Patel AN, Henry TD, Quyyumi AA, et al. Ixmyelocel-T for patients with ischaemic heart failure: a prospective randomised double-blind trial. *Lancet* 2016; 387: 2412–2421.

[290] Bolli R, Mitrani RD, Hare JM, et al. A Phase II study of autologous mesenchymal stromal cells and c-kit positive cardiac cells, alone or in combination, in patients with ischaemic heart failure: the CCTRN CONCERT-HF trial. *Eur J Heart Fail* 2021; 23: 661–674.

[291] Gómez-Cid L, Grigorian-Shamagian L, Sanz-Ruiz R, et al. The essential need for a validated potency assay for cell-based therapies in cardiac regenerative and reparative medicine. a practical approach to test development. *Stem Cell Rev Rep* 2021; 17: 2235–2244.

[292] Gómez-Cid L, López-Donaire ML, Velasco D, et al. Cardiac extracellular matrix hydrogel enriched with polyethylene glycol presents improved gelation time and increased on-target site retention of extracellular vesicles. *Int J Mol Sci* 2021; 22: 9226.

[293] Gómez-Cid L, Moro-López M, de la Nava AS, et al. Electrophysiological effects of extracellular vesicles secreted by cardiosphere-derived cells: unraveling the antiarrhythmic properties of cell therapies. *Processes* 2020; 8: 924.

[294] Abraham J. The international conference on harmonisation of technical requirements for registration of pharmaceuticals for human use. In: Tietje C, Brouder A (eds) *Handbook of transnational economic governance regimes*. Martinus Nijhoff Publishers, 2009, pp. 1041–1053.

[295] European Medicines Agency (EMA). Guidance on human cell-based medicinal products. (EMEA/CHMP/410869/2006), https://www.ema.europa.eu/en/documents/scientific-guideline/guideline-human-cell-based-medicinal-products_en.pdf (2008).

[296] Food and Drug Administration (FDA). Guidance for industry. Potency tests for cellular and gene therapy products. (FDA-2008-D-0520), http://www.fda.gov/regulatory-information/search-fda-guidance-documents/potency-tests-cellular-and-gene-therapy-products (2011).

[297] Bravery CA, Carmen J, Fong T, et al. Potency assay development for cellular therapy products: an ISCT review of the requirements and experiences in the industry. *Cytotherapy* 2013; 15: 9–19.

[298] Pimpaneau V, Gianelli F, Poiseau AD. The challenges of potency assay development for cell-based medicinal products in Europe. *Regul Rapp* 2015; 12: 6.

[299] Barkholt L, Voltz-Girolt C, Raine J, et al. Regulatory watch: European regulatory experience with advanced therapy medicinal products. *Nat Rev Drug Discov* 2019; 18: 8–9.

[300] Stacey G, Andrews P, Asante C, et al. Science-based assessment of source materials for cell-based medicines: report of a stakeholders workshop. *Regen Med* 2018; 13: 935–944.

[301] Jansen of Lorkeers SJ, Eding JEC, Vesterinen HM, et al. Similar effect of autologous and allogeneic cell therapy for ischemic heart disease. *Circ Res* 2015; 116: 80–86.

[302] Gara E, Molnár AÁ, Merkely B, et al. Assessing the therapeutic readiness of stem cells for cardiovascular repair. *Expert Opin Biol Ther* 2017; 17: 911–914.

[303] Luo L, Li T-S. Mini review: Recent advances in the cell-based therapies for cardiac regeneration. *Curr Stem Cell Res Ther* 2020; 15: 649–660.

[304] Chinnadurai R, Rajan D, Qayed M, et al. Potency analysis of mesenchymal stromal cells using a combinatorial assay matrix approach. *Cell Rep* 2018; 22: 2504–2517.

[305] Pritchett T, Little L. "Hard cell": potency testing for cellular therapy products. *BioProcess Int* 2012; 10: 36–48.

[306] Porat Y, Abraham E, Karnieli O, et al. Critical elements in the development of cell therapy potency assays for ischemic conditions. *Cytotherapy* 2015; 17: 817–831.

[307] Food and Drug Administration (FDA). Guidance for industry. Standards development and the use of standards in regulatory submissions reviewed in the Center for Biologics Evaluation and Research. (FDA-2017-D-6535), https://www.fda.gov/regulatory-information/search-fda-guidance-documents/standards-development-and-use-standards-regulatory-submissions-reviewed-center-biologics-evaluation (2019).

[308] Guadix JA, López-Beas J, Clares B, et al. Principal criteria for evaluating the quality, safety and efficacy of hMSC-based products in clinical practice: current approaches and challenges. *Pharmaceutics* 2019; 11: E552.

[309] European Medicines Agency (EMA). Guidance on potency testing of cell-based immunotherapy medicinal products for the treatment cancer (EMA/CHMP/BWP/271475/2006 rev.1), https://www.ema.europa.eu/en/potency-testing-cell-based-immunotherapy-medicinal-products-treatment-cancer-0 (2016).

[310] Ghiroldi A, Piccoli M, Cirillo F, et al. Cell-based therapies for cardiac regeneration: a comprehensive review of past and ongoing strategies. *Int J Mol Sci* 2018; 19: 3194.

[311] Turner D, Rieger AC, Balkan W, et al. Clinical-based cell therapies for heart disease—current and future state. *Rambam Maimonides Med J* 2020; 11: e0015.

[312] Almeida SO, Skelton RJ, Adigopula S, et al. Arrhythmia in stem cell transplantation. *Card Electrophysiol Clin* 2015; 7: 357–370.

[313] Cingolani E, Goldhaber JI, Marbán E. Next-generation pacemakers: from small devices to biological pacemakers. *Nat Rev Cardiol* 2018; 15: 139–150.

[314] Zhao H, Wang F, Tang Y, et al. HCN2 and TBX3 reprogram human-induced pluripotent stem cells-derived cardiomyocytes into pacemaker-like cells. *DNA Cell Biol* 2020; 39: 289–298.

[315] Roell W, Lewalter T, Sasse P, et al. Engraftment of connexin 43-expressing cells prevents post-infarct arrhythmia. *Nature* 2007; 450: 819–824.

[316] Vagnozzi RJ, Maillet M, Sargent MA, et al. An acute immune response underlies the benefit of cardiac stem cell therapy. *Nature* 2020; 577: 405–409.

[317] Du Y-Y, Zhou S-H, Zhou T, et al. Immuno-inflammatory regulation effect of mesenchymal stem cell transplantation in a rat model of myocardial infarction. *Cytotherapy* 2008; 10: 469–478.

[318] de Couto G, Liu W, Tseliou E, et al. Macrophages mediate cardioprotective cellular postconditioning in acute myocardial infarction. *J Clin Invest* 2015; 125: 3147–3162.

[319] Dong Y, Undyala VV, Gottlieb RA, et al. Autophagy: definition, molecular machinery, and potential role in myocardial ischemia-reperfusion injury. *J Cardiovasc Pharmacol Ther* 2010; 15: 220–230.

[320] Uemura R, Xu M, Ahmad N, et al. Bone marrow stem cells prevent left ventricular remodeling of ischemic heart through paracrine signaling. *Circ Res* 2006; 98: 1414–1421.

[321] Davis ME, Hsieh PCH, Takahashi T, et al. Local myocardial insulin-like growth factor 1 (IGF-1) delivery with biotinylated peptide nanofibers improves cell therapy for myocardial infarction. *Proc Natl Acad Sci USA* 2006; 103: 8155–8160.

[322] Xu H, Yao Y, Su Z, et al. Endogenous HMGB1 contributes to ischemia-reperfusion-induced myocardial apoptosis by potentiating the effect of TNF-α/JNK. *Am J Physiol Heart Circ Physiol* 2010; 300: H913–H921.

[323] Bao L, Meng Q, Li Y, et al. C-kit positive cardiac stem cells and bone marrow–derived mesenchymal stem cells synergistically enhance angiogenesis and improve cardiac function after myocardial infarction in a paracrine manner. *J Card Fail* 2017; 23: 403–415.

[324] Burchfield JS, Dimmeler S. Role of paracrine factors in stem and progenitor cell mediated cardiac repair and tissue fibrosis. *Fibrogenesis Tissue Repair* 2008; 1: 4.

[325] Nguyen EH, Daly WT, Le NNT, et al. Versatile synthetic alternatives to Matrigel for vascular toxicity screening and stem cell expansion. *Nat Biomed Eng* 2017; 1: 0096.

[326] Lehman N, Cutrone R, Raber A, et al. Development of a surrogate angiogenic potency assay for clinical-grade stem cell production. *Cytotherapy* 2012; 14: 994–1004.

[327] Ohnishi S, Sumiyoshi H, Kitamura S, et al. Mesenchymal stem cells attenuate cardiac fibroblast proliferation and collagen synthesis through paracrine actions. *FEBS Letters* 2007; 581: 3961–3966.

[328] Tseliou E, Fouad J, Reich H, et al. Fibroblasts rendered antifibrotic, antiapoptotic, and angiogenic by priming with cardiosphere-derived extracellular membrane vesicles. *J Am Coll Cardiol* 2015; 66: 599–611.

[329] Guthrie K, Bruce A, Sangha N, et al. Potency evaluation of tissue engineered and regenerative medicine products. *Trends Biotechnol* 2013; 31: 505–514.

[330] Altman P, Foo CWP. *Methods of measuring potential for therapeutic potency and defining dosages for autologous cell therapies*. US10520505B2, https://patents.google.com/patent/US9752123B2/en (2019, accessed 21 April 2021).

[331] Rutten MJ, Laraway B, Gregory CR, et al. Rapid assay of stem cell functionality and potency using electric cell-substrate impedance sensing. *Stem Cell Res Ther* 2015; 6: 192.

[332] Andriolo G, Provasi E, Lo Cicero V, et al. Exosomes from human cardiac progenitor cells for therapeutic applications: development of a GMP-grade manufacturing method. *Front Physiol* 2018; 9: 1169.

[333] Campbell A, Brieva T, Raviv L, et al. Concise review: Process development considerations for cell therapy. *Stem Cells Transl Med* 2015; 4: 1155–1163.

[334] Ibrahim AG-E, Li C, Ciullo A, et al. Small molecule inhibitors and culture conditions enhance therapeutic cell and EV potency via activation of beta-catenin and suppression of THY1. *Nanomedicine* 2021; 33: 102347.

[335] Ibrahim AGE, Li C, Rogers R, et al. Augmenting canonical Wnt signalling in therapeutically inert cells converts them into therapeutically potent exosome factories. *Nat Biomed Eng* 2019; 3: 695–705.

[336] Li T-S, Hamano K, Nishida M, et al. CD117+ stem cells play a key role in therapeutic angiogenesis induced by bone marrow cell implantation. *Am J Physiol Heart Circ Physiol* 2003; 285: H931-937.

[337] Sultana N, Zhang L, Yan J, et al. Resident c-kit+ cells in the heart are not cardiac stem cells. *Nat Commun* 2015; 6: 8701.

[338] Zhou Y, Pan P, Yao L, et al. CD117-positive cells of the heart: progenitor cells or mast cells? *J Histochem Cytochem* 2010; 58: 309–316.

[339] Cheng K, Ibrahim A, Hensley MT, et al. Relative roles of CD90 and c-kit to the regenerative efficacy of cardiosphere-derived cells in humans and in a mouse model of myocardial infarction. *J Am Heart Assoc* 2014; 3: e001260.

[340] Ye J, Boyle AJ, Shih H, et al. CD45-positive cells are not an essential component in cardiosphere formation. *Cell Tissue Res* 2013; 351: 201–205.

[341] Zarychta-Wiśniewska W, Burdzińska A, Zielniok K, et al. The influence of cell source and donor age on the tenogenic potential and chemokine secretion of human mesenchymal stromal cells. *Stem Cells Int* 2019; 2019: 1613701.

[342] Tuttle CSL, Waaijer MEC, Slee-Valentijn MS, et al. Cellular senescence and chronological age in various human tissues: A systematic review and meta-analysis. *Aging Cell* 2020; 19: e13083.

[343] Zhuo Y, Li S-H, Chen M-S, et al. Aging impairs the angiogenic response to ischemic injury and the activity of implanted cells: Combined consequences for cell therapy in older recipients. *J Thorac Cardiovasc Surg* 2010; 139: 1286-1294.e2.

[344] Fafián-Labora J, Fernández-Pernas P, Fuentes I, et al. Influence of age on rat bone-marrow mesenchymal stem cells potential. *Sci Rep* 2015; 5: 16765.

[345] Kretlow JD, Jin Y-Q, Liu W, et al. Donor age and cell passage affects differentiation potential of murine bone marrow-derived stem cells. *BMC Cell Biol* 2008; 9: 60.

[346] Kulkarni R, Bajaj M, Ghode S, et al. Intercellular transfer of microvesicles from young mesenchymal stromal cells rejuvenates aged murine hematopoietic stem cells. *Stem Cells* 2018; 36: 420–433.

[347] Ahmadi M, Rezaie J. Ageing and mesenchymal stem cells derived exosomes: Molecular insight and challenges. *Cell Biochem Funct* 2021; 39: 60–66.

[348] Fafián-Labora J, Lesende-Rodriguez I, Fernández-Pernas P, et al. Effect of age on pro-inflammatory miRNAs contained in mesenchymal stem cell-derived extracellular vesicles. *Sci Rep* 2017; 7: 43923.

[349] Wang Y, Fu B, Sun X, et al. Differentially expressed microRNAs in bone marrow mesenchymal stem cell-derived microvesicles in young and older rats and their effect on tumor growth factor-β1-mediated epithelial-mesenchymal transition in HK2 cells. *Stem Cell Res Ther* 2015; 6: 185.

[350] Davis C, Dukes A, Drewry M, et al. MicroRNA-183-5p increases with age in bone-derived extracellular vesicles, suppresses bone marrow stromal (stem) cell proliferation, and induces stem cell senescence. *Tissue Eng Part A* 2017; 23: 1231–1240.

[351] Okada M, Kim HW, Matsu-ura K, et al. Abrogation of age-induced microRNA-195 rejuvenates the senescent mesenchymal stem cells by reactivating telomerase. *Stem Cells* 2016; 34: 148–159.

[352] Su T, Xiao Y, Xiao Y, et al. Bone marrow mesenchymal stem cells-derived exosomal miR-29b-3p regulates aging-associated insulin sesistance. *ACS Nano* 2019; 13: 2450–2462.

[353] Rafatian G, Kamkar M, Parent S, et al. Mybl2 rejuvenates heart explant-derived cells from aged donors after myocardial infarction. *Aging Cell* 2020; 19: e13174.

[354] Wu Q, Zhan J, Pu S, et al. Influence of aging on the activity of mice Sca-1 + CD31 − cardiac stem cells. *Oncotarget* 2016; 8: 29–41.

[355] Castaldi A, Dodia RM, Orogo AM, et al. Decline in cellular function of aged mouse c-kit+ cardiac progenitor cells. *J Physiol* 2017; 595: 6249–6262.

[356] Hsiao L-C, Perbellini F, Gomes RSM, et al. Murine cardiosphere-derived cells are impaired by age but not by cardiac dystrophic dysfunction. *Stem Cells Dev* 2014; 23: 1027–1036.

[357] Cesselli D, Beltrami AP, D'Aurizio F, et al. Effects of age and heart failure on human cardiac stem cell function. *Am J Pathol* 2011; 179: 349–366.

[358] Simpson DL, Mishra R, Sharma S, et al. A strong regenerative ability of cardiac stem cells derived from neonatal hearts. *Circulation* 2012; 126: S46-53.

[359] Yan C, Xu Z, Huang W. Cellular senescence affects cardiac regeneration and repair in ischemic heart disease. *Aging Dis* 2021; 12: 552–569.

[360] Wagner W, Horn P, Castoldi M, et al. Replicative senescence of mesenchymal stem cells: a continuous and organized process. *PLOS ONE* 2008; 3: e2213.

[361] Markers & methods to verify mesenchymal stem cell identity, potency, & quality. *www.rndsystems.com*, https://www.rndsystems.com/resources/articles/markers-and-methods-verify-mesenchymal-stem-cell-identity-potency-and-quality (accessed 19 January 2022).

[362] Takasugi M, Okada R, Takahashi A, et al. Small extracellular vesicles secreted from senescent cells promote cancer cell proliferation through EphA2. *Nat Commun* 2017; 8: 15729.

[363] Beer L, Zimmermann M, Mitterbauer A, et al. Analysis of the secretome of apoptotic peripheral blood mononuclear cells: impact of released proteins and exosomes for tissue regeneration. *Sci Rep* 2015; 5: 16662.

[364] Lei Q, Liu T, Gao F, et al. Microvesicles as potential biomarkers for the identification of senescence in human mesenchymal stem cells. *Theranostics* 2017; 7: 2673–2689.

[365] Fujii M, Kawai Y, Endoh M, et al. Expression of RAB27B is up-regulated in senescent human cells. *Mech Ageing Dev* 2006; 127: 639–642.

[366] Urbanelli L, Buratta S, Sagini K, et al. Extracellular vesicles as new players in cellular senescence. *Int J Mol Sci* 2016; 17: 1408.

[367] Xiang J, Wan C, Guo R, et al. Is hydrogen peroxide a suitable apoptosis inducer for all cell types? *Biomed Res Int* 2016; 2016: e7343965.

[368] Claycomb WC, Lanson NA, Stallworth BS, et al. HL-1 cells: a cardiac muscle cell line that contracts and retains phenotypic characteristics of the adult cardiomyocyte. *Proc Natl Acad Sci USA* 1998; 95: 2979–2984.

[369] Vandesompele J, De Preter K, Pattyn F, et al. Accurate normalization of real-time quantitative RT-PCR data by geometric averaging of multiple internal control genes. *Genome Biol* 2002; 3: research0034.1.

[370] White AJ, Smith RR, Matsushita S, et al. Intrinsic cardiac origin of human cardiosphere-derived cells. *Eur Heart J* 2013; 34: 68–75.

[371] Fonsatti E, Maio M. Highlights on endoglin (CD105): from basic findings towards clinical applications in human cancer. *J Transl Med* 2004; 2: 18.

[372] Pierelli L, Bonanno G, Rutella S, et al. CD105 (endoglin) expression on hematopoietic stem/progenitor cells. *Leuk Lymphoma* 2001; 42: 1195–1206.

[373] Perner S, Brüderlein S, Hasel C, et al. Quantifying telomere lengths of human individual chromosome arms by centromere-calibrated fluorescence in situ hybridization and digital imaging. *Am J Pathol* 2003; 163: 1751–1756.

[374] Carpentier G. Contribution: Angiogenesis Analyzer. *ImageJ News*, 5 October 2012.

[375] Youssef NS, Said AM. Immunohistochemical expression of CD117 and vascular endothelial growth factor in retinoblastoma: possible targets of new therapies. *Int J Clin Exp Pathol* 2014; 7: 5725–5737.

[376] Demetrius L. Aging in mouse and human systems: a comparative study. *Ann N Y Acad Sci* 2006; 1067: 66–82.

[377] Harding J, Roberts RM, Mirochnitchenko O. Large animal models for stem cell therapy. *Stem Cell Res Ther* 2013; 4: 23.

[378] Verjans R, van Bilsen M, Schroen B. Reviewing the limitations of adult mammalian cardiac regeneration: noncoding RNAs as regulators of cardiomyogenesis. *Biomolecules* 2020; 10: 262.

[379] Shin HS, Shin HH, Shudo Y. Current status and limitations of myocardial infarction large animal models in cardiovascular translational research. *Front Bioeng Biotechnol* 2021; 9: 673683.

[380] Ge Z, Lal S, Le TYL, et al. Cardiac stem cells: translation to human studies. *Biophys Rev* 2014; 7: 127–139.

[381] Shammas MA. Telomeres, lifestyle, cancer, and aging. *Curr Opin Clin Nutr Metab Care* 2011; 14: 28–34.

[382] Chen J, Du X, Chen Q, et al. Effects of donors' age and passage number on the biological characteristics of menstrual blood-derived stem cells. *Int J Clin Exp Pathol* 2015; 8: 14584–14595.

[383] Choi J-S, Lee B-J, Park H-Y, et al. Effects of donor age, long-term passage culture, and cryopreservation on tonsil-derived mesenchymal stem cells. *CPB* 2015; 36: 85–99.

[384] Siennicka K, Zołocińska A, Dębski T, et al. Comparison of the donor age-dependent and in vitro culture-dependent mesenchymal stem cell aging in rat model. *Stem Cells Int* 2021; 2021: 6665358.

[385] Tomohiko Kazama TN, Yasuji Inamo YN. Influence of donor age and passage number on angiogenic activity in human adipose-derived stem cell-conditioned media. *J Stem Cell Res Ther* 2015; 05: 307.

[386] Mansell E, Sigurdsson V, Deltcheva E, et al. Mitochondrial potentiation ameliorates age-related heterogeneity in hematopoietic stem cell function. *Cell Stem Cell* 2021; 28: 241-256.e6.

[387] Harvey E, Zhang H, Sepúlveda P, et al. Potency of human cardiosphere-derived cells from patients with ischemic heart disease is associated with robust vascular supportive ability. *Stem Cells Transl Med* 2017; 6: 1399–1411.

[388] Kaur G, Cai C. Current progress in the rejuvenation of aging stem/progenitor cells for improving the therapeutic effectiveness of myocardial repair. *Stem Cells Int* 2018; 2018: 9308301.

[389] Avolio E, Gianfranceschi G, Cesselli D, et al. Ex vivo molecular rejuvenation improves the therapeutic activity of senescent human cardiac stem cells in a mouse model of myocardial infarction. *Stem Cells* 2014; 32: 2373–2385.

[390] Lähteenvuo J, Rosenzweig A. Invited review: The role of angiogenesis in cardiovascular aging. *Circ Res* 2012; 110: 1252–1264.

[391] Saha P, Kim M, Tulshyan A, et al. Hypoxia-inducible factor 1-alpha enhances the secretome to rejuvenate adult cardiosphere-derived cells. *J Thorac Cardiovasc Surg* 2021; S0022-5223(21)01046–1.

[392] Tanaka Y, Hosoyama T, Mikamo A, et al. Hypoxic preconditioning of human cardiosphere-derived cell sheets enhances cellular functions via activation of the PI3K/Akt/mTOR/HIF-1α pathway. *Am J Transl Res* 2017; 9: 664–673.

[393] Wang L, Jia Q, Xinnong C, et al. Role of cardiac progenitor cell-derived exosome-mediated microRNA-210 in cardiovascular disease. *J Cell Mol Med* 2019; 23: 7124–7131.

[394] Climent AM, Sanz-Ruiz R, Fernández-Avilés F. Cardiac rejuvenation: a new hope in the presbycardia nightmare. *Eur Heart J* 2017; 38: 2968–2970.

[395] Uren NG, Camici PG, Melin JA, et al. Effect of aging on myocardial perfusion reserve. *J Nucl Med* 1995; 36: 2032–2036.

[396] Gazoti Debessa CR, Mesiano Maifrino LB, Rodrigues de Souza R. Age related changes of the collagen network of the human heart. *Mech Ageing Dev* 2001; 122: 1049–1058.

[397] Zhao Z-A, Han X, Lei W, et al. Lack of cardiac improvement after cardiosphere-derived cell transplantation in aging mouse hearts. *Circ Res* 2018; 123: e21–e31.

[398] Carr CA, Stuckey DJ, Tan JJ, et al. Cardiosphere-derived cells improve function in the infarcted rat heart for at least 16 weeks – an MRI study. *PLOS ONE* 2011; 6: e25669.

[399] Kasai-Brunswick TH, Costa AR da, Barbosa RAQ, et al. Cardiosphere-derived cells do not improve cardiac function in rats with cardiac failure. *Stem Cell Res Ther* 2017; 8: 36.

[400] Bernardes de Jesus B, Blasco MA. Assessing cell and organ senescence biomarkers. *Circ Res* 2012; 111: 97–109.

[401] Ma Z-G, Yuan Y-P, Wu H-M, et al. Cardiac fibrosis: new insights into the pathogenesis. *Int J Biol Sci* 2018; 14: 1645–1657.

[402] Tominaga K, Suzuki HI. TGF-β signaling in cellular senescence and aging-related pathology. *Int J Mol Sci* 2019; 20: 5002.

[403] Sanjabi S, Zenewicz LA, Kamanaka M, et al. Anti- and pro-inflammatory roles of TGF-β, IL-10, and IL-22 in immunity and autoimmunity. *Curr Opin Pharmacol* 2009; 9: 447–453.

[404] Crisóstomo V, Baéz-Diaz C, Blanco-Blázquez V, et al. The epicardial delivery of cardiosphere derived cells or their extracellular vesicles is safe but of limited value in experimental infarction. *Sci Rep* 2021; 11: 22155.

[405] Rogers RG, de Couto G, Liu W, et al. Cardiosphere-derived cell exosomes modulate mdx macrophage phenotype and alter their secretome. *The FASEB Journal* 2019; 33: lb611–lb611.

[406] Coppé J-P, Desprez P-Y, Krtolica A, et al. The senescence-associated secretory phenotype: the dark side of tumor suppression. *Annu Rev Pathol* 2010; 5: 99–118.

[407] Fontes JA, Rose NR, Čiháková D. The varying faces of IL-6: from cardiac protection to cardiac failure. *Cytokine* 2015; 74: 62–68.

[408] DeCicco-Skinner KL, Henry GH, Cataisson C, et al. Endothelial cell tube formation assay for the in vitro study of angiogenesis. *J Vis Exp* 2014; 51312.

[409] Bo-Htay C, Palee S, Apaijai N, et al. Effects of d-galactose-induced ageing on the heart and its potential interventions. *J Cell Mol Med* 2018; 22: 1392–1410.

[410] Pascau J, Gispert JD, Soto-Montenegro M, et al. Small-animal PET registration method with intrinsic validation designed for large datasets. In: *2007 IEEE Nuclear Science Symposium Conference Record*. 2007, pp. 3751–3753.

[411] Wu W, Hou C-L, Mu X-P, et al. H2S donor NaHS changes the production of endogenous H2S and NO in D-Galactose-induced accelerated ageing. *Oxid Med Cell Longev* 2017; 2017: 5707830.

[412] Chang Y-M, Chang H-H, Kuo W-W, et al. Anti-apoptotic and pro-survival effect of Alpinate Oxyphyllae Fructus (AOF) in a D-Galactose-induced aging heart. *Int J Mol Sci* 2016; 17: 466.

[413] Li X, Zhang Y, Yuan Y, et al. Protective effects of selenium, vitamin e, and purple carrot anthocyanins on D-galactose-induced oxidative damage in blood, liver, heart and kidney rats. *Biol Trace Elem Res* 2016; 173: 433–442.

[414] Liu C, Ni C, Liu W, et al. Effects of long-term nonylphenol exposure on myocardial fibrosis and cardiac function in rats. *Environ Sci Eur* 2021; 33: 96.

[415] Chen L, Ji Q, Zhu H, et al. miR-30a attenuates cardiac fibrosis in rats with myocardial infarction by inhibiting CTGF. *Exp Ther Med* 2018; 15: 4318–4324.

[416] Liao P-H, Hsieh DJ-Y, Kuo C-H, et al. Moderate exercise training attenuates aging-induced cardiac inflammation, hypertrophy and fibrosis injuries of rat hearts. *Oncotarget* 2015; 6: 35383–35394.

[417] Chen B, Li Q, Zhao B, et al. Stem cell-derived extracellular vesicles as a novel potential therapeutic tool for tissue repair. *Stem Cells Transl Med* 2017; 6: 1753–1758.

[418] Kennedy TL, Russell AJ, Riley P. Experimental limitations of extracellular vesicle-based therapies for the treatment of myocardial infarction. *Trends Cardiovasc Med* 2021; 31: 405–415.

[419] Chen P, Wang L, Fan X, et al. Targeted delivery of extracellular vesicles in heart injury. *Theranostics* 2021; 11: 2263–2277.

[420] Sánchez PL, Fernández-Santos ME, Costanza S, et al. Acellular human heart matrix: A critical step toward whole heart grafts. *Biomaterials* 2015; 61: 279–289.

[421] Izquierdo I, Rosa I, Bravo SB, et al. Proteomic identification of putative biomarkers for early detection of sudden cardiac death in a family with a LMNA gene mutation causing dilated cardiomyopathy. *J Proteomics* 2016; 148: 75–84.

[422] Peñas-Martínez J, Barrachina MN, Cuenca-Zamora EJ, et al. Qualitative and quantitative comparison of plasma exosomes from neonates and adults. *Int J Mol Sci* 2021; 22: 1926.

[423] Bonzon-Kulichenko E, Pérez-Hernández D, Núñez E, et al. A robust method for quantitative high-throughput analysis of proteomes by 18O labeling. *Mol Cell Proteomics* 2011; 10: M110.003335.

[424] Perez-Hernandez D, Gutiérrez-Vázquez C, Jorge I, et al. The intracellular interactome of tetraspanin-enriched microdomains reveals their function as sorting machineries toward exosomes. *J Biol Chem* 2013; 288: 11649–11661.

[425] Shilov IV, Seymour SL, Patel AA, et al. The Paragon Algorithm, a next generation search engine that uses sequence temperature values and feature probabilities to identify peptides from tandem mass spectra. *Mol Cell Proteomics* 2007; 6: 1638–1655.

[426] Tang WH, Shilov IV, Seymour SL. Nonlinear fitting method for determining local false discovery rates from decoy database searches. *J Proteome Res* 2008; 7: 3661–3667.

[427] Montero A, Acosta S, Hernández R, et al. Contraction of fibrin-derived matrices and its implications for in vitro human skin bioengineering. *J Biomed Mater Res A* 2021; 109: 500–514.

[428] Johnson TD, Lin SY, Christman KL. Tailoring material properties of a nanofibrous extracellular matrix derived hydrogel. *Nanotechnology* 2011; 22: 494015.

[429] Chen MH, Wang LL, Chung JJ, et al. Methods to assess shear-thinning hydrogels for application as injectable biomaterials. *ACS Biomater Sci Eng* 2017; 3: 3146–3160.

[430] Grover GN, Rao N, Christman KL. Myocardial matrix-polyethylene glycol hybrid hydrogels for tissue engineering. *Nanotechnology* 2014; 25: 014011.

[431] Filipe V, Hawe A, Jiskoot W. Critical evaluation of Nanoparticle Tracking Analysis (NTA) by NanoSight for the measurement of nanoparticles and protein aggregates. *Pharm Res* 2010; 27: 796–810.

[432] González MI, Martín-Duque P, Desco M, et al. Radioactive labeling of milk-derived exosomes with 99mTc and in vivo tracking by SPECT imaging. *Nanomaterials* 2020; 10: 1062.

[433] Abella M, Vaquero JJ, Sisniega A, et al. Software architecture for multi-bed FDK-based reconstruction in X-ray CT scanners. *Comput Methods Programs Biomed* 2012; 107: 218–232.

[434] García-Vázquez V, Cussó L, Chamorro-Servent J, et al. Registration of small-animal SPECT/MRI studies for tracking human mesenchymal stem cells. In: Roa Romero LM (ed) *XIII Mediterranean Conference on Medical and Biological Engineering and Computing 2013*. Cham: Springer International Publishing, 2014, pp. 399–402.

[435] Gobeaux F, Mosser G, Anglo A, et al. Fibrillogenesis in dense collagen solutions: a physicochemical study. *J Mol Biol* 2008; 376: 1509–1522.

[436] Suri S, Schmidt CE. Photopatterned collagen–hyaluronic acid interpenetrating polymer network hydrogels. *Acta Biomaterialia* 2009; 5: 2385–2397.

[437] Sargeant TD, Desai AP, Banerjee S, et al. An in situ forming collagen-PEG hydrogel for tissue regeneration. *Acta Biomater* 2012; 8: 124–132.

[438] Engler AJ, Griffin MA, Sen S, et al. Myotubes differentiate optimally on substrates with tissue-like stiffness: pathological implications for soft or stiff microenvironments. *J Cell Biol* 2004; 166: 877–887.

[439] Evans ND, Gentleman E. The role of material structure and mechanical properties in cell–matrix interactions. *J Mater Chem B* 2014; 2: 2345–2356.

[440] Martens TP, Godier AFG, Parks JJ, et al. Percutaneous cell delivery into the heart using hydrogels polymerizing in situ. *Cell Transplant* 2009; 18: 297–304.

[441] Chen CW, Wang LL, Zaman S, et al. Sustained release of endothelial progenitor cell-derived extracellular vesicles from shear-thinning hydrogels improves angiogenesis and promotes function after myocardial infarction. *Cardiovasc Res* 2018; 114: 1029–1040.

[442] Zhang Y, Kumar P, Lv S, et al. Recent advances in 3D bioprinting of vascularized tissues. *Mater Des* 2021; 199: 109398.

[443] Reing JE, Zhang L, Myers-Irvin J, et al. Degradation products of extracellular matrix affect cell migration and proliferation. *Tissue Eng Part A* 2009; 15: 605–614.

[444] Li F, Li W, Johnson S, et al. Low-molecular-weight peptides derived from extracellular matrix as chemoattractants for primary endothelial cells. *Endothelium* 2004; 11: 199–206.

[445] Annabi N, Nichol JW, Zhong X, et al. Controlling the porosity and microarchitecture of hydrogels for tissue engineering. *Tissue Eng Part B Rev* 2010; 16: 371–383.

[446] Antzelevitch C, Burashnikov A. Overview of basic mechanisms of cardiac arrhythmia. *Card Electrophysiol Clin* 2011; 3: 23–45.

[447] Perna F, Leo M. Epidemiology, classification and description of cardiac arrhythmias. In: Fioranelli M, Frajese G (eds) *Sports Cardiology: From Diagnosis to Clinical Management*. Milano: Springer Milan, pp. 155–177.

[448] Khurshid Shaan, Choi Seung Hoan, Weng Lu-Chen, et al. Frequency of cardiac rhythm abnormalities in a half million adults. *Circ Arrhythm Electrophysiol* 2018; 11: e006273.

[449] Macle L, Nattel S. Arrhythmias in 2015: Advances in drug, ablation, and device therapy for cardiac arrhythmias. *Nat Rev Cardiol* 2016; 13: 67–68.

[450] Gopinathannair R, Olshansky B. Management of tachycardia. *F1000Prime Rep* 2015; 7: 60.

[451] Cho HC, Marbán E. Biological therapies for cardiac arrhythmias: can genes and cells replace drugs and devices? *Circ Res* 2010; 106: 674–685.

[452] King JH, Huang CL-H, Fraser JA. Determinants of myocardial conduction velocity: implications for arrhythmogenesis. *Front Physiol* 2013; 4: 154.

[453] Aronis Konstantinos N., Berger Ronald D., Ashikaga Hiroshi. Rotors. *Circ Arrhythm Electrophysiol* 2017; 10: e005634.

[454] Lau DH, Clausen C, Sosunov EA, et al. Epicardial border zone overexpression of skeletal muscle sodium channel SkM1 normalizes activation, preserves conduction, and suppresses ventricular arrhythmia: an in silico, in vivo, in vitro study. *Circulation* 2009; 119: 19–27.

[455] Igarashi T, Finet JE, Takeuchi A, et al. Connexin gene transfer preserves conduction velocity and prevents atrial fibrillation. *Circulation* 2012; 125: 216–225.

[456] Golan DE, Tashjian AH, Armstrong EJ. *Principles of pharmacology: the pathophysiologic basis of drug therapy*. Philadelphia, United States: Lippincott Williams & Wilkins, 2011.

[457] Haugan K, Miyamoto T, Takeishi Y, et al. Rotigaptide (ZP123) improves atrial conduction slowing in chronic volume overload-induced dilated atria. *Basic Clin Pharmacol Toxicol* 2006; 99: 71–79.

[458] Rossello RA, Kohn DH. Gap junction intercellular communication: a review of a potential platform to modulate craniofacial tissue engineering. *J Biomed Mater Res B Appl Biomater* 2009; 88: 509–518.

[459] Comtois P, Kneller J, Nattel S. Of circles and spirals: bridging the gap between the leading circle and spiral wave concepts of cardiac reentry. *Europace* 2005; 7 Suppl 2: 10–20.

[460] Cha Y-M, Friedman PA. *Mayo Clinic electrophysiology manual*. Oxford, United Kingdom: Oxford University Press, 2013.

[461] Qu Z, Xie F, Garfinkel A, et al. Origins of spiral wave meander and breakup in a two-dimensional cardiac tissue model. *Ann Biomed Eng* 2000; 28: 755–771.

[462] Zipes DP, Jalife J. *Cardiac electrophysiology: from cell to bedside e-book: expert consult*. Amsterdam, The Netherlands: Elsevier Health Sciences, 2009.

[463] Lim HS, Hocini M, Dubois R, et al. Complexity and distribution of drivers in relation to duration of persistent atrial fibrillation. *J Am Coll Cardiol* 2017; 69: 1257–1269.

[464] Albert CM, Stevenson WG. The future of arrhythmias and electrophysiology. *Circulation* 2016; 133: 2687–2696.

[465] Raymond-Paquin A, Andrade J, Macle L. Catheter ablation: an ongoing revolution. *J Thorac Dis* 2019; 11: S212–S215.

[466] Sadraddin H, Gaebel R, Skorska A, et al. CD271+ human mesenchymal stem cells show antiarrhythmic effects in a novel murine infarction model. *Cells* 2019; 8: E1474.

[467] Park H, Park H, Mun D, et al. Extracellular vesicles derived from hypoxic human mesenchymal stem cells attenuate GSK3β expression via miRNA-26a in an ischemia-reperfusion injury model. *Yonsei Med J* 2018; 59: 736–745.

[468] Mayourian J, Cashman TJ, Ceholski DK, et al. Experimental and computational insight into human mesenchymal stem cell paracrine signaling and heterocellular coupling effects on cardiac contractility and arrhythmogenicity. *Circ Res* 2017; 121: 411–423.

[469] Hwang HJ, Chang W, Song B-W, et al. Antiarrhythmic potential of mesenchymal stem cell is modulated by hypoxic environment. *J Am Coll Cardiol* 2012; 60: 1698–1706.

[470] Ramireddy A, Brodt CR, Mendizabal AM, et al. Effects of transendocardial stem cell injection on ventricular proarrhythmia in patients with ischemic cardiomyopathy: results from the POSEIDON and TAC-HFT trials. *Stem Cells Transl Med* 2017; 6: 1366–1372.

[471] Cho JH, Kilfoil PJ, Zhang R, et al. Reverse electrical remodeling in rats with heart failure and preserved ejection fraction. *JCI Insight* 2018; 3: 121123.

[472] Cho Jae Hyung, Kilfoil Peter J, Solymani Ryan, et al. Abstract 15421: Anti-arrhythmic effects of heart-derived cell therapy in a rat model of heart failure with preserved ejection fraction. *Circulation* 2017; 136: A15421–A15421.

[473] Askar SFA, Ramkisoensing AA, Atsma DE, et al. Engraftment patterns of human adult mesenchymal stem cells expose electrotonic and paracrine proarrhythmic mechanisms in myocardial cell cultures. *Circ Arrhythm Electrophysiol* 2013; 6: 380–391.

[474] Eun LY, Song H, Choi E, et al. Implanted bone marrow-derived mesenchymal stem cells fail to metabolically stabilize or recover electromechanical function in infarcted hearts. *Tissue Cell* 2011; 43: 238–245.

[475] Raposo G, Stoorvogel W. Extracellular vesicles: Exosomes, microvesicles, and friends. *J Cell Biol* 2013; 200: 373–383.

[476] Marbán E. The secret life of exosomes: what bees can teach us about next-generation therapeutics. *J Am Coll Cardiol* 2018; 71: 193–200.

[477] Climent AM, Guillem MS, Fuentes L, et al. Role of atrial tissue remodeling on rotor dynamics: an in vitro study. *Am J Physiol Heart Circ Physiol* 2015; 309: H1964-1973.

[478] Del-Canto I, Gómez-Cid L, Hernández Romero I, et al. Ranolazine-mediated attenuation of mechanoelectric feedback in atrial myocyte monolayers. *Front Physiol* 2020; 11: 922.

[479] van Gorp PRR, Trines SA, Pijnappels DA, et al. Multicellular in vitro models of cardiac arrhythmias: focus on atrial fibrillation. *Front Cardiovasc Med* 2020; 7: 43.

[480] Brundel BJJM, Kampinga HH, Henning RH. Calpain inhibition prevents pacing-induced cellular remodeling in a HL-1 myocyte model for atrial fibrillation. *Cardiovasc Res* 2004; 62: 521–528.

[481] Hong J, Choi JH, Kim TY, et al. Spiral reentry waves in confluent layer of HL-1 cardiomyocyte cell lines. *Biochem Biophys Res Commun* 2008; 377: 1269–73.

[482] Mace LC, Yermalitskaya LV, Yi Y, et al. Transcriptional remodeling of rapidly stimulated HL-1 atrial myocytes exhibits concordance with human atrial fibrillation. *J Mol Cell Cardiol* 2009; 47: 485–492.

[483] Tsai C-T, Chiang F-T, Chen W-P, et al. Angiotensin II induces complex fractionated electrogram in a cultured atrial myocyte monolayer mediated by calcium and sodium-calcium exchanger. *Cell Calcium* 2011; 49: 1–11.

[484] Tsai C-T, Chiang F-T, Tseng C-D, et al. Mechanical stretch of atrial myocyte monolayer decreases sarcoplasmic reticulum calcium adenosine triphosphatase expression and increases susceptibility to repolarization alternans. *J Am Coll Cardiol* 2011; 58: 2106–2115.

[485] Dias P, Desplantez T, El-Harasis MA, et al. Characterisation of connexin expression and electrophysiological properties in stable clones of the HL-1 myocyte cell line. *PLOS ONE* 2014; 9: e90266.

[486] Houston C, Tzortzis KN, Roney C, et al. Characterisation of re-entrant circuit (or rotational activity) in vitro using the HL1-6 myocyte cell line. *J Mol Cell Cardiol* 2018; 119: 155–164.

[487] Kofron CM, Mende U. In vitro models of the cardiac microenvironment to study myocyte and non-myocyte crosstalk: bioinspired approaches beyond the polystyrene dish. *J Physiol* 2017; 595: 3891–3905.

Declarations

Funding

This research was funded by the Instituto de Salud Carlos III, Ministerio de Ciencia e Innovación, Spain: PI16/01123; PI19/00161; Red de Terapia Celular, Tercel, (RD16.0011.0029) and CIBERCV (CB16.11.00292).

In particular, the work done in Chapter 6 was additionally supported by Comunidad de Madrid, projects S2017/BMD-3867 and EXOHEP-CM S2017/BMD-3727, co-funded by European Structural and Investment Fund, FSE, to RB and by Instituto de Salud Carlos III through the project PT20/00044, co-funded by European Regional Development Fund "A way to make Europe". Chapter 7 was additionally funded by the Instituto de Salud Carlos III, Ministerio de Ciencia e Innovación, Spain: PI17/01059.

Institutional review board statement and informed consent

All the studies were conducted according to the guidelines of the Declaration of Helsinki. Human cardiac biopsy collection for EDC, CDC and EV production was approved by the Ethics Committee *Comité de Ética de Investigación con Medicamentos del Hospital General Universitario Gregorio Marañón* (protocol code 331/16 and date of approval 15/12/2016). Informed consent was obtained from all subjects involved in the studies.

Experiments in rats described in Chapter 5 were approved by the Ethics Committee *Comité de Ética de Experimentación Animal del Hospital Gregorio Marañón* and by the Competent Authority (protocol code 296/19, approved in 2019). For the study in Chapter 6 pig heart collection for decellularization and procedures for retention studies in mice were approved by the Ethics Committee *Comité de Ética de Experimentación Animal del Hospital Gregorio Marañón* and by the Competent Authority (protocol code 115/15 approved in 2015, and protocol code 097/16 approved in 2016 respectively).